Università degli Studi di Cagliari

DOTTORATO DI RICERCA

Scienze della Terra

Ciclo XXIV

ZIRCON U-PB AND LU-HF ISOTOPIC DATA FROM SOME PERI-GONDWANA VARISCAN TERRANES (SARDINIA-CORSICA BLOCK AND CALABROPELORITAN ARC): NEW INSIGHTS ON THE CENOZOIC GEODYNAMIC EVOLUTION OF THE CENTRAL MEDITERRANEAN BASIN

Settori scientifici disciplinari di afferenza

GEO/03

Presentata da: Dott.ssa Pamela Pavanetto

Coordinatore Dottorato: Prof.ssa Rosa Cidu

Tutor: Dott. Antonio Funedda

Prof. Massimo Matteini

Prof. Alfredo Loi

Esame finale anno accademico 2010 - 2011

What more can we require? Nothing but time.

James Hutton

Acknowledgments

The PhD thesis is officially the work of one person, but actually it comes from a continuous exchange of ideas, debates and experiences collected during the course of years of research as well. Without the stimulating environment and people met at meetings, summer schools and at the universities where I stayed, this thesis would not have been possible.

I wish to thank my supervisors Dr. Antonio Funedda, Prof. Alfredo Loi and Prof. Massimo Matteini.

Firstly I wish to express the greatest appreciation to Dr. Antonio Funedda for starting with me this study, for the continuous support and attention gave me and for offering me huge opportunities of scientific and human growth. I will always be grateful for the encouragement you gave me!

Many thanks to my co-supervisor Prof. Alfredo Loi, for his attention in my study and for being always available to help me through discussions and important notions of scientific thinking. Thanks especially to the co-supervisor Prof. Massimo Matteini, for his human and scientific support, not only for constructive explications, discussions or reviews but also for offering me the possibility to stay, and to stay very well, in Brasilia!

All my gratitude goes to Dr. C.J. Northrup for his scientific support, understanding and the interest shown about this research.

Special thanks to Prof. Etta Patacca and Prof. Paolo Scandone for transferring their huge knowledge and enthusiasm. Thank you for experiencing with us the PRIN 2007 field trip and meetings, for the time you dedicated to share precious geological discussions, critics and honest evaluation of ideas. Many thanks also to all the PRIN 2007 team for theirs contribute to this great experience.

Many thanks to the lab supervisor Prof. Cerri (University of Sassari) and his staff, thanks especially to Dr. Stefano Cuccuru and Dr. Leonardo Casini; thanks to the team of the University of Lausanne, Prof. Müntener, Dr. Ulianov, mainly to Prof. Bussy for his critical suggestions. Many thanks to Prof. Elton Dantas and to all the members of the Laboratório de Geocronologia da Universidade de Brasilia for their warm welcome, with a special thank to Prof. Faride Chemale for his helpfulness and critical conversations during the results elaboration. Many special thanks to all the members of my department in Cagliari for their support in these many years of work.

I wish to thank all my colleagues, or better my friends, met at the Dister department. Thanks to my PhD-colleague and friend Daniela, to share with me the adventure of this XXIV doctorate cycle. A special thank to my office-mates Cristina and Fabrizio for the hours of consultations, the days of wild-field trips and the months of fun! An enormous thank to Maurizio for his unlimited support and friendship!

I would like to thank particularly the wonderful "amigos" met in Brasilia who provided for me a true home in Brazil. Thanks especially to my

friends Fabiane e Paulo, for sharing their time with me and for helping me to discover my "Brazilian mood". A particular thank to my friend the Prof. Natalia Hauser, for the huge friendship shown me, for the support gave me and for sharing the same passion for life.
Thanks to all my "Colina" flatmates, for helping me to familiarize with the natural charm of Brazilian people, and a special big thank to Márcia for her exemplar strength of will and to Mariana for giving me her daily Bahian smiles. Muito obrigada!

Further, I would like to thank the various friends close to me, especially in these last months of draft! I must show my thankfulness to Lori, Bea, Angi, Valeria, Marina, Andrea and Antonio for their amazing sustain, dancing and cooking!
A special hug goes to my superlative flatmates Bea and Ale for their understanding and for the funny moments we shared! Thanks girls!

My thanks would be incomplete without acknowledging my Family! I would like to express all my gratitude to my great sister ***Eleonora*** *and to my parents, who always supported and encouraged me in all of my decisions, including when changing my mind! A huge thanks!*

A big, big THANK YOU to all of you!!

ABSTRACT

The reconstruction of pre-Variscan plates configuration in the Mediterranean area, is still poorly understood. Different hypotheses have been proposed to explain the relationships between peri-Tyrrhenian blocks such as Sardinia-Corse block (SCB) and Calabrian-Peloritain Arc (CPA), which before the opening of South Tyrrhenian Basin belonged to a branch of Southern Variscan Realm (Alvarez & Shimabukuro, 2009). Is still ambiguous if the CPA in the early time was formed by an amalgamation of two or more continental terranes that collided during Tertiary (Bonardi et al., 1980; Scandone, 1982) or was a single terrane during the middle and late Tertiary (Amodio-Morelli et al., 1976).

With the aim to provide a contribution in unraveling the peri-Tyrrhenian area evolution of the peri-Gondwana terranes, amalgamated during Variscan and widespread during Cainozoic opening (and closing) of Tethys, both Variscan and Tertiary rocks cropping out in the two Blocks have been investigated, either magmatic or sedimentary.

The first part of the research was focused on the magmatic bodies supposed belonging to the European Variscides with the aim to provide more constrains to the Variscan magmatic evolution and so to draft the analogies between the present-day, separated blocks. In detail, the geochemical data from magmatic and detrital zircons of the basement rocks highlight analogies or differences between the tectono-sedimentary sectors of the Sardinian Variscides (nappe and foreland zones) and between them and the Calabria Variscides. The geochemical whole rocks analyses and U-Pb data obtained show that the Variscan basement which crops out in the Northern part of the CPA (Sila region) is characterized by the similar features of that in the SCB: the Middle Ordovician and Late Palaeozoic magmatic products recognized in the two blocks look similar. Some of these data can provide new insights also about the Ordovician evolution of the Northern Gondwana margin.

To compare the and better constrain the relationships between the two blocks, detrital zircons were sampled in Tertiary rocks in NE Sardinia, E Corsica and Calabria, commonly regarded as closely related to the tectonic evolution of the Central-western Mediterranean. The analyses performed suggest some differences on the classical paleo-geographic positions of the SCB respect to the CPA and some assumptions can be made also about their relationships with other peri-

Gondwana terranes. The association of U-Pb and Lu-Hf study performed on Tertiary detrital zircon populations is a good tool to furnish more data for recognize the pre-Variscan inputs suffered by the peri-Tyrrhenian area, and to highlight differences and similarities between them.

The first consideration that can be made is that the two blocks suffered different crustal evolution. The main difference between them has given by the Grenvillian zircons input studied in the Tertiary deposits. The Southern part of CPA (Aspromonte and Peloritani) is characterized by the lacking of Mesoproterozoic age, whereas the Northern part of CPA (Sila) together with the SCB, are characterized by an important Grenvillian input. These considerations have a geodynamic implications about the misunderstood early evolution of the studied zones The Southern part of CPA shows strong similarities with Cadomiam terranes, which permit to correlate it with the evolution of Variscides now cropping out in North Africa. The SCB and the Northern part of CPA could be associated to the other European Variscan terranes (e.g. Iberia) characterized by widespread Grenvillian zircons. A supplementary assumption that stem out from these analyses is that the early position of SCB and Northern part of CPA, were possibly close to the Amazonian craton or nearness to the West African craton (Arabian-Nubian shield and the Sahara Metacraton), quite different from more of the proposed reconstructions.

Finally, considering all these data in the complicated evolution of southern Tyrrhenian basin, here is supported the “two-terrane model” (slightly different from that proposed by Alvarez and Shimabukuro, 2009) which considers the CPA composed by a northern CPA terrane connected with the SCB from the end of the Variscan orogeny until the almost the Eocene. The southern CPA terrane suffered a different evolution before the opening of the Tyrrhenian Sea. According to the roll-back model of the westward subduction of Adria plate under Europe during Neogene-Pliocene the whole CPA, likely amalgamated in the early Miocene, was then tear apart from SCB and drifted away eastwards during the open of the South Tyrrhenian basin.

CONTENTS

1 INTRODUCTION

1.1 AIM OF THE RESEARCH

This research is part of a national project (PRIN project 2007), which has the aim of reconstructing the peri-Tyrrhenian puzzle, relocating in their original positions elements today dispersed in Southern Tuscany, Calabria and Eastern Sicily. It is supposed they formed a continuous belt bordering Sardinia and Corsica before the opening of the Algero-Provençal Basin and of the Tyrrhenian Basin. The PRIN project is mainly focused on studying and comparing both the basement and cover rocks in the Sardinia-Corsica block (SCB) and in the Calabria-Peloritani Arc (CPA), and this PhD research helps to reconstruct the linkages between these blocks and their paleogeographic relationships before fragmenting into their present positions and configuration.

Geodynamic models and reconstructions of pre-Variscan plate configurations in the Tyrrhenian area are still extremely complex and speculative (Stampfly and Borel 2002, von Raumer et al. 2002, Trombetta et al., 2004; Alvarez & Shimabukuro, 2009). Different hypotheses have been proposed to explain the relationships between Sardinia and Calabria before the opening of the Tyrrhenian Basin. Some of these are contradictory and no single model explains unambiguously the position of Variscan terranes during the time.

Evidence for the paleo-tectonic linkages, the terranes derivations, and the tectonic setting of the SCB and CPA as peri-Tyrrhenian blocks before the opening of the Algero-Provençal Basin can be found in the geology of the SCB basement and the Tertiary deposits cropping out both in the SCB and CPA.

To understand the relationships between outcrops now bordering the Tyrrhenian sea, it is necessary to know the positions of these blocks before the basin opened, and the Variscan and pre-Variscan geology help to constrain their paleogeographic positions. Two separated approaches were taken as part of this work. First, I studied Paleozoic plutonic and volcanic rocks in the Pre-Alpine basement of the SCB and the CPA tectonic units, investigating the similarities between the SCB and CPA reflected in their variscan magmatic evolution. Second, I evaluated Tertiary sedimentary deposits

that formed on both crustal blocks during the interval when the oceanic basins began to open. The deposits chosen are considered coeval and developed during the convergence and collision between Southern Europe and Adria in the late Oligocene-Lower Miocene (Oggiano et al., 2009). Such deposits are widely distributed on Sardinia and the Corsica islands, and studying them is important because the SCB represented the foreland of the North-Apennynic chain that contains in its structures a good chrono-stratigraphic record of the Tertiary regional tectonic evolution.

Geochronological analyses of key sedimentary deposits were conducted to evaluate the sedimentary provenance and determine the plate tectonic setting of the basins, permitting the recognition of paleotectonic linkages and terrane derivations.

Detrital zircon geochronology can be a useful tool to help reconstruct paleogeography in complex and enigmatic settings like the terranes bordering the Tirrhenyan basin. Age distributions distinguish different source regions where the zircons were derrived (Bahlburg et al. 2010; e.g. Sircombe, 1999; Friedl et al., 2000; Dickinson and Gehrels, 2003; Cawood et al., 2007; Linnemann et al., 2007; Veevers and Saeed, 2008; Elliot and Fanning, 2008; Condie et al., 2009). In fact similarities of age distributions and relative abundances of zircons in different but coeval lithostratigraphic units can be used to identify a common source region or provenance (Bahlburg et al. 2010).

However, the age population in a sedimentary rock does not unequivocally identify its source. The presence of a similar age spectrum in several crustal blocks may not uniquely link the actual provenance of these rocks if the crustal evolution of these blocks are not constrained independently by other techniques. Consequently, in addition to U-Pb age determinations, I have documented Hf isotopic signatures of zircon grains using LA-ICP-MS. This integrated method is a powerful tool to more confidently identify and compare provenance (Patchett, 1983; Amelin et al., 2000; Bodet and Scherer, 2000; Augustsson et al., 2006; Flowerdew et al., 2007; Scherer et al., 2007; Willner et al., 2008; Bahlburg et al., 2009). The initial Hf isotopic composition of a dated zircon constrains geochemical features of the source magmatic rocks from which the zircons were eroded. Relatively radiogenic Hf isotopic compositions are consistent with juvenile crust, whereas unradiogenic Hf isotopic compositions reflect an evolved crust source. The Hf isotopic compositions of detrital zircons record their time-integrated isotopic evolution and help to distinguish between different crustal domains as sources of the sediment.

The goals of this research are to address the following questions:

1) Have the Saridinia-Corsica block and Calabro-Peloritan Arc shared the same tectonic evolution after their separation from North-Gondwana (?) margin?

2) Do the Saridinian-Corsica block and Calabro-Peloritani arc basements and Tertiary deposits show the same ages and geochemical features?

3) Do existing geodynamic models adequately explain these features, or can new models be developed to better describe the evolution of these regions?

1.2 TERRANES DISTRIBUTIONS SINCE RODINIA MACROCONTINENT UNTIL THE PRESENT DAY GEOGRAPHIC CONFIGURATION (BY BIBLIOGRAPHIC DATA)

The evolution of the Southern European Variscides (and particularly the Sardinian and Corsican Palaeozoic sequences, and likely part of the Calabro-Peloritani Arc), has been well studied, and many paleogeographic reconstructions have been proposed for time intervals raging from the Cambrian to the present. Neverthless, more gaps remain about the pre-Cambrian evolution of these zones. Most authors agree that the Southern Variscan Realm (Rossi et al., 2009) resulted from the convergence between the northern Gondwana margin and Laurentia-Baltica (Matte, 2001), followed by a diachronous continent-continent collision from Devonian to Carboniferous time. However, the Late Palaeozoic tectonic processes affected crustal blocks (or terranes) that had already been involved in preceeding orogenic cycles, and the recognition of "tectonic traces" produced during the earlier history helps us to resolve the palaegeographic puzzle and reconstruct the older positions of each block. In the following sections, we describe their evolution, from the amalgamation of the Rodinia Supercontinent to the present day, focusing on the main processes that occurred and the paleo-positions of terranes as proposed in various models by previous authors.

1.2.1 PROCESSES LINKED TO THE RODINIA SUPER-CONTINENT

The Rodinia supercontinent was assembled ca. 1,1 Ga ago and was present up to 750 million years ago. His brokering up was following by the opening of the Panthalassic Ocean.

The tectonic events associated to the Rodinia assemblage taken place between **1200-980 Ma** are the associated to the mountain-building event called **Grenville Orogeny**.

*Distinct tectonic events have been associated to the Mesoproterozoic period. One of the most important tectonic events recognized, called the **Elzevirian Orogeny (**Streepey et al. 2004), was the accretion of an island arc occurred at **1.30-1.20** Ga. The Elzevir back arc basin was closing at ca. 1.19 Ga (Corrigan & Hanmer, 1997).*

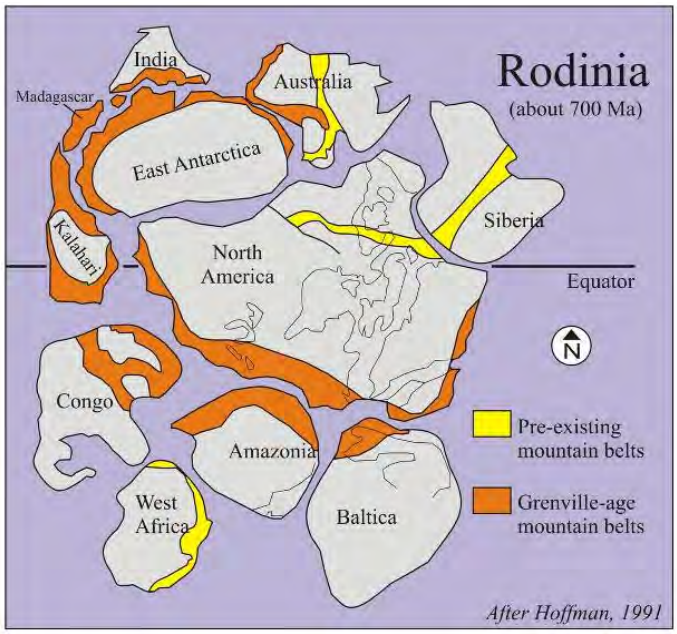

Fig. 1-1 Reconstruction of Rodinia assessment at about 700 Ma ago, after Hoffman, 1991.

Evidence associated to this island arc have been recognised along the **Grenville orogenic belt** (Fig 1-1; Corriveau, Louise, 1990; Mosher et al., 2008).

From **1.18 to 1.14 Ga** the area was interested by common extension (Corrigan & Hanmer, 1997), likely due to lithospheric cooling. During this time have been formed large sedimentary basins, suggesting a general quiescence of the margin. From **1.16 to 1.13** Ga, also some areas have been affected by thrusting and of terranes-emplacement (Corrigan & Hanmer, 1997). From **1.12 to 1.09** Ga westward thrusting occurred Following Corrigan & Hanmer (1997) and until **1.05** Ga the extension was the main tectonic activity that affected the margin.

The mechanism for tectonic regime changing, from compression to extension, is to be expected like the consequence of more processes occurred as gravitational collapse, mantle delamination, formation of a plume underneath a supercontinent (Streepey et al., 2004).

The Neoproterozoic period was affected by diachronic rifting processes along the supercontinent.

Starting by 850 to 800 Ma (Torsvik, 2003) a rift occurred in many continental masses, first on the northern hemisphere (e.g. present-day Australia, eastern Antarctica, India and the Congo and Kalahari cratons) and then on the southern emisphere (e.g. Laurentia, Baltica, Amazonia and the West African and Rio de la Plata cratons). The evidences of this rifting have been recognised up ca. 750 Ma (McMenamin & McMenamin, 1990). Later, during the Ediacaran period, the rift developed into the Adamastor Ocean.

During the **Ediacaran period,** at ca. 610 Ma, a separated rifting gave the formation of the Iapetus

Ocean. Two branches formed this ocean: one part formed between Baltica and Laurentia at the East, and the other one, at the West, between Amazonia and Laurentia.

1.2.2 PAN-AFRICAN OROGENESIS

At ca. 550 Ma with the **Pan-African orogenesis** some cratons were accreted again with Amazonia, West Africa and the Rio de la Plata craton (Pisarevsky et al., 2008) creating the Gondwana continent, which remain stable for hundreds of millions of years.

At ca.550 Ma Laurussia and Gondwana collided to the Congo craton (made up of much of north-central Africa) forming a new supercontinent called **Pannotia (or Vendian supercontinent)**

The Pan-African magmatism is widely spread in the Anti-Atlas domain, where has been described three main stages (Gasquet et al., 2005):

- ocean opening and subduction (790-690 Ma, with peaks at 790 and 690 Ma);
- ocean closure and arc-continent collision (690-605 Ma, with peaks at 660 and 615 Ma);
- transition from an active (compressive–transtensive) to a passive (extensional) margin associated with growth of foreland basins (605-530 Ma, with peaks at 590, 550 and 530 Ma). In this period have been formed voluminous high-K calc-alkaline plutonism and volcanism showing mantellic and crustal signatures (e.g. Gasquet et al. 2005).

Calabrian augen gneisses show a close correspondence to the Pan-African post-collisional granitoids found in the northern edge of the West African craton, the Moroccan Anti-Atlas (Micheletti et al., 2007).

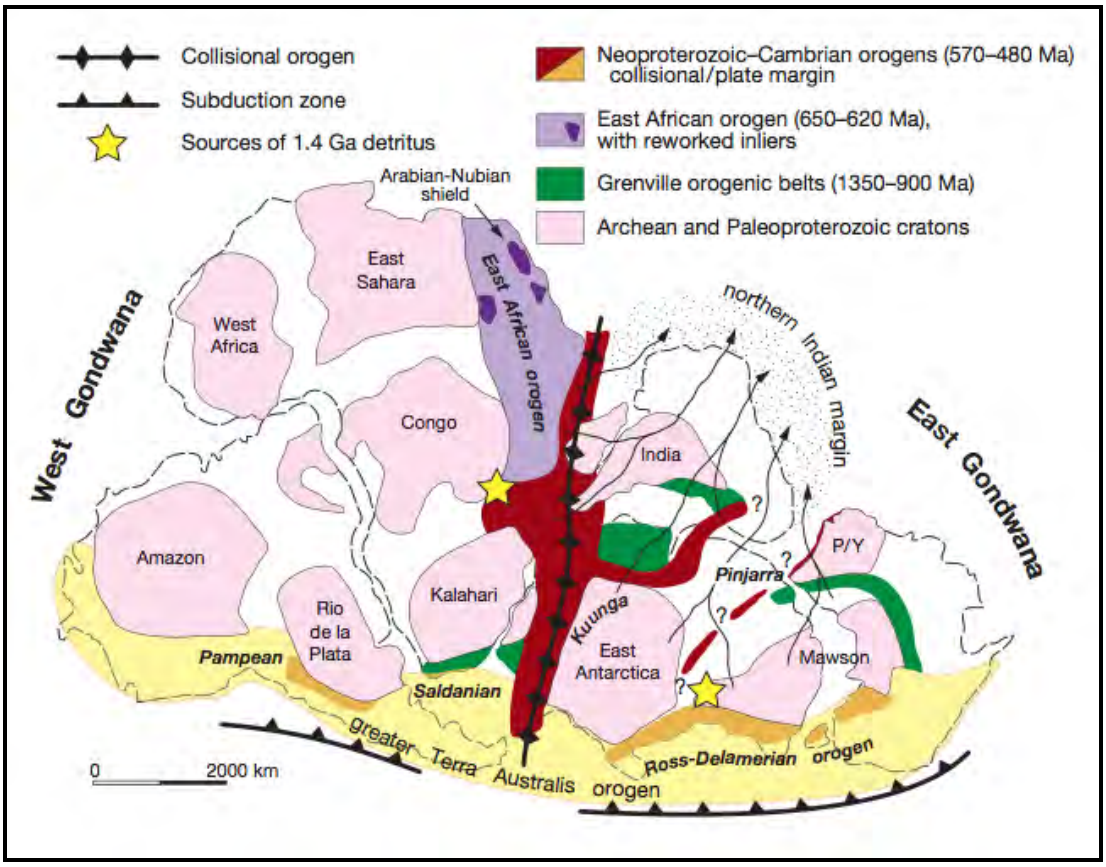

Fig. 1-2. Gondwana reconstrucion at about 500 Ma, after Myrow et al., 2010.

1.2.3 PROCESSES LINKED TO THE GONDWANA CONTINENT

At ca. 570 and 510 Ma, with the connection of the East Gondwana to the West Gondwana, was sutured the supercontinent called Gondwana.

At the end of the Ediacaran (550–500 Ma) several orogens contributed to the Gondwana final amalgamation (Buchan and Craig, 2004). Firstly was involved the **Brasiliano Orogen**, the **East African Orogen**, the **Malagasy Orogen**, and the **Kuunga Orogen.**

Gondwana assembly was extended beyond the separation of Laurentia from West Gondwana opening of the Iapetus Ocean. These final stages enclosed six major cratons: Amazonia, West Africa, Congo, Kalahari, Greater India, Australia-Antarctica, welded together by the Brasiliano/Pan-African orogenic belts (Fig.).

The orogenic belts were formed by the closures of the several Neoproterozoic oceans and were internally dislocated by the collisional indentations and lateral extrusions.

The consumption of the basins between East and West Gondwana and the African cratons (West Africa, Congo-Sao Francisco and Kalahari; Hoffman, 1991; Dalziel, 1991, 1992) was due to the fan-like aggregation of Gondwana about a mean rotation pole in the Weddell Sea region.

At the eastern part of continent, the closure of the Mozambique Ocean (Dalziel, 1991, 1992), turn into the East African Orogen (Stern, 1994; Shackleton, 1996).

At the western part, the Adamastor Ocean (Hartnady et al., 1985) closure developed into the Brasilian orogen and contiguous orogens (Trompette, 1994). Simultaneously, the Laurentia was separated from East Gondwana by the Pacific ocean opening and and from West Gondwana by the Iapetus ocean opening.

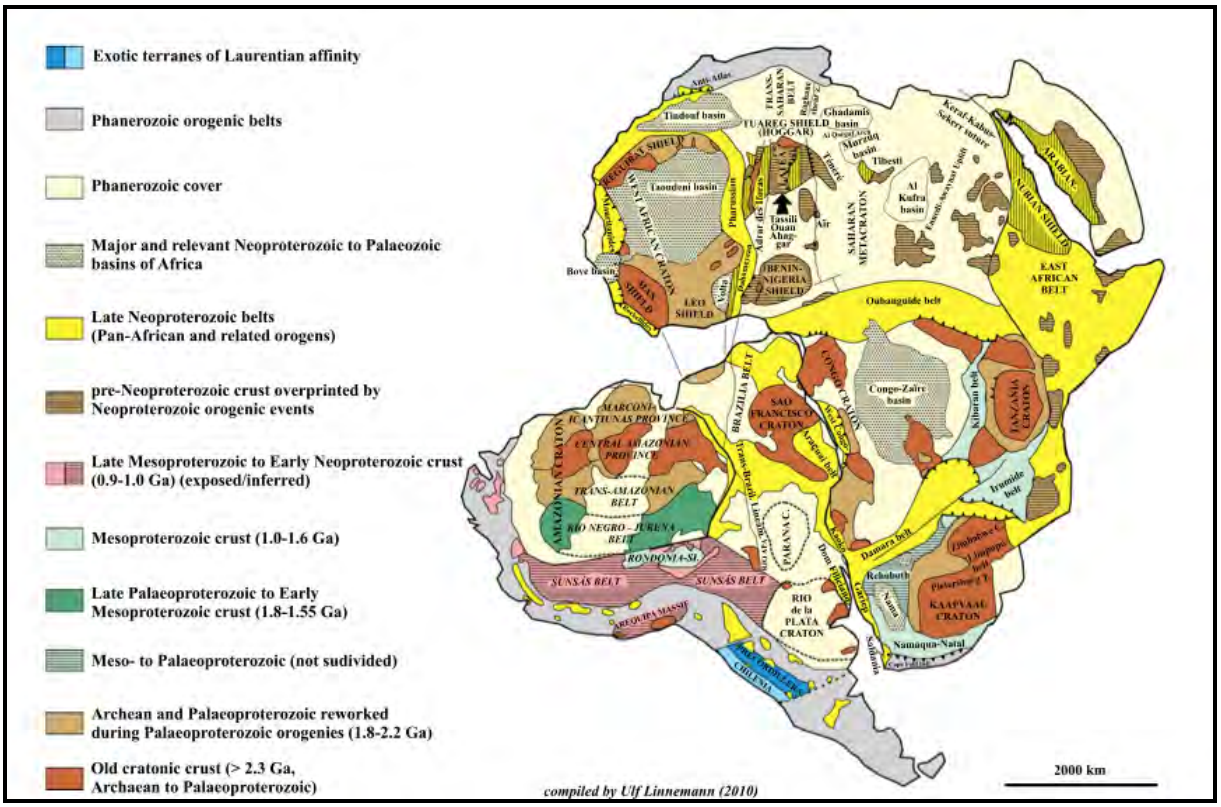

Fig. 1-3 The orogenic provinces amalgamated in the Gondwana continent, after Linnemann, 2010, 2011.

In the Late Precambrian, the Gondwana supercontinent was formed by West Gondwana (South America and Africa) and East Gondwana (India and Australia; e.g. Jacobs & Thomas 2004). Instead, the North Gondwana is composed by the Cadomian and Cimmerian terranes.

Among the Laurentia, Baltica and Gondwana continents have been detected several crustal blocks now cropping out in central and southern Europe. These parts of continent show Precambrian or Cambrian affinity with the margin of Gondwana (Winchester et al., 2002) as suggested by theirs basements constituted mainly by Cadomian apports.

For the reasons expressed upon, these terranes are usually considered as **peri-Gondwanan**

'terranes', even if their position and palaeo-geographical constrains are still debated and they will be described in detail in a following paragraph. According the model proposed by von Raumer and Stampfli (2008), the dispersion of crustal blocks derived from the North Gondwana margin started from the Late Cambrian to the Devonian with different of kinematic regimes, including local back-arc spreading, intra-continental rifting, and even the spreading of a mid-ocean.

Following the model proposed for NW and SW Iberia by Gutiérrez-Alonso et al. (2003) the major events that shaped the northern margin of Gondwana in the Neoproterozoic-Early Palaeozoic boundary (Fig. 1-4) are as follows:

- At 600 Ma the terranes were part of the active northern margin of Gondwana, characterized by a magmatic arc and a variety of back-arc basins (e.g. Murphy et al., 2000).
- At 570 Ma occurred the subduction alongside the margin carried on until either ridge-trench collision (Murphy et al., 2000) or a change in subduction regime (Feŕnandez-Suárez et al., 2000) caused the transition to a transform regime. The stop of subduction was diachronous along the margin (e.g. Murphy et al., 2000; Gutiérrez-Alonso et al., 2003).

The rest of the South America-derived terranes (that later contributed to form the Armorica Terrane Assemblage) have supposed drifted along the Gondwana margin from a South American realm towards the African margin.

The detritus derived by the erosion and dispersal of these crustal fragments have been found in the Mesoproterozoic zircon inputs forming the Armorican quartzite. The dispersal is supposed that has been occurred along the major transform faults that nearly parallel to the Gondwana margin.

From the early stages after the break-up of Rodinia (ca. 800 Ma), the evolution of Neoproterozoic-Early Palaeozoic northern margin of Gondwana was active during about 300-250 (Pisarevsky and Natapov, 2001).

This prolonged period of activity, were generated the proto-Avalonian–Cadomian terranes (western Pacific stage; Murphy et al., 2000), with following arc construction and accretion of terranes (Andean stage). The subduction-arc construction led to a later transform activity (Cordilleran stage). The final margin stage of the extensions conducted to the opening of the Rheic Ocean and the drift of the Avalonian terranes.

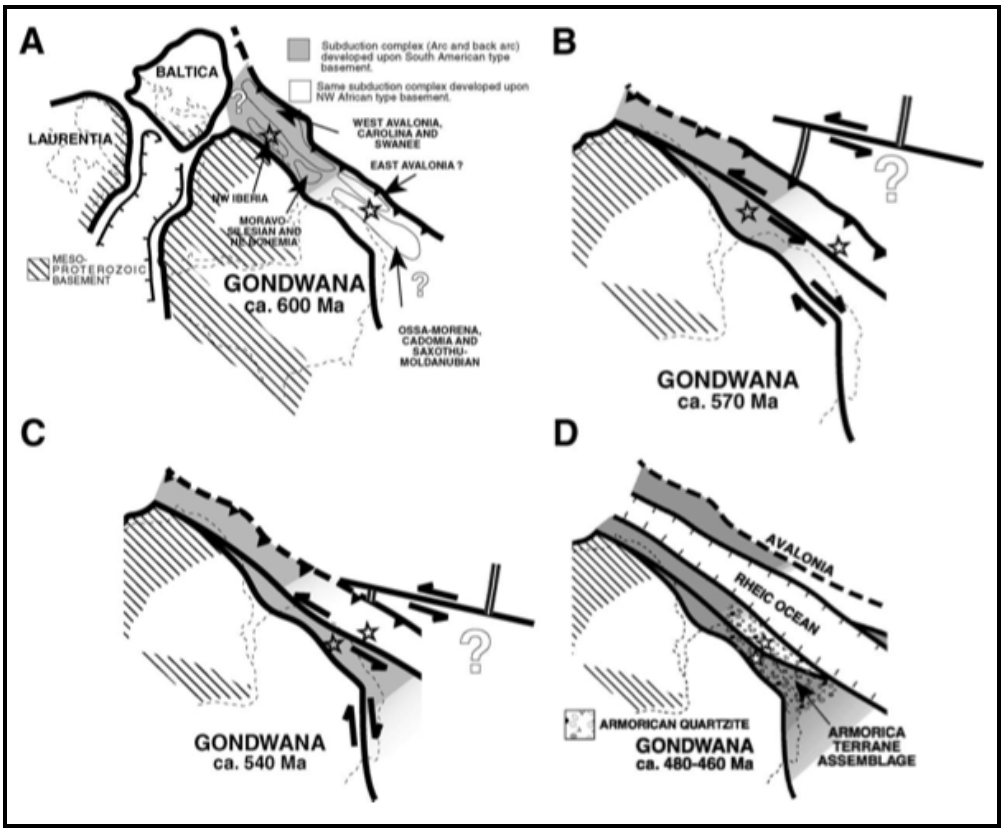

Fig. 1-4 Neoproterozoic terrane distribution (A–B) and Early Paleozoic tectonic evolution (C–D) along the northern Gondwanan margin (see text for details). Stars represent the hypothetical location of NW and SW Iberia/North Armorica. (A) modified after Nance and Murphy (1994) and Fernández-Suárez et al. (2000, 2002b), Gutiérrez-Alonso et al., 2003.

1.2.3.1 PERI-GONDWANA TERRANES: A PUZZLE OF MICROPLATES

Is considered that these "blocks" represented independent palaeogeographical units, attributed to microcontinents or microplates (see also Saveirs and Sintubin, 2009 for the use of terms plate, microplate, terranes). In many palaeogeographical maps, several of these terranes are indeed represented as independent islands ‘floating’ between Gondwana in the high southern latitudes and Laurentia and Baltica in lower latitudes (e.g. Winchester et al., 2002; Belka et al., 2002; Williams et al., 2003).

1.2.3.1.1 AlKaPeca

The Alboran microplate (Andrieux et al. 1971), or Mesomediterranean terrane (Guerra et al, 1993) or AlKaPeca (Bouillin et al. 1986) is constituted by the amalgamation of several microplates: Alboran + Kabilie + Peloritan + Calabria. These terranes were placed in the central position in the

peri-Gondwanian Cadomian terranes (Stampfli and Borel 2002; von Raumer et al. 2002). Although an exact definition of the links between various terranes is still discussed (Trombetta et al. 2004). Fragments of the Alkapeka are considered to crop out in the Alpine and Variscan chains of southern Europe and North Africa (Calabria, Peloritani Mountains, Sardinia, Southern Spain, Maghrebides). According to some researchers, the Calabria–Peloritani Arc represents an "exotic terrane" in the Mediterranean scenario, likely belonging to the Alboran micro-continent (Andrieux et al., 1971) and with this microplate might shared the position close to the northern edge of the West-African craton (Fig. 1-5; Micheletti et al., 2007).

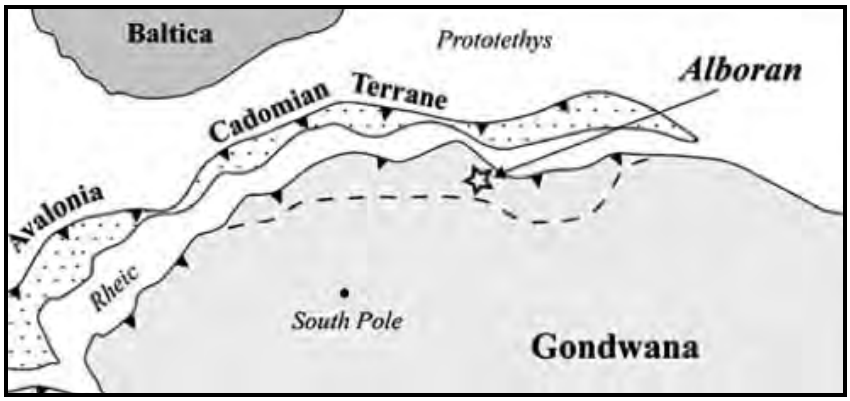

Fig. 1-5 Paleogeographic reconstruction of the Alboran microplate after Micheletti et al., 2007.

1.2.3.1.2 Armorica, Hun Superterrane, Galatian terrane

According to Carmignani et al. (1994c), the Variscan collision has involved the northern Gondwana margin and some small continental plates, the so-called Armorica-Terrane-Assemblage (ATA) of Franke (2000), the Hun Superterrane (von Raumer et al., 2003) or, more recently, the Galatian Terrane (von Raumer and Stampfli, 2008; Fig. 1-6).

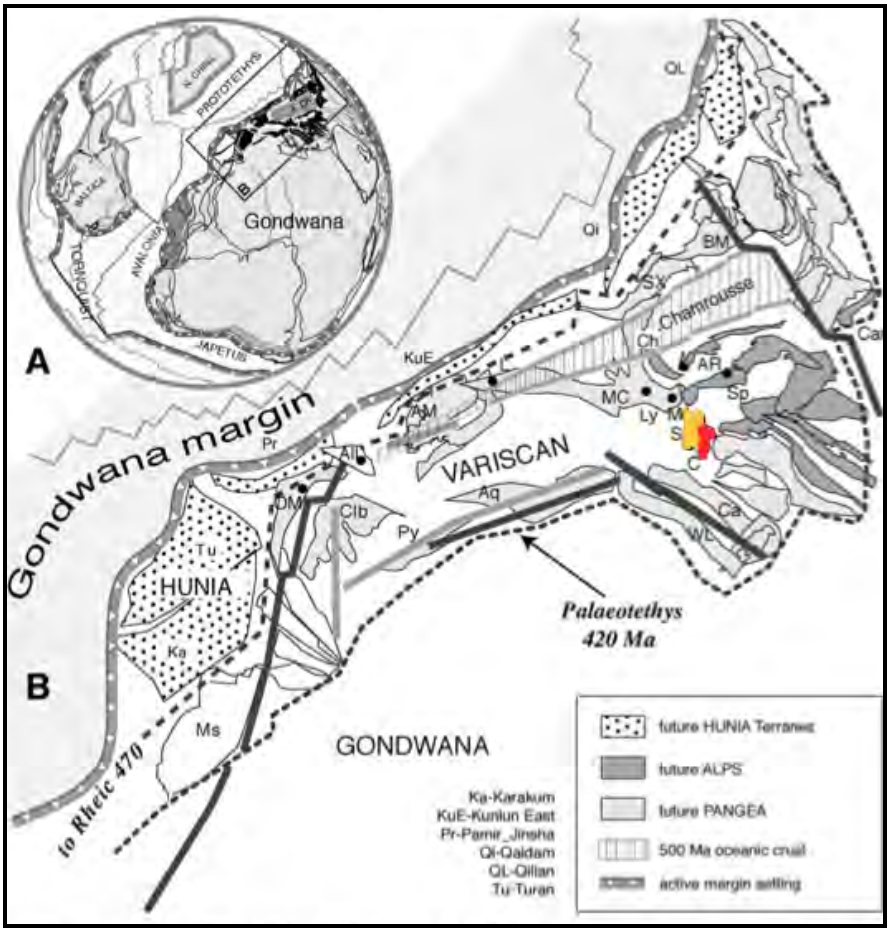

Fig. 1-6 Plate-tectonic situation for the Late Cambrian period (500 Ma), with the reconstruction of the peri-Gondwanan terranes at the Gondwana margin. After von Raumer and Stampfli, 2008. In yellow has been draft the Sardinia and in red has been reported the Calabria. The original model doesn't report the Corsica and Peloritani Mts.

1.2.3.1.2.1 Armorica and/or ATA

The elucidation of Armorica existence and its position are especially important because very different reconstruction of the geodynamic evolution could be proposed for the South Variscan Realm.

The name Armorica is established on the Armorican Massif of Brittany, NW-France. In fact some workers (see review in Servais & Sintubin, 2009 and in Robardet, 2003), attributed the term "Armorica" only to the Armorican Massif. However, in the literature, the expression "Armorica" was usually applied to a much larger area. The original definition of the "Armorica microplate" is based on palaeomagnetic studies (Van der Voo 1979), and included southwestern England and

Wales, various regions of European Variscides, and probably also the Avalon Peninsula and New England. In the beginning, the “Armorica” also included the Avalonia (Van der Voo 1979) and later was restricted to the numerous terranes with a Cadomian basement in Variscan (and Alpine) fold belts cropping out in Europe.

Also in others models are not discriminated the Armorica from Avalonia (Neugebauer, 1989; Lefort, 1990; Piqué, 1991; Piqué et al., 1994) and the southern France and Iberia were considered like part of the Gondwana margin or like a single microplate (e.g. Iberia).

With the designation of Avalonia like a detached plate (Cocks & Fortey, 1982), also has been revaluated the term of the "Armorica microplate" restricting the expression to the Variscan regions of southern and central Europe (Van der Voo, 1988).

Then Matte (1986, 1991) clarified the denomination of "Armorica" considering part of this, the regions sandwiched between two sutures related to two distinct oceans in the pre-Variscan paleo-geography. The Armorica terrenes comprised the Armorican Massif regions, part of the Iberian Peninsula, Saxo-Thuringia and Bohemia and southern France, Corsica-Sardinia. These terranes were considered or like a separate microplate or included in Gondwana (Rey et al., 1997; Faure et al., 1997; Matte 1991). For other workers (e.g. Cocks & Torsvik 2002), ‘Armorica’ is constituted by the Armorican Massif (in Normandy and Brittany), the Massif Central and the Montagne Noire, with several massifs from the Iberian Peninsula.

The presence of the ophiolitic remnants supported the presence the two oceans:

1. the Rheic Ocean, comprises between the Variscan regions of southern Europe and northern Europe, whose suture has been individuated in the North of the Mid-North Armorican Domain;

2. the South-Armorican Ocean (= Ligerian Ocean or Massif Central Ocean), whose suture would be detected between the Mid-North Armorican and the South Armorican regions and prolonged into the Massif Central.

In the latest works the term "Armorica" has become the **Armorican Terrane Assemblage (ATA),** considering it like an "archipelago" of continental crustal blocks detached by several small oceanic basins (Tait et al., 1994; Tait, 1999; Tait and Bachtadse, 2000; Crowley et al., 2000). The ATA is constituted by three main massifs (Iberian, Armorican and Bohemian) with the addition of several crustal blocks such as Saxothuringia Teplá-Barrandia and Moldanubia (and likely comprises ‘Perunica’).

Also Ziegler (1990) admits the presence of several blocks situated between Gondwana and Laurussia but considers a "stepwise accretion" process for amalgamation of Palaeozoic crustal of western and central Variscan Europe, derived by steps of waccretion of various Gondwana-derived microcratons to Laurussia.

Considering that the palaeomagnetic data for the Silurian and the Devonian of the South European regions (the classical Armorica microplate) are still rare and ambiguous, the reality of an Armorica microplate cannot be considered as established (Robardet, 2003).

Even if is present in the literature a paucity of unambiguous data, the lithological indicators of palaeoclimate and palaeo-bio-geographical data about the North Gondwana and the “Armorica” (in his more large sense), suggest that the southern European regions remained permanently closely connected with Gondwana, composing its northern margin (Robardet, 2003).

During the Lower and Middle Cambrian, Gondwana was drifting towards lower latitudes (McKerrow et al., 1992; McKerrow and Cocks, 1995) dominated by a warm to humid climate. During this period intense erosion and denudation process affected the Pan-African, Cadomian and related Neoproterozoic orogens forming a peneplain on the surface of Gondwana. During the Ordovician, large amounts of high maturity sands were accumulated in opened shallow marine shelf basins formed by the rifting and widespread thermal subsidence.

From the above reported framework of models follow that the existence of the Armorica microplate or ATA is still matter of discussion (Servais and Sintubin 2009; Lewandowski, 2003), "a number of authors have turned aside from the original signification of the term Armorica and adapted this denomination in their own way” (as wrote Robardet, 2003).

1.2.3.1.2.2 Hunia

More recent plate-tectonic reconstructions suggest that the location of Gondwana-derived terranes should also be assumed located along the Cambrian Gondwana margin and accreted to the North-Chinese block in the Silurian period (VonRaumer and Stampfli, 2008). So would be considered that also a detrital input from some Asian blocks (Hunia) is possible to detect in the peri-Gondwana terranes.

The Hun terrane (or **Hun superterranes**) is composed by the continental fragments, whose derived from the Gondwana continent, in lateral continuity with the Armorican block (Stampfli et al., 2002). These terranes are figured as a ribbon-like assemblage of basement rocks (Stampfli et al., 2002) detached from the northern African margin (Stampfli et al., 2002) like suggest by Stratigraphic (Paris and Robardet, 1990) and paleomagnetic data performed from the eastern European Hunic terranes (Schätz et al., 1997; Krs and Pruner, 1999). This detachment is considered the first mains separation that occurred between Armorica and Gondwana (Early Devonian; Stampfli et al., 2002).

1.2.3.1.2.3 Galatian

The definition of Galatian terranes are still object of discussion in the modern literature.
von Raumer and Stampfli (2008) associated the separation of a chain of blocks, called the **"Greater Galatian Superterrane",** from Gondwana, with the start of the the **Palaeo-Tethys** Ocean opening, from mid-Devonian times.
Cocks and Torsvik (2002), Scotese (2004), and Ruban et al. (2007) discussed various problems connected with the plate tectonic reconstruction of the Palaeo-Tethys Ocean. Although is considering the lacking of geological and palaeomagnetic data from now constituting the Middle East and Central Asia (cf. Kalvoda and Bábek, 2010) several models have been point out about the Galatian terranes. Also the Rheic, Proto-Tethys, Rhenohercynian, and Palaeo-Tethys oceans are not delineate without a doubt by the recent literature (Cocks and Torsvik, 2002; Scotese, 2004; Stampfli and Borel, 2002; von Raumer and Stampfli, 2008).
Also forthcoming discussions are recently started about the presence of a large watermass between Gondwana and Laurussia before the Early Devonian were recently point out (Dojen, 2009; Spina and Vecoli, 2009).

1.2.4 VARISCAN OROGENESIS

The Variscan belt is part of an intra-Palaeozoic peri-Atlantic orogen extending in Europe from the Bohemian Massif (Germany, Poland and Czech Republic) to the Armorican Massif (France), and from the Iberian Massif (Portugal and Spain) to the Morocco in the northwest Africa (Casini and Oggiano, 2008; Melleton et al., 2010; Keppie et al., 2010). It was formed between 380 and 250 Ma as a result (Matte, 2001) of the diachronous collision between Laurussia (Baltica and Laurentia) and northern Gondwana during the closure of the Rheic Ocean (Matte, 2001; Nance et al., 2010; Pereira et al., 2010). This time-span overlaps that of the Acadian (USA, Canada) and Alleghanian (USA, Mauritania) orogenesis (Kroner et al., 2008).
The Variscan belt of Europe consists of six main zones: the Northern Foreland, the Rhenohercynian Zone, the Saxo-Thuringian Zone, the Tepla-Barrandian, the Moldanubian Zone, and the Southern European Variscides (Fig. 1-7). The northern boundary is delineated by the northward decrease of Variscan deformation and the widespread appearance of structures developed during the Caledonian orogenic event (540-408 Ma; Matte, 1991).

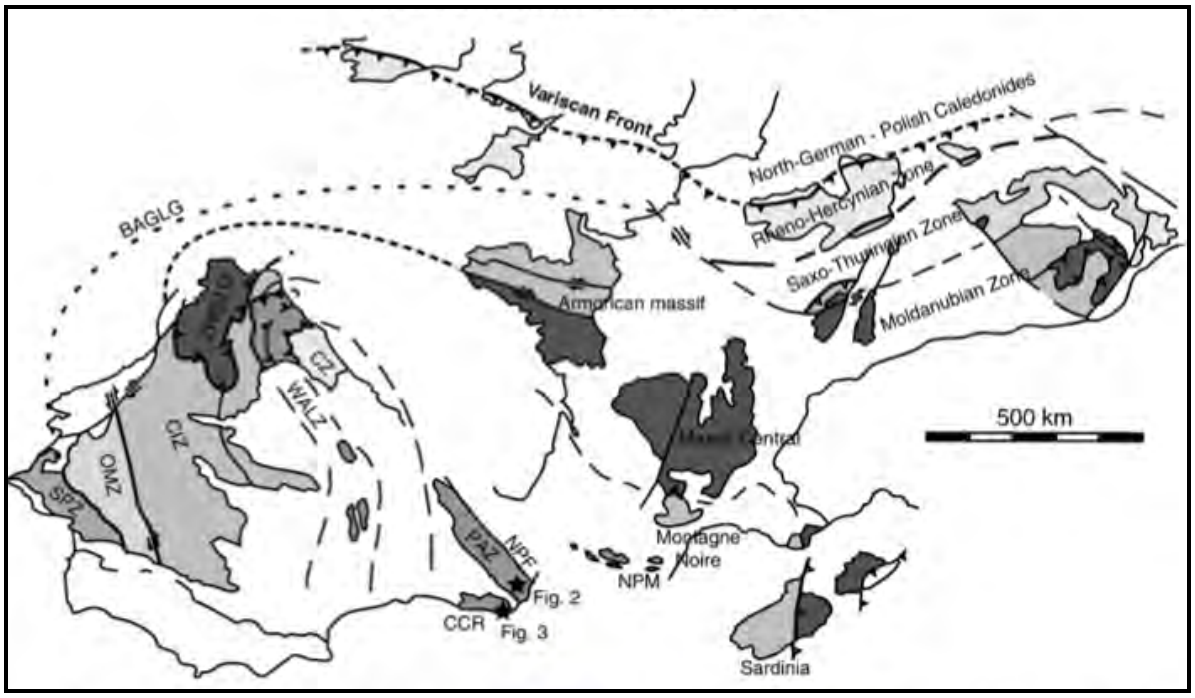

Fig. 1-7. Variscan orogene in Europe, CZ, Cantabrian Zone; WALZ, West Asturian Leonese Zone; GTOMZ, Galicia-Trásos-Montes Zone; CIZ, Central Iberian Zone; OMZ, Ossa Morena Zone; SPZ, South Portuguese Zone; PAZ, Pyrenean Axial Zone; CCR, Catalan Coastal Ranges; NPF, Northern Pyrenean Fault; NPM, North Pyrenean Massifs; BAGLG, Beja-Acebuches-Galicia-Lizard-Giesen oceanic suture Zone. Reconstuction after Navidad et al., 2010.

Especially for the Southern Variscan Realm (Rossi et al., 2009), and here Sardinia-Corse block and Calabria-Peloritani arc, following a model proposed by Capelli e Vai (1992) and Carmignani et al. (1994a) and than reworked (Rossi et al., 2009; Fig. 1-8), the collision involved the northern Gondwana margin and some small continental "microplates" (see previous paragraph).

Recently, Gaggero et al., (2012) considering geochemical geochronological data found three distinct ordovician magmatic cycles in the Variscan basement of Sardinia: 1) an Early Ordovician cycle (492–480 Ma) with mildly alkaline signature is linked to a rifting stage; 2) a middle Ordovician cycle (~ 465 Ma) ranges from subalkaline to alkaline suite linked to a volcanic arc; 3) an Upper Ordovician-Silurian cycle (~ 440 Ma) has alkaline signature and is linked to the rift-drift stages. Based on these data the authors refused the model of von Raumer and Stampfli (2008) that invoke a pattern of local back-arc basins or intra-continental rifts during the Early Cambrian, followed by Upper Cambrian–Early Ordovician closure (von Raumer and Stampfli, 2008), because in the Sardinian Variscides there is no evidence of plate, or microplate, convergence at the boundary between Cambrian and Ordovician, that begin later in the Middle-Upper Ordovician.

To the Variscan orogeny are associated magmatic products. The presence of extensional Early Carboniferous intracontinental basins and the intrusion of post-kinematic S-type granites in the

Southern Variscan Realm provide a minimum age for this deformation at 350-360 Ma (Matte, 1991).

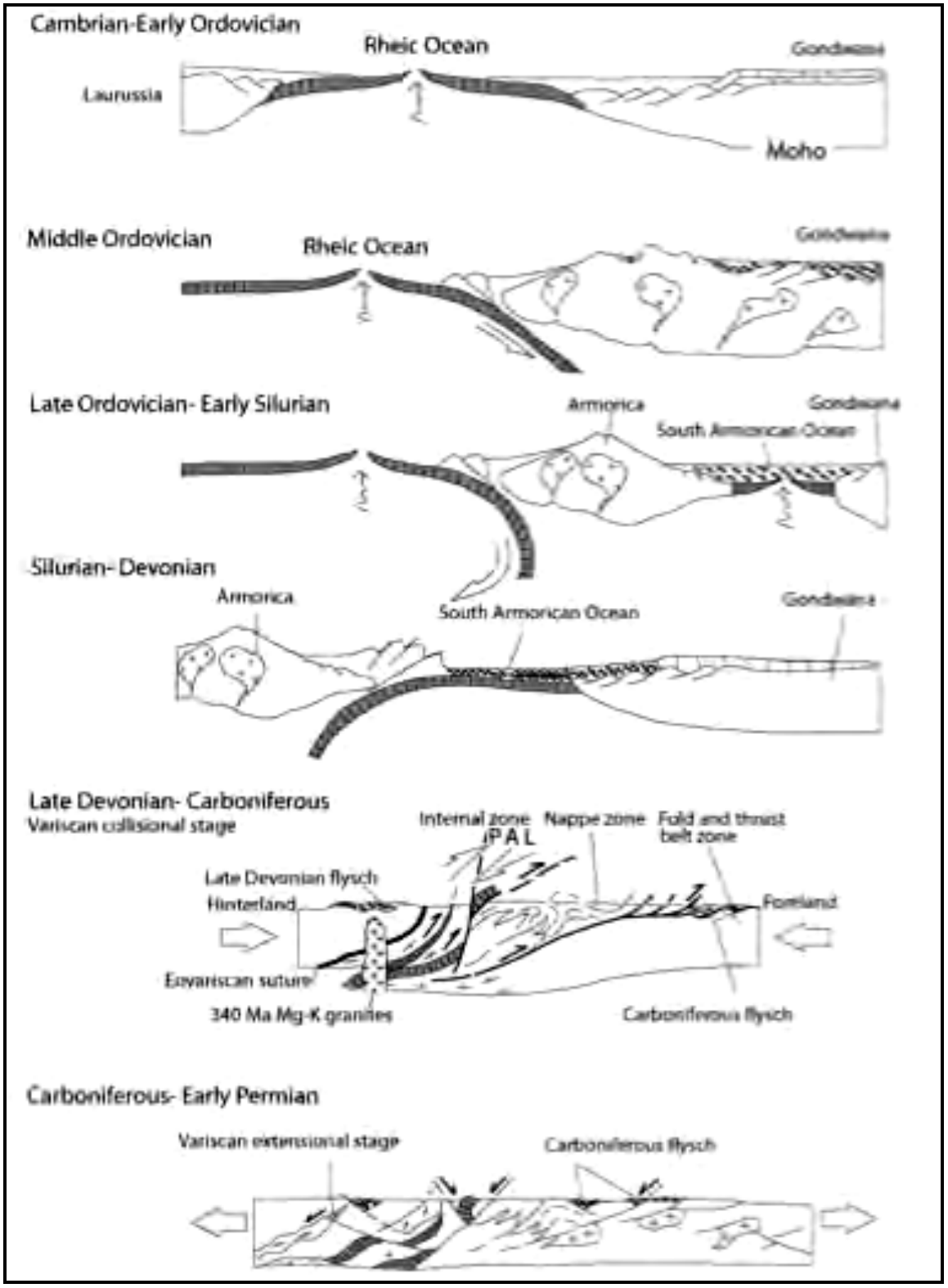

Fig. 1-8. Geodynamic evolution of Sardinian-Corse block; after Rossi et al., 2009

1.3 EVOLUTION OF THE TYRRHENIAN BASIN AND PRESENT-DAY CONFIGURATION

The formation of the Tyrrhenian basin, situated along the suture between Africa and Europe, and also the controversy of the bordering areas geology (Apennines, Calabria, Sicily, Sardinia, Corsica; Fig. 1-9) have long captivated the geologists. Only with the agreement of the plate tectonics paradigm (around 1970), restoring the Tyrrhenian Sea to a pre-drift configuration, the Alpine Corsica was a continuous block directly into the Alpine part of Calabria (Haccard et al., 1972; Alvarez et al., 1974; Alvarez, 1976). The progressive opening of Tyrrhenian Sea, starting in the Miocene (Alvarez et al., 1974; Chiarabba et al., 2008), was due to the slab roll-back which rifting southeastward the Calabria from Sardinia.

It is commonly accepted that before the opening of the Tyrrhenian Sea, Calabria and Sardinia were very close together and probably formed a single continuous continental mass. Indeed, with before the counter-clockwise rotation of Corse-Sardinia away from France (Nairn & Westphal, 1968; De Jong et al., 1969; Zidjderveld et al., 1970, Alvarez 1971; Gattaceca et al., 2004), the whole Corse-Sardinia-Calabria continental crust would have been part of Europe, probably until the Oligocene (Cherchi and Montadert., 1982) or the Lower Miocene (Carmignani et al., 1995; Oggiano et al., 2009).

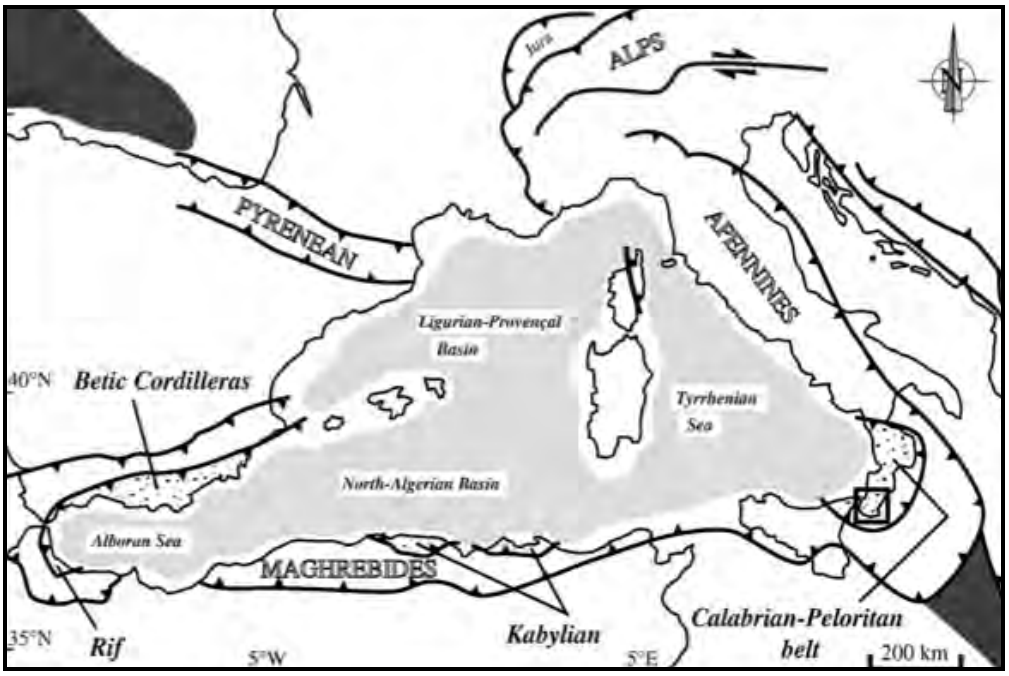

Fig. 1-9. Simplified sketch map of Central Western Mediterranean region, after Heymes et al., 2010

However, in which way the Sardinia and Calabria blocks were linked before the opening of the South Tyrrhenian basin is still matter of discussion. In the follow we report, modified, the very effective synthesis of different models and interpretations proposed by Alvarez and Shimabukuro (2009).

1.3.1 ONE OCEAN MODEL (CALABRIA AND SARDINIA SHARED THE SAME POSITION FROM VARISCAN TIME)

The earliest reconstructions placed the Calabria-Peloritani Arc at east of Sardinia, each having roughly their present configuration (Boccaletti and Guazzone, 1974; Alvarez, 1976).

Different but ambiguous reconstructions have tent to explain how the Calabria and Sardinia have been attached.

In the main reconstructions, the Calabria was considered a unique terrane during the middle and late Tertiary, although affected by Africa-vergent thrusts recognized in the northeastern Sila and Peloritani mountains.

In the **one-ocean model the** Calabrian continental crust is considered a single block with Sardinia since Vriscan times up to Tertiary times. In this scenario is considered an ocean only on the East. This consideration implies that is present an important discontinuity between the HP/LT rocks of the Alps and those of Calabria, which likely were producted in different subduction zones with opposite polarity.

Also has been accepted in this model that the Calabria derived by an amalgamation of two continental terranes that collided in the Tertiary (Bonardi et al., 1980, 1982; Scandone, 1982). This hypothesis is based on geological differences between the Northern Calabria-Peloritani subterrane and Southern Calabria-Peloritani subterrane. The Northern Calabria-Peloritani subterrane (labeled Sila) shared the evolution with Sardinia from the end of the Variscan until the mid-Tertiary. The Southern Calabria-Peloritani subterrane (Serre, Aspromonte, Peloritani) was a microcontinent that did not collide with Sardinia and the northern subterrane until before the opening of the Tyrrhenian Sea.

The mechanism by which the Calabria-Sardinia breakup took place is also still debated and three main models have been proposed: (1) symmetrical rifting (Fig. 1-10a) where both the Sardinian and Calabrian were characterized by thinned lower and upper continental crust (Finetti, 2005), (2) asymmetrical rifting (Fig. 1-10b) with the master fault dipping southeast, admitting exhumation of lower continental crust on the Sardinian margin, and outcrops of upper continental crust on the Calabrian margin (Wang et al., 1989) or (3) asymmetrical rifting with the master fault dipping

north-west (Fig. 1-10c) with exhumation of lower continental crust on the Calabrian margin, and outcrop of upper continental crust on the Sardinian margin. This final model large correspond at the field scenario occurring in Calabria but no evidence have been found also for the Sardinia.

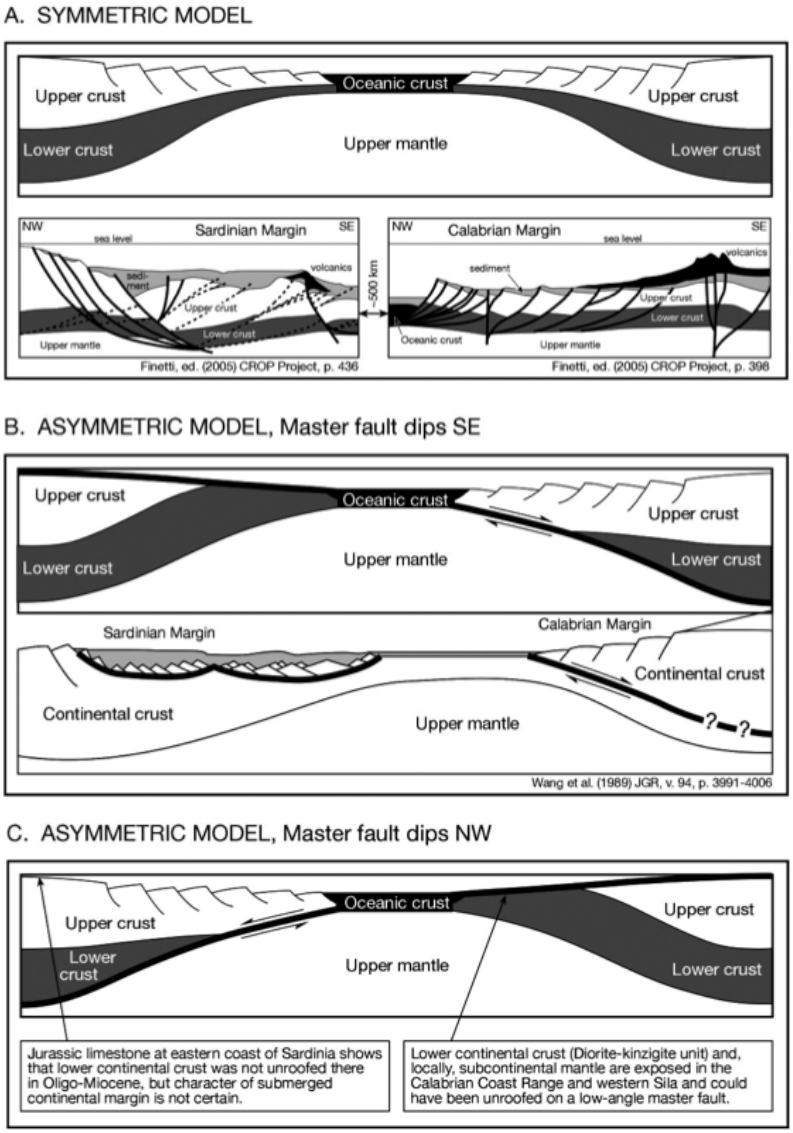

Fig. 1-10. Different models of the opening of the Tyrrhenian basin, after Finetti et al. (2005).

1.3.2 TWO-OCEANS MODEL (CALABRIA AND SARDINIA SEPARATED UNTIL EARLY CENOZOIC)

A more complicated scenarios could be presented if the Calabria and Sardinia were separated until the early Cenozoic. Thus is possible to consider the Calabria belonging to one- or two-terrane model (Vai, 1992, 2001) and the occurrence of two oceans (*Fig. 1-12a*). When and how long the two calabrian blocks were an unique terrane is still confused. Anyway, in this case a single block of

continental crust corresponding to Sardinia and Calabria can not existed, before the Cretaceous or the Jurassic. The suture between Calabria and Sardinia could be taken place in the early Tertiary. Thus a more complex setting must be draft, considering changing plate boundaries and microcontinents (Vai 1992, 2001), if the Sardinia-Calabria massif were accreted before the opening of the Tyrrhenian Sea beginning in the Miocene.

In the one-terrane model (Fig. 1-11, a-b), Calabria was represented like single block since the Variscan (Schenk & Schreyer, 1978; Grassner & Schenk, 2001) from the northernmost Serre to the northwestern Sila and the northern Catena Costiera (Piluso and Morten, 2004). The pattern of this suture would be more easier, delineated by the Calabrian HP/LT belt in continuity with the HP/LT rocks of Alpine Corsica and the Alps, before to the opening of the Tyrrhenian basin.

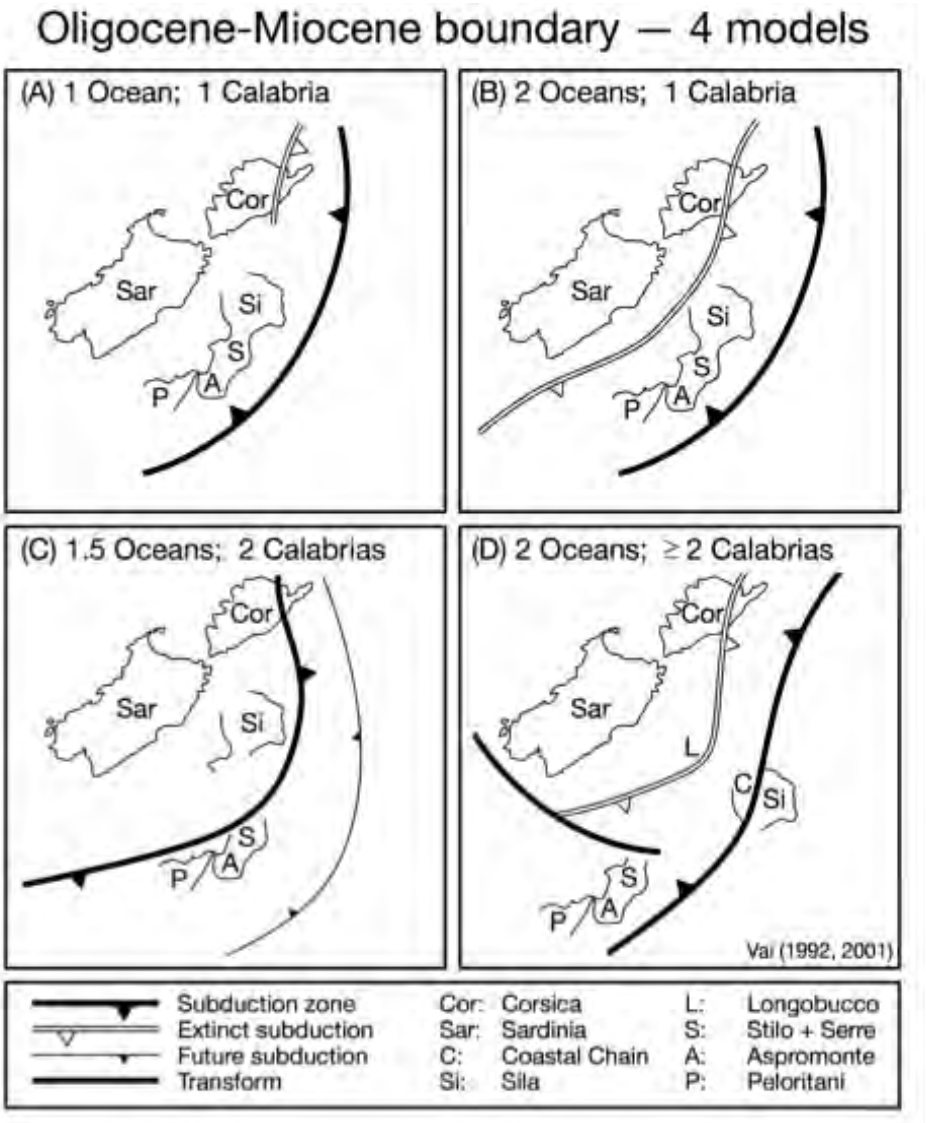

Fig. 1-11. Cartoon of the possible plate-boundary configurations between Corse-Sardinia block and Calaria-Peloritani Arc during Tertiary. After Alvarez & Shimabukuro, 2009 and Vai 1992, 2001

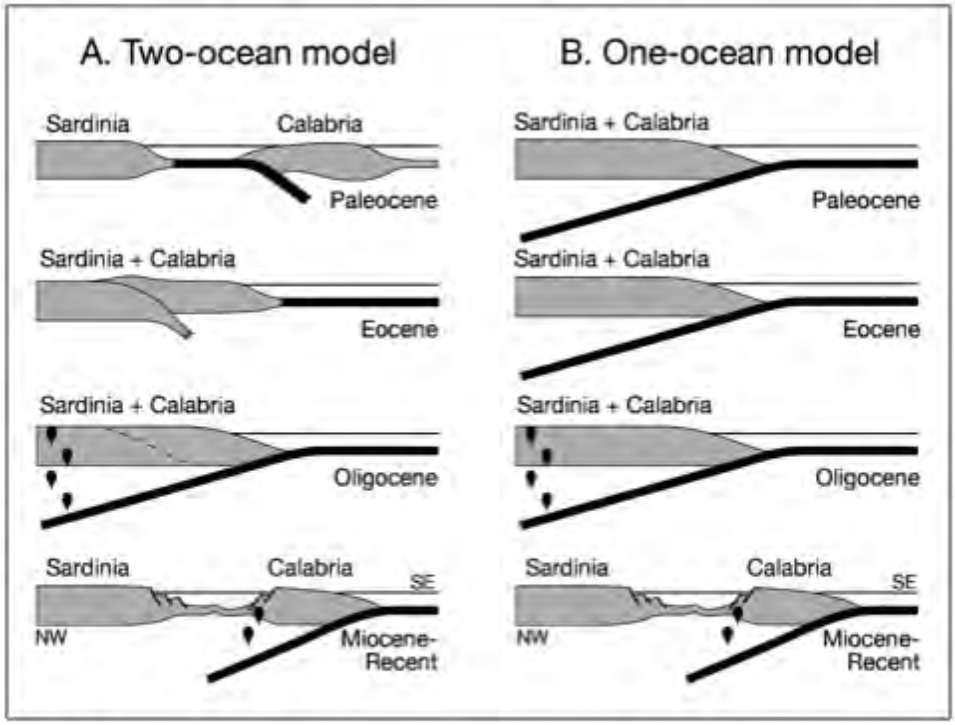

Fig. 1-12. In the two-ocean model (A), Calabria was a microcontinent (or two separate ones, if the two-terrane model is correct) with oceans on either side, subducted by two, oppositely-dipping subduc- tion zones. In the one-ocean model (B), Calabria was part of Sardinia (and of Europe) until microplate motions related to a single direction of subduction.

Indeed if is accepted that the Calabria was formed by two (or more) blocks (Fig. 1-11, c-d), all separated by Sardinia, a more complicate geodynamic scenario must be draft: an east-dipping subduction (linked to early Alpine movements), then a later Apennine west-dipping subduction between Coastal Chain and Sila, marked by the Calabrian HP/LT (Vai, 2001) and finally a transform fault that bounded to the south the earlier subduction zone.

Despite this fairly unambiguous history of microcontinent motions since the Miocene, the **earlier history** of the circum-Tyrrhenian region remains very obscure.

1.4 GEOLOGIC FEATURES OF THE SARDINIA-CORSICA BLOCK

In this part of chapter will be done a simplified framework of the geology of the Sardinia and Corsica basement and of the Tertiary covers linked to the opening of the Tyrrhenian basin and now cropping in the Est Sardinia and in central Corsica.

Because of the Palaeozoic samples have been collected from the Sardinia basement, here this complex will be better described than the Corsica basement whose has been done a simplified description mainly in comparison to the Sardinian structures.

1.4.1 PALAEOZOIC BASEMENT

One of the most complete exposure of southern branch of the Variscan system (Southern European Variscides) is located throughout the Corsica-Sardinia continental block (Fig. 1-13).

A North–South section of the Sardinia-Corsica block (Fig. 1-13) well shows the architecture of this part of the chain with well expressed the geometry, structural and lithological framework of the tectono-metamorphic zones (Internal, Nappe and Foreland zones) mainly formed during Variscan convergence and collision. (Carmignani et al., 2001). In Sardinia, in particular, is well preserved a complete tectono-stratigraphic sequence ranging from allocthonous high grade amphibolites in the North (Inner zone) to autochthonous low grade metamorphic rocks in the South (Foreland). Three main tectono-metamorphic zones are from far recognized (Carmignani et al., 1994c) and generally accepted from all the authors: 1) an Inner (or internal according the different authors) zone or "Axial zone", with medium- to high-grade metamorphic rocks and migmatites (northern Sardinia) of Precambrian (?) to lower Paleozoic age; 2) a Nappe zone characterized by several tectonic units all (Fig. 1-14) subdivided in: internal nappe (central-northern Sardinia), with crystalline units consisting of low- to medium-grade metamorphic rocks, and external nappe zone (central- southern Sardinia), with low-grade metamorphic rocks; 3) an External zone (southern Sardinia, Iglesiente-Sulcis), considered the Variscan foreland in this segment of the chain with no-or very low-metamorphism.

The structural frame of the Corsica-Sardinia Variscides transect is best exposed in Sardinia where a nappe stack were built in the course of a complex polyphase deformation (Carmignani et al., 1994c) followed by a post-collison extension (Conti et al., 2001) (Fig. 1-15).

The shortening event (D1) can be divided into three main synmetamorphic deformation phases: firstly south-verging overturned folds and top-to-south thrusts with the emplacement of several tectonic units one over each others; afterward a late nappe emplacement occured with a top-to-the-west tectonic transport that generated the stronger deformation in the External zone (Conti et al., 2001); a third phases occurred with another change of the shortening direction, north-south again, that folded all the nappe pile, resulting in large upright antiforms and synforms with an axial extension up to 50km and that are one of the more evident regional structural in the Sardinian basement. The extensional event (D2) is characterized by recumbent folds that deformed the nappe pile, and by low-angle normal faultsthat re acivated older thrust in a brittle-ductile environment; the extension probably started when the tangential shortening ceased and the whole nappe pile suffered an isostatic balancig.. The D2 phase ended with the emplacement of late-orogenic granitoids and the development of Late Carboniferous Lower Permian basins that are common features in the South European Variscides related generally to an intraplate strike slip tectonics (Pittau et al.,

2008).

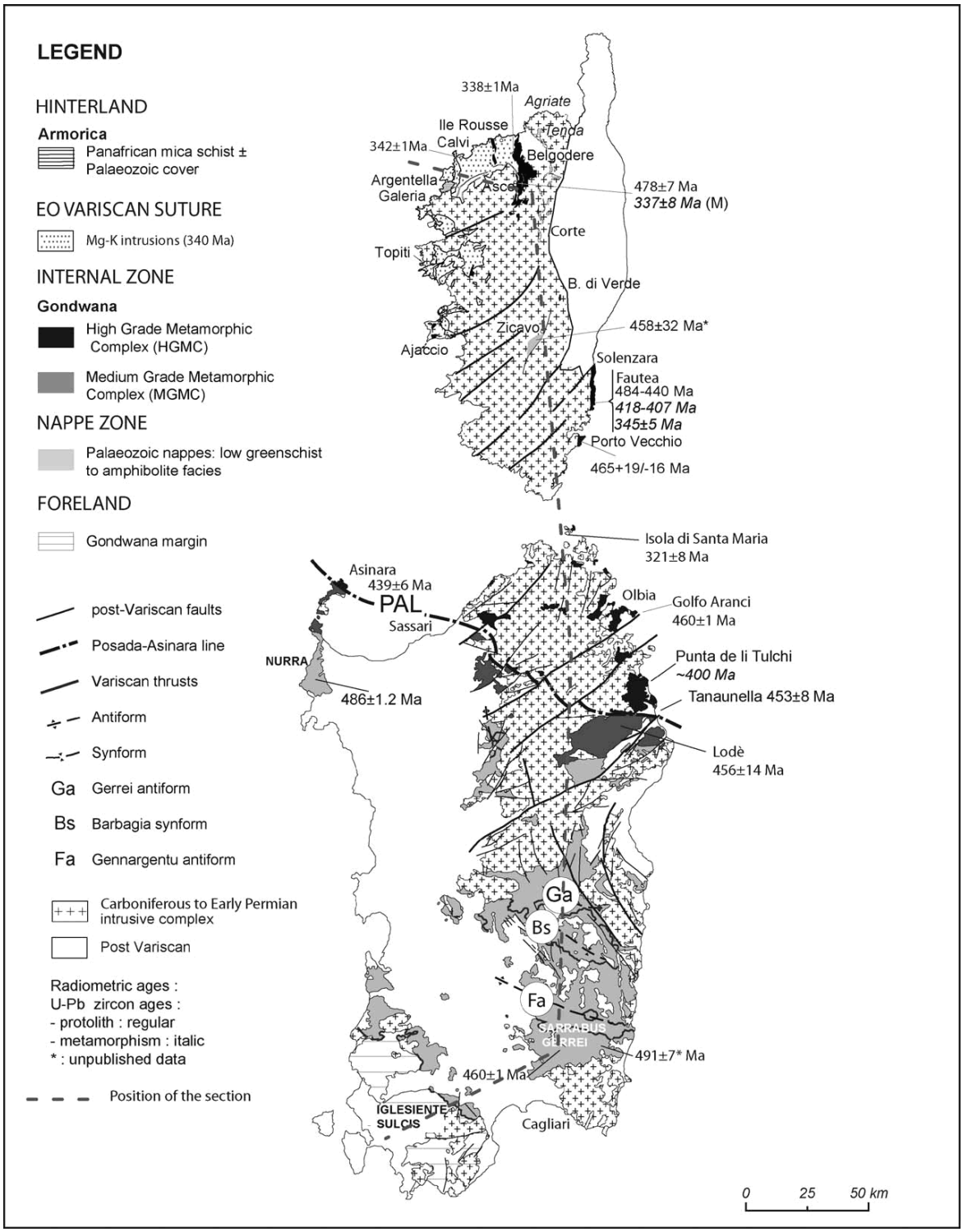

Fig.1-13 The main Variscan zones in Sardinia and Corsica (after Carmignani et al. 2004; Rossi et al., 2009)

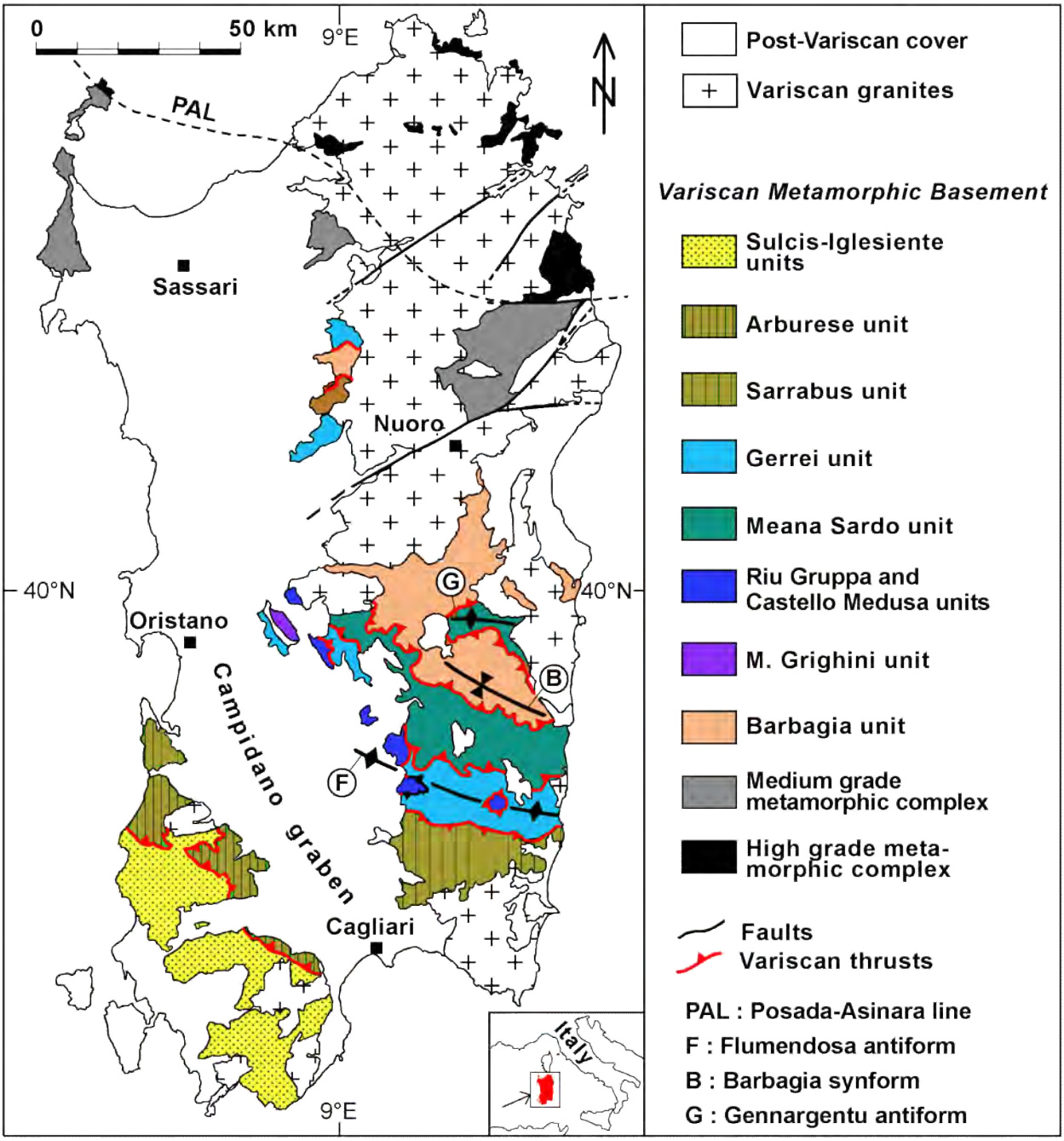

Fig. 1-14 Sketch map of the Sardinian Variscides with detailed the several tectonic units.

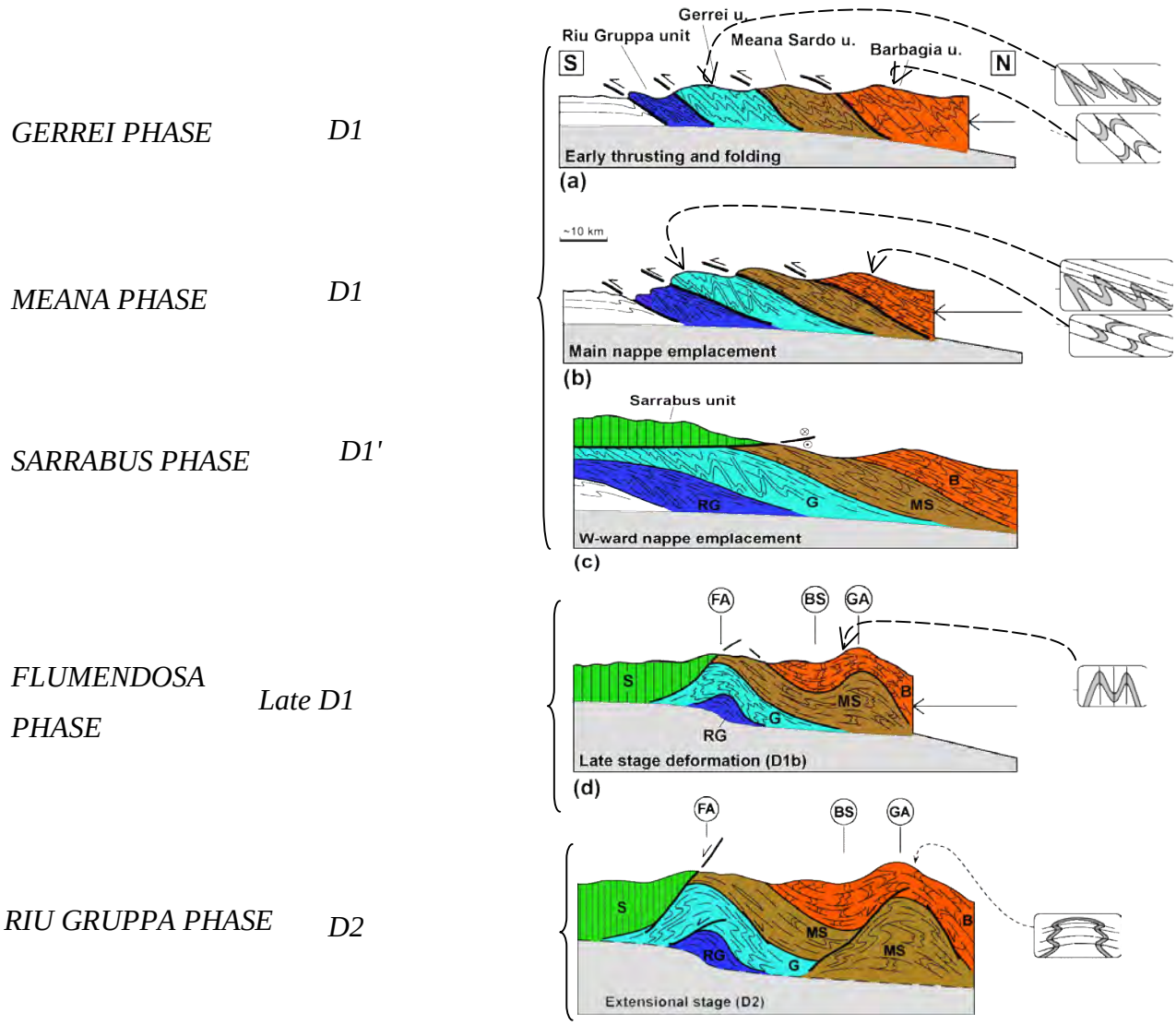

Fig. 1-15 Reconstruction of the tectonic evolution of the External nappe in Sardinia (after Conti et al., 2001 modified)

1.4.1.1 INTERNAL ZONE

In Corsica, the high-grade metamorphic complex (HGMC) comprises leptynite–amphibolite complexes with eclogite boudins, orthogneiss and metasediments derived from an Early Palaeozoic protolith that includes gneiss (amphibolite with granulite) which is commonly anatectic (Palagi et al., 1985) and locally contains eclogite boudins (Libourel et al., 1985). The protolith of metamorphic rocks, affected by HP/HT metamorphism (Libourel, et al., 1988) has been estimated in between 484± 7 and 440 ± 6 Ma; the peak metamorphism ranging between 418 ± 6 and 407 ± 6 Ma.

The Internal Zone of Sardinia has been further subdivided into two metamorphic complexes: the High Grade Metamorphic Complex (HGMC) and the Low-Medium Grade Metamorphic Complex

(LMGMC) (Carmignani, 2001; Franceschelli et al., 2005). The High Grade Metamorphic Complex is made up of migmatites and gneisses, characterized by amphibolite metamorphic grade, reaching the sillimanite + K-feldspar zone (Franceschelli et al., 2005). Rarely embedded within the HGMC are isolated bodies of mafic and ultramafic metamorphic rock, whose protoliths are probably of Precambrian age, and which are intruded by Ordovician orthogneisses (Carmignani et al., 1994c). Some of these utramafic bodies contain relic granulites that are interpreted to be portions of layered basic bodies that intruded in the lower crust (Carmignani et al., 1994a). L-MGMC occupies the area closest to the Posada Asinara Line (PAL), cropping out on the southern portion of the island of Asinara, northern Nurra, Anglona, and the northern Baronie regions, and is structurally juxtaposed over the Nappe Zone (Carosi et al., 200?). The most recent published papers concerning the Variscan system and the role of Sardinia show no general consensus on the origin of the PAL and its relationship to the Hun superterrain (Franke et al., 2000; Matte, 2001; Stampfli et al., 2002; von Raumer et al., 2003).

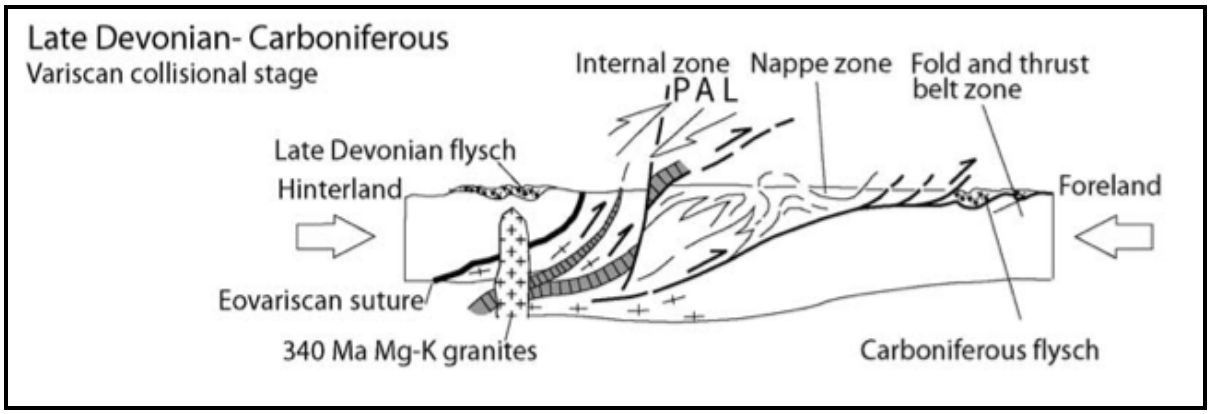

Fig. 1-16. Late Devonian–Carboniferous: collision between Armorica and Gondwana sutured in the PAL, occurring between the deposition of Early Tournaisian formations (about 360 Ma) and the emplacement of Mg–K plutonic rocks at c.a. 340 Ma. (After Matte et al., 1986; Carmignani et al., 2004; Rossi et al., 2009)

The Posada Asinara Line (PAL) is an important tectonic lineament, whose interpretation is still matter of debate bertween the authors that in turn attributed it to:

a suture between the Armorica (HGMC) and Gondwana (southern terranes beyond the PAL; Fig 1-16; Vai et al., 1992; Carmignani et al., 1994c; Matte, 2001; Fig. 1-17). In this model, the occurrence of relic eclogites and highly deformed metabasites within the PAL are interpreted as tectonically dismembered high-grade metamorphic pieces of oceanic crust overriding the nappes (Fig 1-16);

a suture between small Gondwanan provenance terrains (Hun-terrains) and Gondwanan margin (Stampfly et al. , 2002; von Raumer et al. ; 2003) propose that the PAL was part of a complex

system of structurally bounded small terrains (Gondwanan provenance);

an important shear zone to related to a plate-boundary (Stephanian Dextral shear zone, Fig.1-18; Rossi et al., 2009) testimonied by similarities in the rocks both at North and South of the PAL (e.g., Helbing & Tiepolo, 2005; Franceschelli et al., 2005; Giacomini et al., 2006).

In Corsica, the collage between the Galeria External and Internal zones (Armorica–Gondwana collision) can be dated to occur between the deposition of the Early Tournaisian formations (about 360 Ma) and the emplacement of the Mg–K intrusions, i.e. between 345 and 335 Ma.

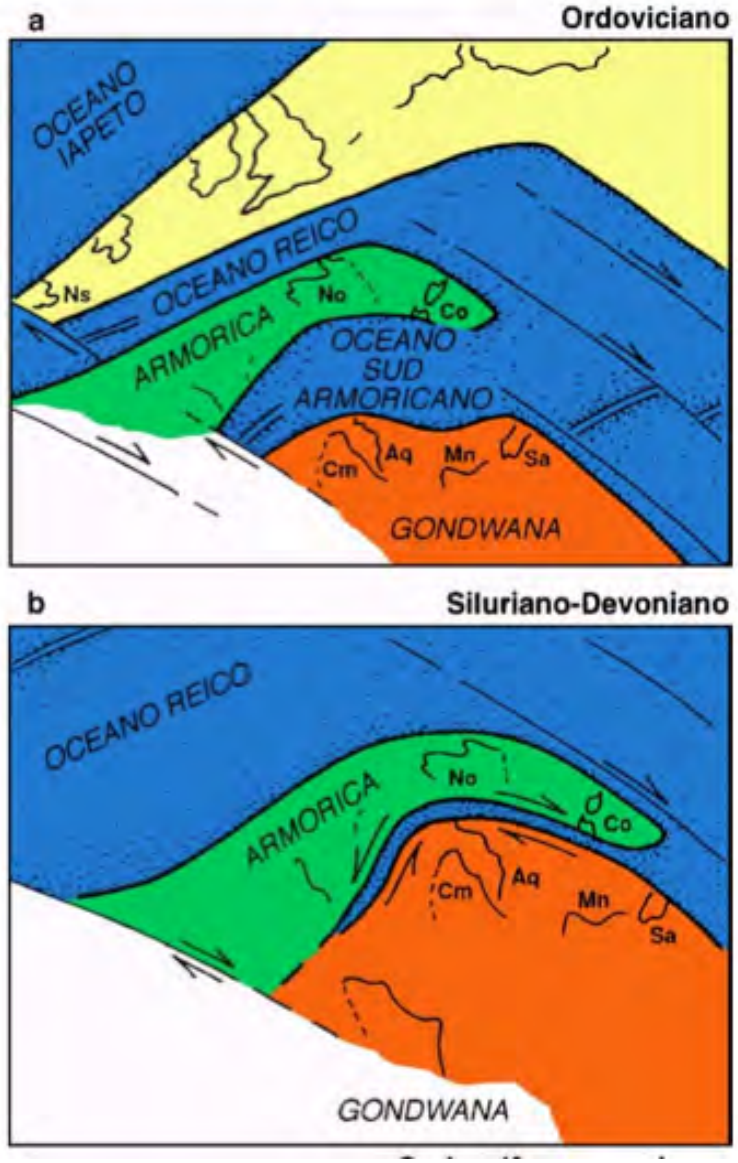

Fig. 1-17. Paleogeographic reconstruction of the Hercynian chain of south Europe: Ordovician paleogeography (after Vai & Cocuzza, 1986; Paris & Robardet 1990; Carmignani et al., 2004); Sa: Sardinia: central and southern Sardinia; CO: Corsica and northern Sardinia; No: Normandie; Cm: Cantabrian chain; Aq: Aquitaine; Mn: Montagne Noire; Ns: Nova Scotia.

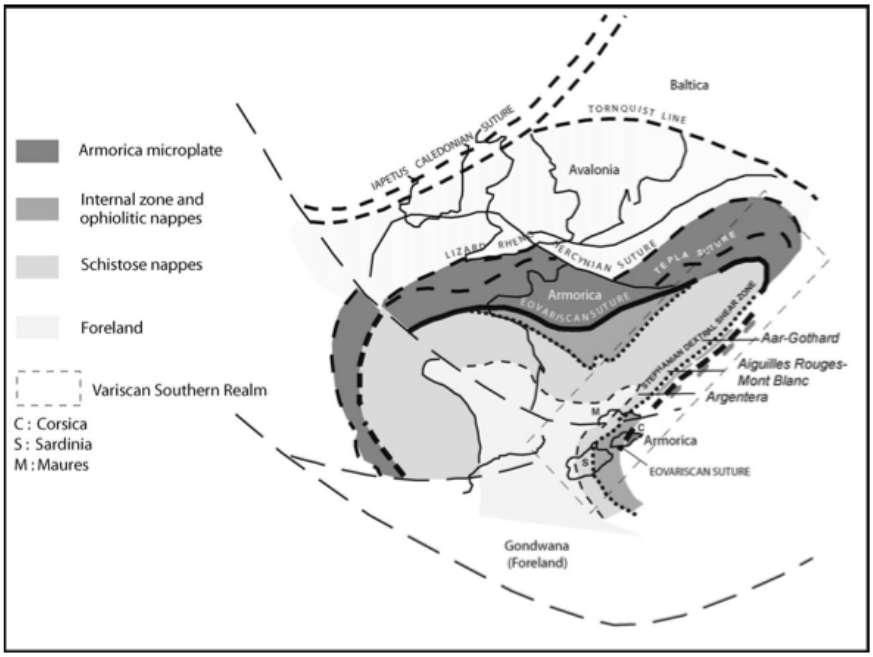

Fig. 1-18 The southern Variscan realm in western Europe. Permian Variscan zonation after Matte 2001

1.4.1.2 NAPPE ZONE

In Corsica, several remnants of the pre-granite intrusion host rocks are scattered as roof pendants and in Zicavo and Topiti could be linked to the Nappe Zone. These rocks display a greenschist to amphibolite facies metamorphism. Three tectonic zone (or fault-separated compart as called by Rossi et al., 2009) compartments are identified close Zicavo: orthogneiss derived from a peraluminous metagranite U–Pb dated at 458 ±32 Ma (Rossi et al., 2009), a metaharzburgite-bearing amphibolitic complex, and metamorphosed black shale. The outcrop near Topiti consists of serpentinite with the original composition of dunite, orthopyroxenite, harzburgite and Cambrian–Ordovician metabasalt (E-MORB).

In Sardinia, the a Cambran to Early Carboniferous succession is involved in the Nappe Zone that extend from Sarrabus in the southeast (External nappes) to Nurra in the northwest (Internal nappes) with deformation and metamorphic grade increasing northward from lower greenschist to amphibolite facies.

The Sardinian Nappe zone consists of several tectonic units (

Fig. *1-14*), characterised by slightly different litshostratigraphic successions,mainly in the ordovician volcanic successions, equilibrated under greenschist facies, embricated and emplaced with a general top to south-west transport.

The External nappe are characterized by a well recognizable and datable lithostratigrtaphic succession, whereas in the Internal nappe the recognizion of a detailed lithostratigraphic succession

is prevented by the lacking of bio-strtatigraphic marker and by a more penterative, polyphasic deformation (Carmignani et al., 1994c; Fig. 1-15).

1.4.1.2.1 Internal Nappe zone

This zone comprises low to medium-grade sequences of metasandstones, quartzites, phyllites, marbles, and a limited amount of metavolcanic rocks (Franceschelli et al., 2005; Carmignani et al., 1995). One of the main different respects to the succession of the Internal Nappe Zone is the low abundance of Ordovician metavolcanic rocks and Devonian age marbles. A Barrovian metamorphic facies is pervasive in the Internal Nappe Zone, ranging from greenschist facies in the Barbagia, Goceano, and southern Nurra regions to intermediate P amphibolite facies proximal to the PAL (Carmignani et al., 1994b).

The structural evolution of the Internal nappe is characterized by the occurrence of at least two penetrative widespread folding events, with syn-metamorphic foliations developed under upper-greenschist facies mertamorphism.

1.4.1.2.2 External Nappe Zone

The tectonic units involved in the External nappe pile crop out from South Anglona in the north to the SW in Sulcis Iglesiente region. But the best exposed, and studied, section crops out along the Flumendosa Valley, at the core of the homonym Antyform with the same name. From the bottom the main tectonic units recognized are (Fig. 1-14 and Fig. 1-19): a) M. Grighini U.; b) Riu Gruppa U.; c) Gerrei U.; d) Meana Sardo U.; e) Sarrabus and dell'Arburese U. Here will be considered like a part of the Nappe zone a small area of Spartivento previously considered as Precambrian (Rasetti, 1972; Cocozza, 1979; Minzoni, 1981; Pillola and Gross, 1982; Junker and Schneider, 1983; Carannante et al., 1984; Gandin and Debrenne, 1984), that in the meanwhile of this study we have defined as Bithia Tectonic U. (Pavanetto et al., 2012).

In The Iglesiente and Arburese areas the nappefront overrides a foreland severely deformed but unmetamorphosed or weakly affected by metamorphic recrystallization.

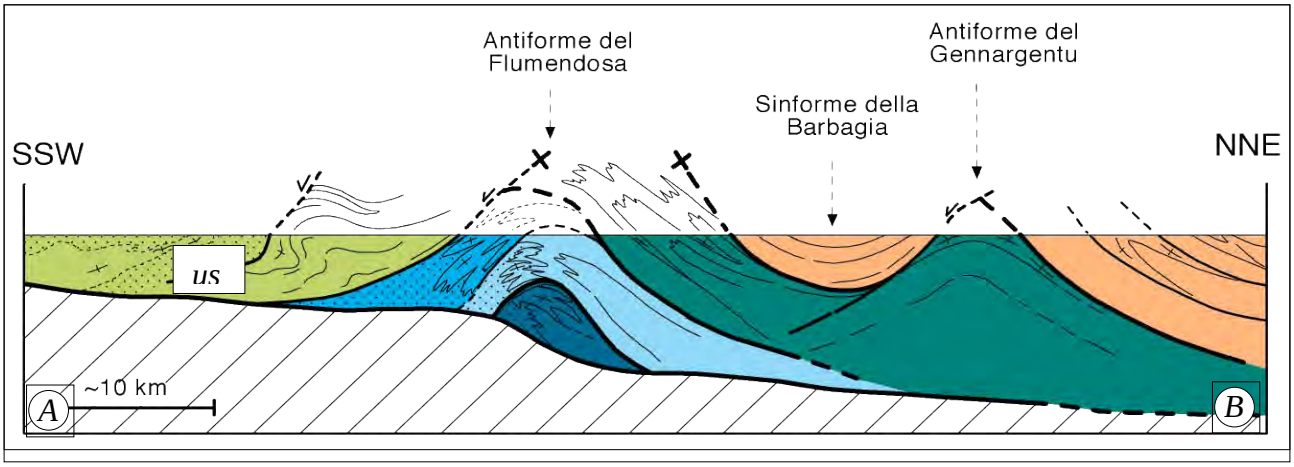

Fig. 1-19. Schematic geological section of the Nappe zone in the Central-southeastern basement of Sardinia

Four synthems can be distinguished:

a) A Middle-Cambrian- Lower Ordovician (Naud and Pittau Demelia, 1987) lithostratigraphic succession that mainlyconsists of metasandstones, phyllites and quartzites (Arenarie di San Vito fm., Calvino 1961) affected by Variscan lower-greenschist facies metamorphism. Interbedded in the uppermost part of the succession has been recently detected a volcanic suite that pre-dates the Sardic Unconformity (Oggiano et al., 2010): it consists of welded rhyolitic ignimbrites (491 ± 3.5 Ma, U–Pb zircon age), trachy-andesitic pyroclastic fall deposits and dacite to trachyte lava flows. In the Meana Sardo tectonic unit, the volcanic rocks within the pre-Sardic sequence occur as dykes and epiclastic crystal-rich tuffites. This succession is sealed by a Middle Ordovician angular unconformity (Sardic Unconformity: Carmignani et al., 2001), which is also recognized in the Eastern Iberian Plate (Casas et al., 2010; Navidad et al., 2010)

b) a Middle Upper Ordovician succession where andesites prevail, that overlies the Sardic Unconformity and is associated with subordinate felsic meta-volcanics, interlayered coarse meta-epiclastic rocks and volcanoclastics. The end of this volcanic activity is marked by rhyolite–rhyodacite lavas, ignimbrites and tuffs, with a combined thickness of less than 100 m (Porfidi grigi del Sarrabus and Porphyroids; Calvino, 1972). In the outermost Nappe Zone (i.e. Sarrabus), meta-dacite occurs as sparse dykes and sills (465.4 ± 1.4 Ma, U–Pb zircon age; Oggiano et al., 2010) within the pre-Sardic sequences, and they are inferred to be the feeder dykes of the Porfidi grigi del Sarrabus. The Middle Ordovician sub-alkalic volcanic suite has reliable stratigraphic and palaeontological constraints. In fact this continental clastic and volcanic sequence unconformably (Sardic Unconformity) lies on metasandstones, which, based on acritarchs assemblages, ranges from middle Cambrian to early (Arenig) Ordovician (Naud and Pittau Demelia, 1987). The transgressive sedimentary covers of the volcanic suite have been attributed to the Upper Ordovician (Katian-Hirnantian age), on the basis of fossil content (Loi et al., 1992; Naud, 1979; Barca and Di

Gregorio, 1979). Also the U-Pb age of 460 ± 1 Ma on a metarhyolite in the external nappes (Giacomini et al., 2006) is consistent with this time span.

c) In trasgression of the volcanic edifice a decametre-thick alluvial deposits of the Gerrei Unit, micaceous metasandstones and mature quartz-arenites cap the volcano-sedimentary succession, indicating high erosion rates after the Middle Ordovician emersion of this sector of the North Gondwana margin. On its fossili content this sedimentary succession is attribuited to the Upper Ordovician (Katian–Hirnantian), which then continued through the Silurian (Black shales and metalimestones) and Devonian into the Early Carboniferous (marble and metalimestones). Three main types of volcanic rock are distinguished within the Upper Ordovician terrigenous succession: 1) effusive products (pillow lavas and hyaloclastics), concordant with the host sediments; 2) sills and larger intrusions; and 3) dykes that cut the entire Lower and Middle Ordovician successions.

d) On the top of the Early Carboniferous metalimestones unconformable rests a thick (up to 100 m at least) terrigenous succession, meta conglomerates and metasandstones, that clearly reworked the older formations, and that is interpreted as a Culm-like deposits (Barca et al., 1992).

The well-exposed products of the Ordovician volcanism in the Nappe Zone (fully described in Result chapter) provide evidence that this collisional structure resulted from an earlier subduction of Rheic oceanic crust beneath the North- Gondwana continental margin. Beginning in the Late Ordovician, back-arc spreading led to rifting on the North-Gondwana margin, which was followed by subduction beneath the Armorica Terrane Assemblage during the Silurian–Devonian. The collision generated a Gondwana-verging orogenic wedge, as testified by both the structural and metamorphic zoning across the Corsica–Sardinia Variscan transect (Rossi et al., 2009).

Here will be take in account three units: the Sarrabus U., the Arburese U. and the Bithia U. and described in the Results chapter (Chapter 3).

1.4.1.2.3 Foreland

The Foreland in Sardinia is represented by the Iglesiente-Sulcis zone

Fig. *1-14*), characterized by the lacking of Ordovician volcanites like the Internal zone. This zone has been interested by a deformative phase, called Sardic phase, coeval with the middle Ordovician convergence phase.

The Sardinian Variscan foreland is mainly terrigenous successions dated from Cambrian to Carboniferous. Classically the Bithia Fm., was also attributed at Foreland zone because of its succession was believed pre-Cambrian (?), but here, considering the recently data about the volcanic rocks inside the Bithia Fm. (dated Ordovician), will be considered like part of Nappe Zone.

The oldest unambigous Fm., the Nebida Fm. (Middle Cambrian) is overlain by a carbonate platform (Gonnessa Formation) capped by Early Ordovician shale (Cabitza Formation, Carmignani 2001). This succession encompasses the entire Cambrian system and the base of the Ordovician, and is unconformably overlain (Sardic unconformity) by Late Ordovician continental conglomerate of the Puddinga Formation. The Caradocian–Ashgillian transgression was followed by a new depositional sequence characterized by Uppermost Ordovician glaciomarine deposits with interbedded basic alkaline rocks (Beccaluva et al., 1981; Leone et al., 1991). The succession ends with Silurian–Devonian black shale (Fluminimaggiore Formation) and limestone capped by culm-like deposits (Pala Manna Formation).

The Palaeozoic succession of the External Zone of southwestern Sardinia recorded no significant metamorphic imprint after the Variscan orogenic events: both the pre-Sardic and post-Sardic sequences at Iglesiente are non metamorphic or anchimetamorphic.

It is likely that these formations belong to the Gondwana margin based on the similarity between the External Zone Palaeozoic of Sardinia (Iglesiente) and the Montagne Noire (France) successions interpreted as Gondwana foreland. The successions of southern Sardinia (Carmiganni et al., 2001) can be compared with the Galeria succession of northern Corsica even if stratigraphic date indicate that the Palaeozoic of Galeria was not deposited in the same area as the Palaeozoic of southern Sardinia, the Maures Massif or Montagne Noire. It was probably part of a microcontinent that separated from Gondwana during the Ordovician, hereafter considered as Armorica (Matte, 2001), and keeping in mind that the latter represents a mosaic of microcontinents (Stampfli & Borel,, 2002).

1.4.2 TERTIARY COVERS

In Sardinia the post-Variscan covers in Sardinia are mainly made up by Mesozoic, lower Eocene and Miocene rocks. The older are genrally marine carbonates aged from middle Triassic to upper Cretaceous that crop out mainly in the NE sector (Nurra), and in the E and central sectors (Baronie Suparamonte, Ogliastra and Sarcidano). The lower Eocene formations overall crop out in the SW, with a mainly paralic succession, and in central-eastern are constituted by silici-clastic to littoral limestones rocks. On thhese directly lays a late Oligocene- Miocene succession, subdivided in three main tecto-sedimentary cycles (Oggiano et al., 2009; Carmignani et al., 2001, cum biblio) characterized by several clastic to carbonatic formations interlayered with huge volcanic products.

Up to seventies the researchers recognised that the only tectonic event that deeply involved the present day Sardinia was the Variscan orogeny, even if an extensional miocenic tectonics (linked

to the Sardinian rift) was recognised. Than, in the early eighties the importance of the extensional tectonics were underlined by several authors (Pecorini and Pomesano-Cherchi, 1969; Cherchi and Montadert, 1982, 1984), but no evidences were reported of shorthening structures during Tertiary. Just Chabrier (1067, 1969, 1970) recognised and described the occurrence of thrusting involving the basement in the Eastern Sardinia; excepted him, the main tectonics recognised by the authors was the occurrence of a late Tertiary strike-slip tectonics (Alvarez & Cocozza, 1974), and they interpreted the overlapping of palaeozoic metamorphites on Tertiary deposits as the consequence of Pleistocenic gravity landslides (Dieni & Massari, 1970, 1971, 1987, Alvarez & Cocozza, 1974).

In the nineties the study of tectonics involving the Mesozoic and Tertiary covers of Eastern Sardinia have been more focused and the occurrence of a pervasive strike-slip faults system were recognised and associated either to important transpressional structures (Carmignani et al., 1992; Carmignani et al., 1994b; Pasci, 1997) that thrust also Palaeozoic basement over the post-Variscan covers (Albo M., Tuttavista M., Supramonte), and to transtensive basins (Chilivani-Berchidda basin, Ottana basin (Oggiano et al., 1995). These authors related this tectonics.to the north-Apenninic belt and in minor part to the Pyrenaic evolution (Carmignani et al, 1992; Carmignani et al., 1994c; Carmignani et al., 1995; Carmignani et al., 2004; Oggiano et al., 2009). In this view, after the Variscan evolution the Sardinia, even if out of the Alpine continental collision zone, was in the between of two orogenic belts: the Pyrenees and the Apennines and recorded the deformation induced by both the events. After that, the island was delimitated by two rifting phases: a) the first one, westward gave rise to the the liguro-provencal basin opening in the Burdigalian; the second one gave rise eastward to the opening of the Southern-Tyrrhenian basin in the Late Miocene-Pliocene. The Oligo-Miocene succession is interlayered with volcanic calcalkaline products correlated to the Northern-apenninic subduction and to the following post-collisional distensive processes (Beccaluva et al., 1994; Carmignani et al., 1994; Carmignani et al., 2001; Lecca et al., 1997). The Late Miocene extension is marked by within-plate basalt flows.

One of more important sedimentary record of the shortening related to the convergence of Apulian Plate and the Southern European margin (Carmignani et al., 1992; Carmignani et al.,1994a; Pasci, 1997; Pasci et al.,1998) is the Cuccuru ‘e Flores conglomerates that will be illustrated in the Result chapter.

Indeed, many open questions remains about the age of the strike-slip tertiary tectonics, and, generally, there is not agreement on the model in which the Central-Western Mediterranean reached its present day configuration (see Oggiano et al., 2009 and Alvarez et al., 2005, where some of these model are reported).

1.5 GEOLOGIC FEATURES OF CALABRIA-PELORITAIN ARC

The Calabria–Peloritani Arc (CPA), forming connection between the Apenninic and Maghrebian Chains, is a composite terrane collided with the Apulia and Ragusa continental margins at its north and south extremities, respectively, and overriding to the East the subducted oceanic lithosphere of the Ionian abyssal plain (Fig. 1-20).

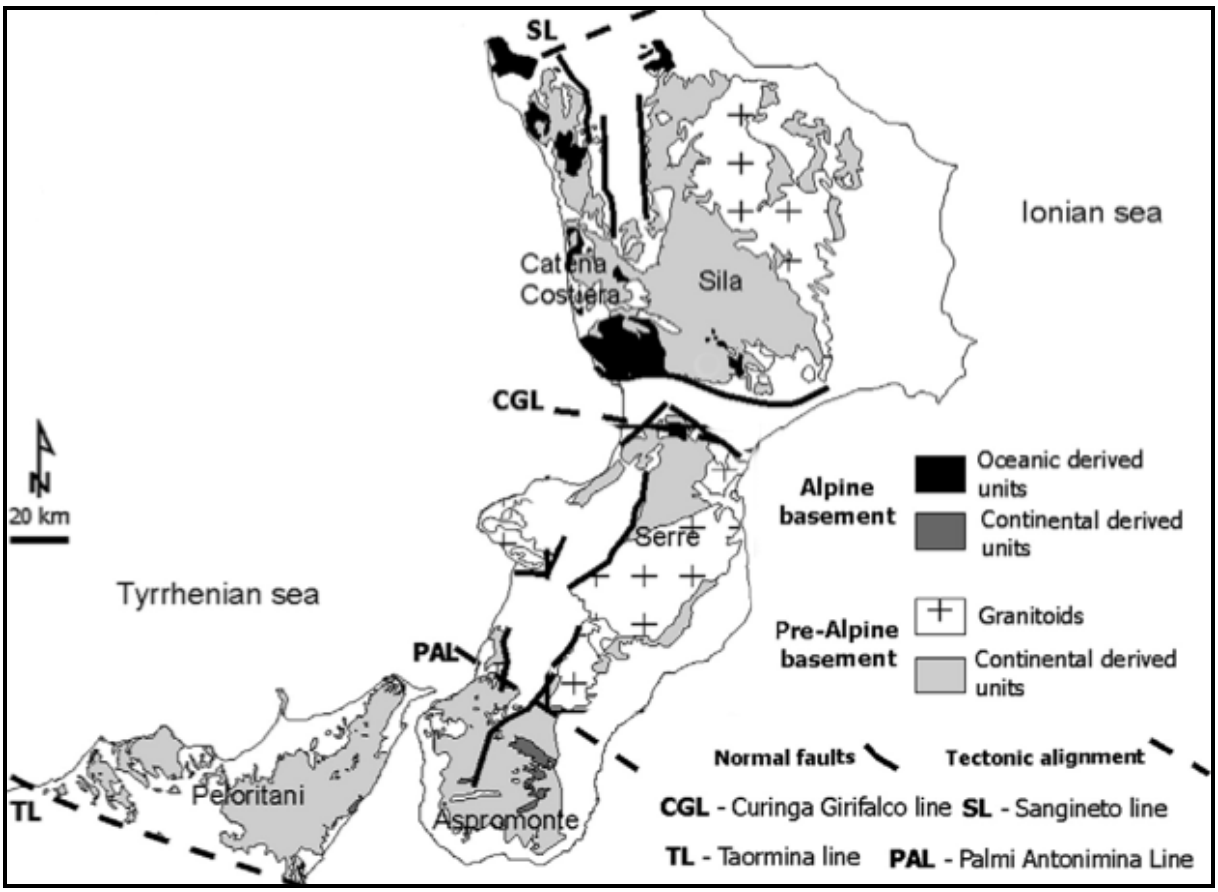

Fig. 1-20. Schematic geological map of the CPA and its main structures. After Angì et al., 2010.

The present tectonic setting of the Calabria–Peloritani segment is the result of pre-Variscan to Cenozoic events (Schenk 1990; Thomson 1994; Caggianelli et al. 2000; Del Moro et al. 2000; Festa et al. 2003). Two distinct models have been proposed for its tectonic evolution:

1. Building of a Cretaceous-Paleogene Europe-verging chain, which was thrust onto Africa-verging Apennine units during early Miocene (e.g. Amodio Morelliet al. 1976).

2. Stacking of European and Tethyan units, subsequently thrust onto the Africa continental margin

in the early Miocene (e.g. Boullin 1984).

The Calabria–Peloritani Arc is made up of a northern terrane which includes the Calabrian Coastal Chain, the Sila Massif and the northern slope of the Serre Massif and a southern terrane which includes the southern part of the Serre Massif, the Aspromonte Massif and the Peloritani Mountains.

The northern sector is constituited by three groups of nappes (Amodio Morell et al.,1976; Scandone, 1982; Bonardi et al., 2001, 2004; Alvarez & Shimabukuro, 2009, Patacca & Scandone, 2011). Moving upsection, they are represented by:

– Piedmont-type and Liguria-type ophiolite-bearing nappes, affected by Alpine metamorphism (Diamante-Terranova, Gimigliano p.p. and Malvito Units);

– Basement nappes with or without a post-Hercynian sedimentary cover, affected by Alpine metamorphism (Bagni Unit and Castagna Unit);

– Basement nappes with a post-Hercynian sedimentary cover not affected by Alpine metamorphism (Sila Unit sensu Messina et al.,1991 and Stilo Unit).

The ophiolite bearing nappes and the overlying Bagni and Castagna Units are supposed to represent the nucleus of a mountain chain built up in Cretaceous-Eocene times with European vergence (e.g. Amodio Morelli et al., 1976; Tortorici et al., 2009) or with African vergence (e.g. Boulin et al.,1986; Dietrich, 1988). These Units have been likely derived from the African continental margin (or from the Mesomediterranean Microplate) in the first case and from the European continental margin if they have an African vergence.

In the southern sector (Bonardi et al., 2001, 2004, 2008), no evidences of the Cretaceous-Eocene mountain chain have been found. The lowest units (Longi-Taormina Unit) crops out in the Peloritani Mountains is represented by a northward-dipping imbricate fan with southward vergence. Moving upsection, the following units or groups of units have been distinguished:

- Basement nappes with post-Variscan sedimentary covers not affected by Alpine metamorphism (Longi-Taormina, Fondachelli and Piraino Units) or affected by very low-grade Alpine metamorphism (Mandanici and Alì Units, sandwiched between the Fondachelli and Piraino Units). These units crop out only in the Peloritani Mountains;

– Basement nappes without Alpine sedimentary covers, not affected by Alpine metamorphism (Mela Unit in the Peloritani Mountains; Africo Unit in Southern Calabria) or affected by low-grade Alpine metamorphism (Cardeto Unit in Calabria);

– Pre-Variscan Aspromonte Unit, showing a low to medium-grade Alpine metamorphic overprint;

– Stilo Unit, composed of a Variscan basement and a post-Variscan sedimentary cover not affected

by Alpine metamorphism. The Stilo Unit is the highest nappe of the Calabrian Arc and crops out both in Southern Calabria and Northern Calabria.

The lowest element of the nappe pile (Longi-Taormina Unit) displays close similarities with the Sila Unit (cropping out in the northern part of Calabria) suggesting these units have derived from the same paleogeographic realm.

In the southern sector of the Calabrian Arc the Stilo-Capo d'Orlando Formation (Bonardi et al.,1980; Cavazza & De Celles, 1993; Cavazza et al.,1997) sealed the entire pile of nappes with its terrigenous deposits. The time in which nappe stacking took place is due by the age of the youngest deposits involved in the shortening and by the age of the oldest thrust-top deposits at the top of the tectonic edifice.

The age of the base of the Capo d'Orlando Formation and of the age of the youngest deposits of the Stilo, Longi-Taormina and Longobucco stratigraphic sequences, could furnish more constrains for a consistent palinspastic reconstructions (Patacca & Scandone, 2011).

About the age of these sequences, there is not a general consensus in the literature. About the top of the Longi-Taormina Unit (Frazzanò Formation) the age attributions span from the early Oligocene (e.g. Weltje, 1992; Lentini et al., 1995) to the Aquitanian (De Capoa et al.,1997).

The top of the Longobucco sequence are more difficult to define with certitude because of the scarcity of information avalaible. The designation of the Paludi Formation, is interpreted as a thrust-top deposit (Bonardi et al., 2005), or as a wildflysch comparable to the Frazzanò Formation.

Reservations exist also on the top of the Stilo stratigraphic sequence, represented by shallow-water limestones. The microfacies of these limestones, showing no trace of reworking, points to a late Rupelian-early Chattian age. However, the ages attributed to these deposits in the geological literature span from the Chattian (e.g. Patterson et al.,1995; Cavazza et al.,1997, 87Sr/86Sr isotope stratigraphy results) to the Aquitanian (Bonardi et al.,2002, 2003).

The age of the Stilo-Capo d'Orlando Formation, present consensus concerning the top of the formation (Burdigalian) but not about the base, which ranges from the Rupelian (e.g. Weltje, 1992) or the Chattian (e.g. Patterson et al., 1995; Catalano & Di Stefano, 1996) to the Burdigalian (Bonardi et al., 2002, 2003). Alsois lacking a reliable geological data to decide whether the lignite-bearing deposits of Agnana and Antonimina represent the lower portion of the Stilo-Capo d'Orlando Formation or belong to an older, pre- orogenic sedimentary cycle (Patacca & Scandone, 2011).

Some authors (e.g. Esu & Kozakis, 1983, Patacca & Scandone, 2011) considered that these deposits have yielded a form of Anthracotherium more primitive than A. magnum and attributed by these

authors to the latemost Suevian-earlymost Arvernian (roughly latemost Rupelian-earlymost Chattian).

The uncertainties on the ages of the above key-deposits have consequences on palinspastic restorations, as well as on the choice of the reference time for the initial fit (Patacca & Scandone, 2011). Following Patacca & Scandone (2011), there woud be two models to considered. If the base of the Stilo-Capo d'Orlando Formation had an Oligocene age, the nappe stacking would have been completed before 25 Ma and the tectonic units forming the Calabrian Arc, shortened and confined in the mountain belt, would occupy a narrow space. Consequently, the space between Europe and Africa established by the boundary condition, i.e. by the relative position of the two plates at that time, would be exclusively filled with the restored Apenninic-Maghrebian paleogeographic domains, apart from a relatively narrow belt occupied by the mountain chain.

In the second case, on the contrary, we should relocate in their original position all the Calabria-Peloritani nappes not yet interested by orogenic transport and consequently a significant portion of the available space would be occupied by these realms.

But considering that the ophiolite-bearing nappes and the Bagni plus Castagna Units were part of the mountain chain while all the other Calabria-Peloritani domains had not been reached by the compression front, the initial fit could be start at 30 Ma (Patacca & Scandone , 2011).

1.6 PROBLEMS STATEMENT

Here will be proposed a schematic list of problems concerning the evolution of the blocks taking in account.

1. There is not a choral paleogeographic draft that take in account where the SCB and CPA were located after the broken and spread out of the Rodinia paleo-contintent up to Gondwana amalgamation;
2. Are not unambiguously identified the parts of SCB and CPA that show the main similarities;
3. There are not data that suggest if the CPA was formed by a single terrane or by a puzzle of micro-plates;
4. There are not unequivocally matches that suggest up to when the SCB and CPA sharing the evolution.

2 METHODOLOGIES

This chapter will describe the approaches chosen and the methodologies used to conduct the research and how the procedures have been performed. Laboratory research focused on chemical and isotopic analysis of magmatic and detrital zircons. Magmatic zircons were analysed at the University of Lausanne, and detrital zircons were analysed at the University of Brasilia during a stay of six month. Other research methodologies included Bibliographic investigation of published work, whole rock geochemistry, and field observation.

2.1. BIBLIOGRAPHIC RESEARCH

Thesis research started with a review and critical study of important published works covering the regional geology and various methods of investigation, particularly in geochemistry and geochronology. A particular focus was given to recent publications about the geology of the two crustal blocks studied (SCB and CPA), and the overall evolution of the European Variscides within the framework of the Gondwana and Rodinia supercontinents.

2.2. FIELD WORK

Field activity occurred in two campaigns, focusing around the collection of samples for geochemistry and geochronology, and documenting the field relationships or context of the samples. The first campaign occurred in April 2009 and focused on the CPA, with the PRIN project team. Key outcrops and magmatic bodies were identified and sampled, and the structural relationships with Calabrian Units were investigated.

The second field campaign was done in 2011, and focused on the Tertiary outcrops of SCB and of the Aspromonte sub-region (southern CPA). This field trip explored the geology of the sedimentary deposits and provided an opportunity to sample parts of the Tertiary stratigraphy.

2.3. WHOLE ROCKS GEOCHEMISTRY

Sample for the determination of major element oxides were sent to Actlabs laboratory (Canada) and results are reported in Table 1 in the Annexes section.

To have the whole rock analysis is the have been performed the total Digestion by ICP, for accurate levels of the base metals Cu, Pb, Zn, Ni and Ag. The trace element have been also detected by ICP-MS and for As, Sb, high W >100ppm, Cr >1000ppm and Sn >50ppm values for these elements provided by Fusion ICP-MS, are order of magnitude only and are provided for general information. Total includes all elements in % oxide to the left of total.

2.4. ZIRCONS GEOCHEMISTRY

Zircon ($ZrSiO_4$) represents a mineral of remarkable utility in geological research. The zircon is large use in geochronology as on of more important timekeeper, considering its radioactive decay of U to Pb.

Because it has a crystalline structure that remains stable over very long periods of geological time, the crystals of zircon are ubiquitarious and permit to draft the early history of the Earth and of the evolution of the crust and mantle.

The ongoing developments in analytical techniques (small-diameter laser, ion and electron beams, high-precision mass spectrometry, different microscopic imaging methods) consent to obtain the ages of tiny volumes of crystals that recorded several growth stages during the time of zircon formation.

Also measuring the U, Th and He contain in the zircon is possible to understand the rates at which recently active landscapes developed and the times at which the exposed rocks cooled to near-surface temperatures.

The Zircon can include variuos elements (P, Sc, Nb, Hf, Ti, U, Th and REE) in his structure in different amounts in trace (up to thousands of ppm) or minor (still to 3 wt%). The possibility to incorporate the elements into the zircon structure occurs through of single-site and coupled-cation substitution mechanisms (Hoskin and Schaltegger 2003). The main controls on the substitution processes have given by the ionic radii of the substituting cations compared with Zr4+ and Si^{4+} cations. The $(OH)_4$ can substitute the SiO_4 because of Zr^{4+} in 8-fold coordination has an ionic radius of 0.084 nm and Si^{4+} in tetrahedral coordination an ionic radius of 0.026 nm. Also the Hf^{4+} (having a ionic radius of 0.083 nm) can be a possible substitution of the 8-fold Zr^{4+} site, and a solid solution towards the mineral hafnon ($HfSiO_4$) exists. In fact zircon usually includes considerable HfO_2 (up

3%), that allow to the zircons to be an indicator of crustal residence and growth evaluation his Hf isotope content (Hawkesworth and Kemp 2006; Scherer et al. 2007).

2.4.1 CL AND BSE IMAGING

The cation replacements in the crystal structure can offer various internal textures in zircon that can be impressed in images. The replacements could be interpreted like growth stages and diffusion−reaction or dissolution–reprecipitation processes in the evolution of the single zircon. The inner structures derived, like the more observed oscillatory and sector zoning, can be imaged mainly using cathodoluminescence (CL) and backscattered electron (BSE) imaging.

For example, the lower mass elements Zr and Si have generally replaced by much heavier elements (U, Th, REE, Hf), well impressed by changes using the backscattered electron (BSE) imaging.

With the technique of the Backscattered electron (BSE) the high-energy electrons produced by elastic collision of an incident electron beam with the electron cone of a sample atom are imaged using a detector within an SEM. The zones showing high light correspond to the high content of Hf in the zircon (Hanchar and Miller 1993; Corfu et al., 2003).

The Cathodoluminescence (CL) imaging technique uses the light emanated from minerals during bombardment by an electron beam, and imaged it using a detector coupled with a scanning electron microscope. To improve the luminescence within minerals are used elements (e.g. Dy), in the other case, have been recognised other elements (e.g. U, Th, Fe) or also defects in the crystal structure generally that smooth the bright of the images. Normally the CL images could reflect the chemical variations within individual crystals showing the internal zoning of the mineral.

In the CL images the brightness are inverted respect of the BSE imaging. The areas within the zircon grains that have a brighter BSE signal are the darkest shown in CL.

In this research have been done both CL technique and BSE technique. The first one has been performed in magmatic zircon analyzed by SEM at the Lausanne University. The BSE technique has been performed at the University of Brasilia (UnB). Has been chosen to perform BSE on detrital zircons because the Hf zircon content here is easier to determine due at its lighter expression (Hanchar and Miller 1993; Corfu et al., 2003) respect of the CL images.

2.4.2 U-PB ISOTOPIC SYSTEM

Zircon is one of the most adaptable chronometer available to the modern geology (Scherer et al., 2007). Its features like geochronometer was recognised since long time by Holmes (1911), before

that the isotopes of Pb could be measured and long before ^{235}U was identified as the second radioactive isotope of uranium.

During his development, the zircon incorporates in its crystal structure modest amounts of uranium (U) and thorium (Th) and excludes lead (Pb). Over time constant decay of U and Th causes accumulation of radiogenic Pb, which provided the basis for accurate and exact determination of the isotopic age of zircon. The special feature of zircon respect the others geochronometers is given by its robustness,in fact for its hardness is a refractory mineral that resists when the host rock is metamorphosed, melted, or mechanically weathered away. Additionally it is characterized by very low diffusion rates for many elements inside, permitting to retain age and other isotopic information as well under high temperatures or magmatism.

Have been recognised three different radioactive decay series that involve the parent isotopes (^{238}U, ^{235}U and ^{232}Th) and studied their daughter products (the isotopes ^{206}Pb, ^{207}Pb and ^{208}Pb). All these decay processes involve a number of intermediate steps and short-lived intermediate isotopes. The decay of ^{238}U to ^{206}Pb takes place by alpha-decay steps (liberating 4He α-particles) together with beta-decay steps (a β-particle has released and occur the transformation of neutron in proton). All these processes produce short-lived isotopes that decay in different time (in order of seconds, years, decades or hundreds of thousands of years).

The U-Pb decay process has been described by a single decay equation relating the number of last parent atoms residual (e.g. ^{238}U) and the number of ultimate radiogenic daughter atoms (e.g. $^{206}Pb^*$) over time, by the following equation:

$$^{206}Pb^*/^{238}U = e\lambda^{238}t - 1$$

where **e** is the exponential function, **t** is time, and **λ** is the decay constant specific to this decay scheme, i.e. λ^{238} = 1.55125e-10. $^{206}Pb^*$ refers to the radiogenic ^{206}Pb accumulated in the crystal as a result of the decay of ^{238}U.

The ^{238}U has a decay of ca. 4468 Ma for half the ^{238}U initially present in the grain to decay to ^{206}Pb – this is the half-life.

Also the $^{207}Pb^*$ has been produced from the decay of ^{235}U and $^{208}Pb^*$ produced from ^{232}Th, with λ^{235} = 9.8485e-10 and λ^{232} = 4.9475e-11. The half-life of ^{235}U is ca. 704 million years and for the ^{232}Th is ca. 14 billion years.

In the zircon laboratory practice is not possible to assume that Th and U are equally ‘closed’ to post-crystallization effects. It is fundamental to correct for any Pb initially present prior to the accumulation of radiogenic Pb in the grain. The inherited or ‘common’ Pb would contribute erroneously to give an

older age. So with the 'common Pb correction' can be analysing non-radiogenic ^{204}Pb and then subtracting the ^{206}Pb and ^{207}Pb that would be associated with this ^{204}Pb at a chosen reference age.
Is it possible to plot mutually compatible sets of daughter/parent ratios, $^{207}Pb^*/^{235}U$ and $^{206}Pb^*/^{238}U$, that would evolve in the zircon grains as time elapses since their formation. This progression is the basis of the concordia diagram (Fig. 1-2,a; Wetherill 1956) where the curve represents the locus of the mutually compatible or concordant $^{207}Pb^*/^{235}U$ and $^{206}Pb^*/^{238}U$ ratios.

As reported upon, when the zircon forms (at time zero), no radiogenic Pb* occurred in the zircon. If the zircon grains are concordant, the two Pb*/U ratios as measured in the grains correspond to the same age (time elapsed), giving directly a measure of age by the position along the concordia curve. The individual analysis points plot as elongated ellipses when the two ratios, and so their errors, are strongly correlated.
The concordia diagram permits also to evaluate zircon whose Pb*/U analyses do not be placed on Concordia curve. So the zircon grains analyses are called discordant where the ages determined from the $^{207}Pb^*/^{235}U$ and $^{206}Pb^*/^{238}U$ ratios do not agree (Fig. 2-1). There are mainly two types of dicordancy: i) the zircons ages are normally discordant if they lie below the concordia curve, ii) or are "reverse discordant" if the analyses lie above the concordia curve (i.e. at a higher $^{206}Pb^*/^{238}U$ for a given $^{207}Pb^*/^{235}U$ ratio).
Also the Tera-Wasserburg (1972) diagram (Fig. 2-1, b) is a way to present the U-Pb data used moreover for the ages younger than 1500 Ma.

(a)

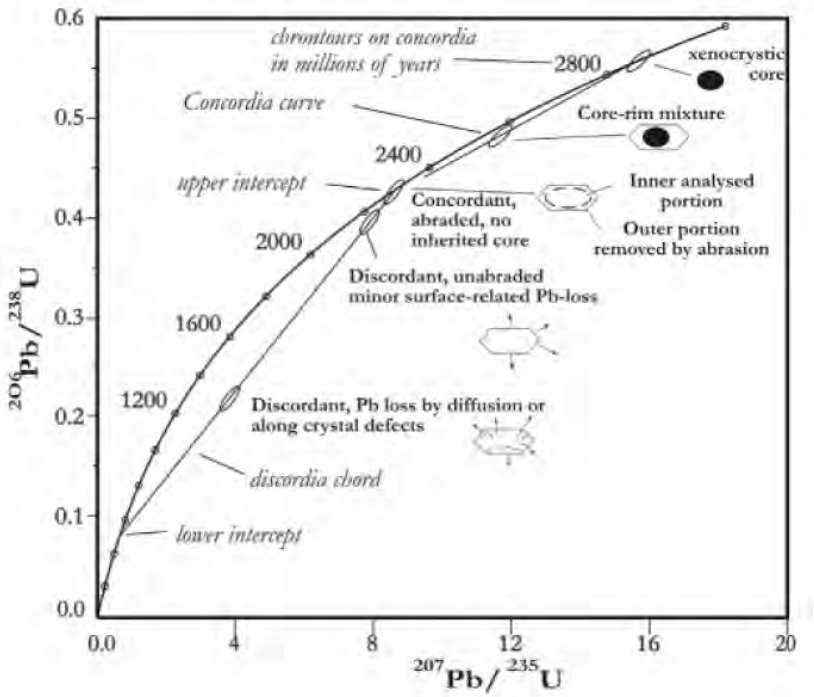

(b)

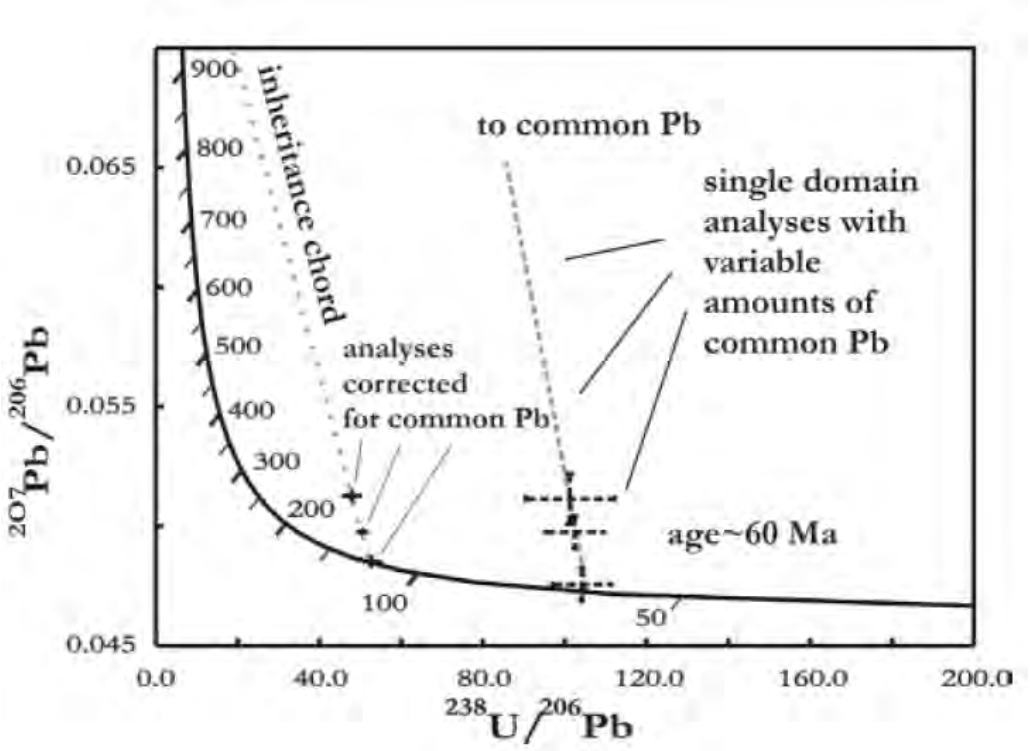

Fig. 2-1. Wetherill and Tera-Wasserburg concordia diagrams with notes (after Parrish and Noble, 2003). (a) The Wetherill Concordia shows several conditions that can be show in the laboratory routine, like the presence of inherited grains, mixed-age crystals that may delineate a chord, concordant data on single crystal, and discordant analyses due to Pb loss consequently radiation damage. (b) The Tera-Wasserburg diagram focus in two case done: on the left have shown more precise common Pb-corrected analyses delineating a chord that likely due by a mixture of inherited and magmatic grains. On the right side have been reported a case of less precise analyses without common Pb-correction; the upper intercept in the box marks the $^{207}Pb/^{206}Pb$ of the common Pb and the lower intercept characterized the $^{238}U/^{206}Pb$ of the crystals giving the interpreted age.*

2.4.3 LU-HF ISOTOPIC SYSTEM

The Lu–Hf isotope system in zircon is considered of huge value mainly by its use as a geochemical tracer. Nowadays the studies with Lu–Hf coupled to U–Pb isotope systems are one of the most powerful tool (Kinny & Maas, 2003) that geologist have.

The Lu–Hf system was first exploited as a geochemical tracer in the early 1980s (Patchett and Tatsumoto, 1980) latter the first effort to establish in-situ zircon hafnium isotopic composition was made by Kinny et al. (1991). But large uncertainties in ε Hf units (±5-7) was obstructing the discussion on the petrogenesis of the parent magma since the development of multiple-collector ICPMS (e.g. Chu et al., 2002; Thirlwall and Walder, 1995) which solved the problems. The ICPMS coupled with a laser ablation system permit to have accurate analysis of Hf isotopic composition on a small part of a single grain (e.g. Griffin et al., 2000; Andersen et al., 2002; Xu et al., 2004).

^{176}Lu is considered like an unstable radionuclide that has a spontaneous β– decay into the stable ^{176}Hf

having a half-life of ca. 35 billion years.
The age equation which is applied to any closed system is expressed by the following:

$$(^{176}Hf/^{177}Hf)_t = (^{176}Hf/^{177}Hf)_{initial} + (^{176}Lu/^{177}Hf)_t \cdot (e^{\lambda t} - 1)$$

where t is the elapsed time, and λ is the ^{176}Lu $\beta-$ decay constant.

^{176}Lu represents the heaviest element of the REEs having ca. 2.6% of natural lutetium. The Lu has a tendency to reside principally in heavy REE-having geochemistry "virtually identical" to zirconium. With respect to refractory elements such as Sm, Nd, Lu, and Hf, Earth is assumed to have the same composition as that of the chondritic uniform reservoir (CHUR) defined by undifferentiated meteorites. Because these elements remained in the silicate portion of Earth (i.e. bulk silicate Earth or BSE) during early core segregation, the BSE is expected to have the same Lu/Hf (and Sm/Nd) values as CHUR. The behaviour of the Lu–Hf system during melting is analogous to that of the Sm–Nd system, with the daughter element Hf fractionating into the melt to a higher degree than the parent element Lu. During the time the fractionation of Lu/Hf among Earth's silicate reservoirs will direct to considerable variation in ^{176}Hf/^{177}Hf. So the Lu–Hf system can be used in the same way as Sm–Nd to monitor the degree of isotopic heterogeneity of Earth's silicate reservoirs, but showing several key advantages.
Considering that Hf is more incompatible than Lu, the crust will have a lower Lu/Hf value than the Bulk Silicate Earth (BSE), but the Lu/Hf value of the depleted mantle will be higher. Over time, the isotopic compositions of the crust and depleted mantle (DM) deviate to lower and higher ^{176}Hf/^{177}Hf values, respectively.

By convention, Hf isotope compositions are expressed as ε_{Hf}, the deviations (in parts per 10^4) from the CHUR composition, whose Lu/Hf and ^{176}Hf/^{177}Hf values are assumed to represent those of the BSE. The notation for these deviations at some time t in the past is $\varepsilon_{Hf}(t)$.
The Lu–Hf isotope system is performed to track the history of chemical differentiation of the Bulk Silicate Earth (BSE) because the fractionation of Lu from Hf taken place during magma generation (Fig. 2-2). The initial Lu/Hf ratio uniform and approximately chondritic, for the Earth has been increasingly modified over time by episodes of partial melting in the upper mantle that, producing basaltic magmas, has depleted the residual mantle in Hf, enriching the basaltic crust generated. Over time, the Hf isotopic composition of the depleted mantle (Lu/Hf > chondrites) and of the enriched crust (Lu/Hf < chondrites) diverges from that of any remaining unfractionated material (Lu/ Hf = chondritic, Fig. 2-3).

The deviations of Hf isotopic composition from chondritic at any time, t, are expressed in epsilon units (parts per ten thousand) and has expressed by the following formula:

$$\varepsilon_{Hf} = [\ (^{176}Hf/^{177}Hf)_{sample} / (^{176}Hf/^{177}Hf)_{chondrites} - 1\ ] \cdot 10^4$$

Samples characterized by higher $^{176}Hf/^{177}Hf$ than chondritic at time t have positive eHf values. Sample having lower $^{176}Hf/^{177}Hf$ than chondritic have negative eHf. Chondrites have eHf = 0. If the deviations from chondritic composition are small could be doubts in the interpretation of Hf isotope ratios.

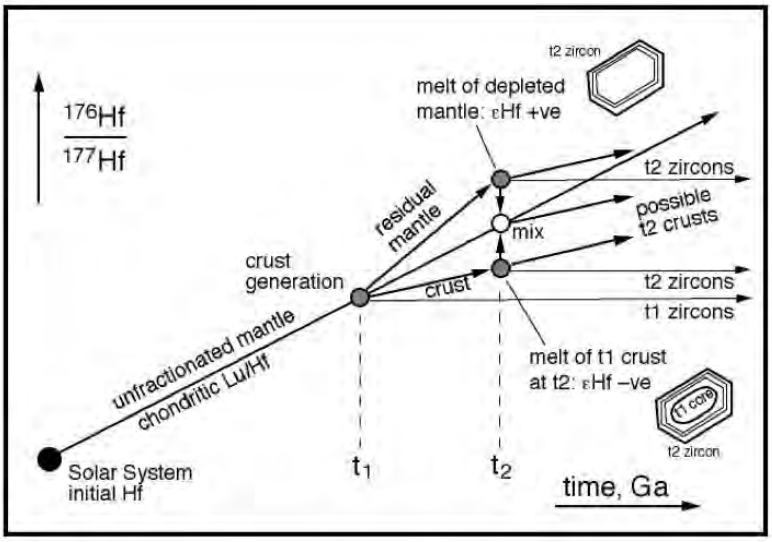

Fig. 2-2. *Schematic Hf isotope evolution diagram, modified after Patchett et al. (1981), showing how an episode of partial melting in Earth's mantle at time t1 is given in divergent Hf isotope evolution paths, for the lately generated crust (low Lu/Hf) and the residual mantle (high Lu/Hf). The zircons formed within that crust have low Lu/Hf, maintaining its initial 176Hf/177Hf ratio. At time t2 a different sources could supply the lately forming crust. If totally derived from depleted mantle (DM), the initial ∑Hf will be positive, nevertheless mixing with an undepleted or enriched source (likely by crustal contamination) may result in low positive, zero, or negative ∑Hf at the time of crystallization depending on the stability of components. Any inherited zircon cores at t2 would be expected to have lower ∑Hf than the newly crystallized host rock.*

The crystallization of zircon results in extreme fractionation of Lu/Hf between zircon and the host magma, because of the Lu/Hf ratio in zircon is very low (usually ~0.002). For that reason, due to the negligible production of ^{176}Hf by ^{176}Lu decay, zircons preserve the initial $^{176}Hf/^{177}Hf$ ratio, giving a permanent record of the Hf isotopic composition of their source at the time of crystallization.

This ratio can be used to determine a T_{DM} Hf model age (with respect to undepleted or depleted mantle). Also the ratio could be useful to determine an initial εHf value with respect to the Hf isotope evolution reference curve for the bulk unfractionated Earth, if the crystallization age of the zircon is known independently from U–Pb dating, (Fig. 2-3). The T_{DM} model age can be interpreted like the crustal residential time of the magma where the zircons crystallised.

The T_{DM} model age follows this formula referred to the depleted mantle (DM):

$$\text{Hf } T_{DM} = 1/\lambda \times \ln \{ [(^{176}Hf/^{177}Hf)_{sample} - (^{176}Hf/^{177}Hf)_{DM} / (^{176}Lu/^{177}Hf)_{sample} - (^{176}Lu/^{177}Hf)_{DM}] + 1 \}$$

The T_{DM} model age could be linked to the more episodes of crustal growth, considering the possibility that the zircons crystallised from magmas derived from mixed source rocks separated from the mantle at different times (Hawkesworth, 2006).

In this thesis the model age has been performed in two stages following (Nebel et al., 2007). The Hf T_{DM} age is estimated by the initial isotopic composition of Hf in the zircon using the average of Lu/Hf crust ratios. The Hf initial composition in zircon represents the $^{176}Hf/^{177}Hf$ during the zircon crystallization with the U-Pb age, previously performed in the same portion of zircon.

T is the crystallization age, so εHf(t) represents the zircon's initial Hf isotope composition. Although the calculated initial $^{176}Hf/^{177}Hf$ value of a zircon is relatively insensitive to age, its $\varepsilon_{Hf}(t)$ is age dependent because the $^{176}Hf/^{177}Hf$ value of the CHUR reference evolves significantly over time. Therefore a εHf(t) value calculated using the $^{207}Pb/^{206}Pb$ age of a discordant zircon might not accurately represent the zircon's initial Hf isotope composition because the $^{207}Pb/^{206}Pb$ age is only a minimum age.

Positive ε Hf(t) values are commonly interpreted to reproduce the growth of juvenile crust by extraction of magmas from a depleted mantle reservoir. In spite of this the interpretation is more complex with zircons with a complicated history. The negative ε Hf(t) values are coherent with significant reworking of ancient crust.

Because of the facility and the time available for this research consents to perform one of these methodologies and the Lu–Hf system has been chosen and performed at Geochronological laboratory at University of Brasilia.

Although the Sm-Nd analysis of the whole rock has been performed in some important studies (e.g. Kröner et al., 1988; Black, 1988), this method have three major restrictions: (1) too much time and facilities expensive; (2) subject to metamorphic troubles that could cause errors in the determinations of initial ratios, ε Nd values and model ages; (3) cold be in amounts irrelevant for sedimentary rocks. Also the Sm–Nd in whole rocks suffered more the metamorphic disturbance than the Lu-Hf system in zircons

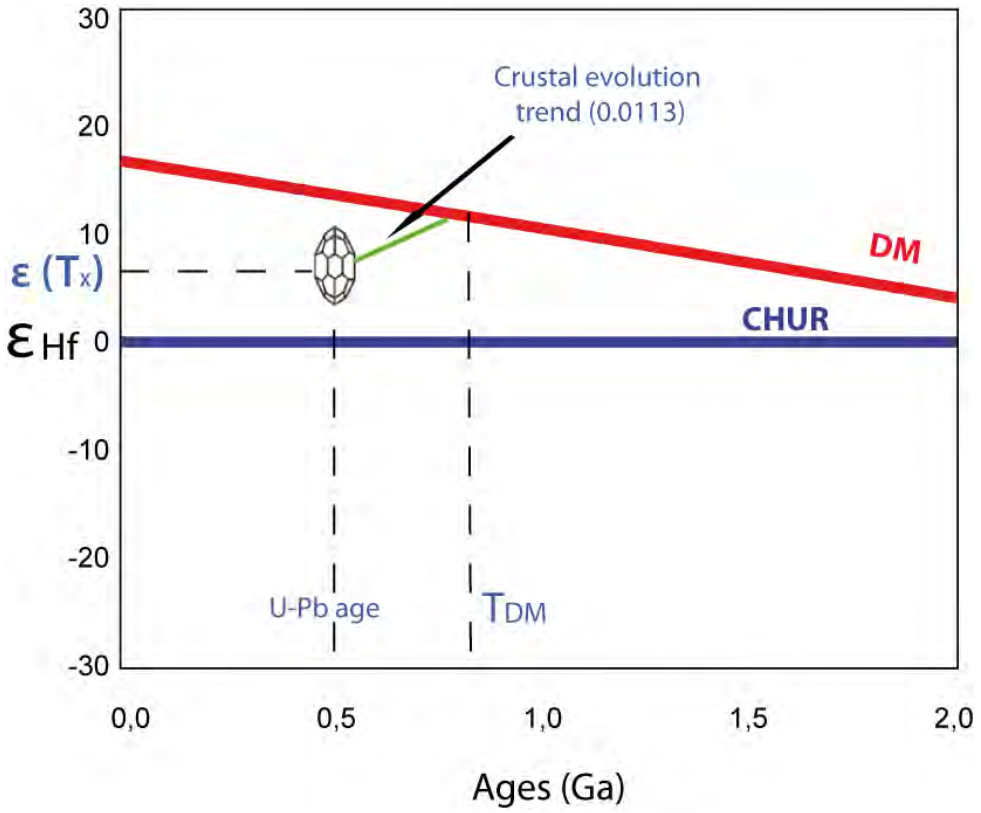

Fig. 2-3, Graphic explains of the variables considered in the Lu-Hf isotopic elaboration. The Epsilon (ε) represents the deviation from the sample "X" isotopic ratio 176Hf/177Hf the respect of the isotopic ratio 176Hf/177Hf of CHUR (Chondritic Uniform Reservoir) or of DM (Depleted Mantle). The εHf(0) represents the deviation at the present time done by laboratory with the 176Hf/177Hf ratio average; the εHf(t) represents the 176Hf/177Hf ratio average deviation at the moment of mineral crystallization.

2.5. PROCEDURES PERFORMED

For in-situ U-Pb and Lu-Hf analyses, zircon concentrates were extracted from 1-10 kg of rock samples by a jaw crusher to a 500μm size, part of sample has been separated by heavy liquid and then concentrated using a Frantz isodynamic separator. Final separation was achieved by hand-picking under a binocular microscope. For the igneous rocks have been selected the more euhedral zircons that the sample shown. For the sedimentary samples, have been selected the majorities of habitus that the samples presented in order to take in account the different populations occurred in the samples. The zircons have been mounted in thin section glasses, where have been collocated a rounded part of Teflon to form the support for the sample. Next has been formed a mix of resins (Struer or Epo fix resin) and hardener (Epo fix hardener) in ratio 2:1. The compost was slowly mixed, in order to evict the bubbles formation, and collocated above the zircons. Then the samples have been put into the oven for 12 hours. The final steps has been to lower the grains almost at their

half by the polishing of epoxy (without the glass) that consisted in several steps with different polish dishes and concluding with alumina powder to shine the zircon surface.

Before analysis, the grains were cleaned with 3% nitric acid.

Cathodoluminescence images have been performed on magmatic zircon at the University of Lausanne. Backscattering electrons (BSE) images used for spot targeting of detrital zircons have been acquired with a Jeol Microprobe at the University of Brasilia.

The U-Pb isotopic analyses of magmatic zircon have been performed in the Mineralogy and Geochemical Institute at the University of Lausanne. Here has been used a sector-field spectrometer Element XR interfaced to a NewWave UP-193 ArF excimer ablation system (Fig. 4-3 a)

(a) (b)

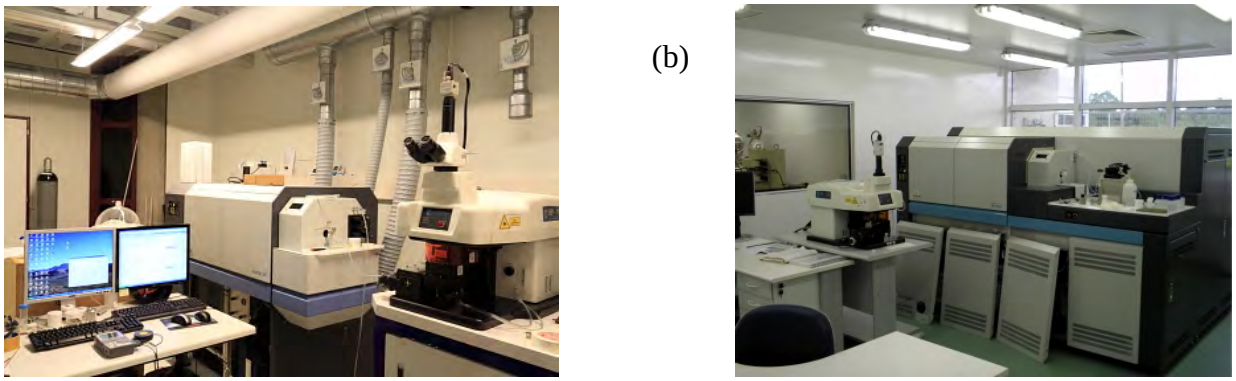

Fig. 4-3, Laboratories where have been performed the samples. (a) Laboratory at the Institute of Minarlogy and Geochemistry of the Lausanne University with a NewWave UP-193 ArF excimer ablation system and a sector-field spectrometer Element XR. (b) Geochronological laboratory at the Brasilia University showing a Thermo-Fisher Neptune MC-ICP-MS coupled with a Nd:YAG UP213 New Wave laser ablation.

The U-Pb and Lu-Hf isotopic analyses performed on detrital zircon grains have been performed at the Laboratory of Geochronology in the University of Brasilia. Here it has been used a Thermo-Fisher Neptune MC-ICP-MS coupled with a Nd:YAG UP213 New Wave laser ablation system (Fig. 4-3 b). The operating conditions and instrument settings of NEPTUNE and laser ablation system during analytical sessions are described in Matteini et al. (2010).

The U-Pb analyses on zircon grains were carried out using the standard-sample bracketing method (Albarède et al., 2004) using the GJ-1 standard zircon in order to control the ICP-MS fractionation. Two to four samples have been analyzed between JG-1 standard analyses, and $^{206}Pb/^{207}Pb$ and $^{206}Pb/^{238}U$ ratios have been time corrected. The raw data were processed off-line and reduced using an Excel worksheet (Buhn et al., 2009). Analyses have performed using spot size of 30 μm and laser induced fractionation of the 206Pb/238U ratio was corrected using the linear regression method (Kosler et al., 2002). During analytical session zircon standard Temora-2 has been analyzed as an unknown sample. In all analyzed zircon grains the common Pb correction was not necessary

due to the low signal of common ^{204}Pb. Concordia diagrams (2σ error ellipses) and upper intercept ages were calculated using the Isoplot/Ex software (Ludwig, 2003), and Lamtrace software for the data performed in Lausanne.

Lu-Hf isotopes were analyzed on selected zircon grains from four different samples, previously analyzed with U-Pb systematic. Lu-Hf isotopic data were collected during 40 seconds ablation time and using a 40 μm diameter spot size. The signals of the interference-free isotopes ^{171}Yb, ^{173}Yb and ^{175}Lu were monitored during analyses in order to correct for isobaric interferences of ^{176}Yb and ^{176}Lu on the ^{176}Hf signal. The ^{176}Yb and ^{176}Lu contribution are calculated using the isotopic abundance of Lu and Hf proposed by Chu et a. (2002). The contemporaneous measurements of ^{171}Yb, ^{173}Yb permit to correct the mass-bias of Yb using a ^{173}Yb/^{171}Yb normalization factor of 1.132685 (Chu et al., 2002). The Hf isotope ratios are normalized to ^{179}Hf/^{177}Hf value of 0.7325 (Patchett, 1983).

The $\varepsilon_{Hf}(t)$ values are calculated using the decay constant $\lambda=1.865*10^{-11}$, proposed by Scherer et al. (2001) and the ^{176}Lu/^{177}Hf and ^{176}Hf/^{177}Hf CHUR values of 0.0336 and 0.282785 (Bouvier et al., 2008). A two-stage T_{DM} age is calculated from the initial Hf isotopic composition of the zircon, using an average crustal Lu/Hf ratio (Gerdes and Zeh, 2006, 2009, Nebel et al., 2007). The initial Hf composition of zircon represents the ^{176}Hf/^{177}Hf value calculated at the time of zircon crystallization, namely the U-Pb age, possibly concordant, previously obtained on the same crystal. The two stages depleted mantle Hf model ages (TDM Hf) are calculated using ^{176}Lu/^{177}Hf=0.0384 and ^{176}Hf/^{177}Hf=0.28325 for the depleted mantle (Chauvel and Blichert-Toft, 2001) and ^{176}Lu/^{177}Hf value of 0.0113 for the average crust (Taylor & McLennan, 1985 and Wedepohl, 1995).

Before Hf isotopes measurements on zircons, replicate analyses of 200 ppb Hf JMC 475 standard solution doped with Yb (Yb/Hf=0.02) were carried out (^{176}Hf/^{177}Hf=0.282162±13 2s, n=4). During analytical session replicate analyses of GJ-1 standard zircon were executed obtaining a ^{176}Hf/^{177}Hf ratio of 0.282006±16 2σ (*n=25*), in agreement with the reference value for GJ standard zircon (Morel et al., 2008). The εHf values for each single grain were calculated at the U-Pb age previously obtained by LA-MC-ICP-MS on the same zircon grain. For slightly discordant (<20%) analyses ^{207}Pb/^{206}Pb ages have been used.

The data about U-Pb and Lu-Hf isotopes performed during the laboratory activities are reported in the Table 2 and 3, in the Annexes section.

3 RESULTS

In this chapter will be shown the geology and the geochemical data relative to the outcrops from which the samples have been collected. Will be illustrate the data first from the Sardinia-Corsica Block basement and the tertiary covers and in the second part of chapter will be reported the data relative to the basement end tertiary covers to the Calabria-Peloritani Arc.

3.1 SARDINIAN-CORSE BLOCK

In this first part of chapter will be illustrated: i) the study about the Palaeozoic evolution of three different tectonic zones belong to the Sardic Variscides and ii) the investigation in some Tertiary deposits linked to the geodynamic evolution of the present-day Tyrrhenian area, so related to the Alps-Apennine system.

In the Palaeozoic basement some Ordovician magmatic bodies (by whole rocks chemical features and age) and correlated deposits (by comparison of detrital zircons), cropping out in the Nappe Zone and in the Foreland Zone, have been studied.

With the aim to better define the provenance and characterize the sources of the sediments of analogous and problematic deposits, two tertiary detrital zircon samples belonging to the Sardinian-Corse Block have been chosen, one cropping out in NE Sardinia and one in E Corsica.

3.1.1 VARISCAN OROGEN

The Nappe Zone of the Sardinia segment of the Variscan orogen consists of several tectonic units, characterised by successions, equilibrated under greenschist facies, embricated and emplaced with

a general top-to-the-southwest transport. Have been distinguished (Carmignani et al., 2001): an External Nappe zone in the central-southern areas characterized by more or less a similar lithostratigraphic succession; an Internal Nappe zone in the central-northern zone, where a lithostratigraphic succession is not well defined. In the external nappe the occurrence of volcanic products is more abundant and more easily linkable to the lithostratigraphic units dated on their fossil content (Beccaluva et al., 1981, Oggiano et al., 2010). For this reason the Internal Nappe and theirs volcanic products will not be take in account. The small area in the SW (Capo Spartivento), recently defined as the Bithia Unit (Pavanetto et al., 2012), where a volcanic sequence dated Middle Ordovician crops out, will be considered like a part of the Nappe Zone, The study will focus on the Ordovician magmatic bodies and on theirs correlated sedimentary deposits.

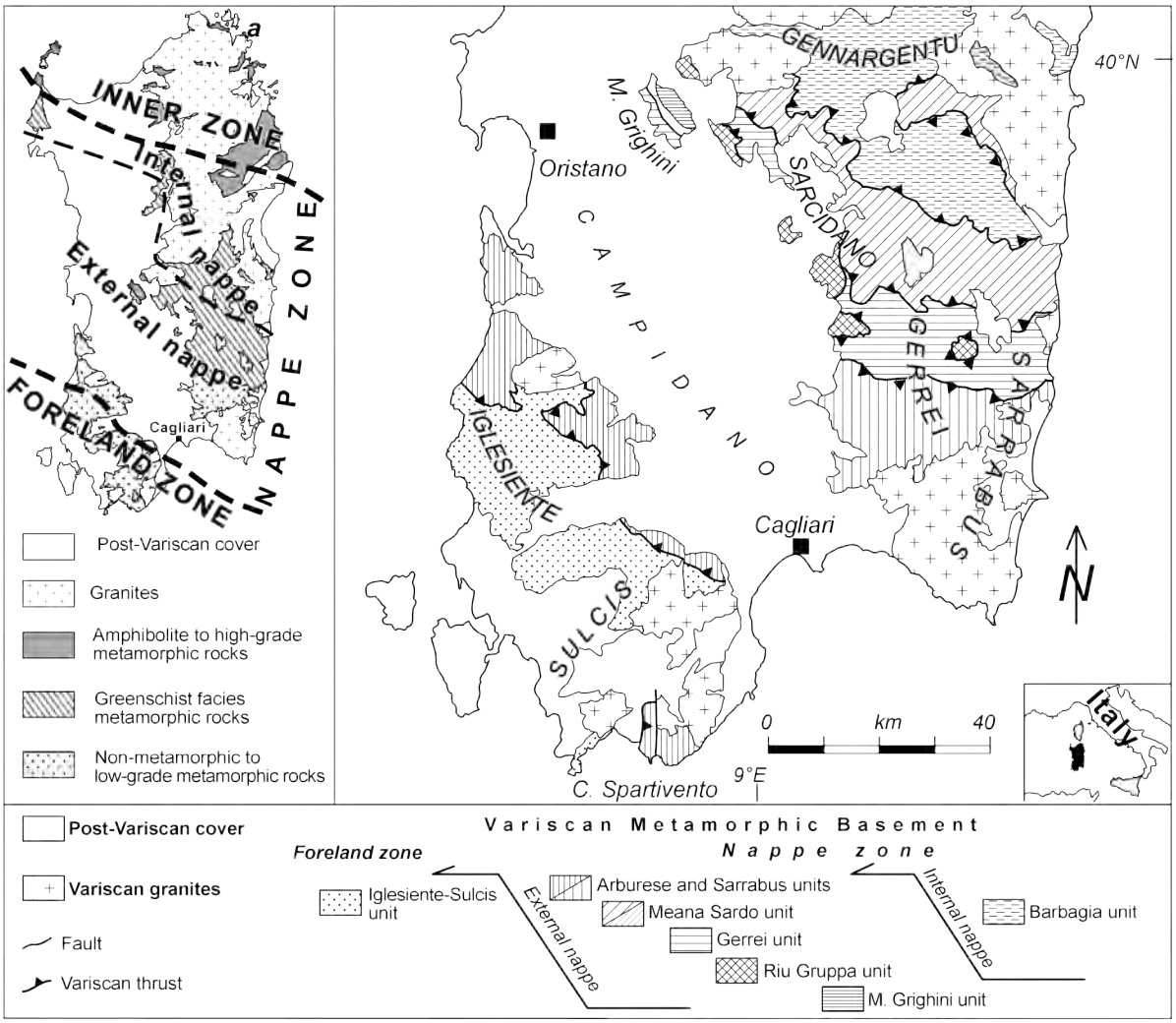

Fig. 3-1 Tectonic sketch map of the Nappe and Foreland zone in the Sardinian Variscides

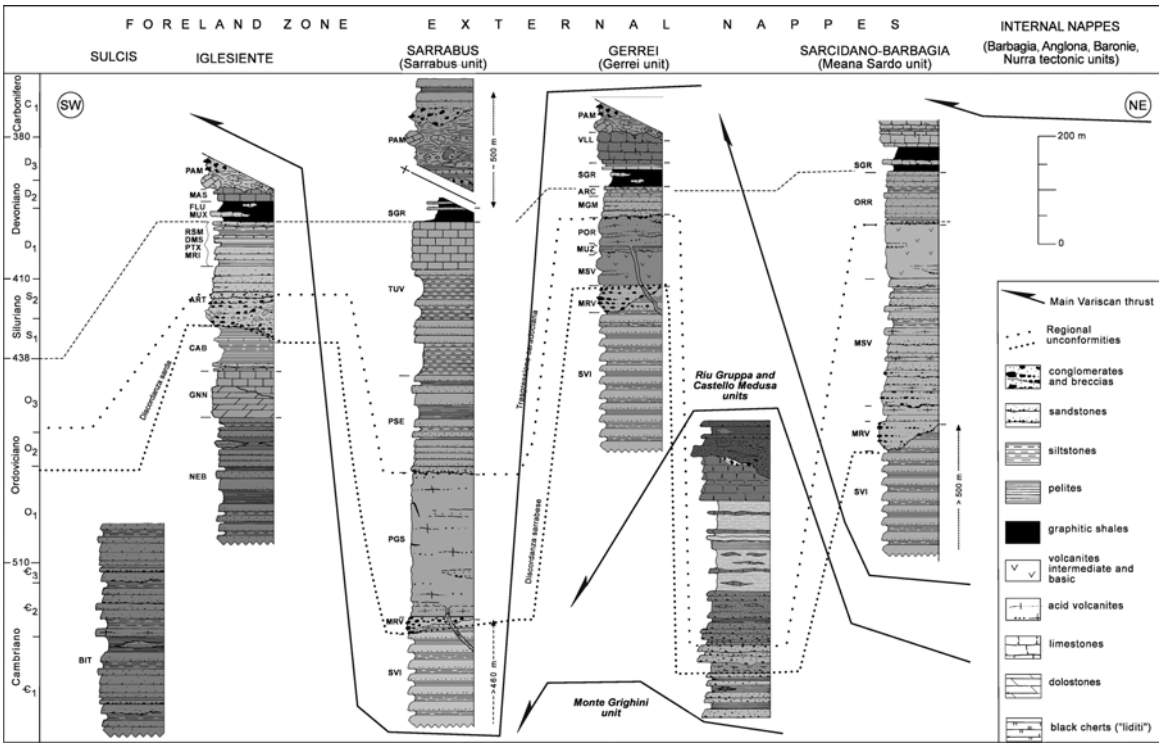

Fig. 3-2 Litho-stratigraphical synthetic columns of the tectonic units in the external nappes and Foreland zone. Abbreviations: ARC: "Argilloscisti di Rio Canoni"; ART: M. Argentu Formation (Puddinga Auct.); BIT: Bithia Formation; CAB: Cabitza Formation; MRV: "Metaconglomerato di Muravera"; DOM: Domusnovas Formation; FLU: Fluminimaggiore Formation; GNN: Gonnesa Formation; MGM: "Metarcose di Genna Mesa"; MUX: Genna Muxerru Formation; MUZ: "metarenarie e quarziti di Su Muzzioni"; NEB: Nebida Formation; ORR: Orroeledu Formation; MAS: Mason Porcus Formation; MRI: Monte Orri Formation; PAM: Pala Manna Formation; MSV: Monte Santa Vittoria Formation; PGS: "Porfidi grigi del Sarrabus"; POR: "Porfiroidi"; PSE: Punta Serpeddì Formation; PTX: Portixeddu Formation; RSM: Rio san Marco Formation; SGR: "Scisti a Graptoliti"; SVI: "Arenarie di San Vito"; TUV: Tuviois Formation; VLL: "Calcari di Villasalto". Note that according recent data also collected during this research the Bithia Unit is considered a klippe of the Arburese unit and not the Precambrian basement of the Variscan foreland succession as represented in this sketch.

In the southwest the nappe stack overrides a foreland severely deformed but non- or weakly-metamorphosed (Fig. 3-1).

The pre-Middle Ordovician lithostratigraphic succession of the external nappes consists of metasandstones, phyllites and quartzites affected by Variscan pumpellyite–actinolite and lower-greenschist facies metamorphism. The ages of these metasedimentary deposits, based on acritarch biostratigraphy, range from Middle Cambrian to Lower Ordovician (Naud and Pittau Demelia, 1987). Interbedded in the uppermost part of the succession is a volcanic suite that pre-dates the Sardic Unconformity (Oggiano et al., 2010): it consists of welded rhyolitic ignimbrites (491 ± 3.5

Ma, U–Pb zircon age), trachy-andesitic pyroclastic fall deposits and dacite to trachyte lava flows (Fig. 3-3). In the Meana Sardo tectonic unit, the volcanic rocks within the pre-Sardic sequence occur as dykes and epiclastic crystal-rich tuffites.

The Nappe Zone (as well the Foreland Zone) is characterised by a Middle Ordovician angular unconformity (Sardic Unconformity: Carmignani et al., 2001 and reference therein), which is also recognised in the Eastern Iberian Plate (Casas et al., 2010; Navidad et al., 2010).

The volcanic succession that overlies the Sardic Unconformity is characterized by a andesitic composition and a geochemistry typical of a calcalkaline suite, associated with subordinate felsic metavolcanics, interlayered coarse metaepiclastic rocks and volcanoclastics. In the Gerrei Unit (Fig. 3-3), micaceous metasandstones and mature quartzarenites cap the volcano-sedimentary succession, indicating high erosion rates of the volcanic edifice. In the Sarrabus and Gerrei units the end of this volcanic activity is marked by rhyolite–rhyodacite lavas, ignimbrites and tuffs, with a combined thickness of less than 100 m (*Porfidi grigi del Sarrabus* and Porphyroids; Calvino, 1972, Carmignani et al, 2001). In the outermost Nappe Zone (i.e. Sarrabus area), metadacite occurs as sparse dykes and sills (465.4 ± 1.4 Ma, U–Pb zircon age; Oggiano et al., 2010) within the pre-Sardic sequences, and they are inferred to have been the feeder dykes of the Porfidi grigi del Sarrabus (Fig. 3-3).

The Middle Ordovician calcalkaline volcanic suite has reliable stratigraphic and palaeontological constraints. In fact this continental clastic and volcanic sequence unconformably (Sardic Unconformity) lays on metasandstones, which, based on acritarchs assemblages, ranges from middle Cambrian to early (Arenig) Ordovician (Naud & Pittau Demelia, 1987). The transgressive sedimentary covers of the volcanic suite have been attributed to the Upper Ordovician (Katian-Hirnantian age), on the basis of fossil content (Loi et al., 1992; Naud, 1979; Barca and Di Gregorio, 1979). Also the U-Pb age of 460 ± 1 Ma on a metarhyolite in the external nappes (Giacomini et al., 2006) is consistent with this time span.

After the Middle Ordovician emersion of this sector of the North Gondwana margin, a large-scale transgression marked the onset of a new sedimentary cycle in the Upper Ordovician (Katian–Hirnantian), which then continued through the Silurian and Devonian into the Early Carboniferous. Three main types of volcanic rock are distinguished within the Upper Ordovician terrigenous succession: 1) effusive products (pillow lavas and hyaloclastics), concordant with the host sediments; 2) sills and larger intrusions; and 3) dykes that cut the entire Lower and Middle Ordovician successions.

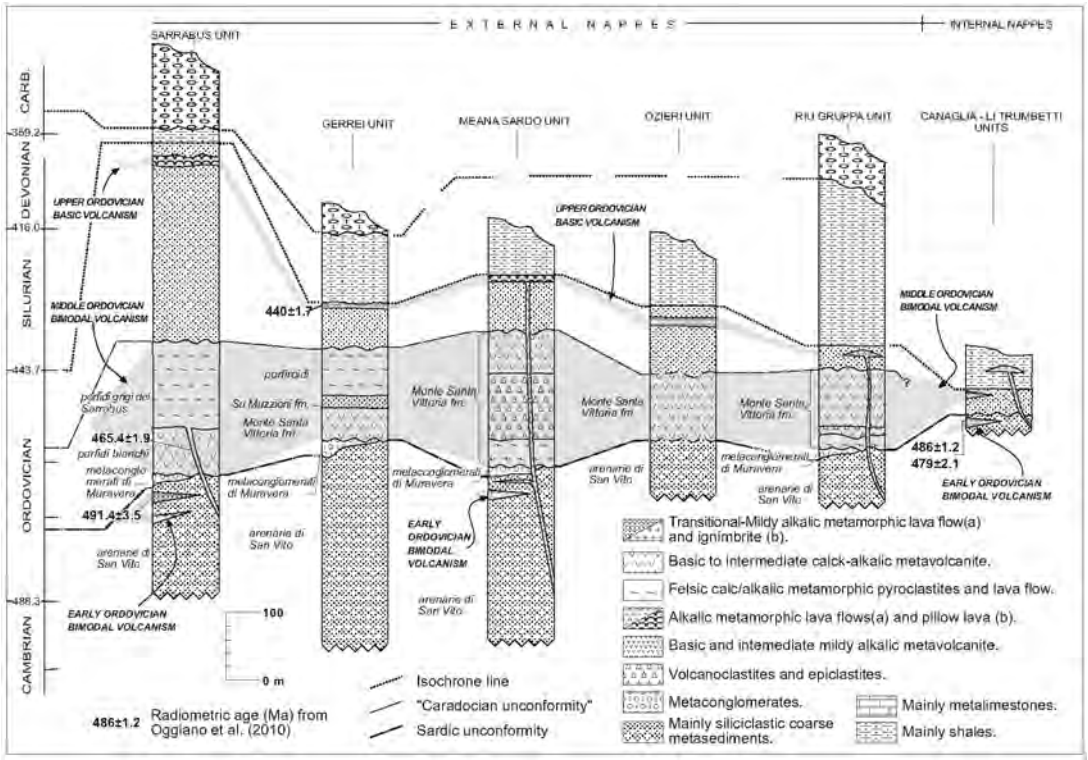

Fig. 3-3 Litho-stratigraphic sketch of the relationships within the Lower Palaeozoic successions, across the Variscan nappes of Sardinia with highlighted the volcanic products in bold characters isotopic age (figure and ages after Gaggero et al., 2012).

In summary, following Oggiano et al. (2010) three main volcanic cycles have been distinguished for the External Nappe zone on the base of radiometric and field evidence:

I. A felsic Upper Cambrian–Lower Ordovician volcanic cycle older than the Sardic phase. The occurrence as dykes cutting the epicontinental clastic arenitic sediments and rare ignimbrites suggest a volcanic passive margin context.

II. The calcalkaline volcanic cycle (Memmi et al., 1983; Di Pisa et al., 1992) embracing the Middle Ordovician. It is referred to as an Andean type arc, developed at the northern Gondwana margin (Carmignani et al., 1994c).

III. An alkaline (Lehman, 1975; Ricci and Sabatini, 1978, Di Pisa et al., 1992), volcanic activity, at the Ordovician–Silurian boundary.

Here will be take in account three units: the Sarrabus U., the Arburese U. and the Bithia U., all belonging to external nappes. Up to now the attribution of the Bithia U. to the Nappe zone or to the Foreland was still ambiguous and considered like a problematic zone. Following Pavanetto et al.,

2012 partially stem out from the present research we finally believe that it is part of the external nappe, probably a klippe of the Arburese unit.

3.1.1.1 PALAEOZOIC SAMPLE COLLECTION

From the Nappe Zone 8 samples have been analyzed (Fig. 3-4). Three are from the Sarrabus Unit: two from volcanic bodies (SM-200 and BS-125,) and one sample has been collected from sedimentary deposit (SST-5100). One sample has been collected from the Arburese U. (CC-150) and two sample from Bithia Unit: one sample has been collected from magmatic body (SAR05-11) and one from a sedimentary deposit (AF0828); two orthogneiss samples (28, SAR-0509) have been collected from Capo Spartivento area (Sulcis sub-region). These two last samples are related to an intrusive Ordovician magmatic body whose relationships with the surrounding rocks are still matter of debate. According Pavanetto et al. (2012) given the type of contact (considered a low-angle normal fault developed in ductile regime) and the different metamorphic evolution it might be considered as a part of the crust of the foreland.

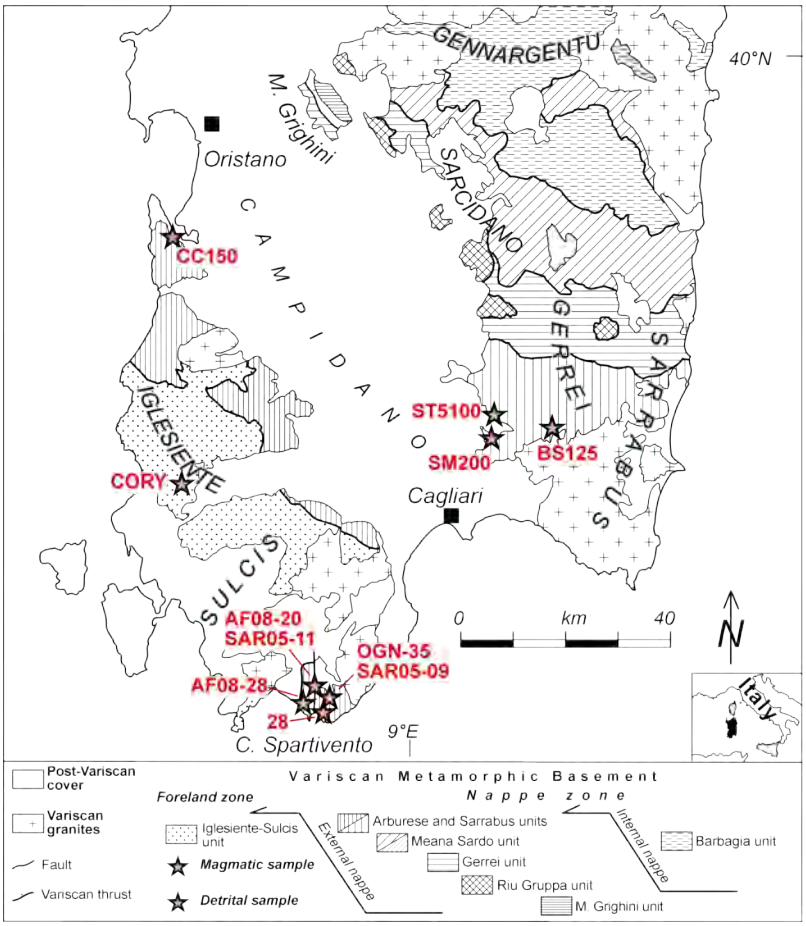

Fig. 3-4 Location of magmatic samples collected in Variscan basement of Sardinia

SAMPLE	LITOLOGY	UNIT/Fm.	SUBREGION	COORDINATES
SM-200	Meta-ryodacites	Sarrabus U.	Sarrabus	9°11'48.02"E, 39°23'11.89"N
ST-5100	Quartz-arenites	Sarrabus U.	Sarrabus	9°11'22.89"E, 39°23'56.05"N
BS-125	Metaryolithes	Sarrabus U.	Sarrabus	9°18'46.47"E, 39°23'10.84"N
CC-150	Metavolcanites	Arburese U.	Arburese	8°31'43.10"E, 39°40'45.19"N
AF08-20 (SAR05-11)	Metavolcanites	Bithia U.	Sulcis	8°48'2.92"E, 38°53'53.37"N
28	Leucocratic orthogneiss	M. Filau orthogneiss	Sulcis	8°49'4.91"E, 38°53'42.83"N
OGN-35 (SAR-0509)	ptitic orthogneiss	M. Filau orthogneiss	Sulcis	8°49'15.55"E, 38°54'9.27"N
AF08-28	Quartz-arenites	Bithia U.	Sulcis	8°48'10.30"E, 38°54'6.06"N
CORI	Quartz-arenites	Cabitza Fm.	Iglesiente	8°28'48.05"E, 8°28'48.05"E
SA-ALB	Meta-conglomerates	Cuccuru 'e Flores cconglomerates	Baronie	° 38' 18.7" E, 40° 32' 13" N,
CO-SOL	Meta-conglomerates	Solaro FLysch	East Corse	9°20'19.30"E, 41°54'15.50"N

Tab. 3-1 Samples collected in the Palaeozoic basement of Sardinia and theirs coordinates.

3.1.1.1.1 Sarrabus and Arburese Units

The Sarrabus and the Arburese units represent the front of the external nappe that are considered the main allochthon complex that overlies directly the Foreland zone (Iglesiente-Sulcis).

Following the main authors (Carmignani et al., 1982, 2001) here the two units have been considered as the same, constituted by the same formations, where the Arburese U. represents the

westward prosecution of the Sarrabus U. beyond the Campidano. Here the two tectonic units will be described together.

The tectonic units suffered two main deformation phases linked to Variscan orogeny. The first phase, relate to the continental collision, has given a crustal thickening with the nappe emplacement, the second phase, occurred when the continental collision ceased, has done the tectonic exhumation with both ductile and fragile deformation and the third one has given a mild deformation with crenulation cleavage, related to the last stage of exhumation. In the Sarrabus U., the first deformation phase develops three sub-units (Carmignani et al., 2001): i) Genn'Argiolas sub-unit; ii) Minderrì sub-unit and iii) P.ta Ruggeri sub-unit. The Genn'Argiolas sub-unit is the most correlated to Arburese U.

Even if the majority of nappes have N-S transport, the Sarrabus and Arburese units were emplaced with a top-to-the-W transport direction during the first Variscan deformation phase (Conti et al., 2001): the Sarrabus U. thrusts over both the Meana Sardo and Gerrei units along the Villasalto thrust, and the Arburese U. thrusts over the Iglesiente area representing the autochthon zone

The Sarrabus U. is constituted by the Arenarie di S. Vito formation. (middle Cambrian-Lower Ordovician), the acid volcanites complex (Middle - Upper Ordovician), the P. Serpeddì Fm. and the Tuviois Fm. (Upper Ordovician) and the post-Ordovician formations (Silurian-Lower Carboniferous) (Fig. 3-2).

Here will be take in account the acid volcanic complex and the P. Serpeddì Fm., from whose the samples have been collected.

3.1.1.1.1.1 Volcanic complex in the Sarrabus / Arburese units

The volcanic complex (as also explain in the previous paragraph) is composed by ca. 200 m of volcanic deposits classically called "porfidi grigi del Sarrabus" and "porfidi bianchi" (Calvino, 1972) from dacitic to rhyolitic in composition (Memmi et al., 1982), generally with a porphiric texture with large phenocrysts of K-feldspar and quartz (Fig. 3-5)

All over in the Sarrabus unit the end of this volcanic activity is marked by rhyolite–rhyodacite lavas, ignimbrites and tuffs, with a combined thickness of less than 100 m, metadacite products occur as sparse dykes and sills (465.4 ± 1.4 Ma, U–Pb zircon age; Oggiano et al., 2010) within the pre-Sardic sequences, and they are inferred to be the feeder dykes of the Porfidi grigi del Sarrabus.

The contact between the volcanic complex and the bottom of sequence (Arenarie di S.Vito) is characterized by the Sarrabese unconformity, derived by the Caledonian orogeny in Sardinia expressed by the Sardic phase (Calvino, 1959).

Fig. 3-5 Outcrop of the Porfidi Grigi del Sarrabus

3.1.1.1.1.1.1 P.ta Serpeddì Formation

It is constituted by 200 m of platform detrital-terrigenous deposits (Loi et al., 1992) of Caradoc, transgressive over the volcanic products (Porfidi Grigi). The formation has been subdivided into three members (Loi, 1993): i) Bruncu Spollittu Mb. at the bottom constituted by conglomerates and coarse sandstones with important placers of heavy minerals (Fig. 3-6); ii) Sa Murta Mb. is formed by decameters thick strata of fine quartz-conglomerates interlayered with microconglomerates to siltites strata; iii) Bruncu de Is Mallorus Mb. is constituted mainly by fine sandstones and coarse siltites with associated heavy minerals strata, by faunistic association it has been attributed a Caradocian age (Barca & Di Gregorio, 1979).

Fig. 3-6 Basal conglomerate with thin heavy mineral layers of the Br.cu Spollittus Mb in the P.ta Serpeddì Fm. near Dolianova.

3.1.1.1.2 Volcanic samples from Sarrabus unit.

The SM-200 sample and the BS-125 are volcanic rocks collected from “Porfidi grigi del Sarrabus” formation.

The SM-200 sample crops out ca. 1,5 km NE to the Dolianova village (see coordinates in the Tab. 3-1). The BS-125 sample crops out ca. 6 km NNE to the Burcei village (see coordinates in the Tab. 3-1). The geochemical data are reported in the Table 1 in the Annexes section.

Plotting the alkali vs. silica into the TAS diagram (Total Alkali Silica, Le Bas et al., 1986) where has been reported the Irvine and Baragar line (1971) the red color, the two samples fall in the dacite field, in the subalkaline field, falling under the red line (Fig. 3-7). Plotting the K_2O versus SiO_2 (Fig. 3-8) the SM-200 sample falls in the High-K cal-Alkaline filed and the BS-125 sample falls in the shoshonitic series.

Plotting the samples in the Cabanis and Lecolle (1989) tectonic diagram (Fig. 3-9) the volcanites have been generated in a calc-alkali setting and projecting the Zr/Y vs Zr in a Pearce et al., (1984) tectonic diagram, all the two samples show a within plate formation (Fig. 3-10).

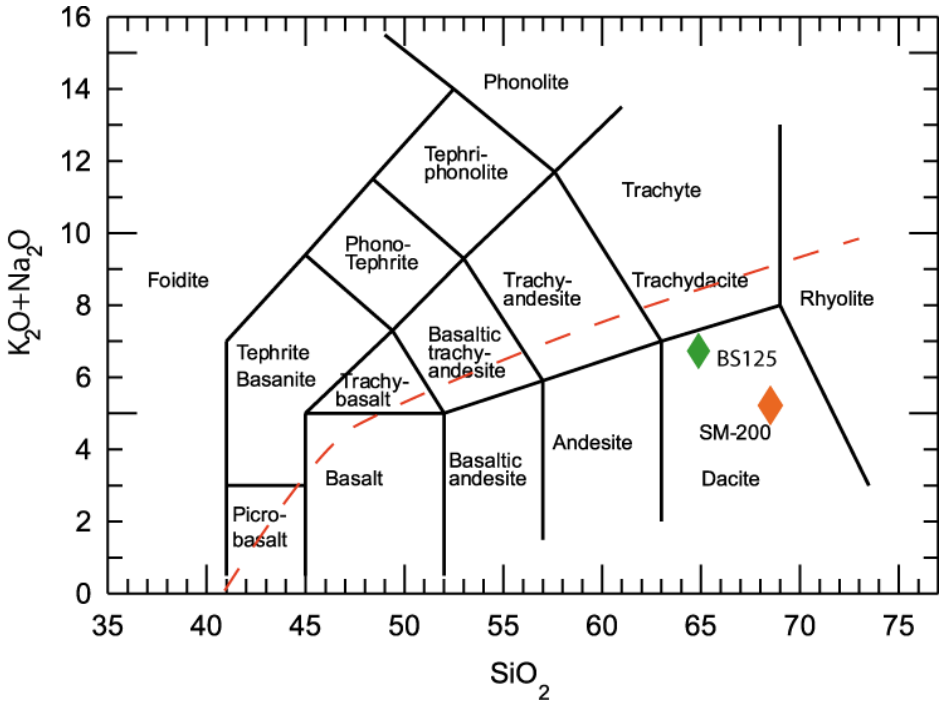

Fig. 3-7 TAS classification diagram with Irvine and Baragar (1979) line (in red) that subdivided the subalkaline from the alkaline field where the SM-200 and the BS-125 samples in the dacite field.

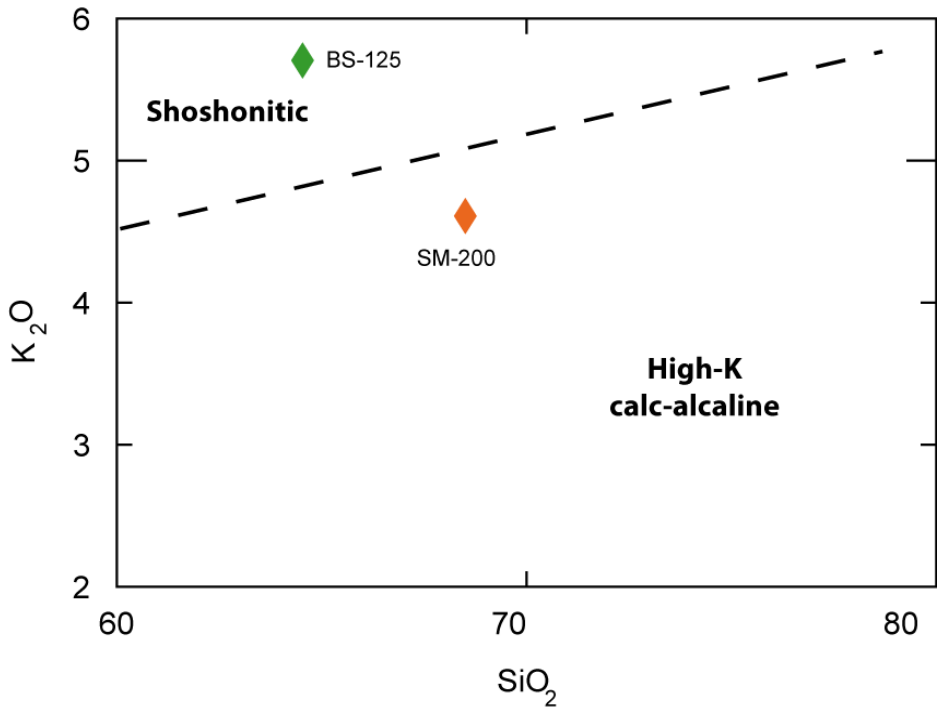

Fig. 3-8 K_2O versus SiO_2 plot showing the High-K calcalkaline signature of the Sarrabus U. volcanic samples.

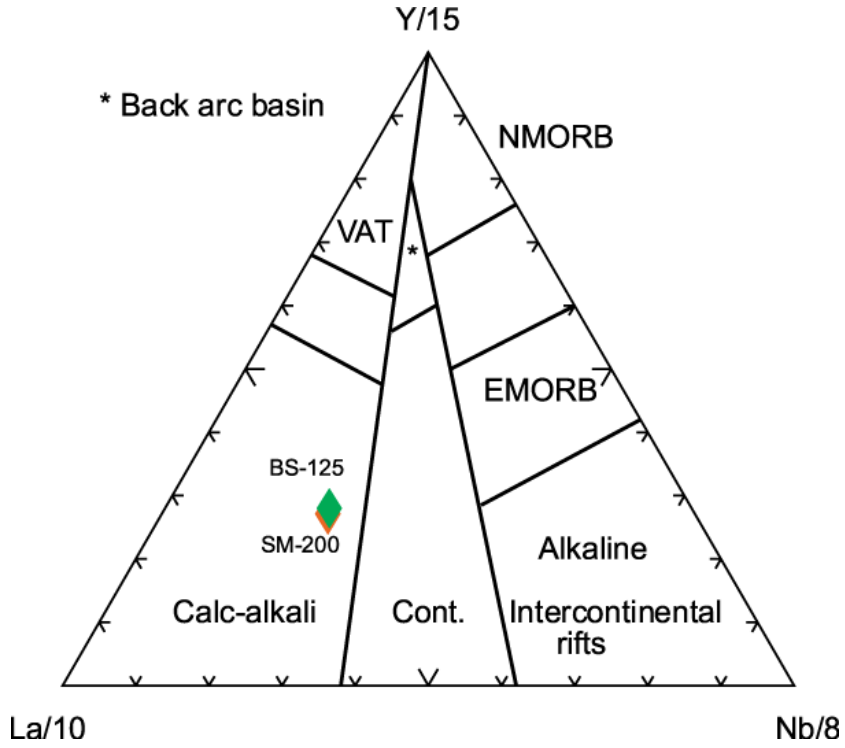

Fig. 3-9 Cabanis and Lecolle (1989) tectonic diagram showing the main formation filed of samples: the volcanic samples from Sarrabus U. (BS-125 and SM-200) fall in the Calc-alkali field.

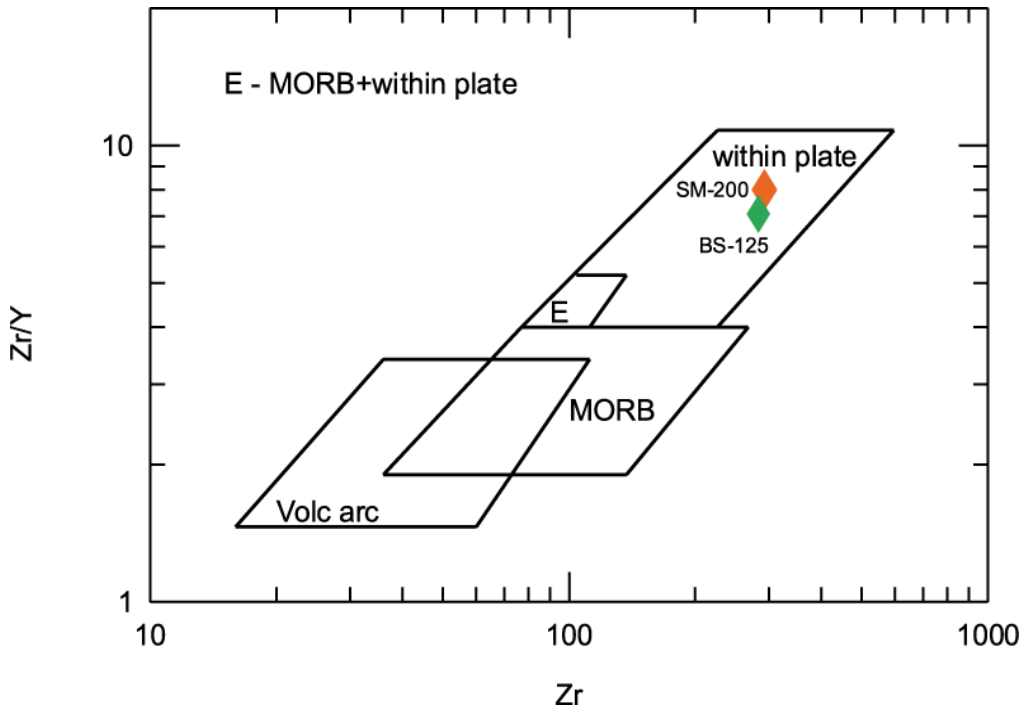

Fig. 3-10 Pearce et al., (1984) tectonic diagram showing a within plate formation for the Sarrabus U. volcanic samples.

Chondrite-normalized rare earth patterns (Sun and McDonough, 1989) of the Sarrabus volcanic samples volcanic samples show the same trend with LREE-enriched with flat-decreasing HREE and with a systematically negative Eu anomaly (Fig. 3-11a) linked to the fractionating plagioclase process.

In the multi-elements diagram primitive mantle-normalized (Sun and McDonough, 1989, Fig. 3-11b) the volcanic Sarrabus U. samples show an enrichment and of large ion lithophile elements (LILE) with a strong positive anomaly in Cs, the SM-200 shows a decreasing in Ba than the other sample, is evident an impoverishment of high field strength elements (HFSE). The strong negative anomalies have shown by Nb, Sr, and Ti. All over negative anomaly of Sr could be linked to the plagioclase fractionating.

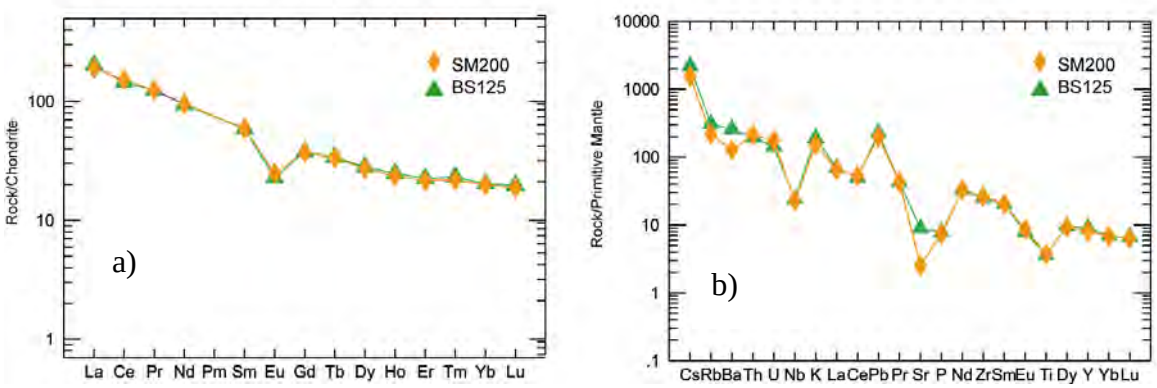

Fig. 3-11 Trace element spiders (Sun and McDonough, 1989) for Sarrabus volcanites (SM-200 and BSE-125); a) REE patterns normalized to chondrite and b) multi-element diagram normalized to primitive mantle.

3.1.1.1.2.1.1 U-Pb isotopes

From the Sarrabus U. SM-200 sample ca.100 zircon grains have been analyzed under optical microscope. Two main groups have been distinguished following Pupin classification (1980): a P-typology with elongated morphology, and a second group of S-typology. The majority of grains show the main length of 150 µm and are euhedral and prismatic with strong magmatic zonation (zircon L1-50; Fig. 3-12). The majority of cores found have given similar age respect of the rimes (zircons L1- 53, L1-71; Fig. 3-12). Ten zircon grains defined a $^{206}Pb/^{238}U$ weighted average age of 458.7 ± 2.8 Ma (Fig. 3-12; Tab. 2 Table 2 in Annexes).

a)

b)

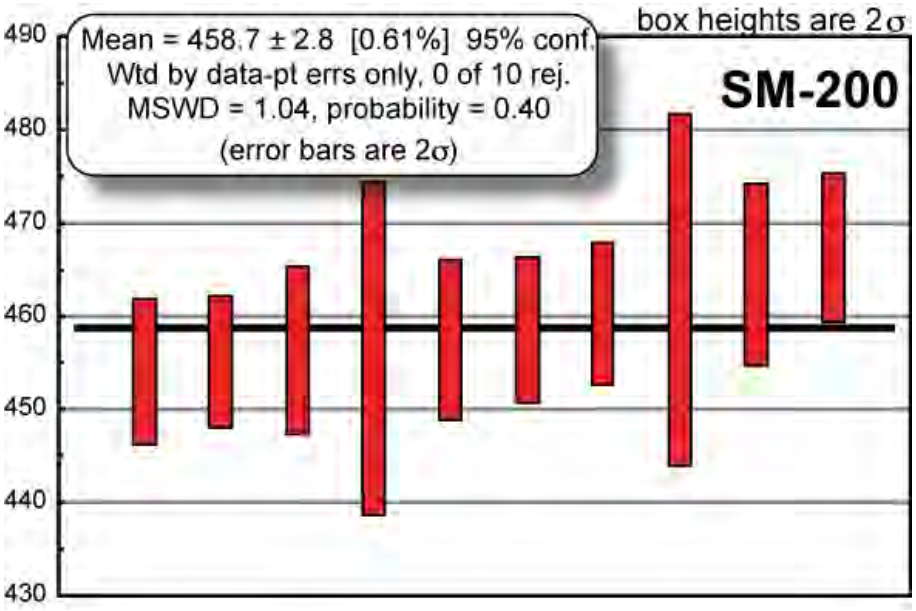

Fig. 3-12 Zircons CL images and $^{206}Pb/^{238}U$ age of SM-200 sample belonging to the Sarrabus U. a) CL zircon images from SM-200 sample showing the inner structures of zircons L1-53, L1-50, L1-71; b) $^{206}Pb/^{238}U$ of SM-200 sample gives an average age of 458.7 ± 2.8 Ma.

From the Sarrabus U. BS-125 sample ca.100 zircon grains have been analyzed under optical microscope. Two main groups have been distinguished following Pupin classification (1982): a P-typology with elongated morphology, and a second group of S typology. The majority of grains show the main length of 100 µm and are euhedral to sub-euhedral (CL images of zircon S L3-75, L3-77, L3-82; Fig. 3-13a) with magmatic zonation, also metamorphic inner structures have been observed. Six zircon grains defined a $^{206}Pb/^{238}U$ weighted average age of 464.6 ± 7.3 Ma (Fig. 3-13; Table 2 in Annexes 2).

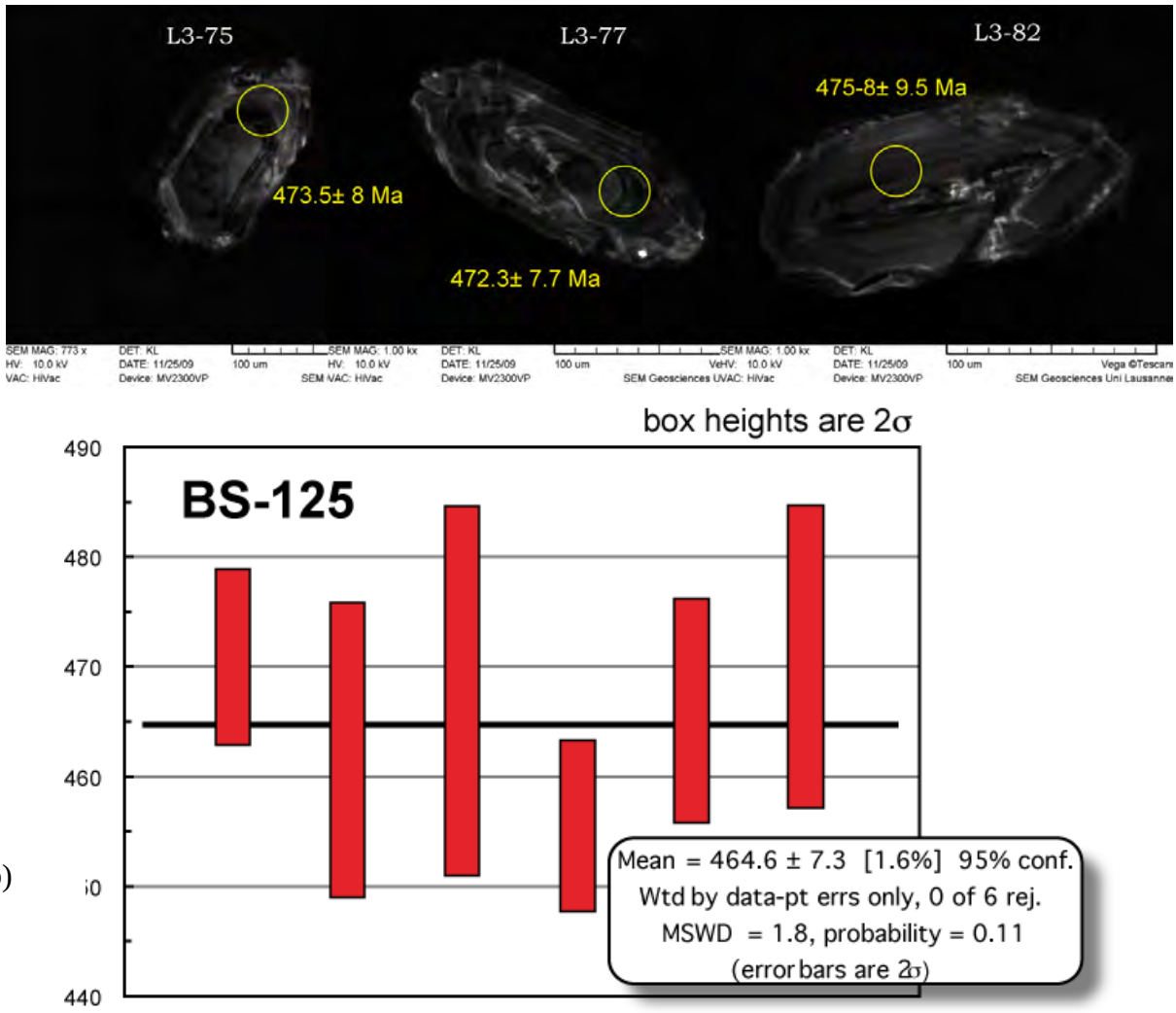

Fig. 3-13 Zircons CL images and $^{206}Pb/^{238}U$ age of BS-125 sample belonging to the Sarrabus U.; a), CL zircon images the inner structures of zircons L3-75, L3-77, L3-82; b) $^{206}Pb/^{238}U$ of SM-200 sample gives an average age of 464.6 ± 7.3 Ma.

3.1.1.1.3 Sedimentary sample from Sarrabus unit

The SST-5100 sample belongs to the Punta Serpeddì Fm. cropping out ca. 2.5 km NNE from Dolianova village (see coordinates in Table 3.1).

The deposit is composed by fossiliferous terrigenous sediments that were deposited in a littoral environment under storm influente (Loi et al., 1992). They are mainly coarse to fine-grained wackes. Quartz (33-73%), albite and orthoclase (0-10%), and lithic fragments (1-31%) are the main clastic components. This age is Middle-Late Ordovician.

This sequence is associated to the thick sequence of metamorphosed calcalkaline volcanic rock (SM-200 and BS-125 samples).

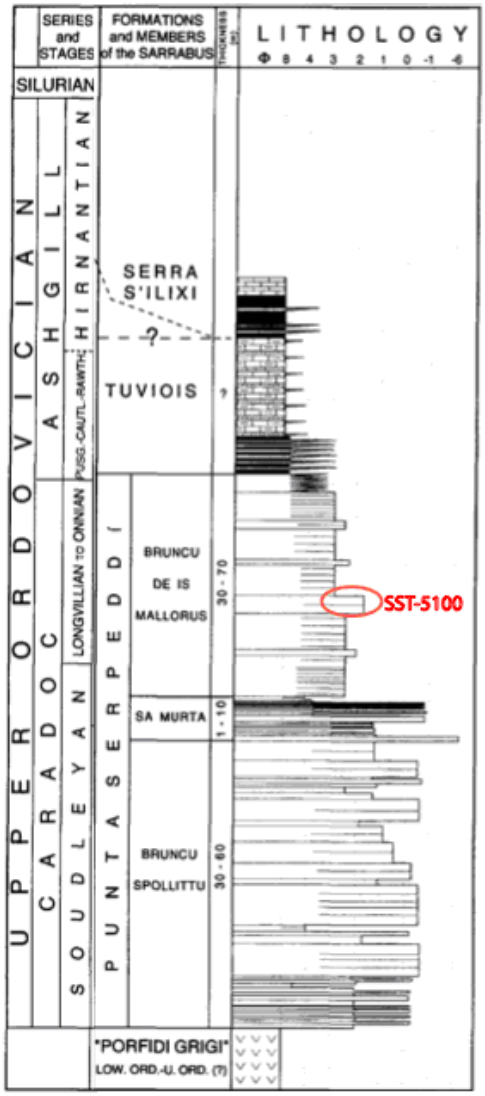

Fig. 3-14 Upper Ordovician successions in the Sarrabus areas. Geometric scale is expressed in Phi units (From Loi & Dabard, 1997). The samples analyzed are marked with the red circle.

3.1.1.1.3.1 Zircon study

Almost 100 zircons have been analyzed and observed under optical microscope, they show from sub-euhedral to rounded shape with main length around 100 mμ, but also grains up to 200 mμ have been found. Two groups of zircon have been observed: one group is characterized by the smallest and more rounded zircons (Fig. 3-16, zircon z62b) with colour from pinkish to brownish, due likely to hydrothermal alteration or metamicsation; a second group is less rounded (Fig. 3-16, zircon z9 and z90) and is characterized by bigger sizes and by is colourless. By BSE imaging (Fig. 3-16a) zircons mainly appears without metamorphic structures, rare cores have been found. The majority of zircons are characterized by several micro-fractures, probably done by stress during the

sedimentary cycles, and inclusions. Some inclusions (Fig. 3-16) have been analyzed by electron microprobe and reveal all over peaks of Al, Na, K, Fe suggesting an alluminosilicate origin.

3.1.1.1.3.1.1 U-Pb isotopes

Seventy U-Pb analyses (Table 2 in Annexes) on single grains from the SST 5100 sample were performed and reported in the Concordia diagram (Wheterill, 1956; Fig. 3-15b). They are concordant except for some slightly discordant Paleoproteroic zircons. The age spectra is spanned between ca. 400 Ma and 2,000 Ma.

The frequency density histogram (Fig. 3-17) shows a polymodal distribution with a main population between 360 Ma and 750 Ma (84% of all zircons) with a main peak at 441 Ma. Minor peaks at 1,000 and 1,900 Ma were also recognized.

3.1.1.1.3.1.2 Lu-Hf isotopes

In situ Hf isotope analyses on sixteen zircons (Table 3 in Annexes), representative of the different zircon populations have been carried out (Fig. 3-18).

Seven Early Ordovician- zircon grains between 432 and Ma and 474 Ma have negative εHf values ranging from 8.4 to -1.1 with Hf TDM model ages between 1.4 and 1.7 Ga.

Five Ediacaran zircon grains, with U-Pb age between 550 to 600 Ma, show negative εHf values ranging from −25.8 to -1.3. They have a TDM model ages between 2.8 and 1.5 Ga.

The Cryogenian zircon (U-Pb age of ~703 Ma) has a strong negative εHf of -36.3 and a Hf TDM model age of 3.4 Ga.

The Tonian age zircons, here represented by two Grenvillian zircons (U-Pb age of ~945 Ma), have positive εHf values (+7.4 to +9.9) and a Hf TDM model age 1.1-1.3 Ga.

The analysed Paleoproterozoic zircon grain (U-Pb age of ~2 Ga) shows a strong negative εHf value (εHf -12.5) and a Hf TDM model age of 3.2 Ga.

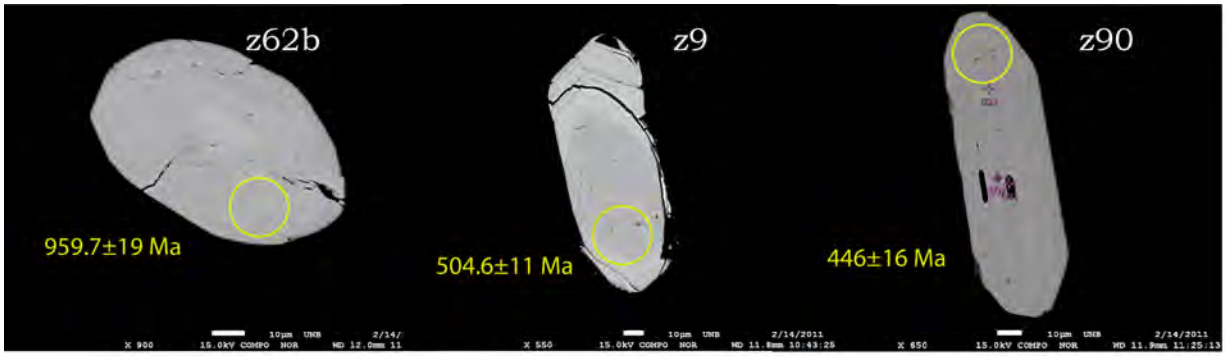

a)

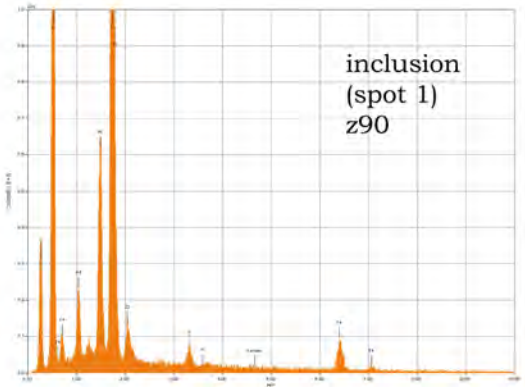

b)

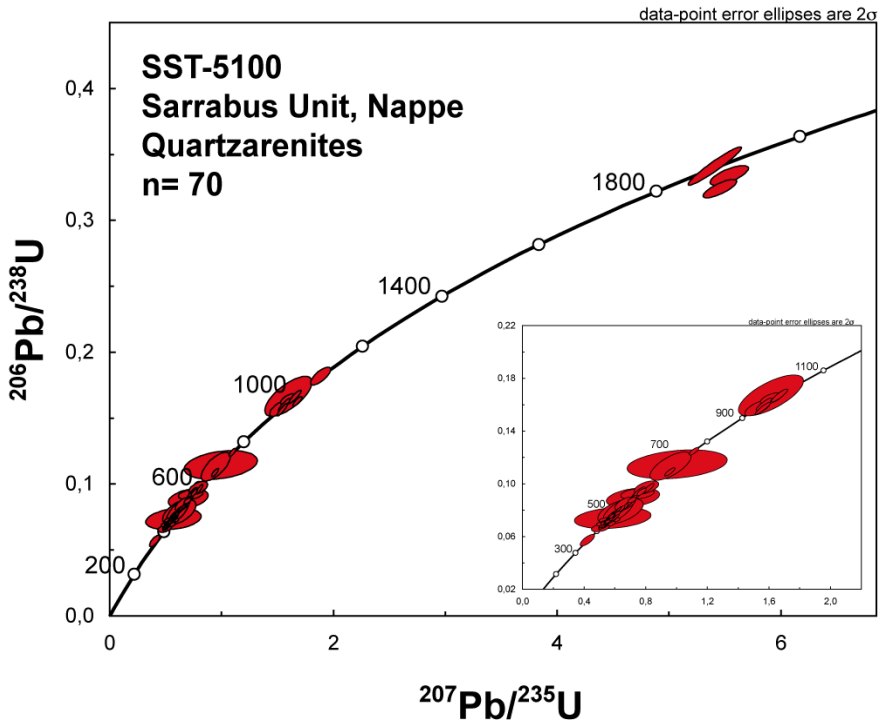

Fig. 3-16 BSE images and U-Pb ages from the SST-5100 sample. a) BSE images with zircons z62, z9 and z90 and relative spectrum of inclusion found in the z90; b) Concordia diagram (Wetherill, 1956) with manly concordant age spanned from ca. 400 Ma to 2,000 Ma.

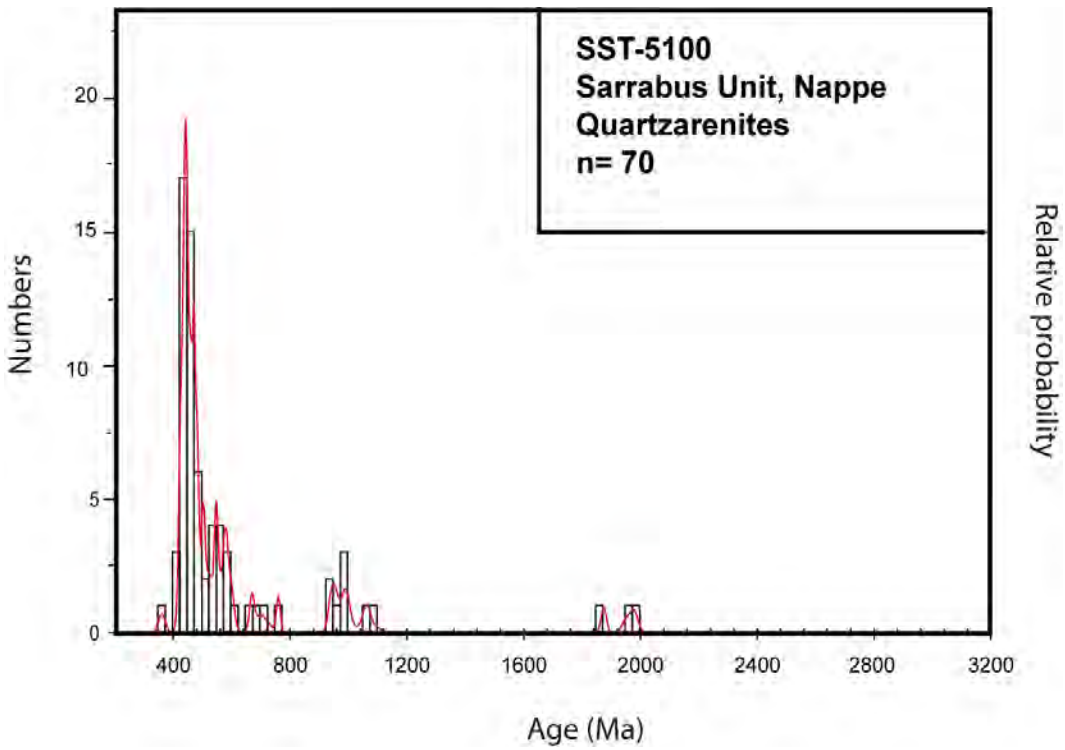

Fig. 3-17 U-Pb results shown in frequency histogram for the ST-5100 sample, for the younger ages (< 900 Ma) have been used the $^{238}U/^{206}Pb$ ratios and for the older have been used the $^{207}Pb/^{206}Pb$. The histogram shows a polymodal distribution of ages, with a main population between ca. 400 and 750 Ma.

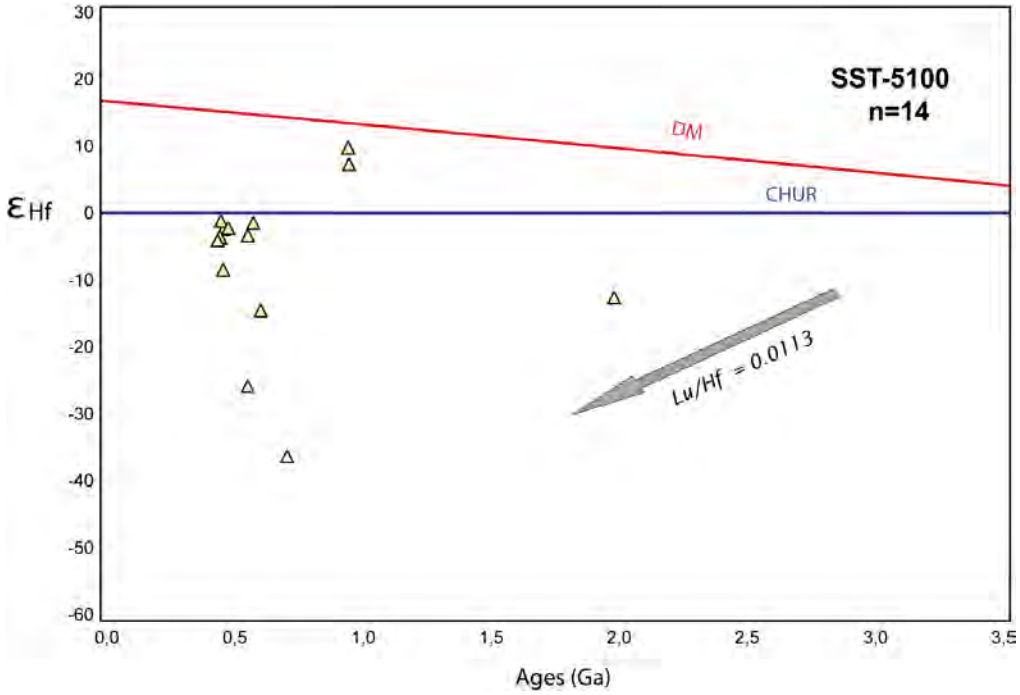

Fig. 3-18 Ages vs εHf values for the ST-5100 sample. The grey arrow represents a crustal evolution trend for Hf isotopic composition, calculated using $^{176}Lu/^{177}Hf$ = 0.0113 (Taylor and McLennan, 1985; Wedepohl, 1995).

3.1.1.1.4 Volcanic sample from the Arburese unit

The CC-150 sample is a metavolcanite of the from Arburese U., ("Porfidi grigi del Sarrabus") collected out near the Marceddì pond, ca. 5 km SE from the S. Antonio di Santadi village (see coordinates in the Tab. 3-1). Because the sample collected is too much alterated the WRA analyses have not been reported.

3.1.1.1.4.1 Zircon study

Almost 100 zircons analyzed show sub-euhedral to euhedral habitus with main length around 100 mμ. The zircons are pinkish to brownish, due likely to hydrothermal alteration or metamictisation. CL imaging (Fig. 3-19a) zircons show a strong magmatic zonation and rare cores.

3.1.1.1.4.1.1 U-Pb isotopes**.**

Of the five zircon grains analyzed (Table 2 in Annexes 2) by LA-ICP-MS, four zircons are concordant and show an age of 465.5 ± 5.4 Ma (Fig. 3-19).

a)

b)

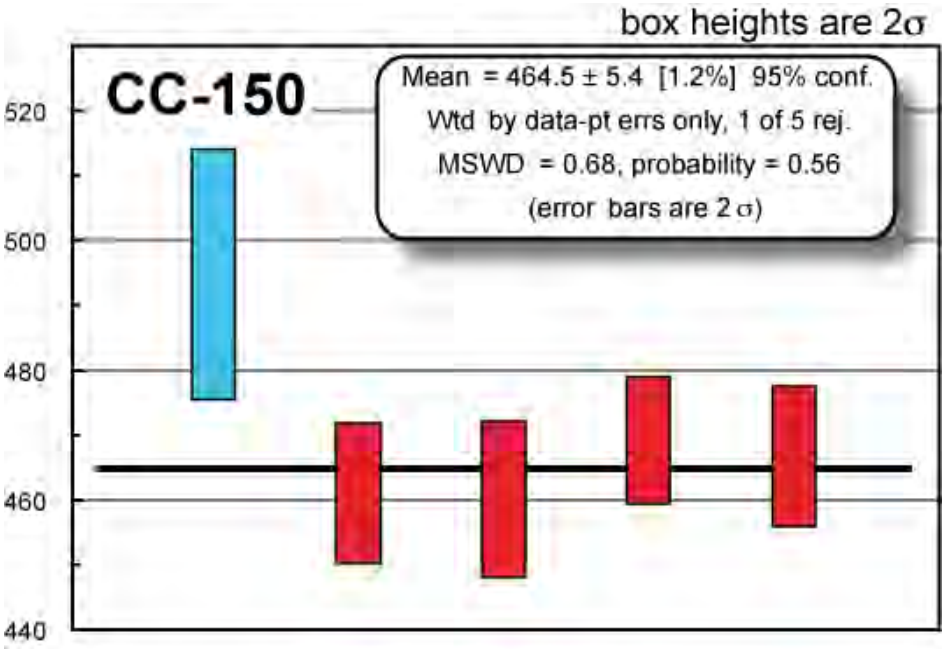

Fig. 3-19 Zircons CL images and $^{206}Pb/^{238}U$ age of CC-150 sample belonging to the Arburese Unit. a) CL zircon images the inner structures of zircons L3-61, L3-60, L3-57; b) $^{206}Pb/^{238}U$ of CC-150 sample gives an average age of 464.5 ± 5.4 Ma. The blue bars represents the rejected analysis.

3.1.1.2 BITHIA UNIT

The Bithia Tectonic Unit (Pavanetto et al. 2012) is a greenschist facies unit that contains at least three principal rock packages including: a metavolcanic sequence, a laminated sandstone and quartzite sequence, and a marble sequence. The primary bedding is not easy to distinguish and where present it has been strongly transposed into tectonic fabrics, so is not possible to have a realistic stratigraphic log.

Here will be described only the sequence from which the samples have been collected:

a) Metavolcanic sequence. These rocks crop out in some narrow strips close to the Capo Malfatano peninsula and Piscinnì bay, and they include some metavolcanic rocks that have not been previously recognized. The metavolcanic rocks have a recrystallized phyllitic matrix containing flattened but recognizable lithic clasts and relict pumice fragments aligned within the main tectonic foliation. The metavolcanic sequence contains interstratified clastic sediments, including conglomerate with clasts derived from the underlying volcanic rocks, and rare greywackes. The geometric upper part of the volcanic sequence consists of meta-igneous rocks with a phyllitic matrix and cm-size porphyroclasts of quartz and K-feldspar, with an "augen gneiss" texture. The authors (Tucci, 1983; Costamagna et al., 2008; Pavanetto et al., 2008) consider the metavolcanic

rocks of the BTU of calcalkaline affinity and include rhyolites, basaltic andesites, and high-K, high-Al basalts (Tucci, 1983; Costamagna et al., 2008). The volcanic rocks have been recently dated (Pavanetto et al. 2012) and give an Upper Ordovician age (U-Pb age of 457.01 ± 0.17).

b) Laminated sandstone & quartzite sequence. This unit crops out close to the metavolcanic sequence. It contains medium-grained sandstones with alternating mm-scale lamina of lighter quartz-rich zones and darker mica-rich zones. This layering may have been considered primary bedding by some authors (Junker and Schneider, 1983; Carosi et al., 1995). However others authors (Pavanetto et al., 2012) interpret this fine-scale compositional layering, which is parallel to a widespread tectonic foliation, as the product of metamorphic and deformational differentiation. The metasandstone sequence also contains rare marble layers less than 1 m thick.

The AF08-20 is a volcanic sample belongs to the Bithia U. cropping out along the SS195 coastal road near to the Chia Village (see coordinates in Tab. 3-1, Fig. 3-20). Here will be described the geochemical features, taking in account the recent U-Pb age data from literature. The geochemical data performed for these samples are reported in the Table 1 in the Annexes section.

Plotting the alkali vs. silica into the TAS diagram (Total Alkali Silica, Le Bas et al., 1986) where has been reported the Irvine and Baragar line (1971) the red colour, the sample falls in the dacite field, in the subalkaline field, falling under the red line. Plotting the K_2O versus SiO_2 (Fig. 3-21) the AF08-20 sample falls in the High-K calalkaline field.

Plotting the samples in the Cabanis and Lecolle (1989) tectonic diagram (Fig. 3-23) the volcanite has been generated in a calcalkaline setting.

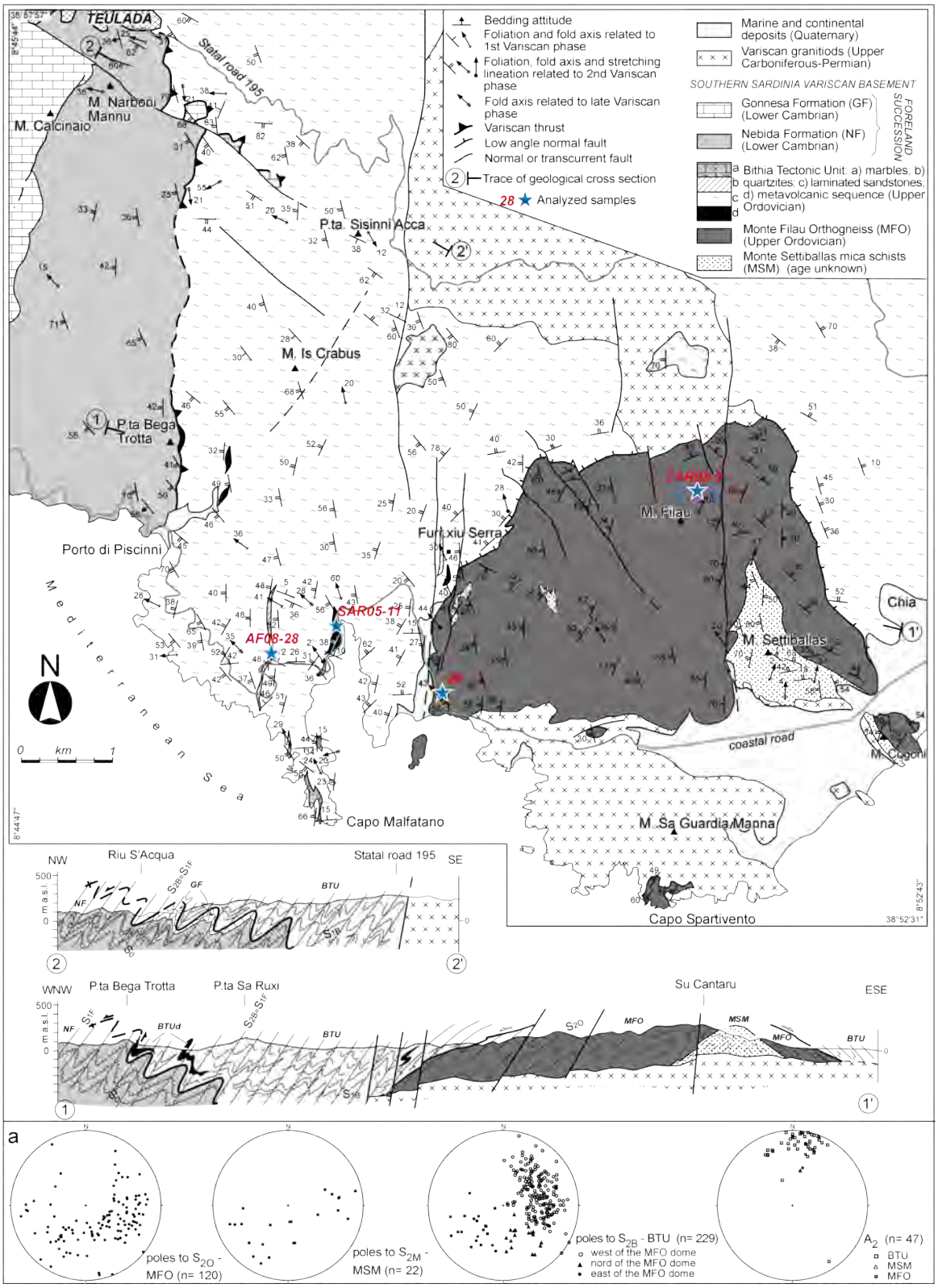

Fig. 3-20 Geological map of the Spartivento area, where the Bithia unit crops out with some of the analyzed samples (after Pavanetto et al., 2012).

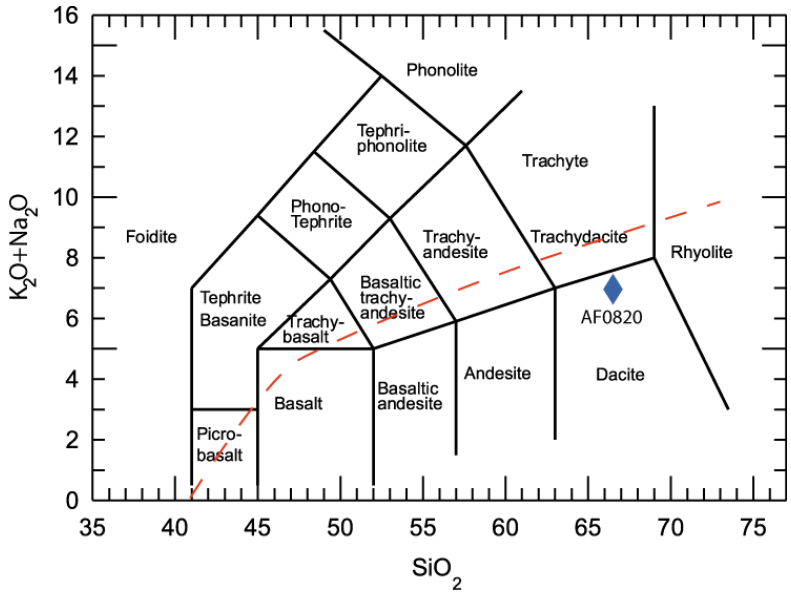

Fig. 3-21 TAS classification diagram with Irvine and Baragar (1979) line (in red) that subdivided the subalkaline from the alkaline field where the AF08-20 samples in the dacite field.

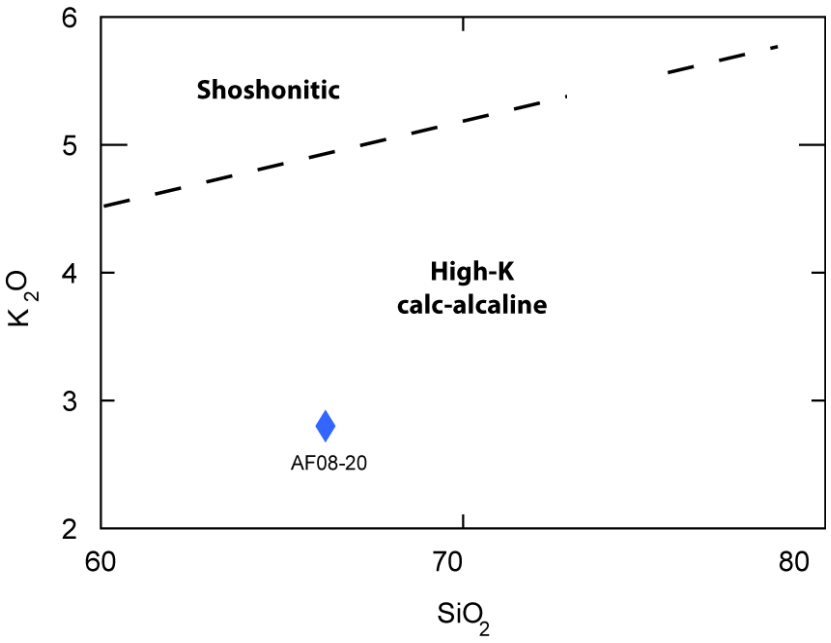

Fig. 3-22 K_2O versus SiO_2 plot showing the High-K calcalkaline signature of the Bihia U. volcanic sample.

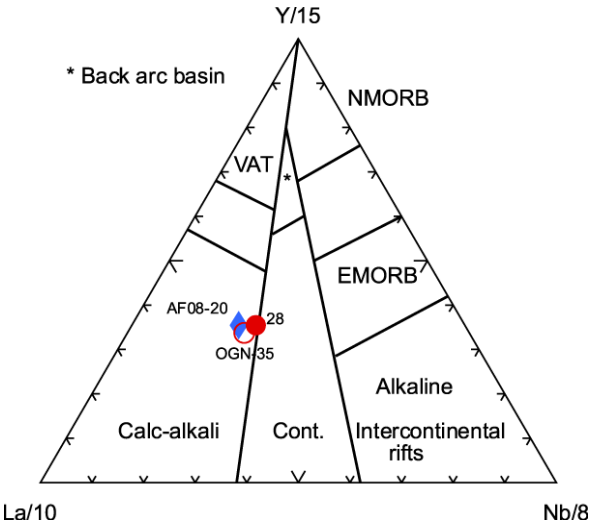

Fig. 3-23 Cabanis and Lecolle (1989) tectonic diagram showing the main formation of sample: the volcanic samples from Bithia U. (AF08-20) falls in the Calc-alkali field.

Chondrite-normalized rare earth patterns (Sun and McDonough, 1989) of the Bithia U. volcanic sample show a trend with are LREE-enriched with flat-decreasing HREE and with a systematically negative Eu anomaly (Fig. 3-24a) linked to the fractionating plagioclase process.

In the multi-elements diagram primitive mantle-normalized (Sun and McDonough, 1989, Fig. 3-24b) the volcanic Bithia U. sample show an enrichment and of large ion lithophile elements (LILE) with a strong positive anomaly in Cs, is evident an impoverishment of high field strength elements (HFSE). The strong negative anomalies have shown by Nb, Sr, and Ti. All over negative anomaly of Sr could be linked to the plagioclase fractionating.

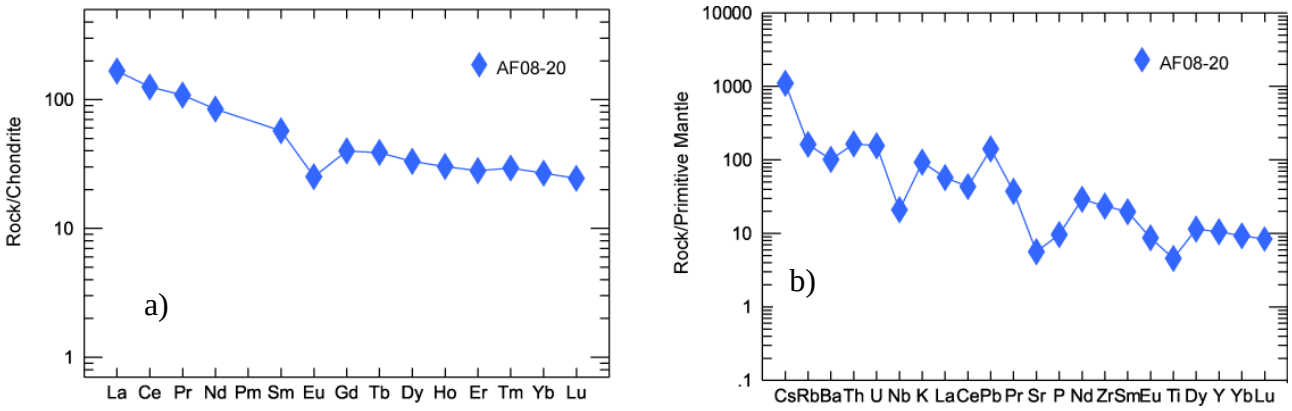

Fig. 3-24 Trace element spiders (Sun and McDonough, 1989) for Sarrabus volcanites (SM-200 and BSE-125); a) REE patterns normalized to chondrite and b) multi-element diagram normalized to primitive mantle.

3.1.1.2.1 Sedimentary sample from Bithia Unit

The AF08-28 sample is a quartzarenite belongs to the *laminated sandstone & quartzite sequence of the* Bithia U. the cropping out in the SS195 coastal road (see coordinates in Tab. 3-1, Fig. 3-20).

3.1.1.2.1.1 Zircon study

Almost 100 zircons have been analyzed and observed under optical microscope. Zircons are pinkish to colourless, sub-euhedral (CL of zircon z36b, Fig. 3-25a) to rounded (CL of zircons z20b, z23 Fig. 3-25b) with main length around 150 mμ, but also grains up to 200 mμ have been found. The majority of zircons show fractures and inclusions, all over of apatite and some alumina-silicate (Fig. 3-25b). Even if the majority of zircons show magmatic zonations, some inherited cores are found (Fig. 3-25b) suggesting crustal recycling.

3.1.1.2.1.1.1 U-Pb isotopes

Seventy-two grains from AFO828 sample have been analysed (Table 2 in Annexes) and the results reported in the Concordia diagram (Wheterill, 1956). Zircons are concordant (Fig. 3-25c) except some slightly discordant Archean grains. The age spectra is spanned between ca. 500 Ma and 3,000 Ma.

a)

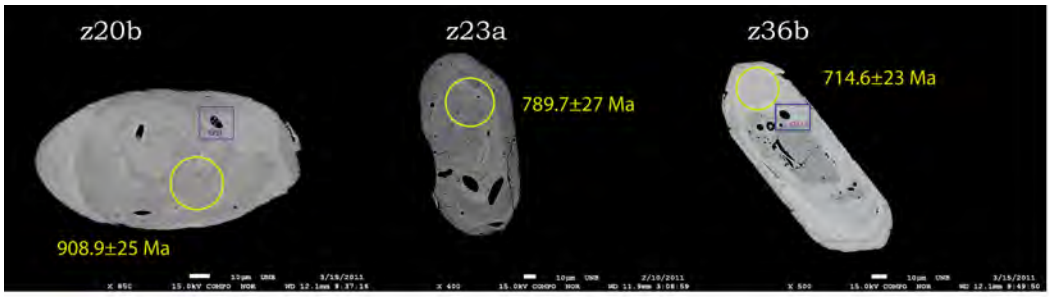

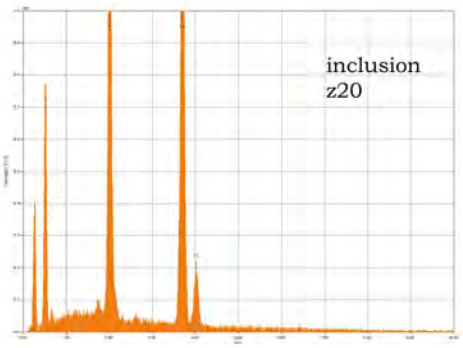

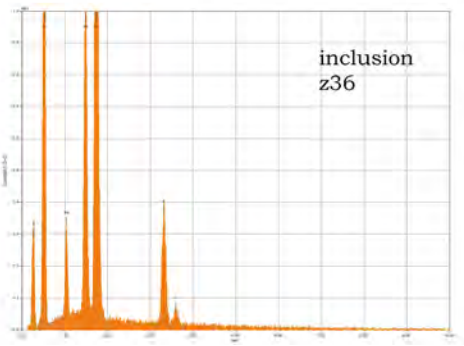

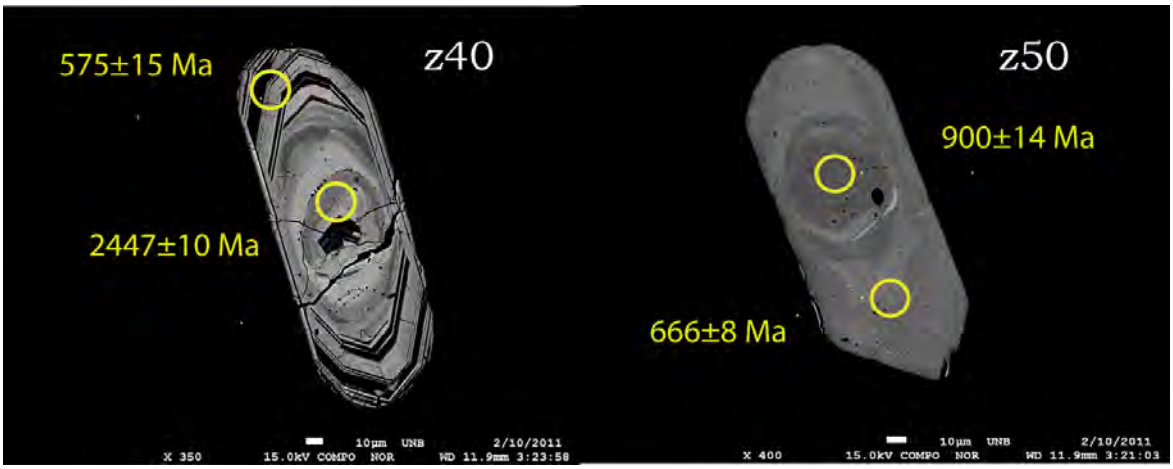

b)

c)

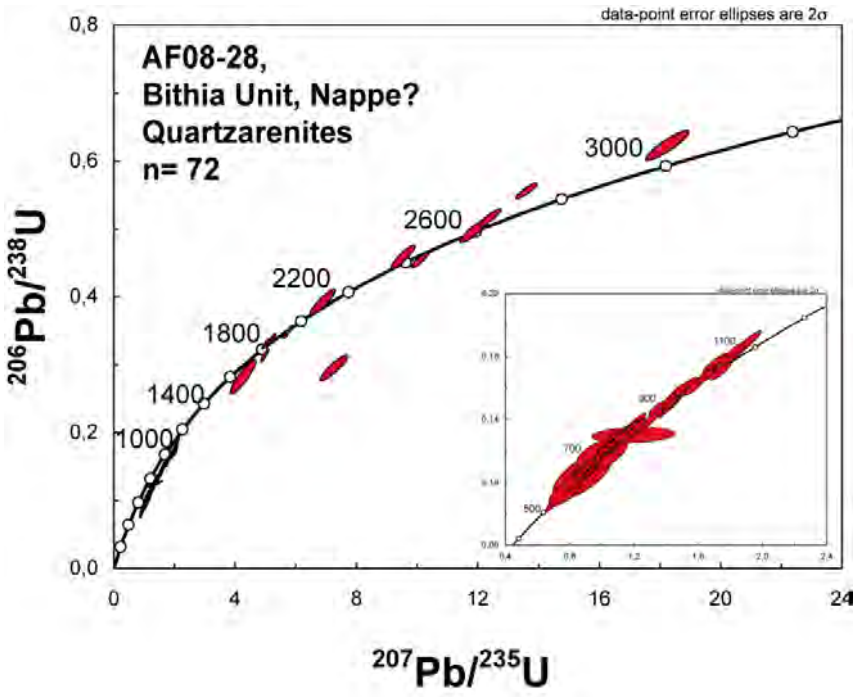

Fig. 3-25 BSE images and U-Pb ages from the AF08-28 sample. a) BSE images with zircons z20, z23, z36 and relative spectrum of inclusion found in the z20 and z36; b) BSE images with zircons z40 and z50 with examples of inherited cores; c) Concordia diagram (Wetherill, 1956) with manly concordant age spanned from ca. 500 Ma to 3,000 Ma.

The frequency histogram (Fig. 3-26) showing a polymodal distribution with two main populations with peaks at 660 and 736 Ma (ca. 45% of all zircons) and a third minor population with ages between 900 and 1,050 Ma. Other minor populations scattered between 1,768 Ma and 2,900 Ma are also recognized.

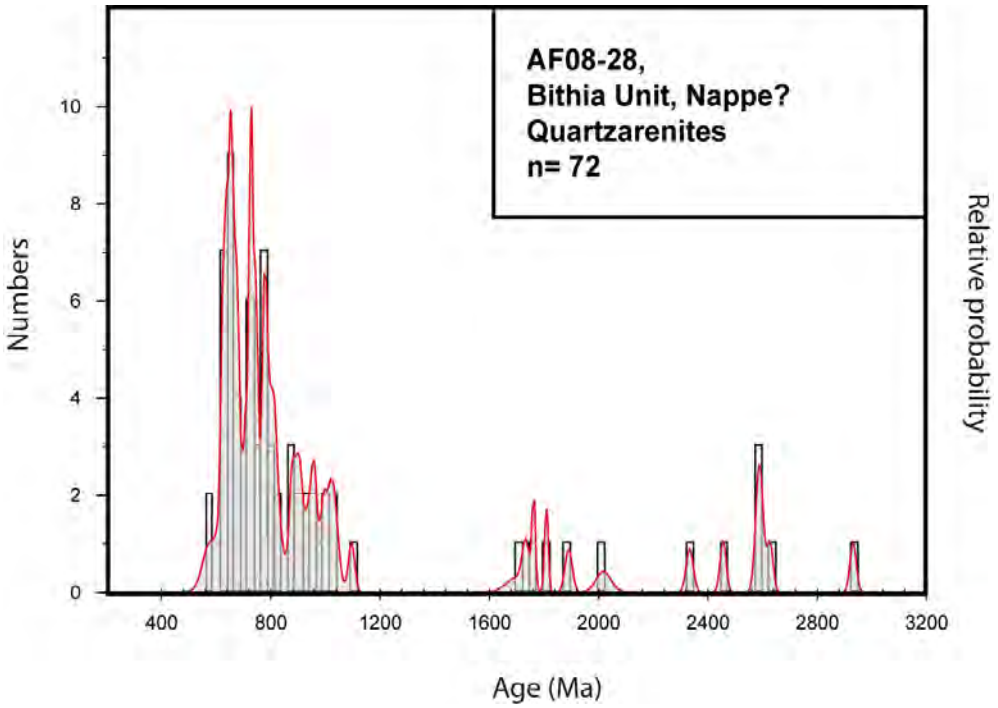

Fig. 3-26 U-Pb results shown in frequency histogram for the AF08-28 sample, for the younger ages (< 900 Ma) have been used the $^{238}U/^{206}Pb$ ratios and for the older have been used the $^{207}Pb/^{206}Pb$. The histogram shows a polymodal distribution of ages, with a main population between ca. 500 and 2,500 Ma.

3.1.1.3 MONTE FILAU ORTHOGNEISS

The 28 and OGN-35 (SAR05-09) are orthogneiss samples collected from the M. Filau Othogneiss., in the Capo Spartivento area (Fig. 3-20).

The sample 28 is a leucocratic orthogneiss sample cropping out in the coastal road SS195 near the Chia village (see the coordinates in Tab. 3-1); the sample OGN-35 is a leucocratic orthogneiss sample cropping out in the M. Filau near the Chia village (see the coordinates in Tab. 3-1).

The M. Filau Othogneiss is a classically interpreted as a structural dome (see the brief description in the paragraph about the Variscan Nappe zone). It derived from a granitic body (Mazzoli and Visonà, 1992) intruded in the Mt. Settiballas Micaschist and that either intruded into the BTU or was structurally juxtaposed with the BTU by ductile shearing, which resulted in the gneissic character of the rock. Two principal lithofacies can be distinguished (Mazzoli and Visonà, 1992; Carosi *et al.*, 1998): (1) medium to coarse grained biotite orthogneiss with an augen texture produced by large microcline or quartz phenocrysts and aggregates of microcline + quartz + oligoclase, generally over 1cm in size; and (2) finer-grained leucocratic orthogneiss that crops out as a border facies of the intrusion. The leucocratic gneiss is commonly present as centimetre to

metre-scale dykes and apophyses within the biotite orthogneiss. The granitic rocks of the MFO are peraluminous (Mazzoli and Visonà, 1992) to alkaline (Delaperriere and Lancelot, 1989), and likely reflect melting of the lower continental crust.

Up to now the age of the plutonic protolith(s) of the MFO has been debated. Some previous workers have proposed a Precambrian age (Junker and Schneider, 1983) based on stratigraphic correlations. Radiometric techniques have yielded inconsistent results, including 478 ± 16 Ma (Upper Ordovician) from multigrain U/Pb zircon analyses (Delaperriere and Lancelot, 1989), and 427 ± 33 Ma (Silurian) from Rb/Sr whole rock analyses (Cocozza et al., 1977). The age of the metamorphic event affecting the MFO has been estimated at 280 ± 4 Ma using the Rb/Sr isochron technique (Cocozza et al., 1977). The geochemical data performed for these samples are reported in the Table 1 in the Annexes section.

According to the Streckeisen classification (Fig. 3-27), the two samples (28 and OGN-35) fall in the monzogranite field showing a peraluminous composition (Shand diagram, 1929; Fig. 3-28). Plotting the SiO_2 vs K_2O compositions, the intrusive samples show an high-K calcalkaline signature with an high index of SiO_2 (values around 75) and K_2O values around 5. Plotting the samples in the Whalen et al., (1987) diagram is observed that the samples derivation from A-type granite type (Chappel and White, 1974; Fig. 3-30). Also plotting the two samples in the Y+Nb / Rb diagram (Pearce et al., 1984; Fig. 3-31) the samples fall in the within plate setting (WPG). Following Cabanis and Lecolle (1989), the setting is ambiguous for the sample 28 that falls between the continental and the calc-alkali fields, the sample OGN-35 falls in the calc-alkali field (Fig. 3-32).

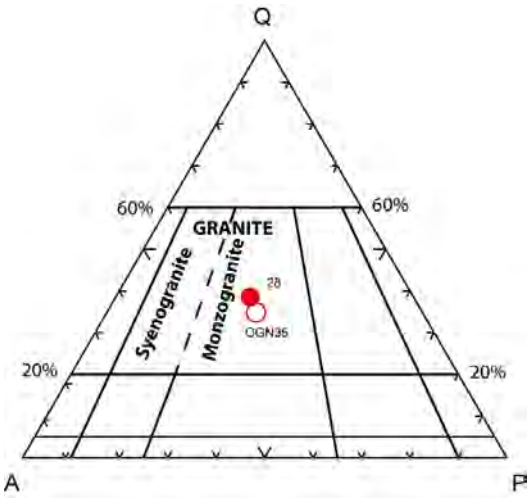

Fig. 3-27 Streckeisen diagram (1979), showing Sulcis intrusive samples (OGN-35 and 28) falling in the monzogranites field.

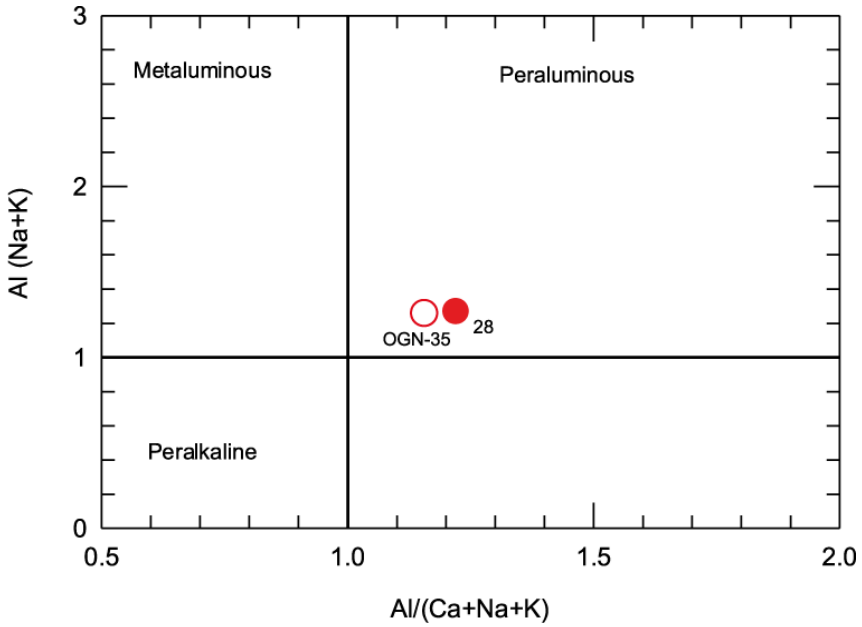

Fig. 3-28 Shand diagram (1929) where is shown the peraluminous features of Sulcis intrusive samples (OGN-35 and 28).

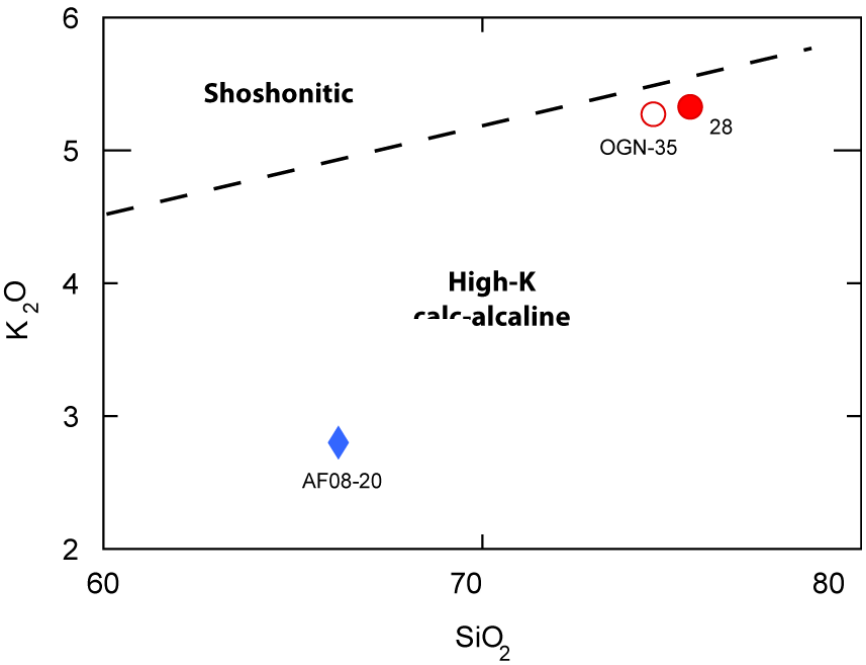

Fig. 3-29 K2O versus SiO2 plot showing the High-K calcalkaline signature of the Sulcis intrusive samples (OGN-35 and 28).

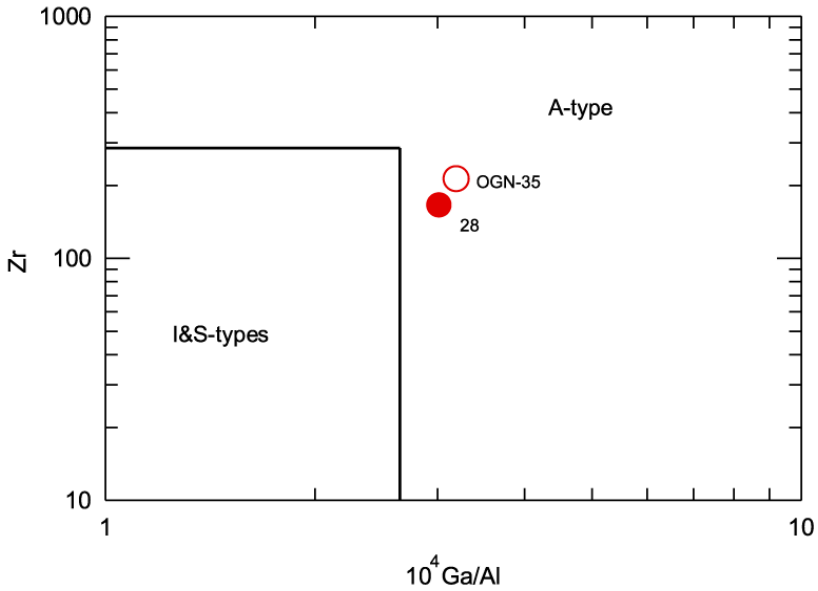

Fig. 3-30 Whalen et al., (1987) diagram showing granitoid type following the Chappel and White (1974) subdivision: the Sulcis intrusive samples (OGN-35 and 28) fall in the A-types.

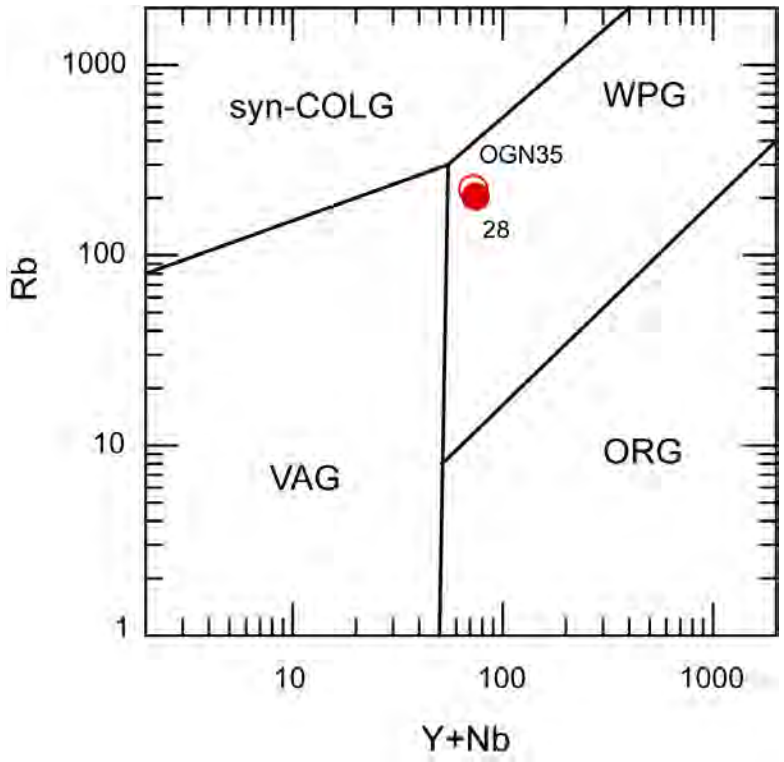

Fig. 3-31 Pearce et al., (1984) tectonic diagram suggesting the tettonic setting of the Sulcis granitic samples (OGN-35 and 28) like a within plate scenario (WPG).

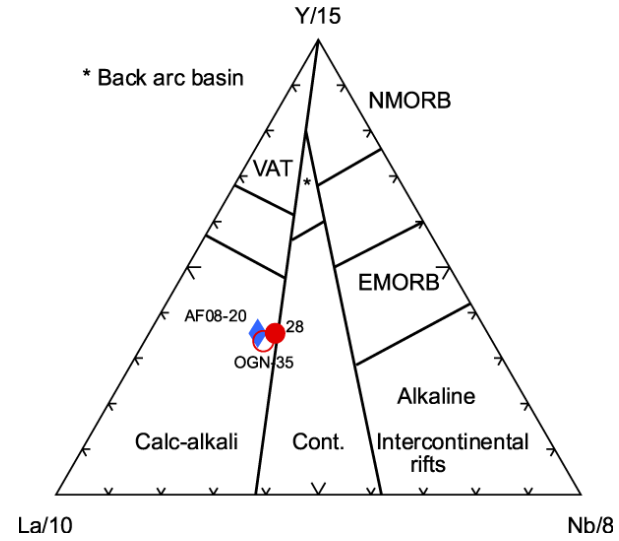

Fig. 3-32 Cabanis and Lecolle (1989) tectonic diagram showing the main formation scenario of samples: the setting is ambiguous for the sample 28 that is between falling in the continental and calc-alkali field, the sample OGN-35 falls in the calc-alkali field.

Chondrite-normalized rare earth patterns according Sun and McDonough (1989) (Fig. 3-33a) of the intrusive Sulcis samples are LREE-enriched with flat HREE with a systematically negative Eu anomaly linked to the important fractionating plagioclase process.

In the multi-elements diagram primitive mantle-normalized by Sun and McDonough (1989 (Fig. 3-33b) the intrusive Sulcis samples show an enrichment of large ion lithophile elements (LILE) and a deletion of high field strength elements (HFSE). Negative anomaly of Ba, Nb, Sr (P in 28 sample) and Ti has been shown. Negative anomaly of the Ba and Sr are linked to the plagioclase fractionating. The HREE show a flat trend.

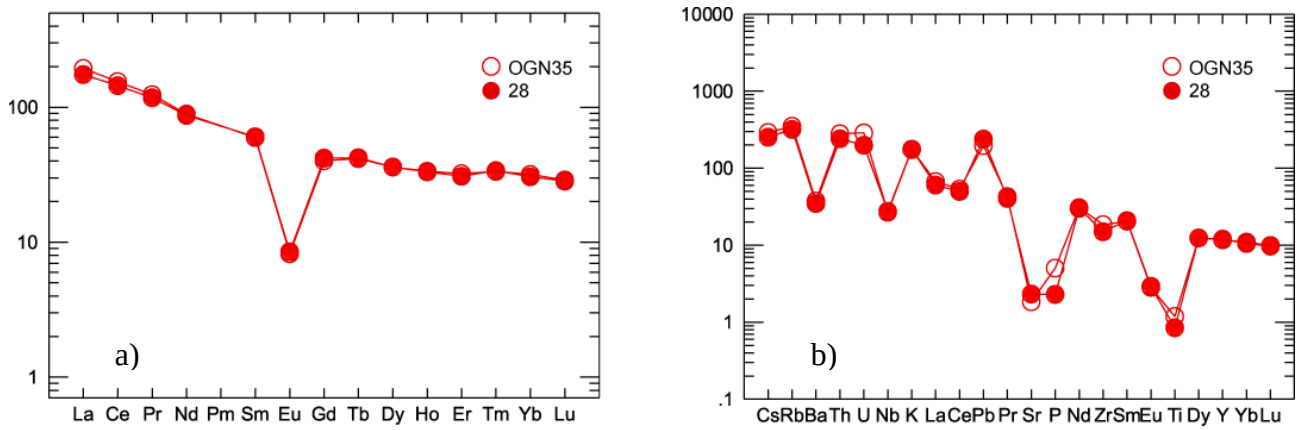

Fig. 3-33 Trace element spider diagrams (Sun and McDonough, 1989) for granitic Sulcis samples (OGN-35 and 28 samples): a) REE patterns normalized to chondrite and b) multi-element diagram normalized to primitive mantle.

3.1.1.3.1.1.1 U-Pb isotopes

From the SAR05-09 (OGN-35) and 28 samples have been observed almost 100 zircons showing maximum length reaching 200 µm. The majority of grains are euhedrals and with strong magmatic zonation (Fig. 3-34). Rare cores have been found. The 5 zircon grains from SAR05-09 (OGN-35) sample that given concordant $^{206}Pb/^{238}U$ ages show an average age of 462 ± 5.7 Ma (Fig. 3-34). Eleven U-Pb analyses on single grains from the 28 sample were performed (Table 2 in Annexes; Fig. 3-34). They are concordant and give an age of 459.6 ± 3.9 Ma (Fig. 3-35).

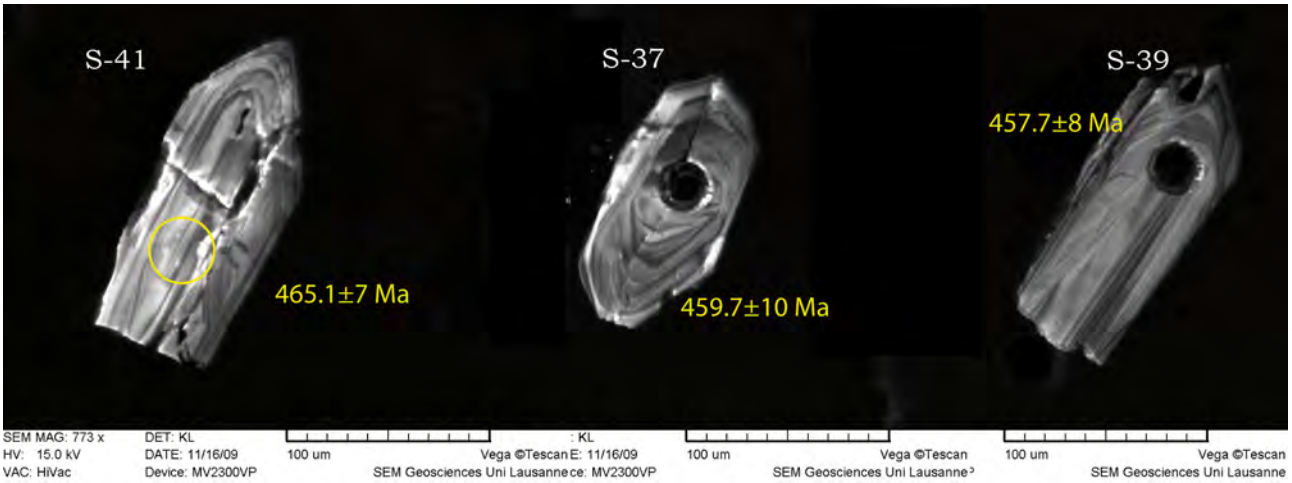

a)

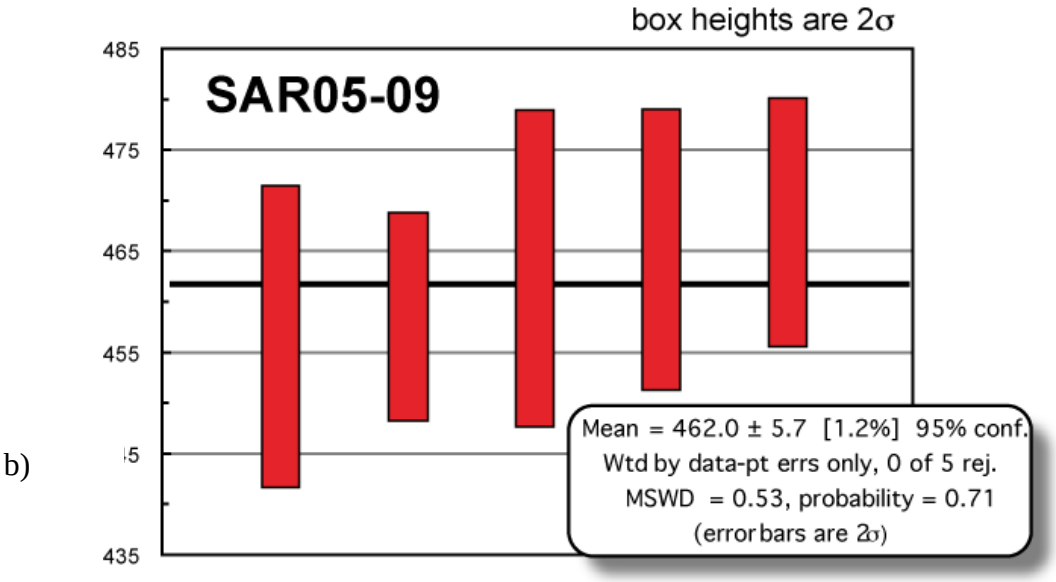

b)

Fig. 3-34 CL zircon images from SAR05-09 (OGN-35) sample. a) CL showing the strong magmatic zonation of S-41-S-37, S-39 zircons; b) $^{206}Pb/^{238}U$ of SAR05-09 (OGN-35) sample gives an average age of 462 ± 5.7 Ma.

a)

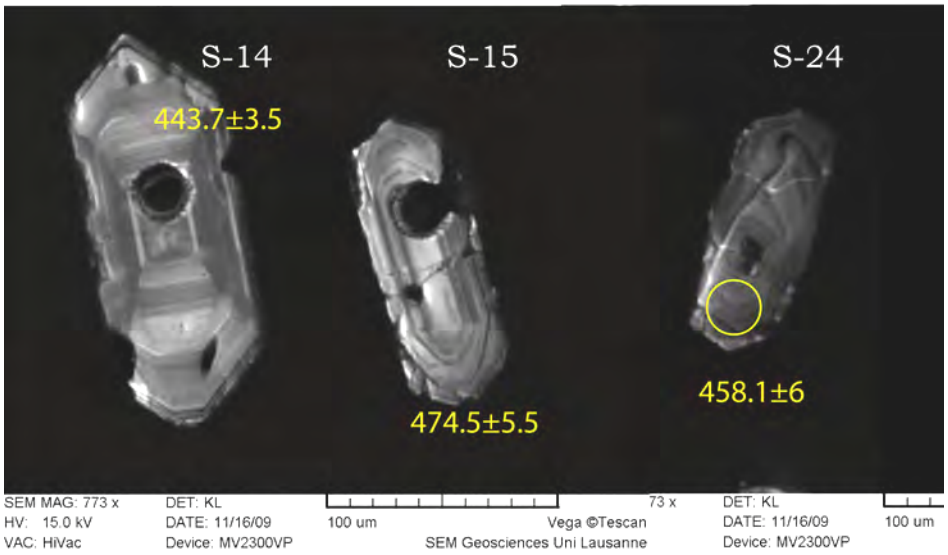

b)

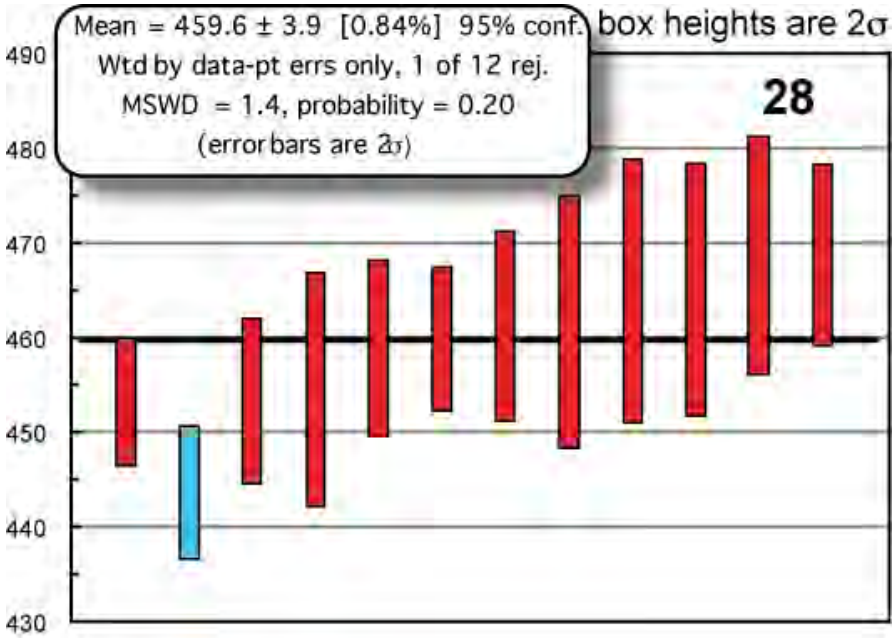

Fig. 3-35 CL zircon images from 28 sample a) CL showing the strong magmatic zonation of S-14-S-15, S-24 zircons; b), $^{206}Pb/^{238}U$ of 28 sample gives an average age of 459.6 ± 3.9 Ma. The blue bar represents the rejected analysis.

3.1.1.4 FORELAND ZONE

The Foreland Zone cropping out in the Iglesiente-Sulcis sub-region (SW Sardinia, Fig. 3-1) is characterized by a Palaeozoic succession dated by Cambrian to Devonian (Fig. 3-2). In the Foreland succession there is no occurrence of volcanic rocks. In the Foreland, the pre-Sardic sedimentary history is dominated by the deposition of epicontinental sediments (Nebida Group),

including carbonate shelf deposits (Gonnesa Group), which are inferred to grade laterally into deeper siliciclastic sequences (Iglesias Group), all of which are topped by the Sardic Unconformity. The sedimentary rocks of the shelf–slope transition indicate passive continental margin conditions during the Late Cambrian–Early Ordovician (Cocozza, 1979; Galassi and Gandin, 1992; Pillola et al., 1995, and references therein). Only the Capo Spartivento orthogneiss, basement of the Foreland, is referred to this setting on the basis of a doubtful date (478 ± 13 Ma, Delaperrière and Lancelot, 1988).

The post-Sardic succession in the Foreland starts with huge amounts of continental, alluvial, fan-related conglomerates (M. Argentu Formation; Martini et al., 1992), and these grade upwards into a trangressive sequence made up mostly of sandstone and silt of Katian–Hirnantian age. No volcanic rocks are found in this highstand episode of the post-Sardic phase.

After the Middle Ordovician emersion of this sector of the North Gondwana margin, a large-scale transgression marked the onset of a new sedimentary cycle in the Upper Ordovician (Katian–Hirnantian), which then continued through the Silurian and Devonian into the Early Carboniferous.

3.1.1.4.1 Sedimentary Foreland Zone sample

The CORI sample is a quartz-arenite belongs to a Cabitza Fm. cropping out in the Sulcis-Ig]esiente area (see coordinates inTab. 3-1). In the Sulcis-Ig]esiente area, the succession is continuous from the Caradoc to the uppermost Ashgill and comprises several mainly terrigenous lithostratigraphic units (Leone et al., 1991).

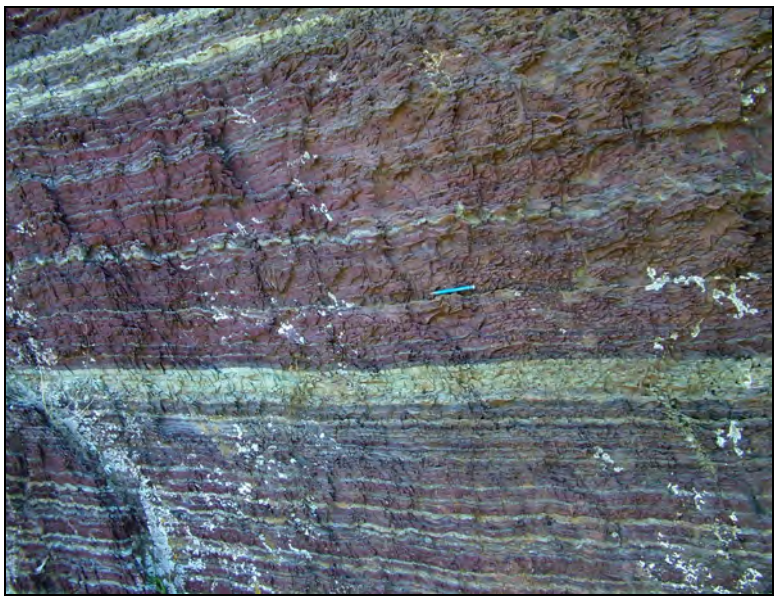

Fig. 3-36 Outcrop of the Cabitza Fm close to the location of sample CORI.

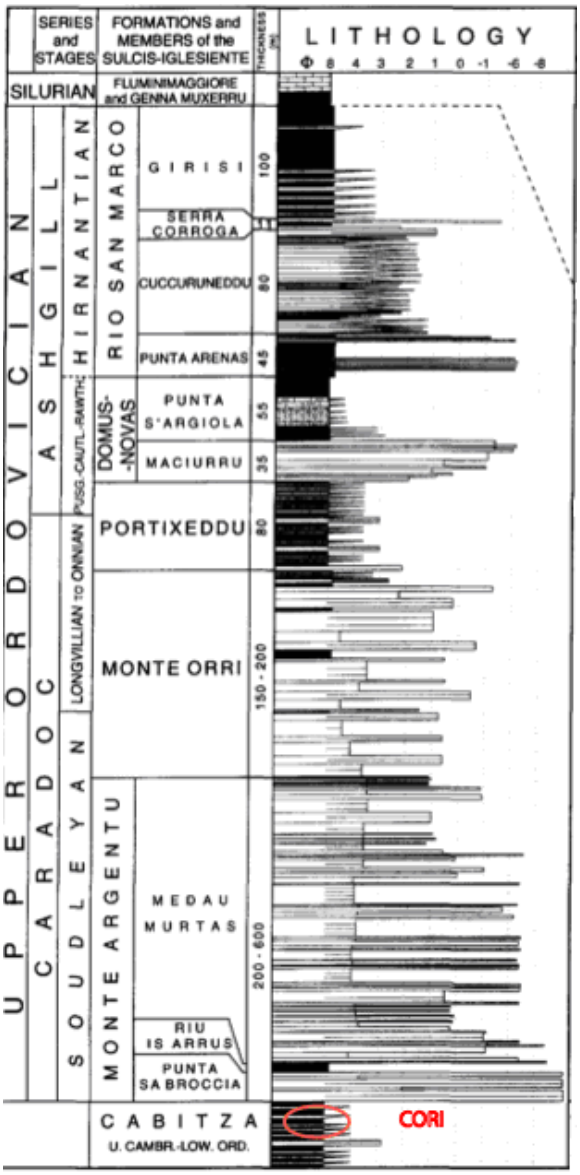

Fig. 3-37 Upper Ordovician successions in the Sulcis Iglesiente area. Geometric scale is exspressed in Phi units (After Loi & Dabard, 1997). The samples analyzed are marked with the red circle.

The Cabitza Formation (Cocozza, 1967) is Cambro-Tremadoc age (Pillola and Gutierrez Marco, 1988). These rocks are mainly terrigenous, comprising conglomerates, sandstones (quartzwackes, lithic wackes, and accessory quartz arenites), siltstones and shales. Sandstones contain 25-80% quartz, 0-4% albite, and 0-3% lithic fragments (Fig. 3-36). They plot in the field of sediments originating from the erosion of an internal craton (Loi & Dabard 1997).

3.1.1.4.1.1 Zircon study

Almost 100 zircons have been analyzed and observed under optical microscope. They are pinkish to brownish colour, sub-euhedral to rounded with main length around 150 mμ, also grains up to 250 mμ have been found. Some zircons show apatite inclusions (BSE of z26 show in Fig. 3-38). By BSE imaging (Fig. 3-38a) have been observed zircons with rare inherited cores.

3.1.1.4.1.1.1 U-Pb isotopes

Eighty-seven grains from CORI sample were U-Pb analyzed (Table 2 in Annexes). Results are reported in the Concordia diagram (Wheterill, 1956; Fig. 3.37b) that shows a concordant age pattern except for the oldest zircon ages. The age spectra is spanned between ca.450 Ma and 2500 Ma.

Projecting the data in a frequency histogram (Fig. 3-39) a bimodal distribution is shown, with a main population between 550 Ma and 1,200 Ma (ca. 50 of all zircons) with main peaks at 647 Ma, ~850 and ~1,000 Ma. Minor populations show ages spanned from 1,800 to 2,700 Ma.

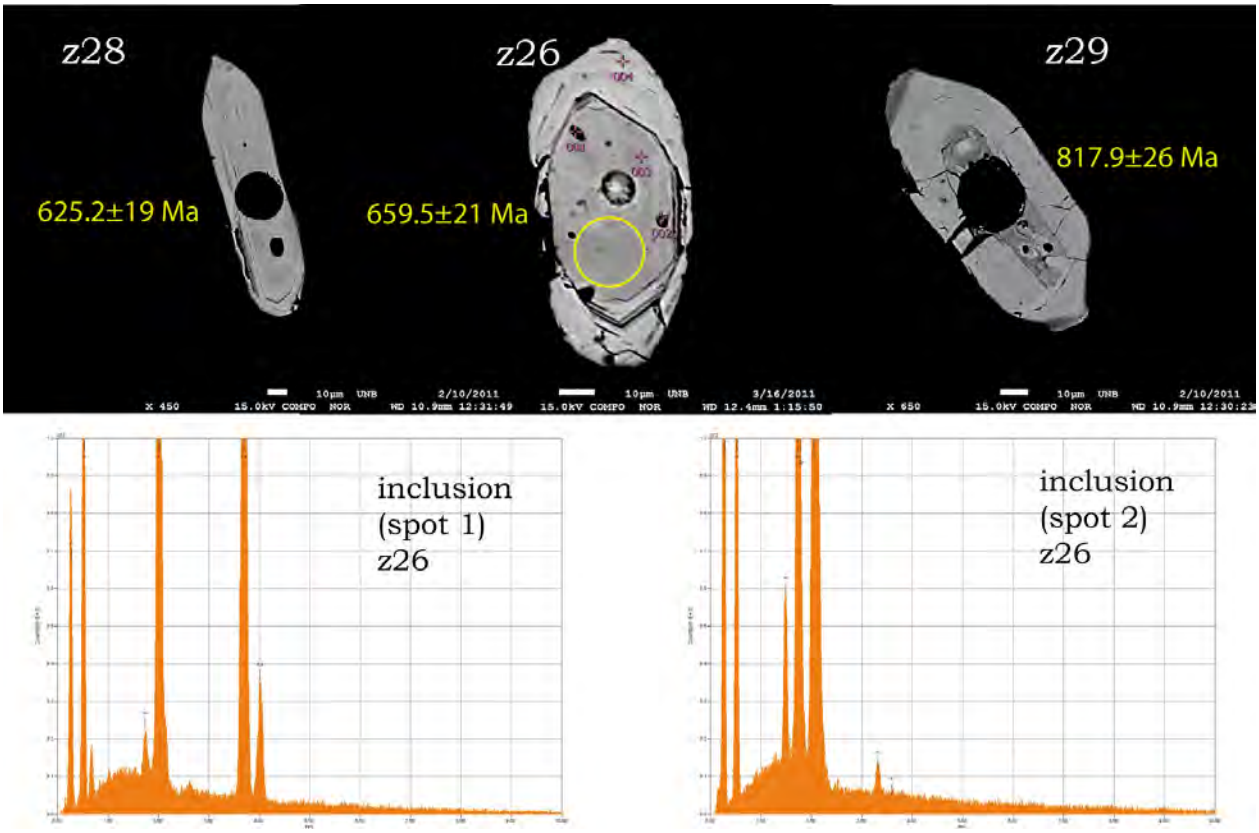

a)

b)

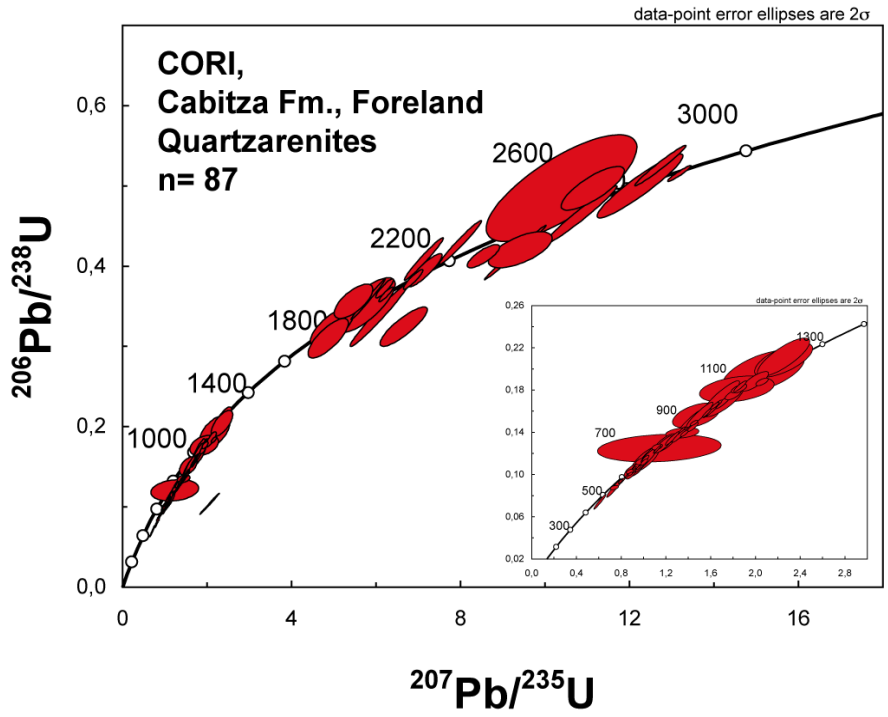

Fig. 3-38 BSE images and U-Pb ages from the CORI sample. a) BSE images with zircons z28, z26 and z29 and relative spectrum of inclusion found in the z90; b) Concordia diagram (Wetherill, 1956) with manly concordant age spanned from ca. 500 Ma to 2,500 Ma.

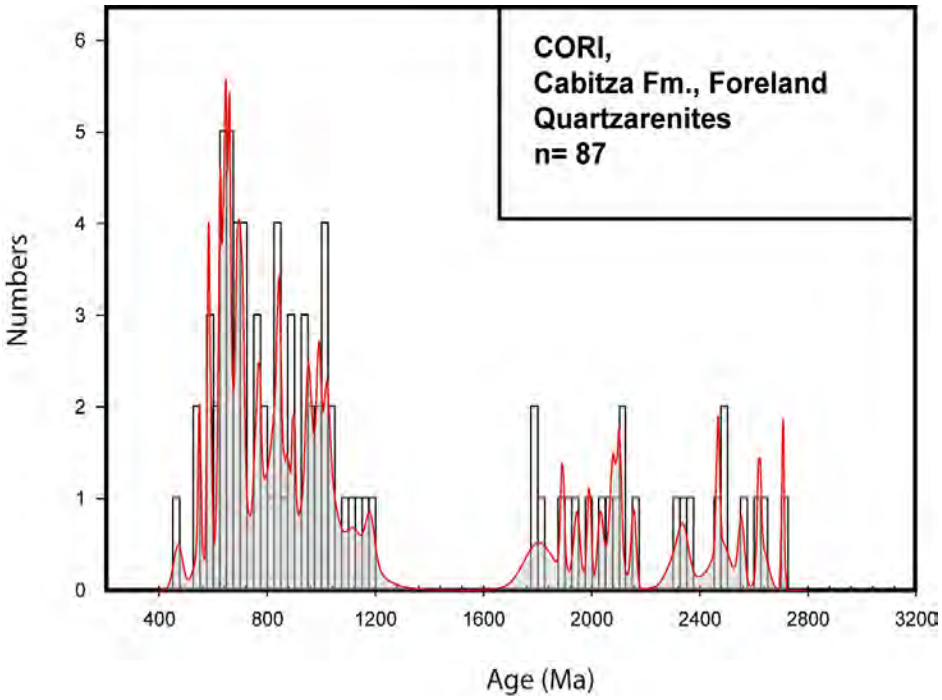

Fig. 3-39 U-Pb results shown in frequency histogram for the CORI sample, for the younger ages (< 900 Ma) have been used the $^{238}U/^{206}Pb$ ratios and for the older have been used the $^{207}Pb/^{206}Pb$. The histogram shows a bimodal distribution of ages, with a main population between ca. 500 and 1,200 Ma.

3.1.2 TERTIARY DEPOSITS

SAMPLE	LITOLOGY	UNIT/Fm.	REGION	COORDINATES
SA-ALB	Meta-conglomerates	"C.ru Flores conglomerate"	Sardinia	9° 38' 18.7" E, 40° 32' 13" N
CO-SOL	Meta-conglomerates	Solaro FLysch	Corsica	9°20'19.30"E, 41°54'15.50"N

Tab. 3-2 Samples collected in the Tertiary deposits of Sardinia and Corsica and theirs coordinates.

3.1.2.1 NE SARDINIA

3.1.2.1.1 Cuccuru 'e Flores conglomerates (CFC) sample

The Cuccuru 'e Flores conglomerates (CFC) is a key stratigraphic point in the understanding of the tertiary tectonics of Sardinia. Although there are a very abundantly literature about this formation still retains some ambiguity about its age, the deposition environment and the provenance of its clasts (Dieni & Massari, 1965; Pasci, 1997; Pasci et al. 1998; Carmignani et al., 2001; Dieni et al., 2008; Oggiano et al. 2009). Finally, also the correlation with other similar sedimetary deposits in the surrounding areas are differently interpreted (Dieni et al., 2008; Oggiano et al., 2010).

The formation, firstly defined by Dieni & Massari (1965) crops out just in NE Sardinia, where is associated to several strike-slip faults (Pasci et al., 1998), as a matter of fact its outcrops are generally lens shaped bounded by sinistral strike-slip faults, the most of them with a very important reverse component.

The CFC is mainly made up by clastic deposits, genreally plygenetic rudites: megabreccias (with some blocks up to 10mc size), conglomerates, sandstones and locally cherty mudstones. Clast come from the Palaeozoic basement (variscan granitoids and metamorphites, dikes, sometime single Ms or K-feldspar), form the Mesozoic cover (limestone and dolostones) and from paleogenic sedimentary formations (sandstones and limestones bearing large foraminipherae, overall nummulites). Generally basement clasts are more rounded than the mesozoic ones. The total thickness is very irregular, but more than 100 m.

The CFC rests gernerally over the Mesozoic and the Lower Eocene, but alaso directly over the Palaeozoic basement.

The depositional environment its not still defined: many authors proposed in the past a continental source (fluvial) (Dieni & Massari, 1965), according some others strictly linked to a active tectonics (Pasci et al., 1998, Carmignani et al., 2001), recently a marine littoral environment has been proposed (Dieni et al., 2008).

Nevertheless the main of the debate about the CFC arises from the tectonic structures related to this deposits. In NE Sardinia two main strike-slip fault systems are recognized, with locally transpressions (M.Albo) and transtensive basins (Chilivani, Ottana, etc.). One system consists of left lateral faults striking NE-SW, the other system consists of right lateral faults striking E-W; both can show also reverse or normal component. The NE-SW system is marked by numerous faults (Nuoro Fault, Tavolara Fault, Olbia Fault and others), and many of the CFC outcrops are located close to these faults, the best are that close M.Albo and the Lanaitto Valley. One of the more large and best exposed is at the conjunction between the E-W striking Cedrino Fault and a NE faults in east side of M. Tuttavista. According Pasci et al. (1998) the CFC suffered a deformation during its deposition at the core of synclinal growth-folds during late Oligocene. Aquitanian. Although this correlation of the conglomerates with the strike-slip faults is accepetd by all the authors, Dieni & Massari (1965, 2008) suggested a completely syn-tectonic source, whereas Pasci et al. (1998) and Oggiano et al., (2010) wrote that just a part of the deposits is linkable with a tectonic activity.

The age of CFC is still controversial, all the authors, except for Dieni et al. (2008) found just reworked fossils, overall Lower Eocene nummulites that not allowed a clearly datation of the deposit. Chabrier (1969), that did not recognized the reworked nummulites, proposed a post Upper Cretaceous age.

Dieni & Massari (1965) proposed a post-Cuisian age (Upper Eocene-Oligocene), as they found the macroforaminiphera described above.

Carmignani et al. (1994a), Oggiano et al. (1995, 2009), Pasci (1997) e Pasci et al. (1998) re-assessed a post Middle Eocene, and of the region still proposed a late Oligocene -Aquitanian age.

Dieni et al. (2008) then proposed a Lower-Middle Eocene based on the occurrence of a palynological content in the matrix and on a correlation to the Cixerri fm. cropping out in SW Sardinia. This data has been refused by Oggiano et al. (2010) since the palynological data look reworked and the palynomorfa described by Dieni et al. (2008) are not yet considered marine, but continental by many authors and not confined to the Eocene.

Also about the correlation of CFC with other formations there still not agreement. Dieni et al. (2008) proposed that it is the same of the Eocene Cixerri fm., whose age is up to now not defined too: ranges from Middle Eocene to Upper Oligocene (Pecorini & Pomesano Cherchi, 1969; Barca & Costamagna, 2000, Funedda et al., 2009). Oggiano et al. (2009; 2010) propsed a correlation to the Ussana fm. (Upper Oligocene- Aquitanian, Pecorini & Pomesano Cherchi, 1969) considering the similar tectono-stratigraphic features.

The sample SA-ALB has been collected in a quarry in the NE side of M. Albo, about 6 km from Siniscola village (see the coordinates in the Tab. 3-2) where the conglomerates prevail. (Fig. 3-41).

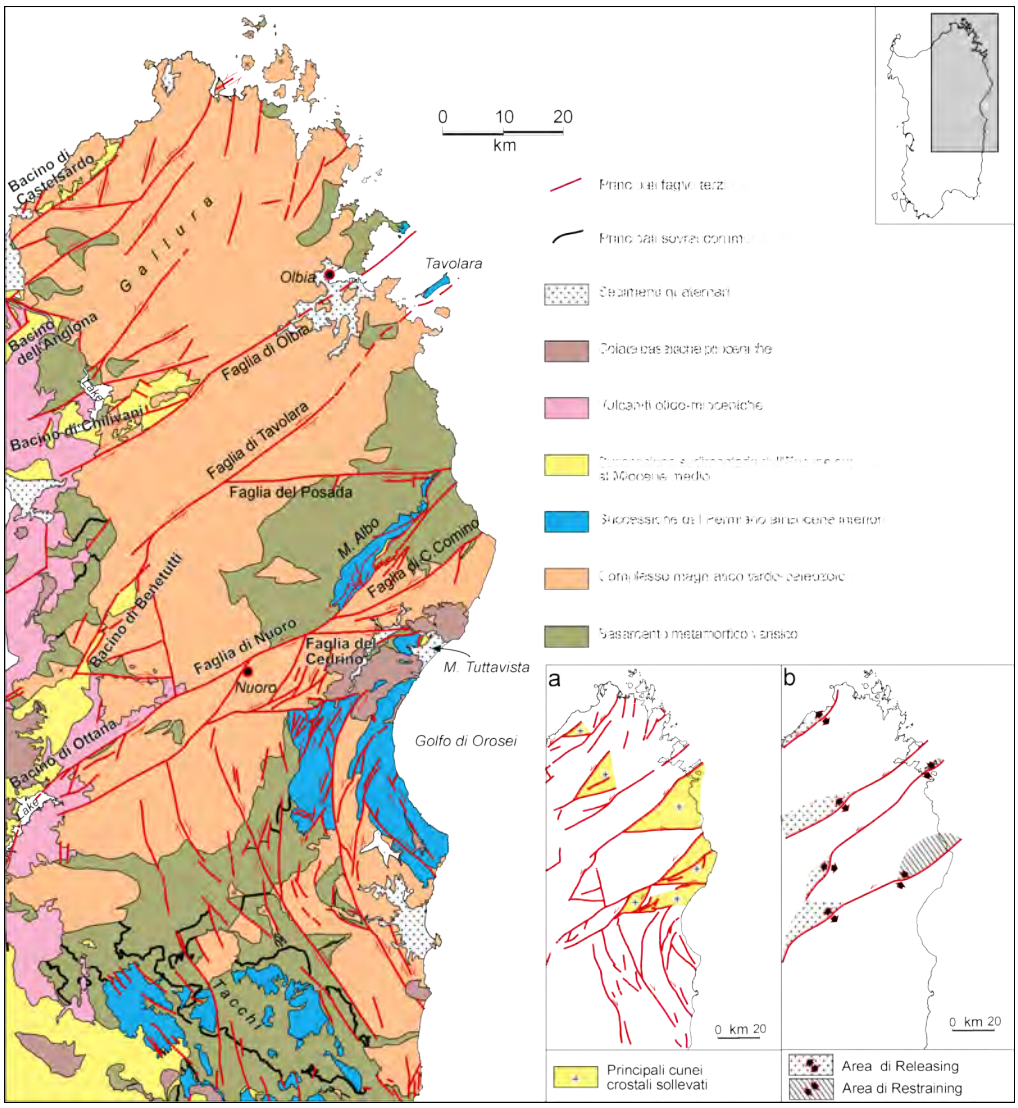

Fig. 3-40 Tectonic sketch map of NE Sardinia with highlighted the main tertiary tectonic features (after Oggiano et al., 2009)

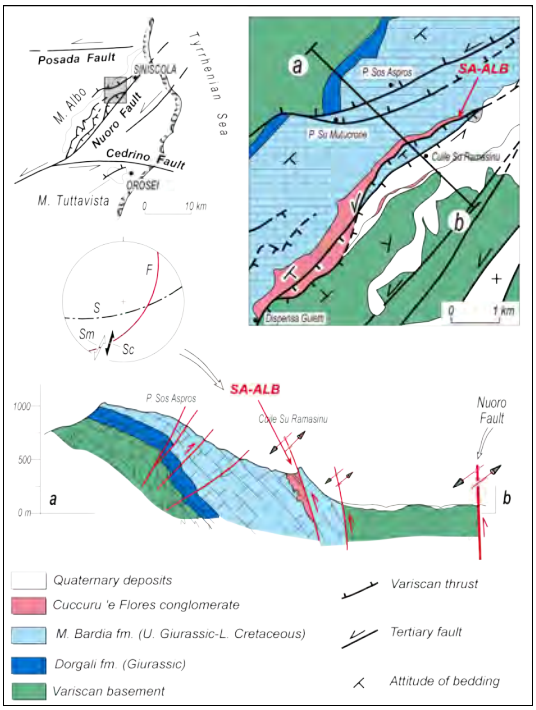

Fig. 3-41 Geological sketch map of the NE sector of M.Albo, where the SA-ALB has been collected; cross section and stereographic projection of s-c relationship and calculated striae. After Carmignani et al., 1994b, modified)

Fig. 3-42 The M. Albo quarry area where the SA-ALB sample has been collected

3.1.2.1.1.1 Zircon study

Almost 100 zircons analyzed and observed under optical microscope. They are pinkish to yellowish colour, sub-euhedral to rounded with main length around 150 mμ, also have been found grains with length of 50 mμ (BSE show in Fig. 3-44). Several fractures (BSE imaging, Fig. 3-44a) have been observed. Rare inherited cores have been found.

3.1.2.1.1.1.1 U-Pb isotopes

U-Pb analysis on sixty-one grains from SA-ALB sample were performed (Table 2 in Annexes) and reported in the Concordia diagram (Wheterill, 1956; Fig. 3-44b), they are concordant except for some Archean grains. The age spectra is spanned between ca. 450 Ma and 300 Ma.

Projecting the data in a frequency histogram (Fig. 3-45) a main polymodal distribution with a population between 500 Ma and 850 Ma (33% of all zircons) is shown, with two main peaks at 682 Ma and 1017 Ma and others secondary peaks at 500 and 850 Ma. A secondary population is concentrated between 1,850 and 2,000 Ma.

3.1.2.1.1.1.2 Lu-Hf isotopes

Twenty-one U–Pb zircon grains representative of the different age populations, were analyzed to obtain Hf isotopic compositions (Table 3 in Annexes, Fig. 3-46). Zircon grains with ages between 600 and 700 Ma show variable εHf values, ranging 2from −16 to +10, with Hf TDM model ages between 0,93 Ga and 2.35 Ga. Four zircon grain around to the 800 Ma age peak show variable εHf values, ranging from −3 to +10, with Hf TDM model ages between 1 Ga and 2.8 Ga. Seven Grenvillian zircons show variable εHf values, ranging from −19 to +14, with Hf TDM model ages between 1 Ga and 2.78 Ga.

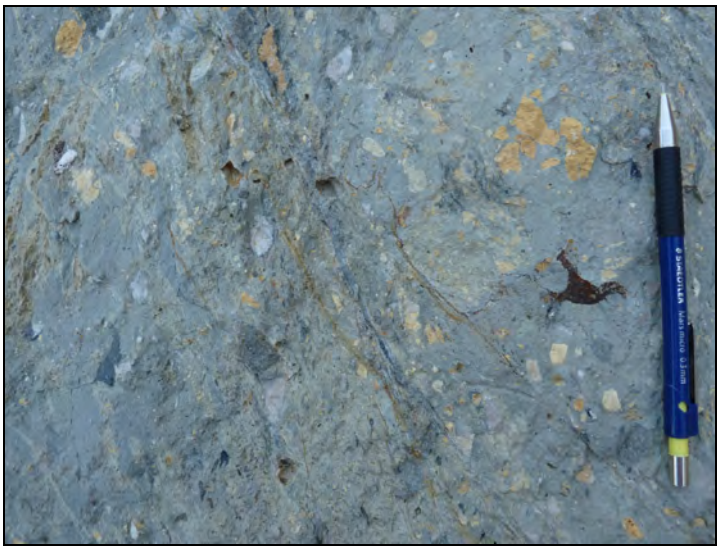

Fig. 3-43 Detail of the outcrop of SA-ALB sample

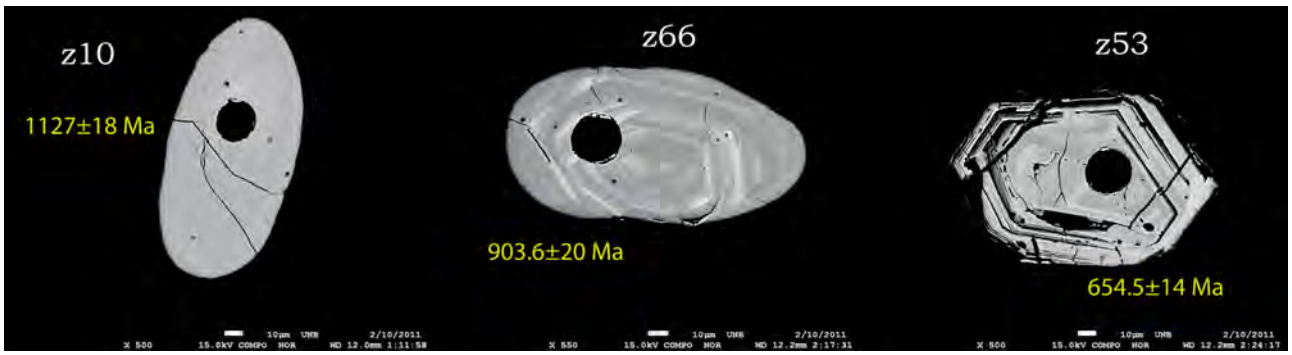

a)

b)

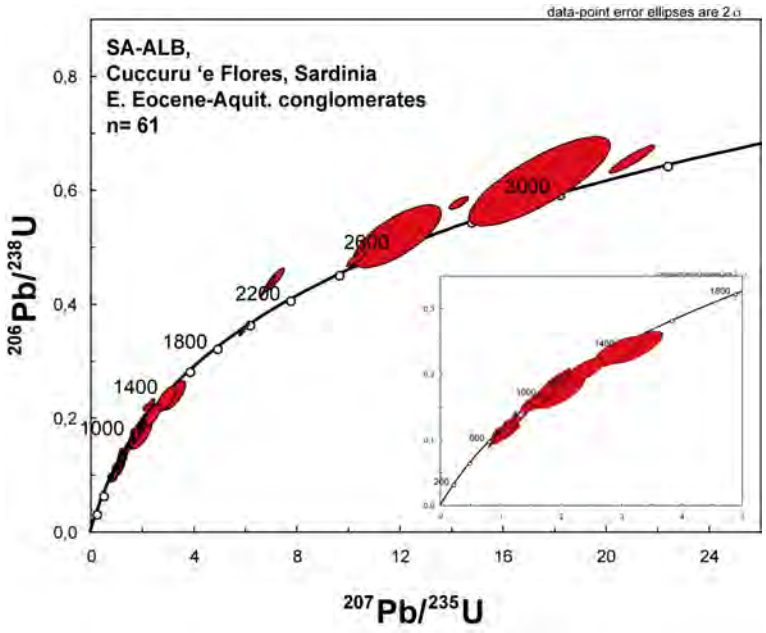

Fig. 3-44 Zircon images from SA-ALB sample a) z10 zircon; b) z66 zircon; c) z53. b) Concordia diagram (Wetherill, 1956) with concordant age and a box with an expansion of measured from 550 Ma to 3,000 Ma.

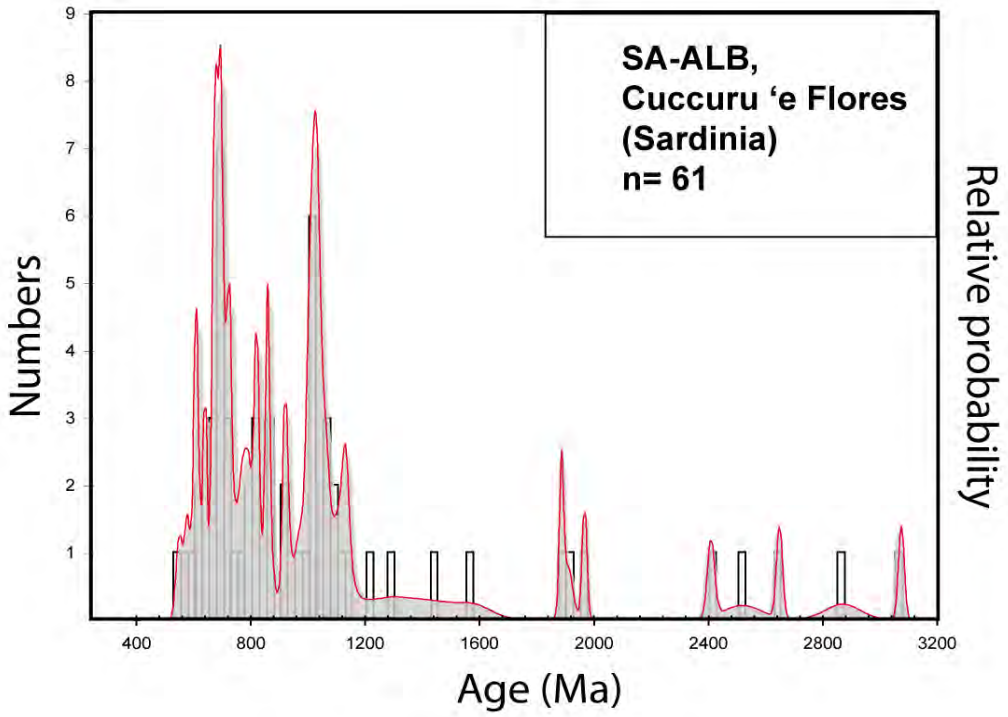

Fig. 3-45 U-Pb results shown in frequency histogram for the SA-ALB sample, for the younger ages (< 900 Ma) have been used the $^{238}U/^{206}Pb$ ratios and for the older have been used the $^{207}Pb/^{206}Pb$. The histogram shows a polymodal distribution of ages, with a main population between 550 and 3,000 Ma.

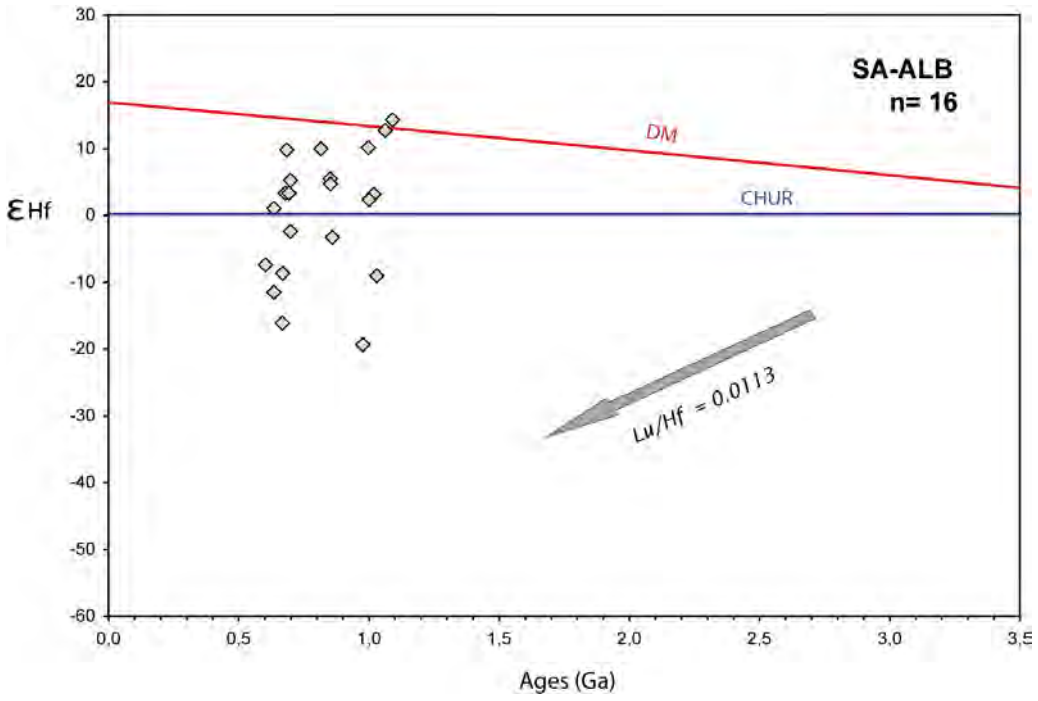

Fig. 3-46 Ages vs εHf values for the SA-ALB sample. The grey arrow represents the crustal evolution trend for Hf isotopic composition, calculated using $^{176}Lu/^{177}Hf$ = 0.0113 (Taylor and McLennan, 1985; Wedepohl, 1995).

3.1.2.2 CORSICA

The left lateral strike-slip faults that crop out either in NE Sardinia and SE Corsica, are often sealed by sediments attributed to Upper Burdihgalian- Langhian (Oggiano et al., 1995), the same is for the alpine thrusts in Corse (Francardo, St. Florent: Orszag-Sperber & Pilot, 1976; Rossi & Rouire, 1980; Jolivet et al., 1990; Daniel et al., 1996). In SE Corsica some syn-tectonic sediments (Solaro Flysch, Vazio conglomerates e di P.ta di a Chiappa conglomerates: Amaudric Du Chaffaut, 1973, Rossi et al., 2008) are related to the strike-slip system, with thickness up to 500 m, and unconformable resting over either Variscan crystallne basement and the meso-cainozoic cover up to the Lower Eocene (P.ta Muffrareccia, Favona). In NE Corse similar deposits (Solaro Flysch, Polasca Flysch) crop out at the base of the Alpine Corse nappe front (Amaudric Du Chaffaut, 1973; Bezert & Caby, 1988; Egal, 1992). Some outcrops in Corsica corroborate this conclusione. At P.ta Calcina the mesozoic cover are preserved in small pieces involved along left strike.slip faults, very similar to that one along the Nuoro Fault in NE Sardinia. Near P.ta di a Chiappa the same tectonic relationships are well exposed.

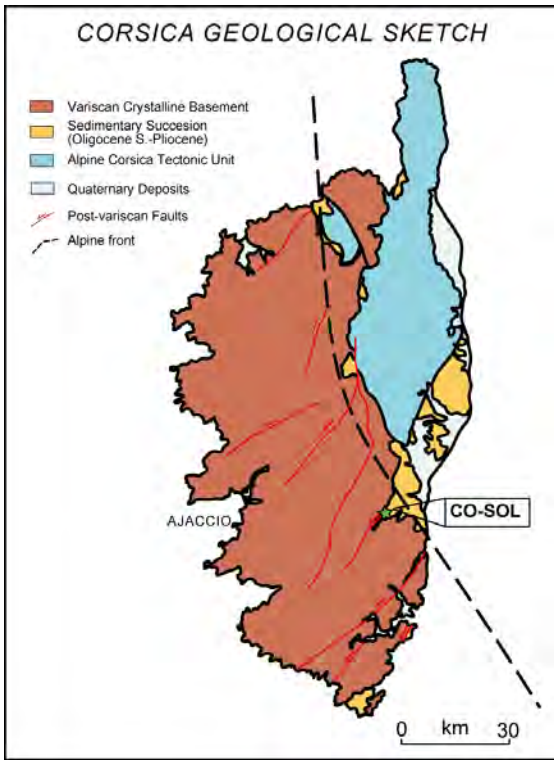

Fig. 3-47 Corsica geological simplified map, modified from Carmignani et al. (2004)

3.1.2.2.1 Solaro Flysch sample

The CO-SOL has been collected from the Solaro Flysch (SF). The SF is a syn-tectonics deposit (Amaudric Du Chaffaut, 1973) cropping out in the Southestern Corsica (see coordinates in Table 2-3). The SF mainly consists of conglomerates and arkose with variable thickness (Fig. 3-47) . The SF is linked with the same strike-slip faults system that affected the Northerneastern Sardinia and is considered like a comparable deposits of CCF (Carmignani et al., 1994b; Dieni et al., 2008). The SF is discordant on the basement and on the Mesozoic to Eocene formations. Locally it gets up a thickness of 500 m. In the deposit are recognized reworked foraminifers (Amaudric Du Chaffaut 1973) with a Priabonian age (Rossi & Rouire 1980), that allow to define that the SF is post-Eocene, but taking in account the tectonics which the SF is linked, have been proposed an age of Late Oligocene-Aquitanian (Carmignani et al., 1994; Oggiano et al., 2009).

The Solaro Flysch contains reworked foraminiphera dated to the Priabonian (Amaudric Du Chaffaut, 1973, Rossi & Rouire, 1980). Thus, the age of all these syntectonic sediments would postdated the Middle Eocene. Considering the tectonostratigraphic framework Carmignani et al. (1994b), Oggiano et al. (1995, 2009, 2010), Pasci (1997) and Pasci et al. (1998) proposed a Upper Oligocene-Aquitanian age.

3.1.2.2.1.1 Zircon study

The almost 100 zircons have been analyzed and observed under optical microscope. They are mainly colourless but pinkish to yellowish colour, sub-euhedral to rounded with main length around 200 mμ (BSE imaging, Fig. 3-49a). Rare inherited cores have been found.

3.1.2.2.1.1.1 U-Pb isotopes

Ninety U-Pb analyses on single grains from the CO-SOL sample were performed (Table 2 in Annexes) and reported in the Concordia diagram (Wheterill, 1956; Fig. 3-49b). They are concordant except for some slightly discordant Archean zircons. The age spectra is spanned between 300 Ma and ca. 2600 Ma.

The frequency histogram (Fig. 3-50) shows a polymodal distribution with a younger population spanned between (25% of all zircons), with a peak around 300 Ma. A secondary population is concentrated between 450 and 600 Ma (37% of all zircons), with the peak marked at 550 Ma

A secondary population is spanned between 650 Ma and 800 Ma (20% of all zircons). Smaller populations have peaks at 900 Ma and 11,000 Ma. Also an Archean input has been shown with the main peak at 2700 Ma.

3.1.2.2.1.1.2 Lu-Hf isotopes

Twenty-two U–Pb-analyzed zircon grains (Table 3 in Annexes; Fig. 3.50) representative of the different age populations, were analyzed for their Hf isotopic compositions. Five zircon grains with Carboniferous age have negative εHf values between −3 to -13 with Hf TDM model ages between 1 Ga and 2 Ga. Six zircon grains with Pan-African ages also show negative εHf values between −47 to -1 with Hf TDM model ages between 1.4 Ga and 3.9 Ga. Hf isotopic compositions. Zircon grains with ages around 600 Ma show variable εHf values, ranging from −6 to 1, with Hf TDM model ages between 1.40 Ga and 1.8 Ga. Zircon grains with ages between 700 and 780 Ma show variable εHf values, spreading from −30 to 6, with Hf TDM model ages between 1.2 Ga and 3 Ga. Two Neoarchean zircon have positive εHf values between 6.8 to 8.2 with Hf TDM model ages between 2.66 Ga and 2.74 Ga.

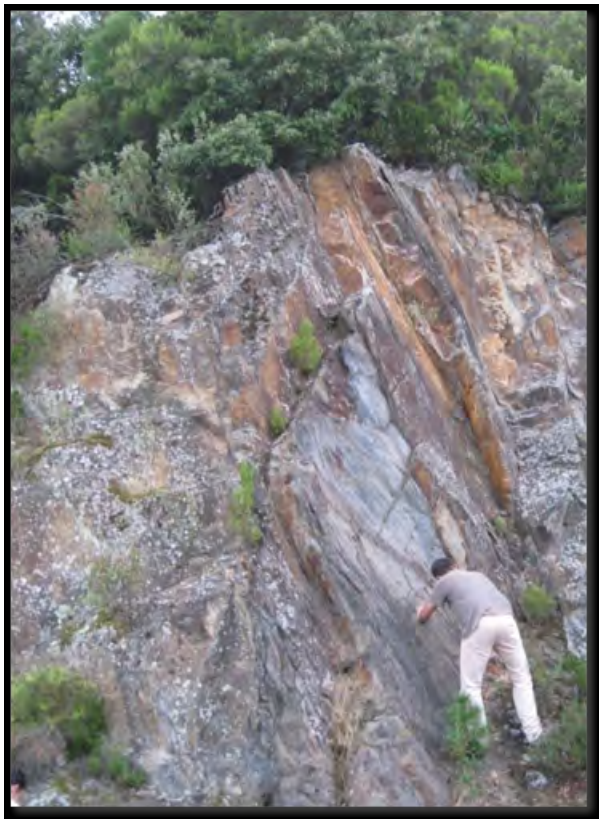

Fig. 3-48 Outcrop of the Quartz-arenite and micro-metaconglomerate belonging to the Solaro Flysch deposits.

a)

b)

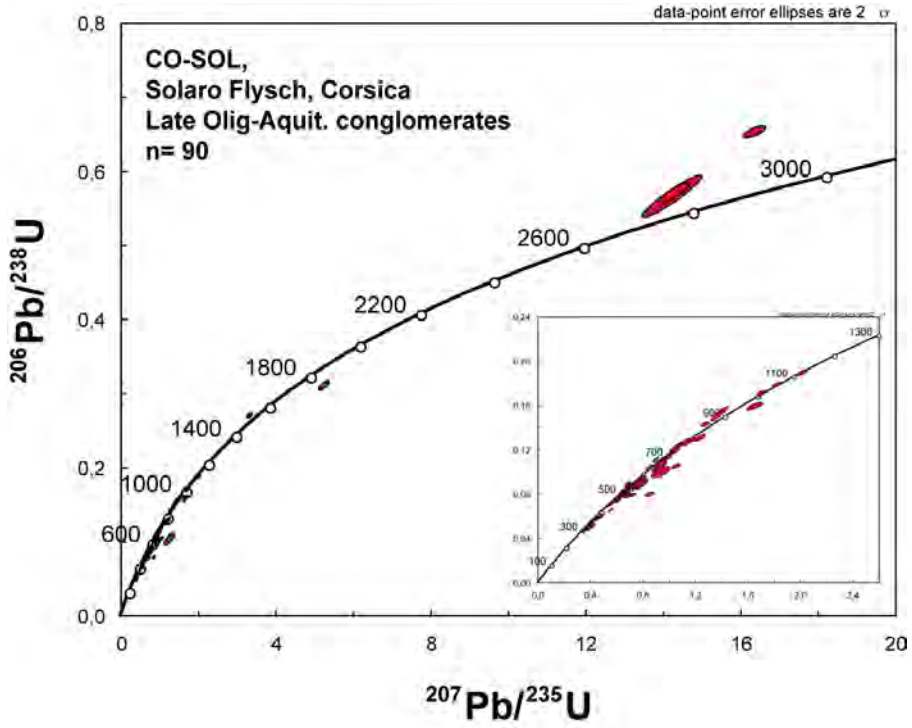

Fig. 3-49 CL zircon images from CO-SOL sample. a) BSE images of z57 zircon, z51 zircon and z20 zircon. b; Concordia diagram (Wetherill, 1956) with concordant age and a box with an expansion of measured from 550 Ma to 3,000 Ma.

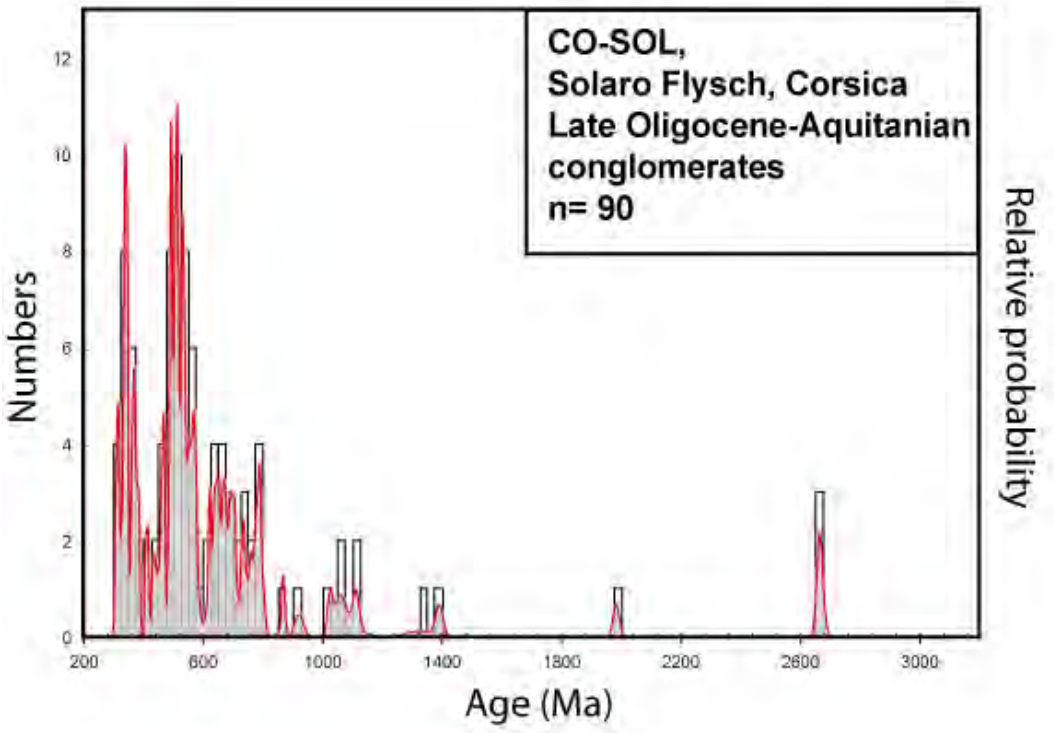

Fig. 3-50 U-Pb results shown in frequency histogram for the CO-SOL sample, for the younger ages (< 900 Ma) have been used the $^{238}U/^{206}Pb$ ratios and for the older have been used the $^{207}Pb/^{206}Pb$. The histogram shows a polymodal distribution of ages, with a main population between ca. 350 and 2,800 Ma.

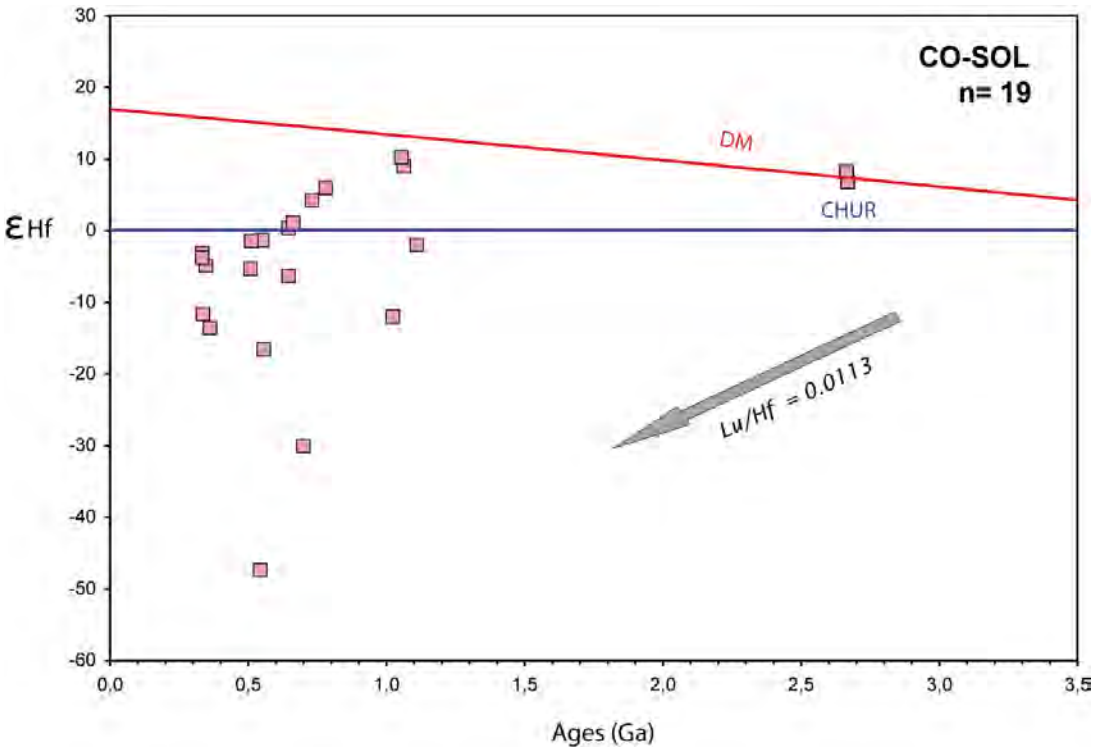

Fig. 3-51 Ages vs εHf values for the CO-SOL sample. The grey arrow represents the crustal evolution trend for Hf isotopic composition, calculated using $^{176}Lu/^{177}Hf$ = 0.0113 (Taylor and McLennan, 1985; Wedepohl, 1995).

3.2 CALABRIAN-PELORITAIN ARC

In this part of chapter will be illustrate i) the study about the Paleozoic evolution of three different tectonic subregion belong to the Calabria Variscides and ii) the investigation in some Tertiary deposits linked to the Tyrrhenian opening.

From Palaeozoic bodies have been studied some magmatic bodies (by whole rocks chemical features and age).

With the aim better define the provenance and characterize the sources of the sediments of analogous and problematic deposits, two tertiary detrital zircon samples belonging to the Calabria-Peloritani Arc have been chosen, one sample cropping out in Serre sub-region and one sample in Aspromonte sub-region.

3.2.1 NORTHERN CALABRIA SECTOR

The northern CPA (Calabria-Peloritani Arc) is constituted of the Catena Costiera and Sila sub-regions.

In the northern sector of CPA three groups of nappes have been discriminated (see Amodio-Morelli et al., 1976; Scandone, 1982; Bonardi et al., 2001, 2004; Alvarez & Shimabukuro, 2009; Patacca & Scandone 2011):

– Piedmont-type and Liguria-type ophiolite-bearing nappes, both affected by Alpine metamorphism (Diamante-Terranova, Gimigliano p.p. and Malvito Units);

– Basement nappes with or without a post-Variscan sedimentary cover, affected by Alpine metamorphism (Bagni Unit and Castagna Unit);

– Basement nappes with a post-Variscan sedimentary covers not affected by Alpine metamorphism (Longobucco Unit, Sila Unit *sensu* Messina et al., 1991 and Stilo Unit).

Here will be take in account the basement not affected by Alpine metamorphism, choosing to analyze the Longobucco Unit (called also Longobucco-Longi Taormina Unit, Amodio-Morelli et al., 1976) cropping out in the Sila sub-region.

3.2.1.1 SILA SUB-REGION BASEMENT

In this study some magmatic bodies belonging to the Longobucco Unit from the Sila sub-region have been investigated. The Longobucco U. basement is constituted by Variscan migmatites and by metamorphic rocks characterized by a low grade (Fig. 3-52).

The metamorphic grade of the Variscan crust increases from the northeast towards the southwest. The Variscan chain in the Sila region commonly dipping to the NE, occupies the uppermost structural position. The lower crust here in the sub-region has a thickness of ca. 7 km and is composed mainly of migmatitic paragneisses with minor metabasites and marbles (Dubois, 1971; Lorenzoni & Zanettin–Lorenzoni, 1983; Graessner & Schenk, 2001).

Instead the upper crust is characterized by considerable granitoids bodies intruded in a older sedimentary successions metamorphosed during Variscan orogeny. Two distinct metamorphic complexes have been recognized: i) the Bocchigliero complex, characterized by a very-low- to low-grade, ii) and the Mandatoriccio complex in greenschist facies to amphibolite facies. The metamorphic rocks consist of phyllites, metavolcanites (also with consistent bodies of porphyroid), metagreywackes, metalimestones.

The Sila batholith, represents a calc-alkaline suite, consisting of tonalite, with minor gabbro and diorite, granodiorite, monzogranite and leucogranite, characterizing the crustal levels from deeper to shallower levels (Messina et al., 1991; Ayuso et al., 1994). The granites have been subdivided in two main types: i) a principal metaluminous to weakly peraluminous suite, cropping both in Sila and Serre subregions, and ii) a minor strongly peraluminous suite (Rottura et al., 1993; Fiannacca et al., 2008). The granite of the two suites show ages ranging from ca. 303 to ca. 290 Ma (mineral and whole-rock Rb/Sr, zircon and monazite U/Pb; Borsi & Dubois, 1968; Schenk, 1980; Del Moro et al., 1982; Graessner et al., 2000).

The evolution of the Sila massif, according with his products due by late Variscan events, was characterized by post-collisional deformation likely by thermal relaxation following the intrusion and then extension of mid-crustal granitoid (Caggianelli et al., 2007). The emplacement of the late Variscan granitoids into the middle crust cold has been related at a brief time near-synchronous with the metamorphic peak (e.g. Graessner et al., 2000; Graessner & Schenk, 2001; Caggianelli & Prosser, 2002; Acquafredda et al., 2006).

Two major scenarios have been proposed in order to explain the Variscan evolution of the Sila Massif. Schenk (1984, 1989, 1990) and Graessner & Schenk (2001) proposed that the metamorphic heating, crustal uplift and isobaric cooling were a direct consequence of a crustal thickening event. Thus the crustal thickening occurred at c. 300 Ma, with a gap of 30–40 Ma, in agreement to the

collisional stage designated for the southern European Variscan belt (Arthaud & Matte, 1977; Burg et al., 1987; Ledru et al., 1989, Rossi et al., 2008). The other scenario, gives a rocks exhumation and granitoid emplacement occurring in a framework of post-collisional lithospheric extension (Caggianelli et al., 2007; Langone et al., 2010), comparable to the French Massif Central evolution (Faure, 1995; Ledru et al., 2001), the Sardinia region (Carmignani et al., 1992; Di Vincenzo et al., 2004) and the Ivrea zone (Brodie & Rutter, 1987; Handy & Zingg, 1991). This is a more auspicial situation for explain coeval processes activity like: i) ascent and emplacement of granitoids in the middle crust (Ayuso et al., 1994; Caggianelli et al., 2000; Caggianelli & Prosser, 2002), ii) LP/HT static metamorphism in the intermediate–upper crust and iii) high-T metamorphism in the lower crust (Schenk, 1980, 1990; Graessner & Schenk, 2001). An other explication for the Calabrian Variscides evolution has given by Graessner (2000) suggesting a geodynamic scenario of a continental arc above a subduction zone. The same geodynamic setting can take in account also for the Serre massif.

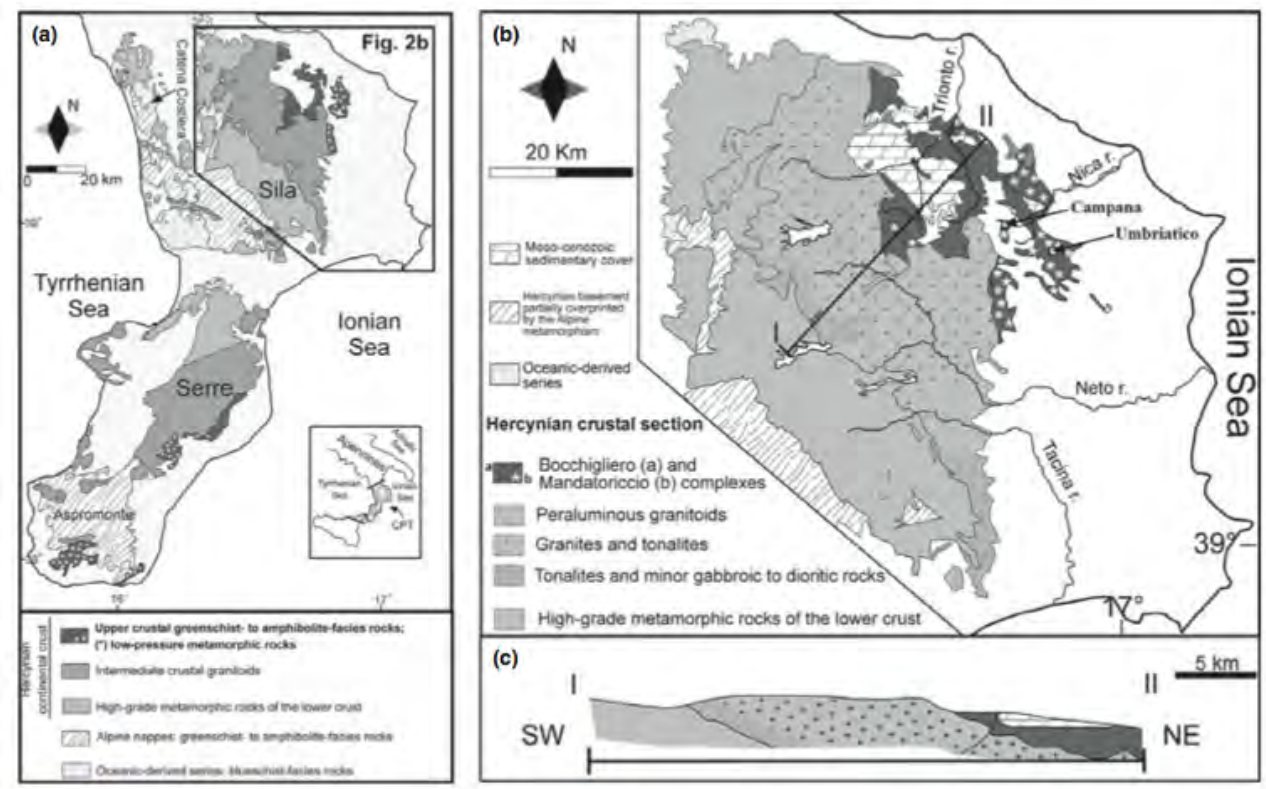

Fig. 3-52-Sila massif sketch, after Micheletti (2007). a) Calabria simplified geological map; b) a Sila sketch with magmatic and metamorphic rocks; c) cross section of Sila massif.

3.2.1.1.1 Sila Sub-Region Basement Igneous Samples

Four samples collected in the Longobucco U. cropping out in the Sila subregion, have been analyzed: three are collected from intrusive bodies (LON-02, LON-03 and TRI-08) and one is from metavolcanic rock (VIV-11). The VIV-11 sample come from a porphyroid collected in the Longobucco U. near to the Vivaio centre, ca. 7 km E to the Cecita lake (see coordinates in the Tab. 3-3). The LON-02 sample has been collected between the Longobucco village and the Cecita Lake; the LON-03 sample has been collected 5 km E from the LON-02; the TRI-08 sample has been collected along the Trionto valley, 1 km NE from the Cropalati village (see coordinates in the Tab. 3-3). The whole rocks geochemical performed in these samples are reported in the Table 1 in Annexes section.

According to the Streckeisen classification (Fig. 3-27) two of the three intrusive samples (LON-02, LON-03) are monzogranite and one sample (TRI-08) falling between monzogranite and granodiorite fields.

Following the Shand diagram (1929), all the samples show a peraluminous composition (Fig. 3-54). Plotting the SiO_2 vs K_2O compositions, the intrusive samples show an high-K calcalkaline signature (

Fig. 3-55) with an high index of SiO_2 (between ca. 73 and 76,5) and K_2O values between 4 and 5.

SAMPLE	LITOLOGY	UNIT	MASSIF	COORDINATES
LON-02	Granitoid	Longobucco	Sila	16°34'3.15"E, 39°25’ 19” N
LON-03	Granitoid	Longobucco	Sila	16°37'31.23"E, 39°24'53.03"N
TRI-O8	Granitoid	Longobucco	Sila	16°44’ 30” E, 39°31’ 12” N
VIV-11	Porphyroids	Longobucco	Sila	16°37'54.653"E, 39°21'55.388N
CAV-05	Quartz-arenites	Longobucco	Sila	16°38'20.93"E, 39°27'55.95"
COR-13	Granitoid	Stilo	Serre	16° 35’ 60"E, 38°49'60" N
PAL-16	Gneiss	Stilo	Aspromonte	15°58'55.723" E, 37°57'03.538" N
CA-PAL	Quartz-arenites	Stilo	Aspromonte	15°58'6.11"E, 37°58'33.88"N

Tab. 3-3 Magmatic and sedimentary samples from CPA with their coordinates. (UTM-WGS 84)

Plotting the samples in the Whalen et al. (1987) diagram (Fig. 1-5) is observed that only the LON-03 has an unambiguous derivation from I&S granite type (Chappel and White, 1974), whereas the other two samples fall in the between of the from I&S and the A-type granite fields (Chappel and

White, 1974) assuming an incertitude between anorogenic (A-type) or a metamorphic rocks source (I-S type) derivation.

Also plotting the three samples in the Y+Nb / Rb diagram (Pearce et al., 1984) (Fig. 3-57) an ambiguous tectonic setting is observed for the LON-03 and LON-02 samples, that fall between the syn-collisional (syn-COLG) and the volcanic arc (VAG) fields. The TRI-08 sample well fits in the volcanic arc setting field. Considering the Pearce et al. (1983) tectonic diagram (Fig. 3-58) the TRI-08 and the LON-02 samples fall in the continental arc field and the LON-03 sample falls in the oceanic arc setting. These settings are confirmed, following Cabanis and Lecolle (1989) (Fig. 3-59), for the TRI-08 and the LON-02 samples, falling in the continental arc field.

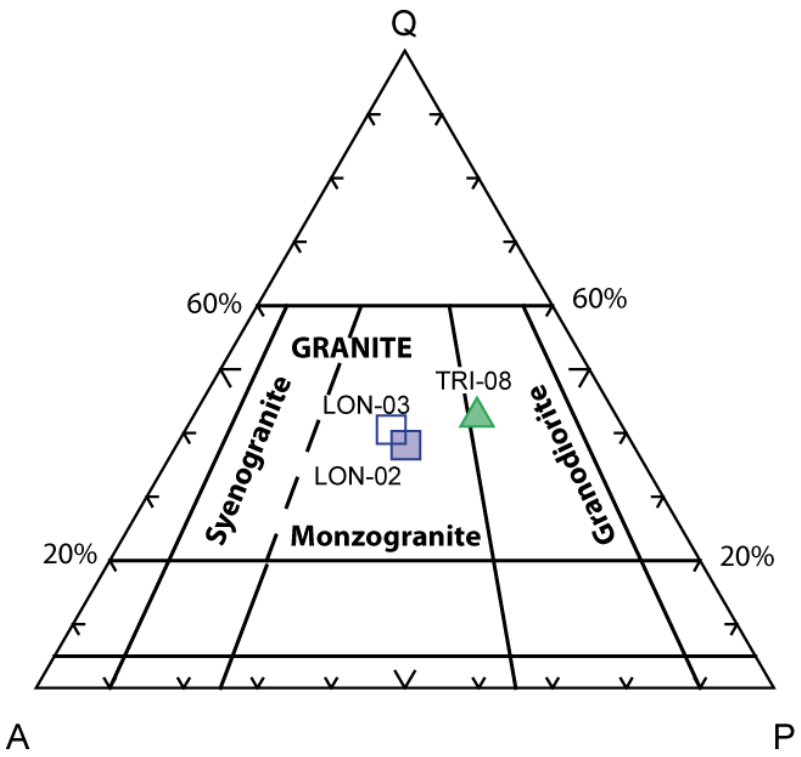

Fig. 3-53 Streckeisen diagram (1979), showing Sila intrusive samples: LON-02, LON-03 fall in the monzogranites field and the TRI-08 sample falls between monzogranite and granodiorite field.

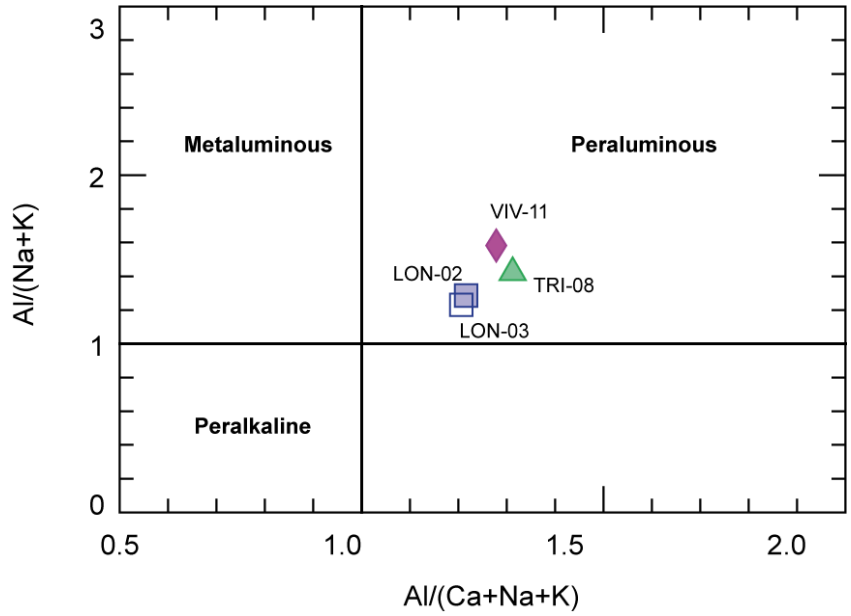

Fig. 3-54 Shand diagram (1929) where is shown the peraluminous features all granitic sample.

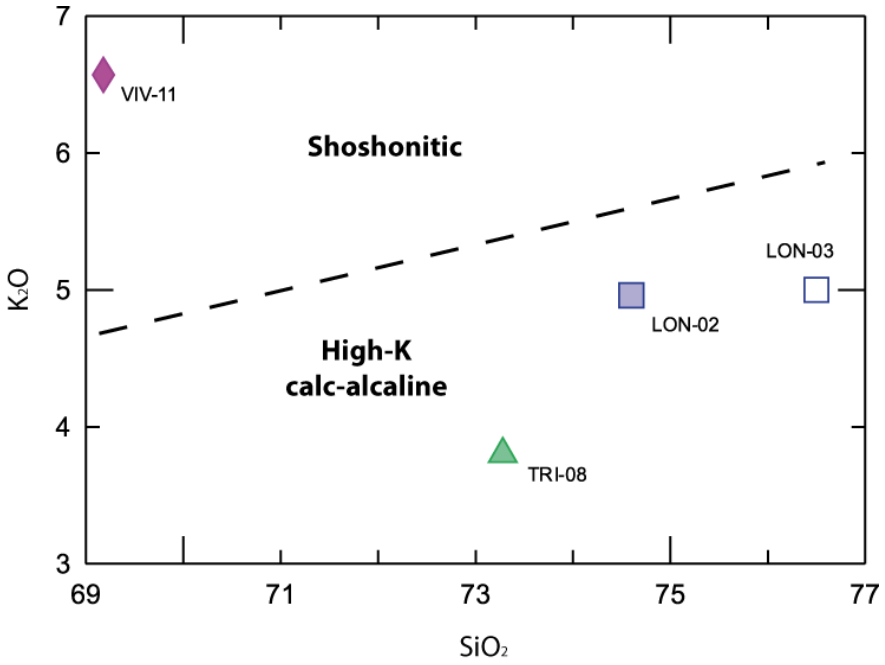

Fig. 3-55 K_2O versus SiO_2 plot showing the High-K calcalkaline signature of the Sila samples.

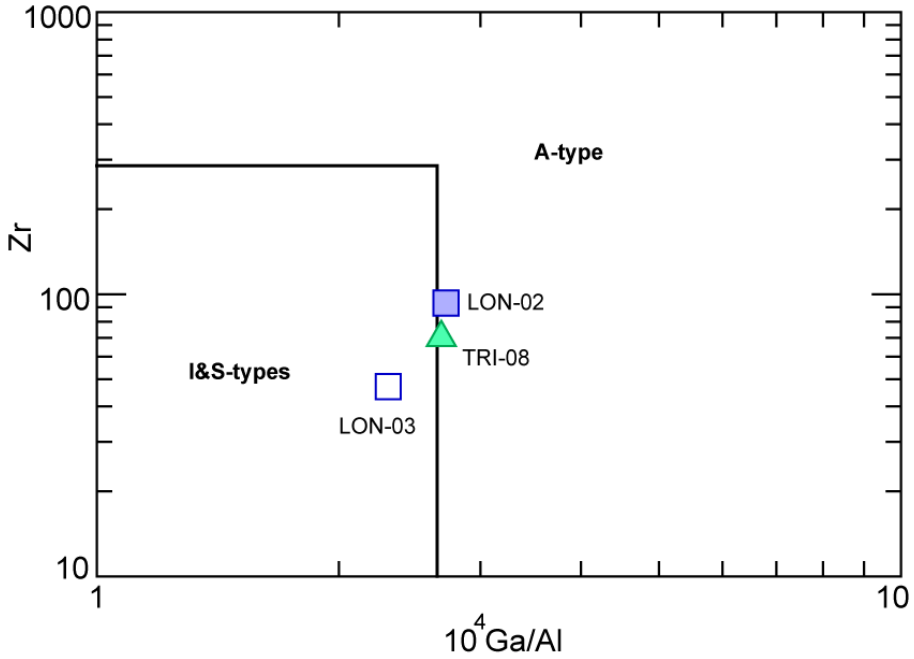

Fig. 3-56 Whalen et al., (1987) diagram showing granitoid type following the Chappel and White (1974) subdivision: the LON-03 shows I&S-types features, LON-03 and TRI-08 fall between the field of I&S-types and A-types.

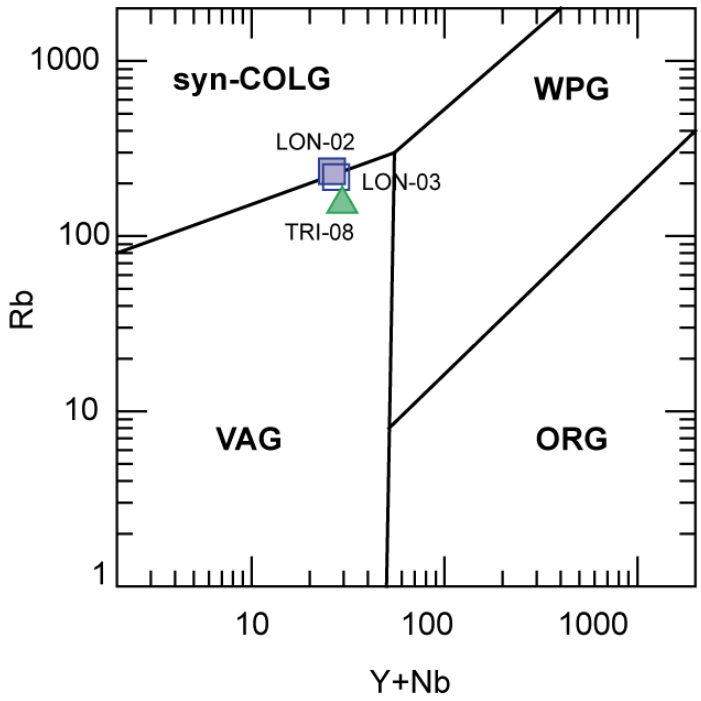

Fig. 3-57 Pearce et al., 1984 tectonic diagram suggesting the volcanic arc setting of the Sila granitic samples: the LON-03 and LON-02 samples falling between the syn-collisional (syn-COLG) and the volcanic arc (VAG); the TRI-08 sample well falls in the volcanic arc setting (VAG).

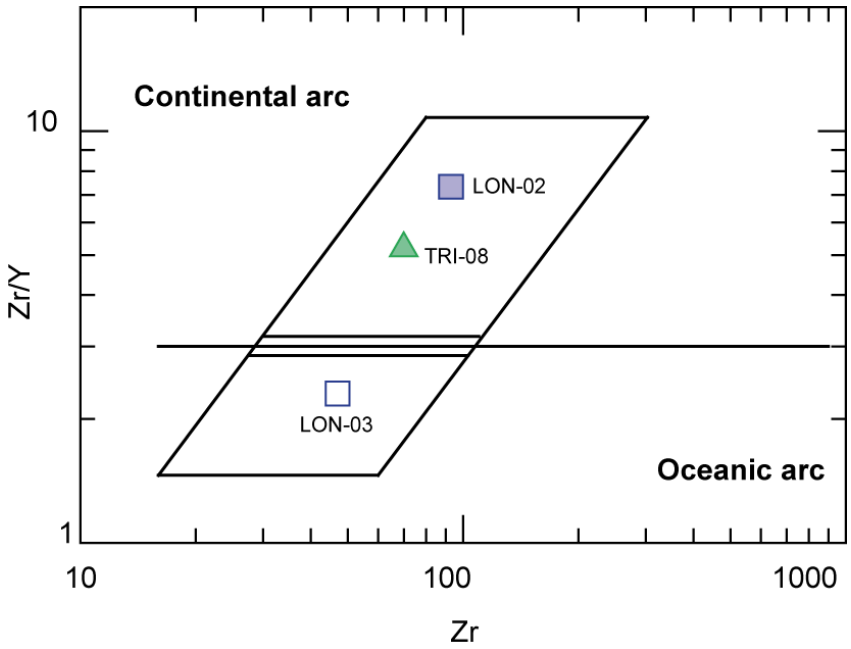

Fig. 3-58 Pearce et al., 1983 tectonic diagram showing a continental arc formation for the LON-02 and the TRI-08 samples and an oceanic arc setting for the LON-03 sample.

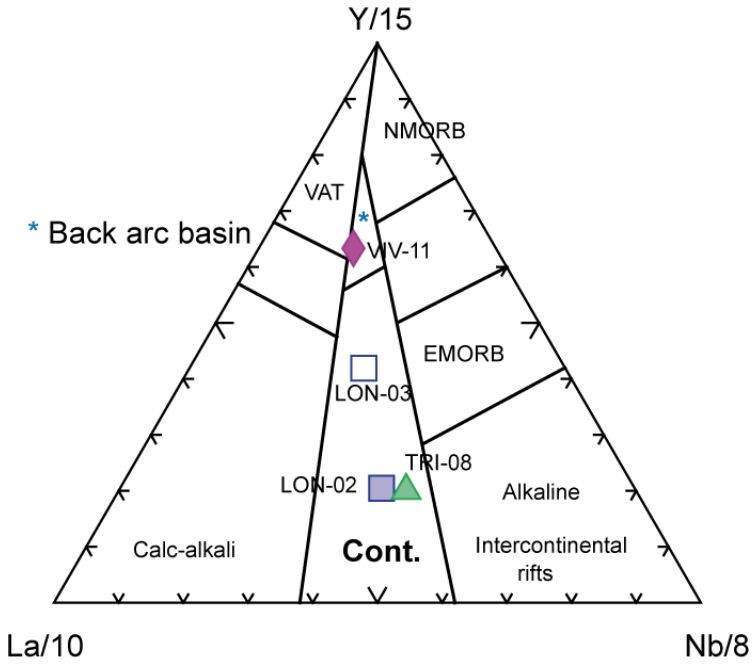

Fig. 3-59 Cabanis and Lecolle (1989) tectonic diagram showing the main formation filed of samples: the volcanic sample (VIV-11) falls in the back arc basin setting, the other granitic samples (LON-02, LON-03 and TRI-08 samples) fall in the continental field.

Chondrite-normalized rare earth patterns according Sun and McDonough (1989) (Fig. 3-60) of the intrusive Sila samples are LREE-enriched with flat HREE for the LON-03 sample and HREE decreasing for the LON-02 and for the TRI-08 with a systematically negative Eu anomaly linked to the important fractionating plagioclase process.

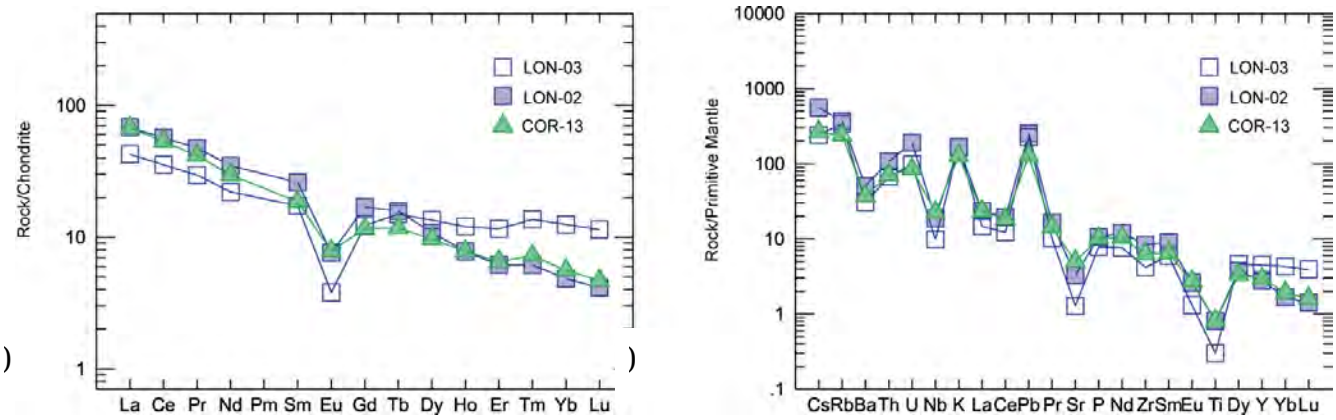

Fig. 3-60 Trace element spider diagrams (Sun and McDonough, 1989) for granitic Sila samples (LON-02, LON-03 and TRI-08 samples): a) REE patterns normalized to chondrite and b) multi-element diagram normalized to primitive mantle.

In the multi-elements diagram primitive mantle-normalized by Sun and McDonough (1989 (Fig. 3-60) the intrusive Sila samples show an enrichment of large ion lithophile elements (LILE) and an impoverishment of high field strength elements (HFSE). A negative anomaly has shown by Ba, Nb, Sr, and Ti. All over negative anomaly of the Ba and Sr are linked to the plagioclase fractionating.

3.2.1.1.1.1.1 U-Pb isotopes

From the LON-02 sample have been analyzed sixteen zircon grains (Tab. 3-3) showing maximum length reaching 200 µm. The majority of grains are euhedrals and prismatics (Fig. 3-61) with magmatic zonation. Rare inherited cores have been found and have given similar age respect of the rimes (zircon L1-31, Fig. 3-61 c).

Fourteen U-Pb analyses on single grains from the LON-02 sample were performed and reported in the Concordia diagram (Wheterill, 1956) giving an age of 298.2 ±1.8 Ma (Fig. 3-61).

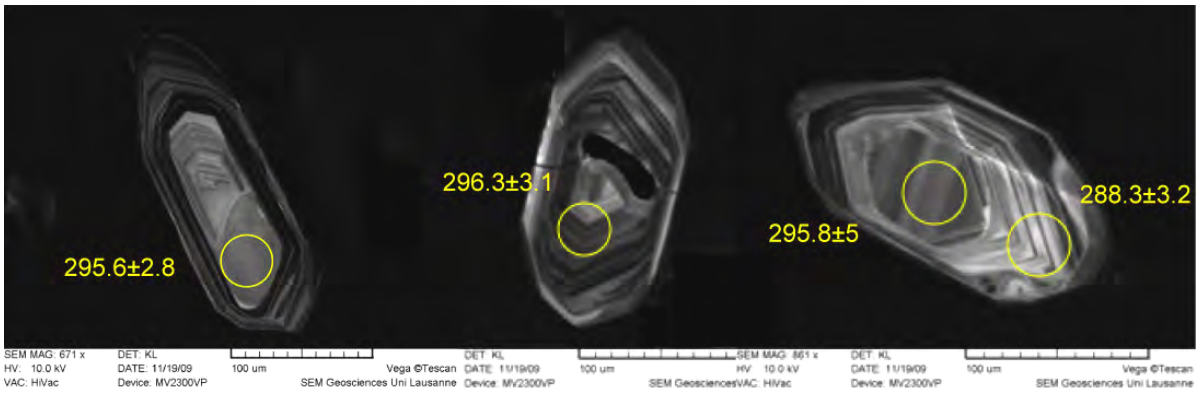

a)

b)

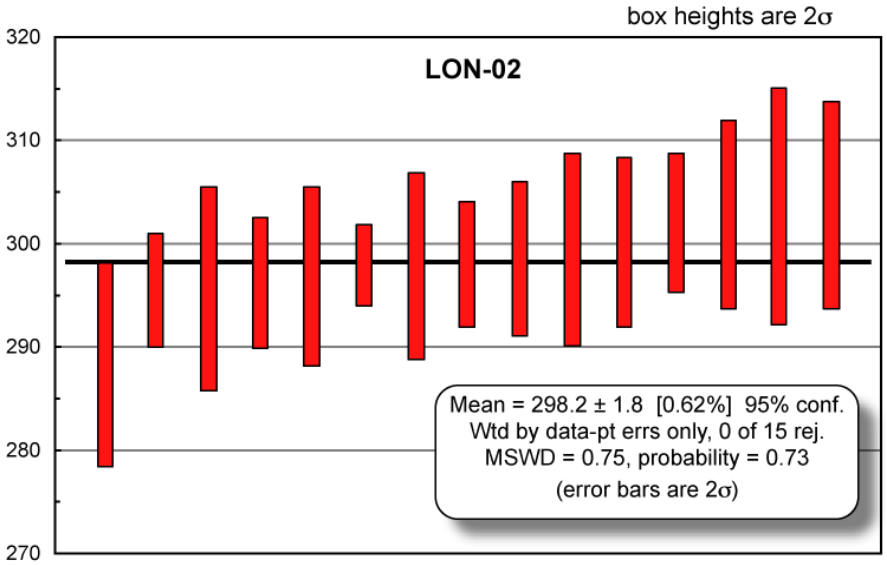

Fig. 3-61 CL zircon images from LON-02 sample: left) L1-18 zircon; centre) L1- 27 zircon; right) L1- 31 zircon with measures done in the core and in the rim. The core shows an older age than the rims of ca. 7 Ma. b) $^{206}Pb/^{238}U$ of LON-02 sample gives an average age of 298.2 ±1.8 Ma.

From the LON-03 sample have been analyzed 13 zircon grains (Table 2 in Annexes). They show maximum length reaching 200 μm. The majority of grains are euhedrals and prismatics (Fig. 3-62) with strong magmatic zonation. Rare inherited cores have been found and have given similar age respect of the rimes (zircon L1-15, Fig. 3-62c). The 12 zircon grains that given concordant $^{206}Pb/^{238}U$ ages show an average age of 303.6 ± 2 Ma (Fig. 3-62). Fourteen U-Pb analyses on single grains from the Trionto Valley granite sample (TRI-08) were performed (Table 2 in Annexes). They show maximum length reaching 200 μm. The majority of grains are euhedral and prismatic (Fig. 3-63) with strong magmatic zonation. Eleven zircons are concordant showing an age of 302.9 ± 4.2 Ma (Fig. 3-63).

a)

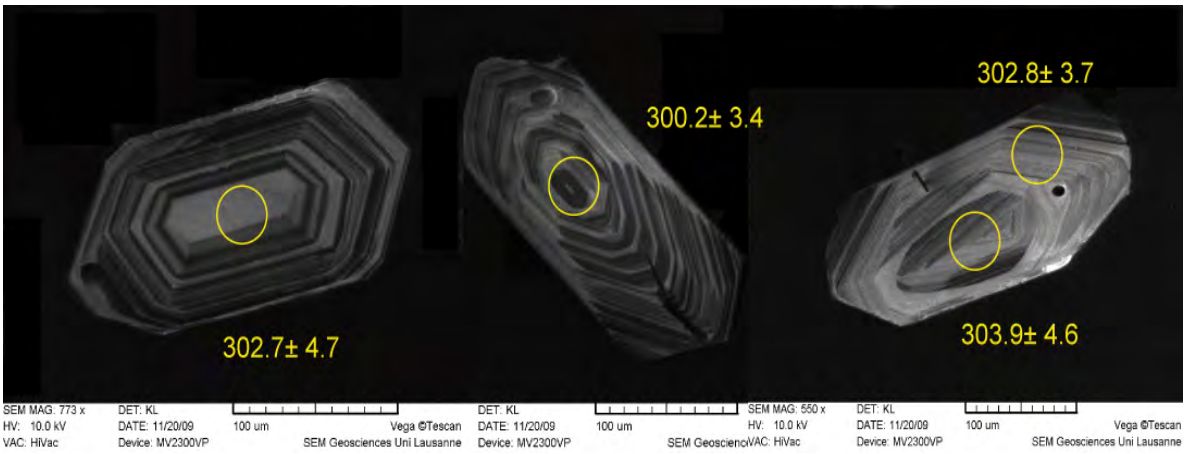

b)

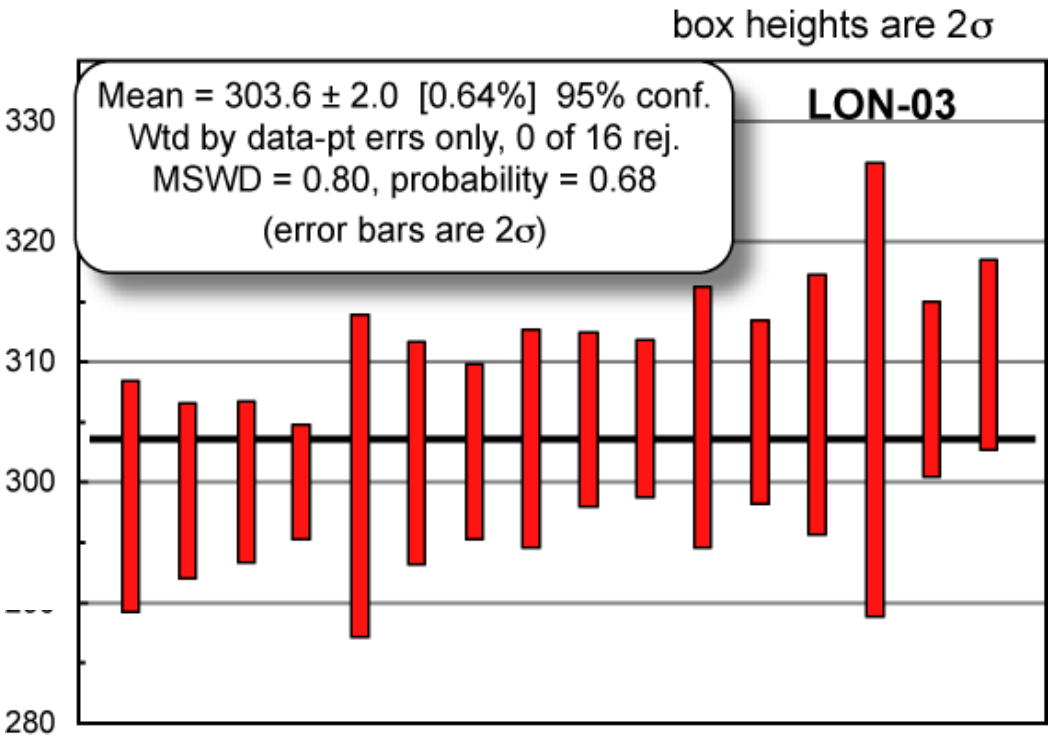

Fig. 3-62 a) CL zircon images from LON-03 sample: left) L1-118 zircon; centre) L1- 109 zircon; right) L1-115 zircon with measures done in the core and in the rim. The core shows an older age than the rims of ca. 1 Ma. b) $^{206}Pb/^{238}U$ of LON-03 sample gives an average age of 303.6 ± 2 Ma.

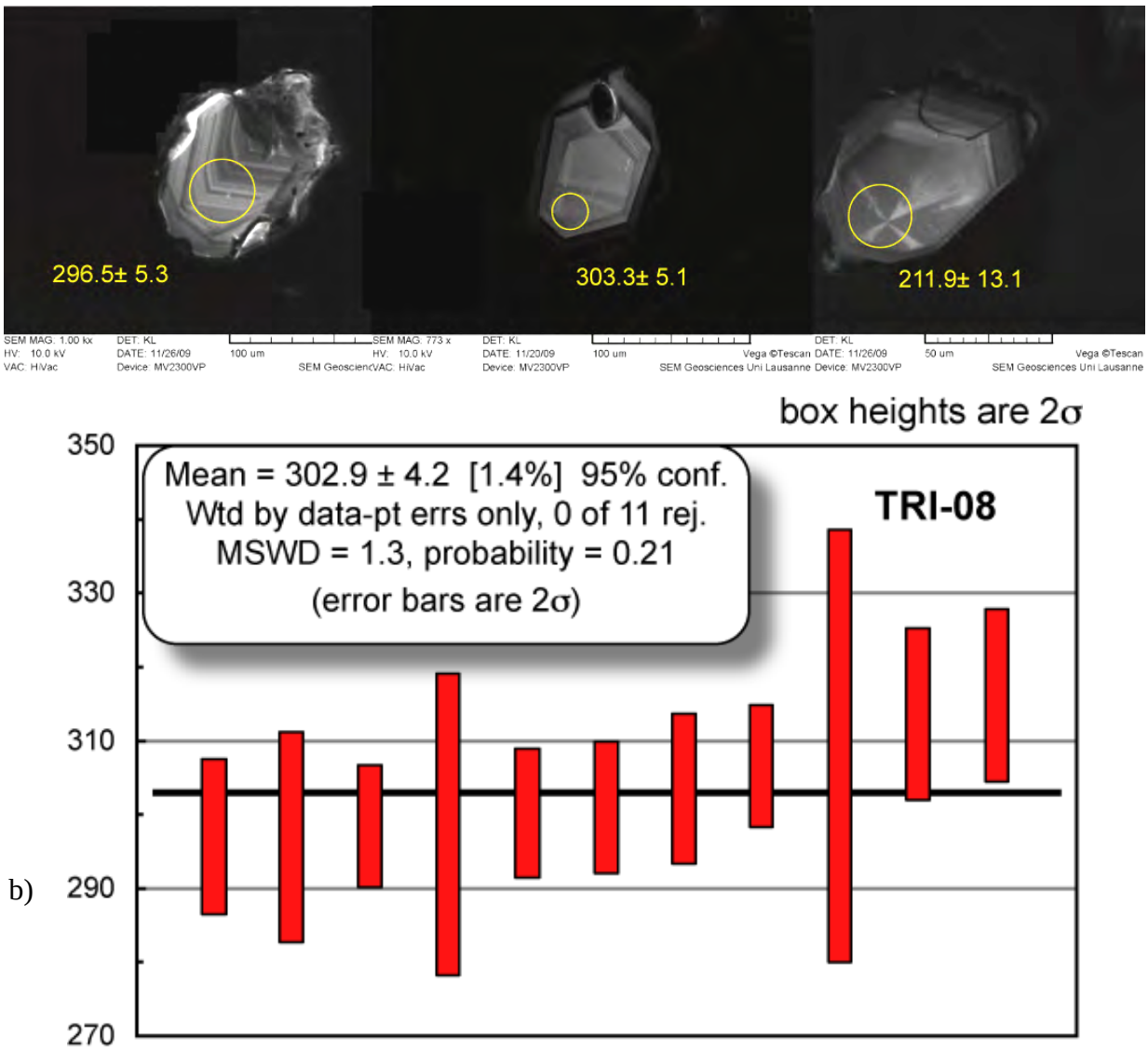

Fig. 3-63.a CL zircon images from TRI-08 sample: left) S2-21 zircon; centre) L1- 139 zircon; right) S1- 39 zircon. b) $^{206}Pb/^{238}U$ of TRI-08 sample gives an average age of 302.9 ± 4.2 Ma.

3.2.1.1.2 Sila Sub-Region Basement Volcanic Sample

The VIV-11 is sample collected from porphyroid cropping out in the Longobucco U. near to the Vivaio centre, ca. 7 km Est to the Cecita Lake (see coordinates Tab. 3-3). The whole rocks geochemical performed in this sample are reported in the Table 1 in Annexes section.

The sample is characterized by K-feldspar phenocryst, quartz and plagioclase. Plotting the alkali vs. silica of Tab. 3-3 into the TAS diagram (Total Alkali Silica, Le Bas et al., 1986) (Fig. 3-7) where the red color the Irvine and Baragar line (1971) has been projected, the sample VIV-11 falls between the trachydacite and the dacite area, in the subalkaline field, falling under the red line.

Considering the diagram about the orogenic series proposed by Peccerillo and Taylor (1976) the sample falls in the shoshonitic series and in the trachyte field (Fig. 3-65). Following the Shand (1929) diagram the sample shows a peraluminous composition (Fig. 3-54).

Plotting the sample in the Cabanis and Lecolle (1989) tectonic diagram (Fig. 3-59) the metavolcanic has been genrated in a back-arc basin setting.

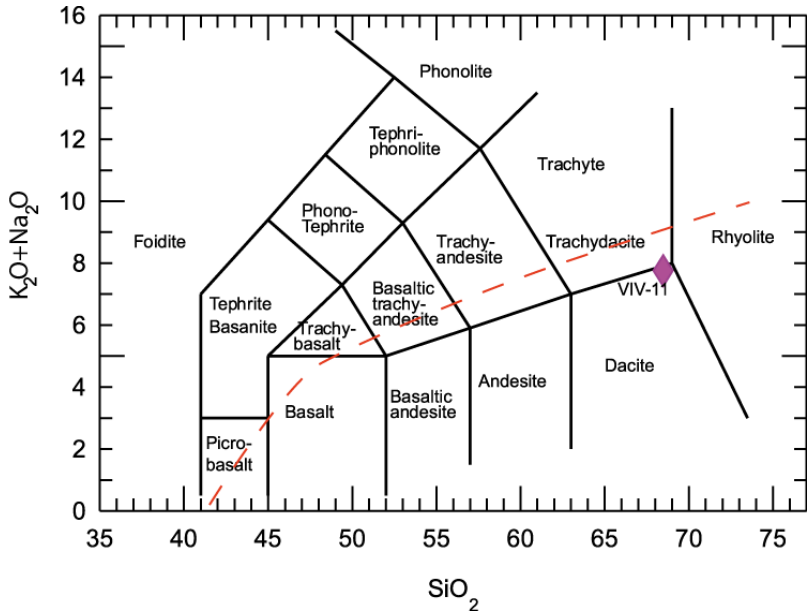

Fig. 3-64 TAS classification diagram with Irvine and Baragar (1971) line that subdivided the subalkaline from the alkaline filed where the VIV-11 porphyroid sample falls between the trachydacite and dacite field.

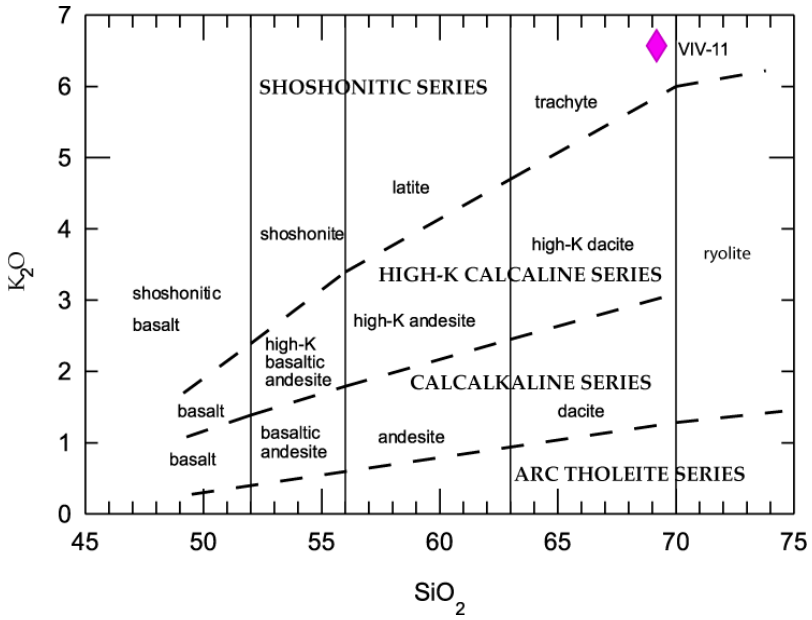

Fig. 3-65 Peccerillo & Taylor (1976) classification diagram where the VIV-11 porphyroid sample falls in the trachyte sample.

Chondrite-normalized rare earth patterns (Sun and McDonough, 1989, Fig. 3-66) of the Sila volcanic sample are LREE-enriched with flat HREE with a systematically negative Eu anomaly linked to the important fractionating plagioclase process.

In the multi-elements diagram primitive mantle-normalized (Sun and McDonough, 1989, Fig. 3-66) the volcanic Sila samples show an enrichment and of large ion lithophile elements (LILE) and an impoverishment of high field strength elements (HFSE). The strong negative anomalies have shown by Nb, Sr, and Ti. All over negative anomaly of Sr could be linked to the plagioclase fractionating.

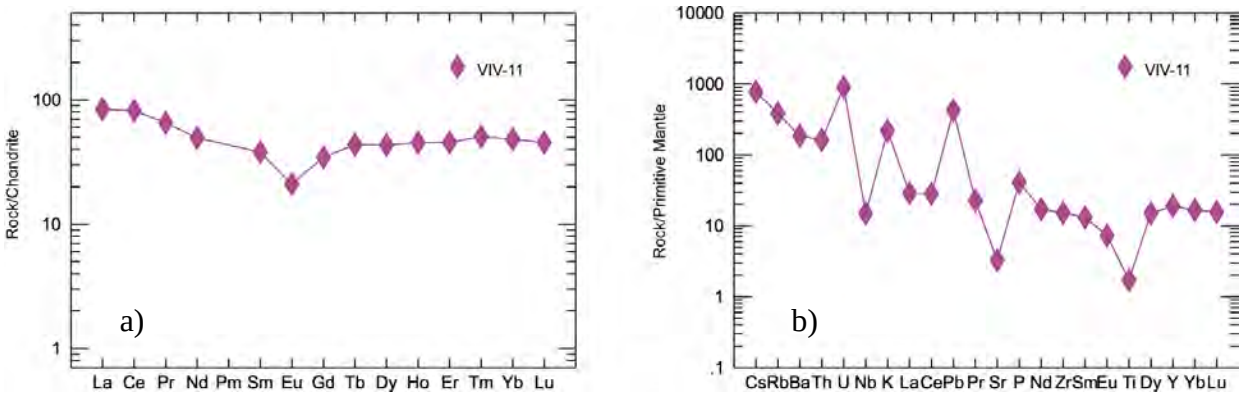

Fig. 3-66 Trace element spiders (Sun and McDonough, 1989) for VIV-11 Sila porhyroid: a) REE patterns normalized to chondrite and b) multi-element diagram normalized to primitive mantle.

3.2.1.1.2.1.1 U-Pb isotopes

From the Sila porphyroid sample (VIV-11) 13 zircon grains have been analyzed (Tab. 3-3) showing maximum length reaching 200 μm. The majority of grains are euhedral and prismatic (Fig. 3-67a) with strong magmatic zonation. Rare inherited cores have been found and have given similar age respect of the rimes (zircon L3- 41, Fig. 3-67a). Eleven zircon grains are concordant and show an average age of 466.4 ± 6.9 Ma (Fig. 3-67b).

a)

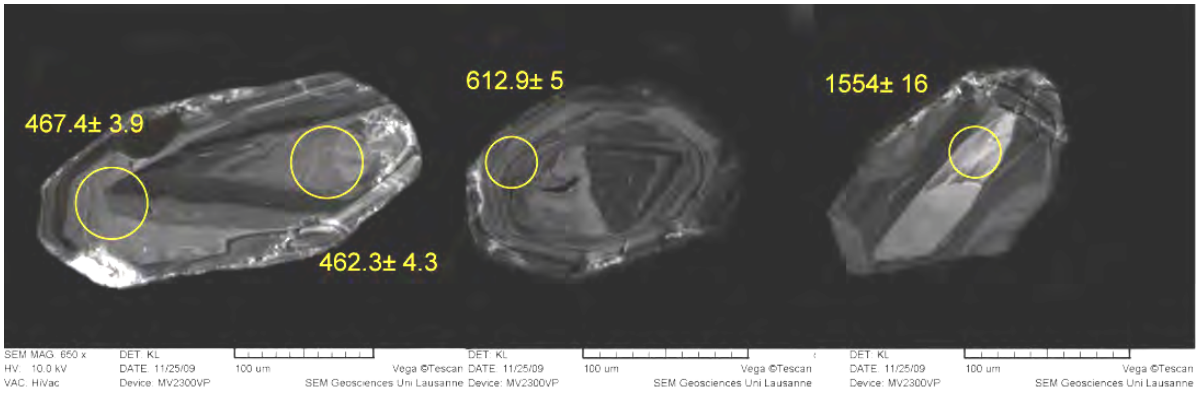

b)

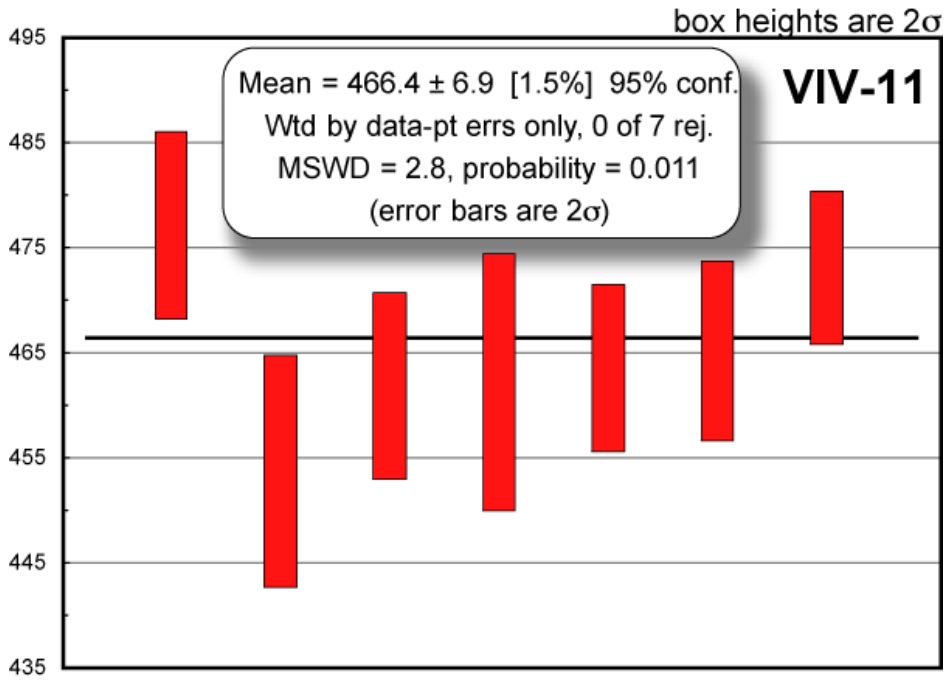

Fig. 3-67 a) CL zircon images from VIV-11 sample left) L3- 41 zircon with measures done in the core and in the rim. The core shows a younger age than the rims of ca. 5 Ma; centre) L3-43 zircon; right). L3- 42 zircon. b) $^{206}Pb/^{238}U$ of VIV-11 sample gives an average age of 466.4 ± 6.9 Ma.

3.2.1.2 SILA SUB-REGION COVERS

3.2.1.2.1 Sila sub-region Tertiary sample

The CAV-05 sample belongs to the Paludi Formation cropping out 3 km NE from the Longobucco village (see coordinates in the Tab. 3-3) The sample has been collected from one of the quartz-arenites strata (Fig. 3-68) of the Paludi Fm of the Bocchigliero Sub-unit (part of the Longobucco Unit), that laying on angular unconformity above the Sila Unit and locally on the Mesozoic covers. The Paludi Fm. is mainly made by polygenic conglomerates, marbles, sandstones with muscovites, quartz-arenites showing a total thickness of nearly 100 meters. The Paludi Fm. is dated Oligocene

at the base and Aquitanian at the top of the sequence by nanoflora data. The main of the researchers considered it like as a pre-collisional flysch (Amodio-Morelli et al. 1976; Bonardi et al. 2004), but it is still ambiguous if it represents a sedimentary episode between two tectonic phases (Dubois, 1976) or if it is the top of the pre-orogenic sedimentary sequence of Sila Unit (Amodio-Morelli et al. 1976).

Fig. 3-68 Quartz-arenite and clay-siltstone strata belonging to the Paludi Fm. The CAV-05 has been collected from the quartz-arenite strata.

According to Bonardi et al. (2004) the turbidites in the Paludi Fm. could be interpreted as the filling of the Southern Apennines foreland wedge-top depo-zone. In this interpretation the conglomerates and sandstones would be the sedimentary foreland onset of the ongoing Calabrian thrust during post eo-alpine tectonic phases related to the beginning of orogenic transport to the Apula plate. This evidence is corroborated by a stratigraphic gap between the younger (Neocomian) sediments of the Sila Unit and the Paludi Fm. (Oligocene (?)-Aquitanian) that also affected the later top-to-the-NE thrusts. Other authors (Thomson, 1994; Caggianelli and Prosser,

2002) considered the Paludi Fm. deposition linked to a rapid exhumation between the Oligocene and the Miocene.

3.2.1.2.1.1 Zircon study

The zircons analyzed are colourless to yellow-brownish colour, sub-euhedral to rounded ~~habitus~~ with main length around 150 mμ (Fig. 3-69).

The majority of zircons are characterized by several micro-fractures, probably done by stress during the sedimentary cycles, and inclusions. Some inclusions (Fig. 3-69) have been analyzed by electron microprobe and reveal all over peaks of phosphor, calcium, carbon and chlorine suggesting an apatitic origin (Fig. 3-69, analysis n.1).

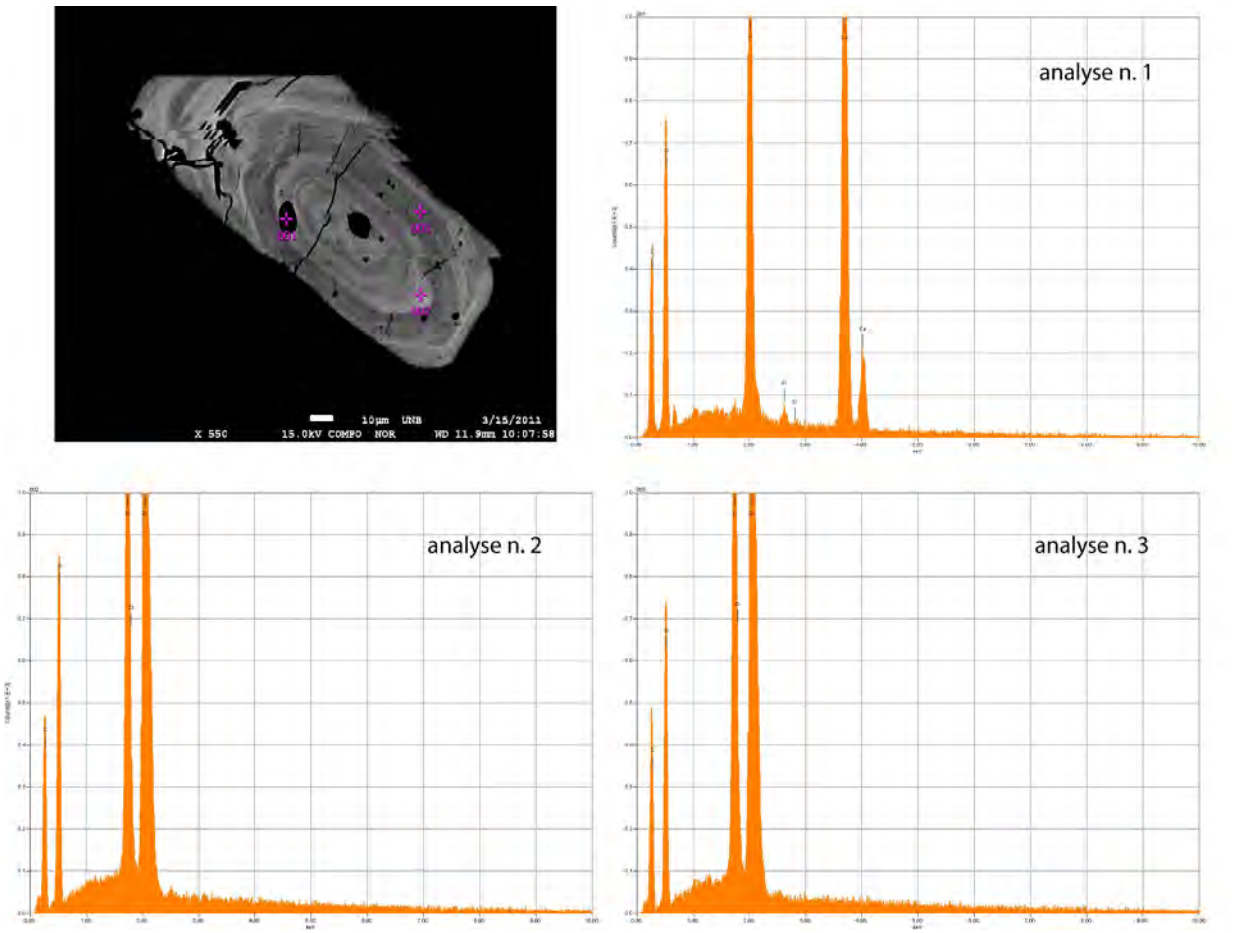

Fig. 3-69 Analyses performed by electron microprobe in the zircon n. 2 (here in BSE imaging) belonging to the CAV-05 samples. The first analysis show an inclusion with apatitic composition, the other two analyses have been done in order to verify the composition between darker (analysis n. 3) and brighter zone with higher U content (analysis n. 2)

.

3.2.1.2.1.1.1 U-Pb isotopes

71 of 76 zircon grains measured From the Paludi Fm. sample (CAV-05), are concordant U-Pb analyses (Table 2 in Annexes). The data have been reported in the Concordia diagram (Fig. 3-70) where the majority of grains are concordant and only few zircons are slightly discordant due to Pb loss. The age spectra is spanned between ca. 280 Ma and 2,900 Ma. The data has been also shown in a frequency histogram (Fig. 3-70) with a polymodal distribution of the ages. The main age population is spanned between 286 and 950. The main population (43% of all zircons) is Palaeozoic with age comprises between ca. 286 and ca. 540 Ma, with two main peaks at ca. 300 Ma and 500 Ma; a second age population is Grenvillian and is focused between 1,000 and 1,100 Ma (8% of all zircons). Also are present single age spots at 1,400 Ma, and a Palaeoproterozoic input between 1,800 and 2,000 Ma and between 2,600 and 2,950 Ma.

3.2.1.2.1.1.2 Lu-Hf isotopes

16 zircon grains from the main populations (Fig. 3-71) have been selected to obtain Lu-Hf measures (Table 3 in Annexes). Four zircons grains between 270 Ma and 315 Ma have negative εHf values ranging from −5.7 to -6.5 with Hf TDM model ages around 1.5 Ga. Seven grains relative to the Cambro-Ordovician population show εHf values spanned from −35 to 2.3 where the two grains around 480 Ma show positive εHf values. The population has a Hf TDM model ages between 1.2 Ga and 3.2 Ga, where only the zircon around 440 Ma show a TDM model age of 3.2 Ga. The Neoproterozoic zircons analyzed show positive εHf values: 1.4 the youngest grain (650 Ma) and 8.3 the oldes one (830 Ma), with Hf TDM model ages of 1.4 and 1.1 Ga respectively. The Grenvillian population shows εHf values spanned from −11.7 to 4.5 and a Hf TDM model ages between 1.5 and 2.4 Ga.

a)

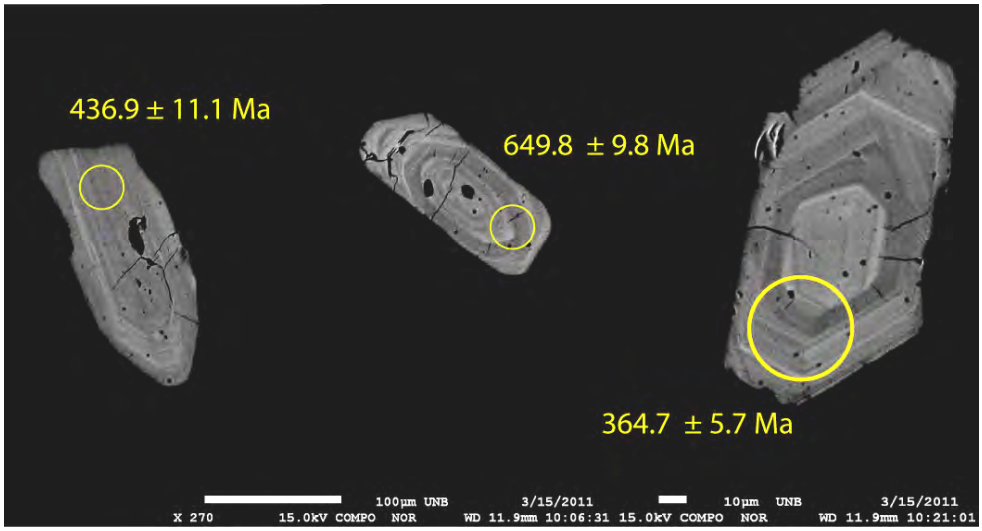

b)

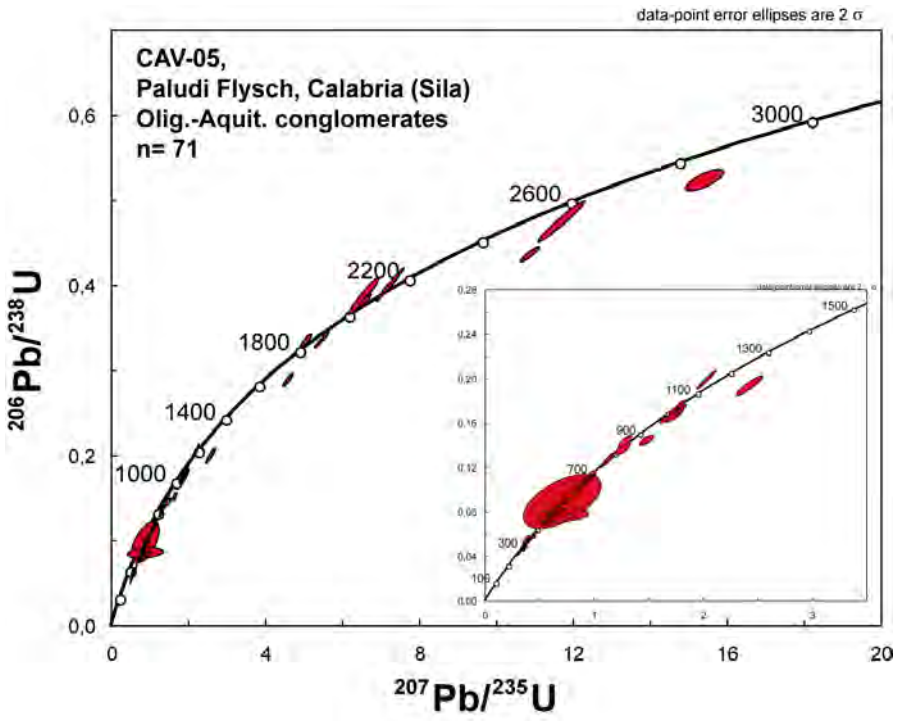

Fig. 3-70 Bse images and U-Pb ages from the CAV-05 sample. a) BSE images with zircons n.2, n.21, and n.15 b) Concordia diagram (Wetherill, 1956) with concordant age and a box with an expansion of measured from 100 Ma to 1,500 Ma.

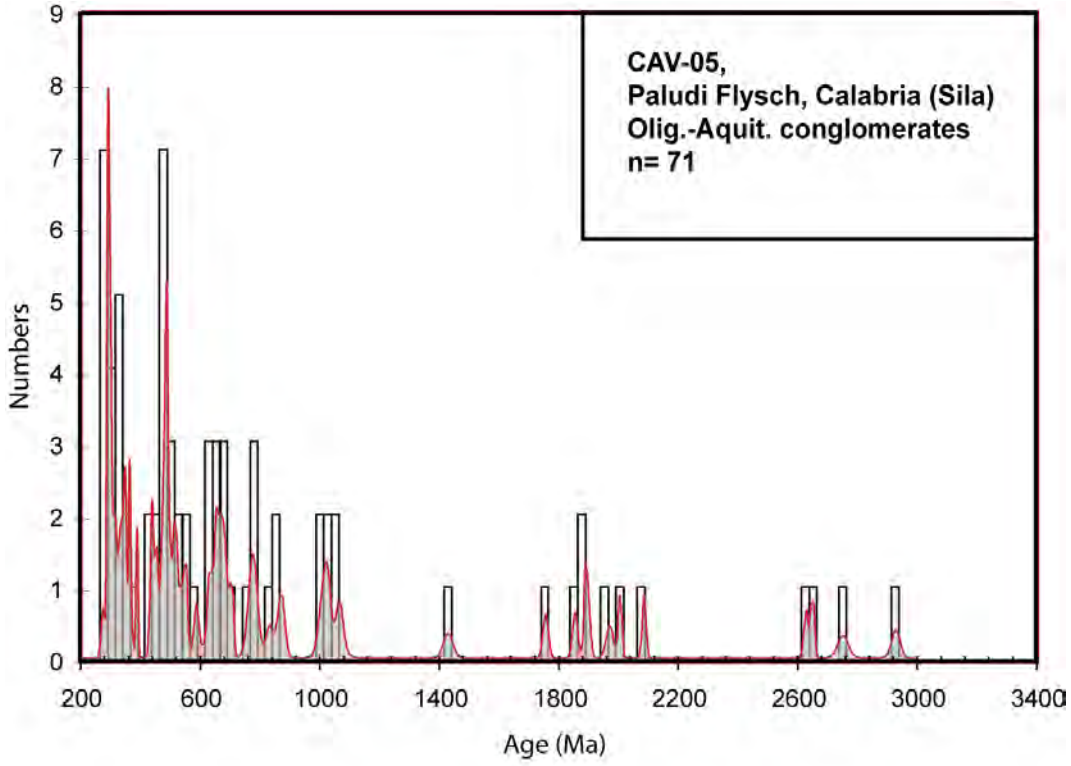

Fig. 3-71 U-Pb results shown in frequency histogram for the CAV-05 sample, for the younger ages (< 900 Ma) have been used the $^{238}U/^{206}Pb$ ratios and for the older have been used the $^{207}Pb/^{206}Pb$. The histogram shows a polymodal distribution of ages, with a main population between 300 and 1,000 Ma.

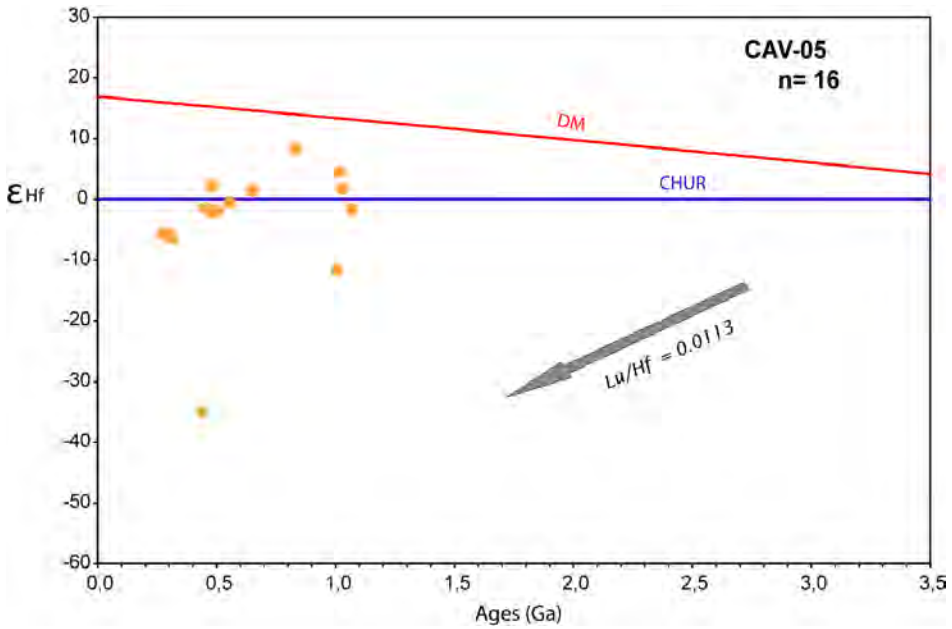

Fig. 3-72 Ages vs εHf values for the CAV-05 sample. Ages vs εHf values for the CAV-05 sample. The grey arrow represents the crustal evolution trend for Hf isotopic composition, calculated using $^{176}Lu/^{177}Hf$ = 0.0113 (Taylor and McLennan, 1985; Wedepohl, 1995)

3.2.2 SOUTHERN CALABRIA SECTOR

From the southern sector of the Calabro-Peloritani Arc (CPA) (Bonardi et al., 2001, 2004, 2008) including the Serre Massif, the Aspromonte Massif and the Peloritani Mountains, in this study the Sila and Aspromonte sub-regions have been take in account.

3.2.2.1 SERRE SUB-REGION BASEMENT

The Serre Massif represents the linkage between the southern (Aspromonte Massif and Peloritani Mountains) and the northern (Sila and Catena Costiera) sectors of the CPO (Fig. 3-74).

The poly-metamorphic crystalline basement in the Serre Massif consisting is characterized by three complexes: i) the basement composed by a granulite facies, represented the deepest level, metagabbros, felsic granulites, metabasites, and metapelitic migmatites (Maccarrone et al., 1983; Schenk, 1984, 1989; Fornelli et al., 2002, 2004; Acquafredda et al., 2006, 2008); ii) Late Variscan batholith (Serre batholith) represented the middle crustal level, consist of foliated tonalite with minor Qtz-diorite and gabbro, and felsic and peraluminous granitoid, represented the upper crustal levels (D'Amico et al., 1982; Rottura et al., 1990; De Vivo et al., 1992; Del Moro et al., 1994; Fornelli et al., 1994). In the south-western part of the batholith crop out the peraluminous Cittanova granite (Atzori et al., 1977; Crisci et al., 1979; D'Amico et al., 1982; Rottura et al., 1990; Graessner et al., 2000) (Fig. 2a); iii) in the southern part of this Massif, crop out the greenschist to amphibolite facies, represented the intermediate and upper crustal level, and meta-sedimentary and metavolcanic Palaeozoic successions (Colonna et al., 1973; Atzori et al., 1977; Bonardi et al., 1984; Acquafredda et al., 1987; Festa et al., 2003), locally intruded by leucogranite dykes (Colonna et al., 1973; Borsi et al., 1976; Bonardi et al., 1984; Del Moro et al., 1994).

According to Schenk (1989), the Serre Massif represents an entire and tilted Variscan crustal section. The peak metamorphic have been estimated only for the lower crust levels and ranges from 750 MPa at 800°C to 550 MPa at 690°C, for the bottom to the top sections (Schenk, 1984). However, Acquafredda et al. (2006) suggested a prograde metamorphism from temperature of about 500°C and pressure of 400-500 MPa to $T < 700$°C and $P \sim 800$ MPa for the migmatites representing the upper part of the lower continental crust.

On the other hand, no reliable P-T values are still available for the upper crustal level of the Massif, which is characterized by the presence of two metamorphic complexes made up of amphibolite to

greenschist facies metamorphic rocks (Stilo-Pazzano Phyllite Complex and Mammola Paragneiss Complex; Colonna et al., 1973), intruded by the late-Variscan granitoids (Rottura et al., 1990).

	Method	Age (Ma)	Data source
Sila metamorphic rocks			
Upper crust	Rb–Sr Wr	330–328 ± 4	Acquafredda *et al.* (1991)
Mid-to-upper crust	Rb–Sr Wr	326 ± 6	Acquafredda *et al.* (1992)
Lower crust	U–Pb Mnz	304–300 ± 0.4	Graessner *et al.* (2000)
Sila granitoids			
Two-mica granites	U–Pb Mnz	304–300 ± 0.4	Graessner *et al.* (2000)
Tonalites–granodiorites	$^{40}Ar/^{39}Ar$ Hbl	293.0 ± 1.0 – 291.5 ± 0.9	Ayuso *et al.* (1994)
Two-mica granites	$^{40}Ar/^{39}Ar$ Ms	293.4–289.4 ± 0.9	Ayuso *et al.* (1994)
Two-mica granites	$^{40}Ar/^{39}Ar$ Bt	292–254 ± 1	Ayuso *et al.* (1994)
Two-mica leucogranites	Rb–Sr Wr	284 ± 14	Caggianelli *et al.* (2003)
Serre metamorphic rocks			
Lower crust	Rb–Sr Wr	450 ± 20	Schenk (1989)
Lower crust	U–Pb Zrn	300 ± 10	Schenk (1980)
Lower crust	U–Pb Mnz	296–289	Schenk (1980)
Lower crust	Sm–Nd Grt, Pl	215	Schenk (1989)
Lower crust	K–Ar Hbl	180	Schenk (1989)
Serre granitoids			
Granites (Serre-Aspromonte)	U–Pb Mnz, Xen	303–302 ± 0.6	Graessner *et al.* (2000)
Tonalite	U–Pb Zrn	295 ± 2	Schenk (1980)
Tonalite	U–Pb Zrn	293.0 ± 1.5	Caggianelli *et al.* (2000)
Granodiorites	Rb–Sr Ms	288–263 ± 4	Fornelli *et al.* (1994)
Granodiorites	Rb–Sr Bt	289–266 ± 4	Fornelli *et al.* (1994)

Fig. 3-73 Metamorphic and granitoids rocks from Sila and Serre massifs after Caggianelli et al., 2007

The Serre Massif granitoids (Fig. 3-73; Fig. 3-74) could be described by two suites: one calcalkaline, metaluminous to weakly peraluminous, and one strongly peraluminous (Rottura et al., 1990). Both the suites have been associated to the late- to post-tectonic evolution and in all probability emplaced in an extensional regime along ductile shear zones (Rottura et al., 1990; Caggianelli et al., 2007).

As well as the Sila massif, the Serre massif represents a complete section through the Variscan continental crust (Schenk, 1980; Graessner & Schenk, 2001) affected by widespread LP/HT metamorphism, intense crustal anatexis and granite magmatism. The metamorphic rocks in granulite facies, representing the lower crust levels, have been separated from the greenschist facies to amphibolite facies metamorphic rocks linked to the intermediate-to-upper crust, by late-Variscan granitoids with ages of 293– 289 Ma (40Ar–39Ar on hornblende; Ayuso et al., 1994) and 303–302 Ma (Graessner et al., 2000).

The structural data (Faure, 1995; Burg et al., 1994; Carmignani et al., 1994c; Caggianelli et al., 2007) offered by the literature suggest a general tectonic framework for the Serre and Sila massifs

evolution. Theirs evolution could be linked to the post-collisional late Variscan evolution based on thermal relaxation following mid-crustal granitoid intrusion and extension (Caggianelli et al., 2007).

This study will be tacking in account the sample from the Stilo U. that is spread out in the Serre massif. Its basement is constituted by variscan granitoids and by metamorphic rocks affected by low to middle grade metamorphism.

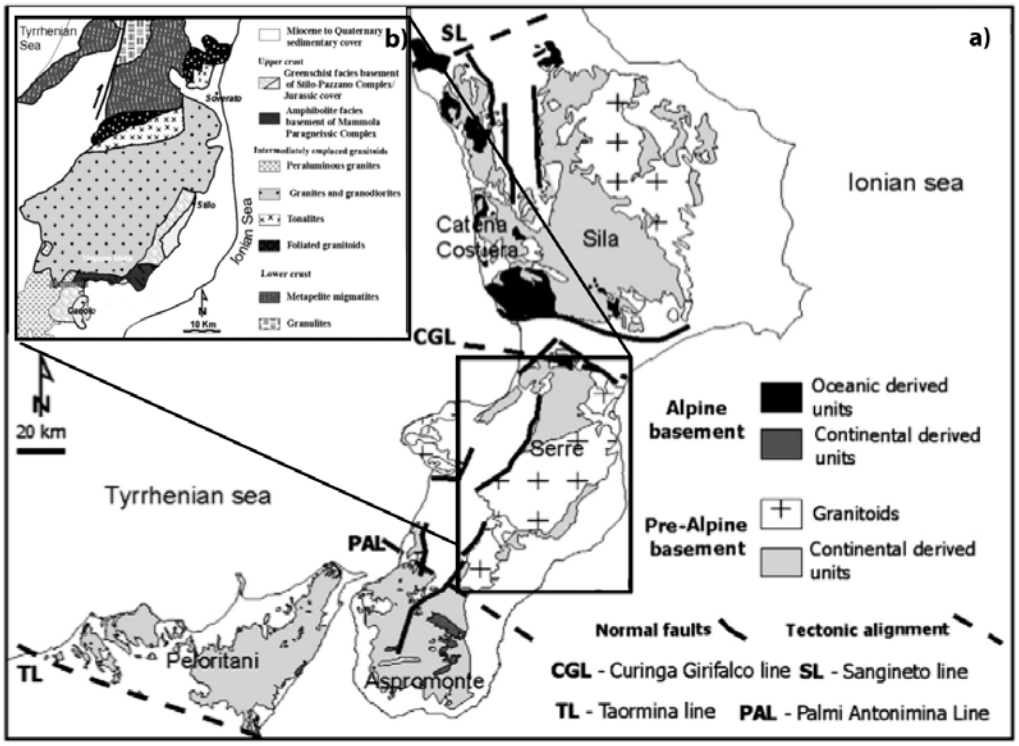

Fig. 3-74 Geological sketches modified from AngÏ et al., 2010. a) Calabria-Peloritani geological sketch with the sub-regions; b) Serre massif simplified geology.

3.2.2.1.1 Serre Sub-Region Basement Igneous Sample

The COR-13 sample is a monzogranite (Fig. 3-75) with a peraluminous composition (Shand, 1929; Fig. 3-76) collected from the Stilo U. cropping out in the Serre sub-region. This sample crops out along the Corace valley, ca. 2 km West-North-West from the Croccelletta centre (see coordinates in the Tab. 3-3). The whole rocks geochemical performed in these samples are reported in the Table 1 in Annexes section.

Plotting the SiO_2 vs K_2O compositions, the intrusive sample shows an high-K calcalkaline signature (Fig. 3-77 with an high index of SiO_2 (ca. 72) and K_2O values of ca. 4.

Plotting the samples in the Whalen et al., (1987) diagram (Fig. 3-78) is observed that the sample has an ambiguous derivation falling in the between of the I&S granite and the A-type fields (Chappel and White, 1974) and assuming an incertitude between anorogenic (A-type) or metamorphic rocks source (I-S type) derivation. Considering Pearce et al. (1984, Fig. 3-79) the sample falls in the volcanic arc (VAG) tectonic setting suggesting a continental arc field according to the Pearce et al. (1983) tectonic diagram (Fig. 3-80).

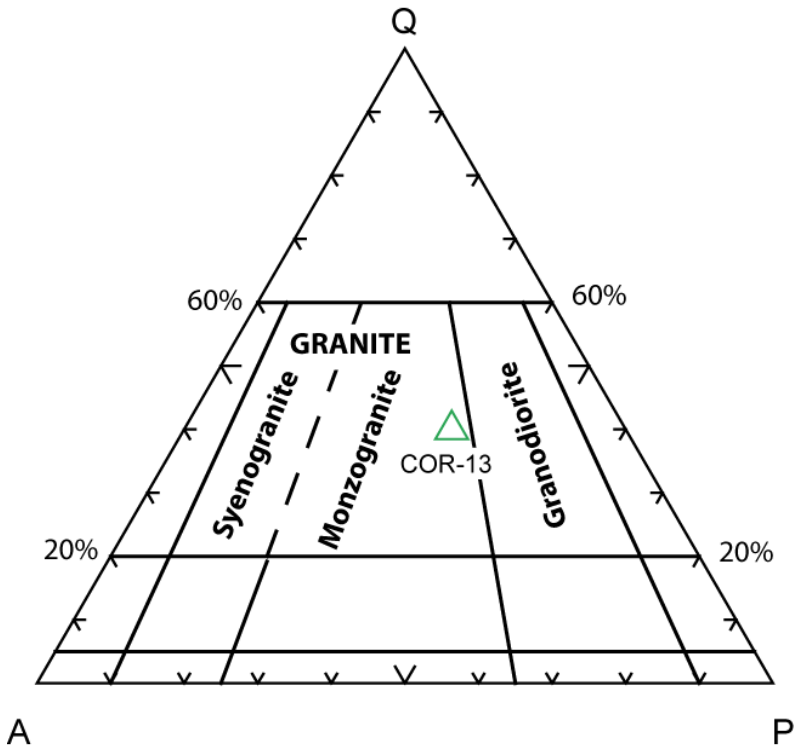

Fig. 3-75 Streckeisen 1979, showing that the COR-13 sample falling in the monzogranite field.

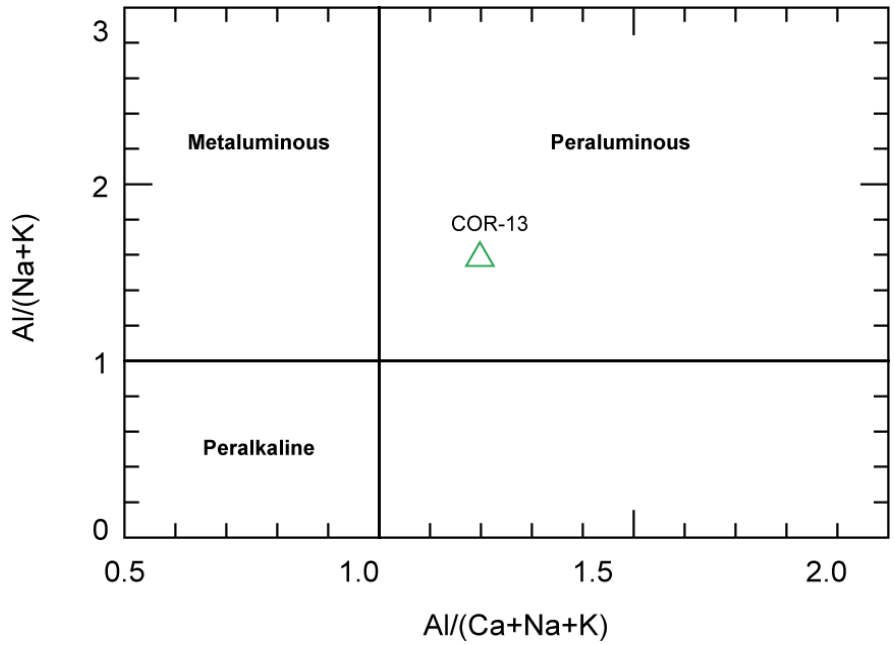

Fig. 3-76 Shand (1929) diagram where is shown the peraluminous features of COR-13sample.

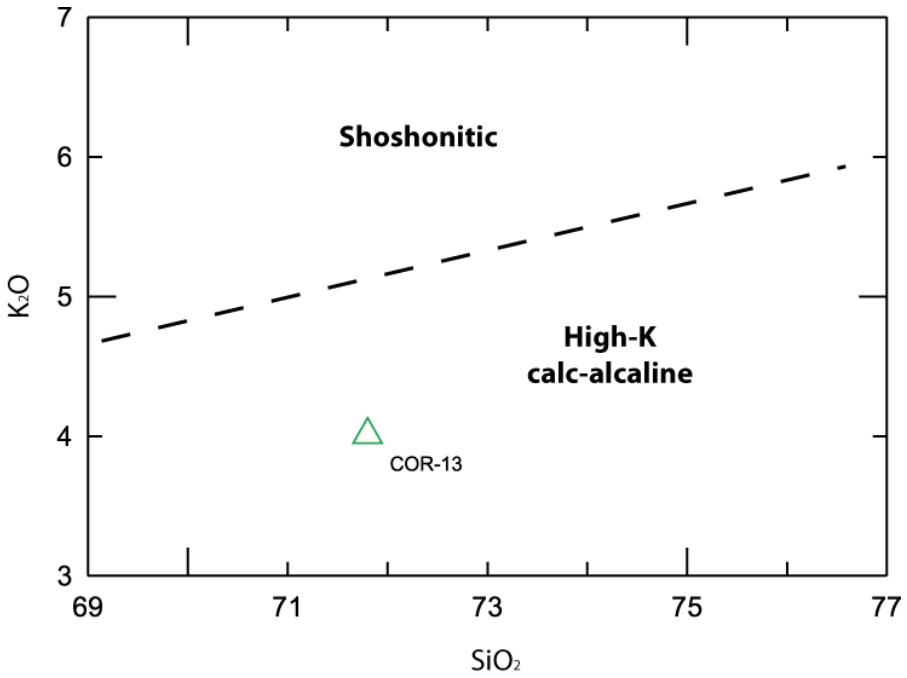

Fig. 3-77 K_2O versus SiO_2 plot showing the High-K cal-Alkaline signature of the COR-13 Serre sample.

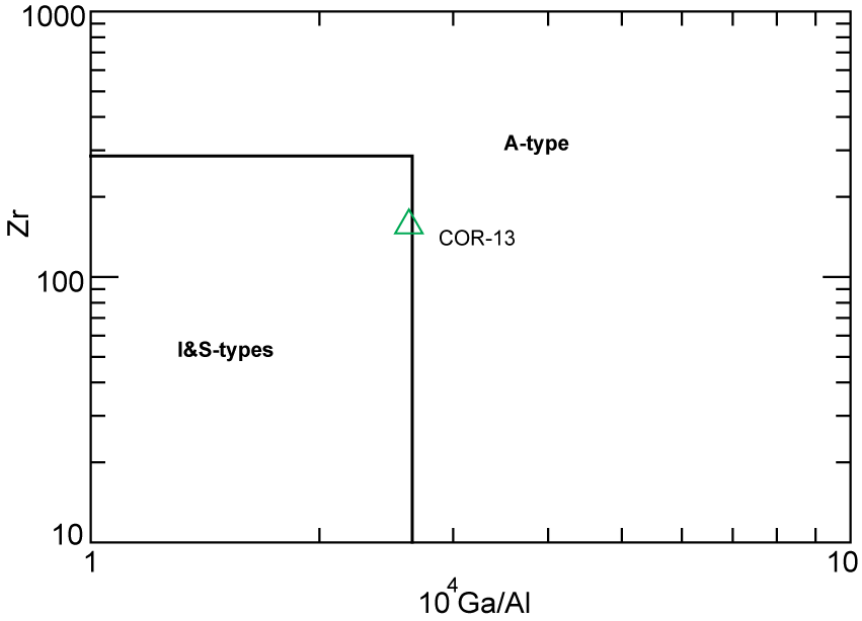

Fig. 3-78 Whalen et al., (1987) diagram showing the ambiguous nature of the COR-13 samples, falling between the I&S-types and A-types.

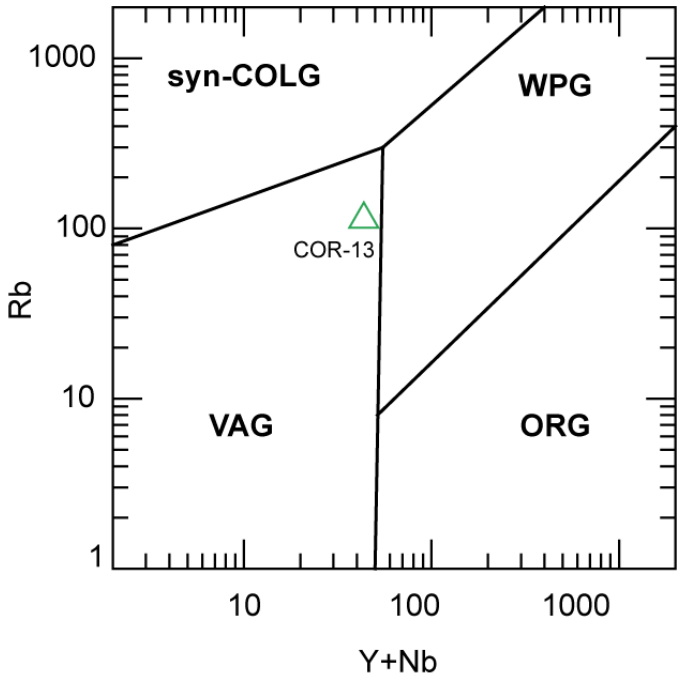

Fig. 3-79 Pearce et al., 1984 tectonic diagram suggesting the volcanic arc (VAG) setting of COR-13 granite.

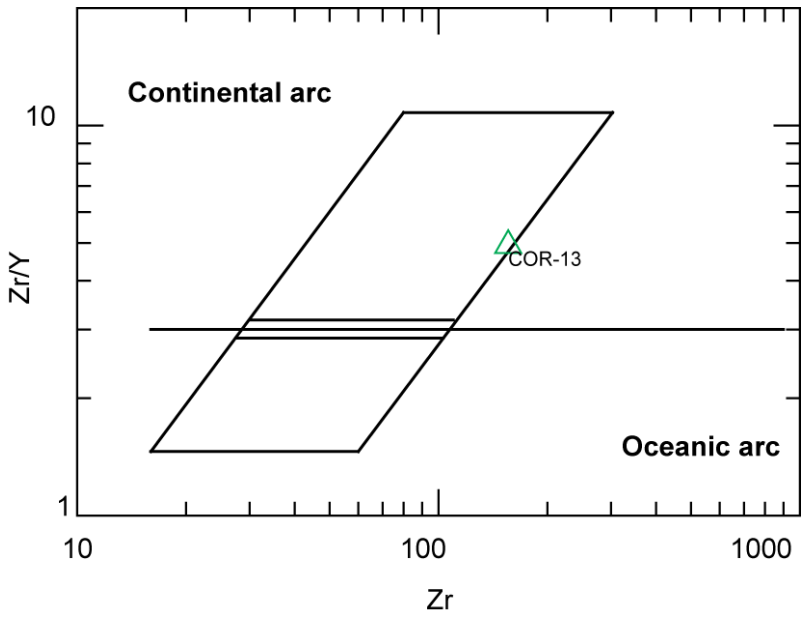

Fig. 3-80 Pearce et al., 1983 tectonic diagram showing the continental arc formation setting of COR-13 sample.

Chondrite-normalized rare earth patterns (Sun and McDonough, 1989 Fig. 3-81a) of the Serre granitic sample are LREE-enriched and HREE-decreasing with a systematically negative Eu anomaly linked to the important fractionating plagioclase process. In the multi-elements diagram primitive mantle-normalized (Sun and McDonough, 1989 Fig. 3-81b) the intrusive Serre samples show an enrichment of large ion lithophile elements (LILE) all over of Pb and an impoverishment of high field strength elements (HFSE). The sample shows the Nb, P, and Ti strong negative anomalies.

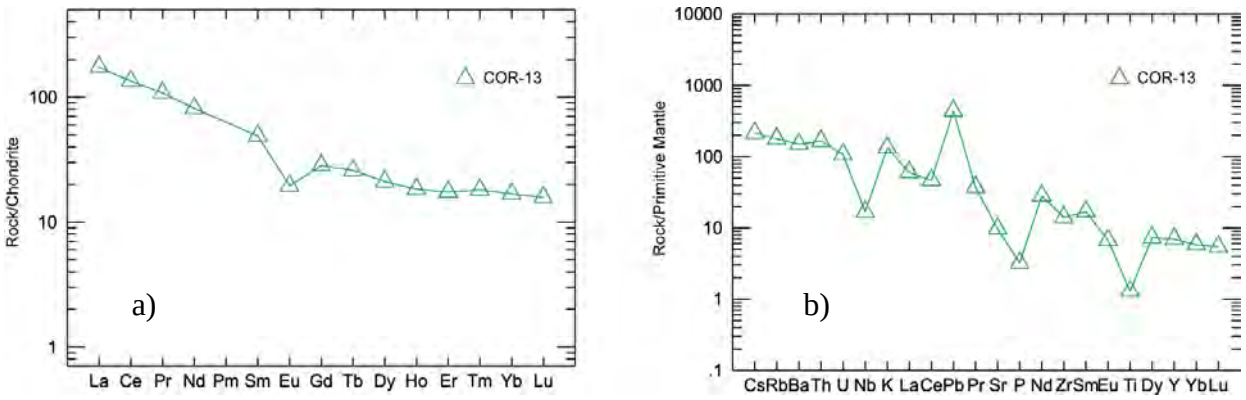

Fig. 3-81 Trace element spiders (Sun and McDonough, 1989) for PAL-16 Calabrian augen gneiss a) REE patterns normalized to chondrite and b) multi-element diagram normalized to primitive mantle.

3.2.2.1.1.1.1 U-Pb isotopes

From the Serre granite sample (COR-13) 15 zircon grains have been analyzed (Table 2 in Annexes). The majority of grains observed, are euhedral and prismatic (Fig. 3-82a), showing maximum length around 200 µm. The majority of grains are with a strong magmatic zonation. All the 15 zircon grains are concordant giving an age of 295.3 ± 1.5 Ma (Fig. 3-82a). The inherited cores found have given similar age than the rims (zircon L1- 89, L1-92, Fig. 3-82a).

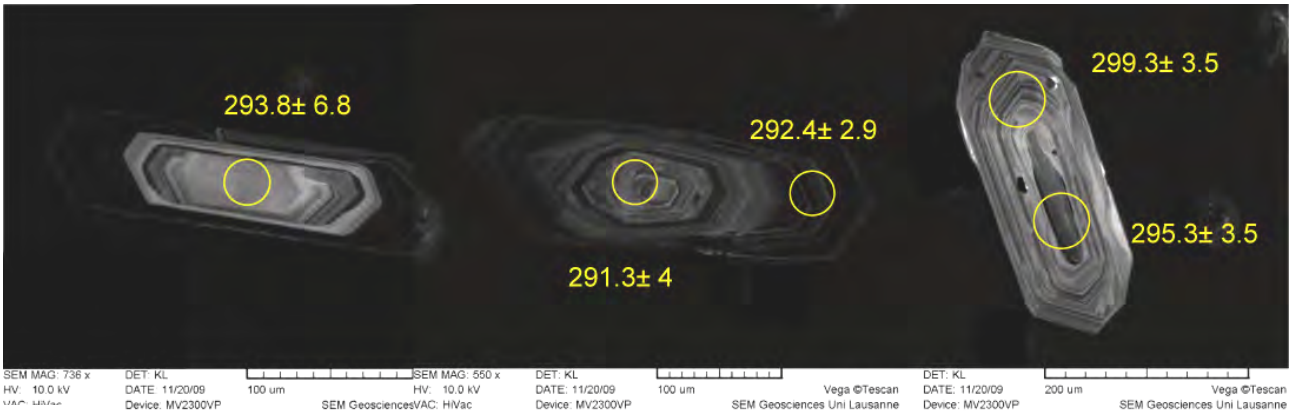

a)

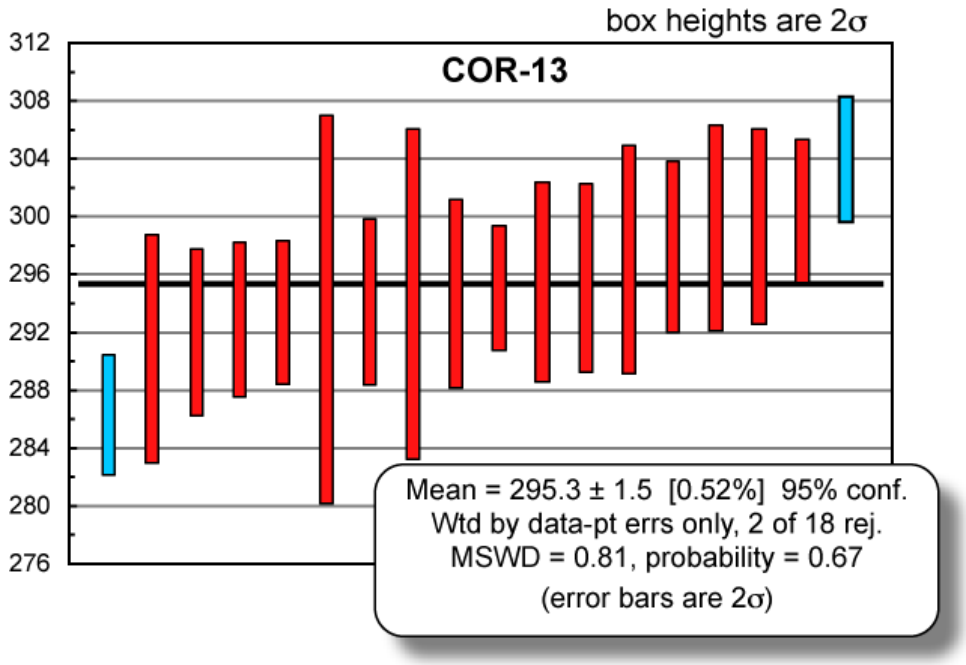

b)

Fig. 3-82 a) CL zircon images from VIV-11 sample: left) L1- 82 zircon; centre) L1- 89 zircon with measures done in the core and in the rim; right) L1- 92 zircon with measures done in the core and in the rim. In the last two samples the core shows a younger age than the rims. b) $^{206}Pb/^{238}U$ of VIV-11 sample gives an average age of 295.3 ± 1.5 Ma. Blue bars represent rejected analyses.

3.2.2.2 ASPROMONTE SUB-REGION BASEMENT

In this part of CPA (Fig. 3-83), the Variscan basement cropping out under the Stilo U has been investigated. The Stilo Unit has been chosen because it is composed by a Variscan basement not affected by Alpine metamorphism (Patacca & Scandone, 2011). The Stilo Unit also represents the highest nappe of the Calabrian Arc.

The Stilo-Unit basement comprises greenschist to amphibolite-facies metamorphic rocks intruded by late-Variscan granitoids (Bonardi et al. 1984). The Aspromonte Unit shows a metamorphism in amphibolite facies and is characterized by huge masses of augen-gneisses associated with biotite–sillimanite–garnet paragneisses and micaschists, minute leucocratic gneisses, amphibole-bearing gneisses, amphibolites, meta-ultramafic rocks, calc-silicate rocks and marbles (Bonardi et al. 1984; Micheletti et al., 2007). Phase assemblages in augen-gneisses and associated metasediments indicate equilibration under low- to high-grade conditions during the Variscan metamorphism (e.g. Bonardi et al. 1984; Schenk 1990; Fornelli et al. 2002).

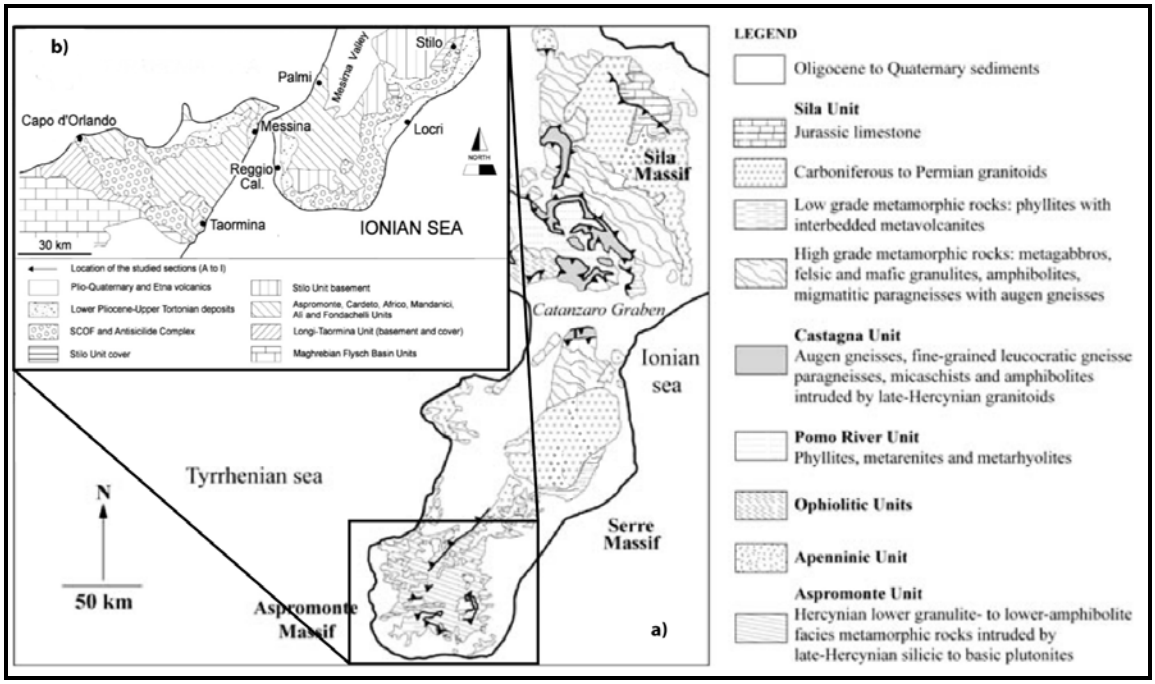

Fig. 3-83 Aspromonte geological map; a) geological sketch of CPA (modified from Micheletti et al., 2007); b) geological simplified map of Aspromonte sub-region (modified from Bonardi et al., 2003)

3.2.2.2.1 Aspromonte Sub-Region Basement Igneous Sample

This PAL-16 sample has been collected from the Stilo U. cropping out ca. 1,7 km South- South-West from the Palizzi village (see coordinates in the Tab. 3-3).

Fig. 3-84 The augen-gneiss in the location where the sample PAL-16 has been collected

The whole rocks geochemical performed in these samples are reported in the Table 1 in Annexes section. The PAL-16 is an augen-gneiss (Micheletti et al., 2007) (Fig. 3-84) having granitic protholit following the Streckeisen (Fig. 3-85) falling in the monzogranite field. Following the Shand (1929) diagram the sample shows a peraluminous composition (Fig. 3-86). Plotting the SiO_2 vs. K_2O the sample shows an high-K calcalkaline signature (Fig. 3-87) with an index of ca. 70 of SiO_2 and 4.6 of K_2O.

This sample has a Y+Nb / Rb ratio typical of a volcanic continental arc (Pearce et al., 1984, Fig. 3-89, Pearce et al., 1983, Fig. 3-90), and it falls in the I&S type (Fig. 3-88), likely S-type (derived from meta-sedimentary sources; Chappell and White, 1974) suggested also by its strongly peraluminous nature. These granite-types, likely are generated by partial melting of metasedimentary rocks as a result of thermal relaxation and/or exhumation of the orogen (England & Thomson 1984).

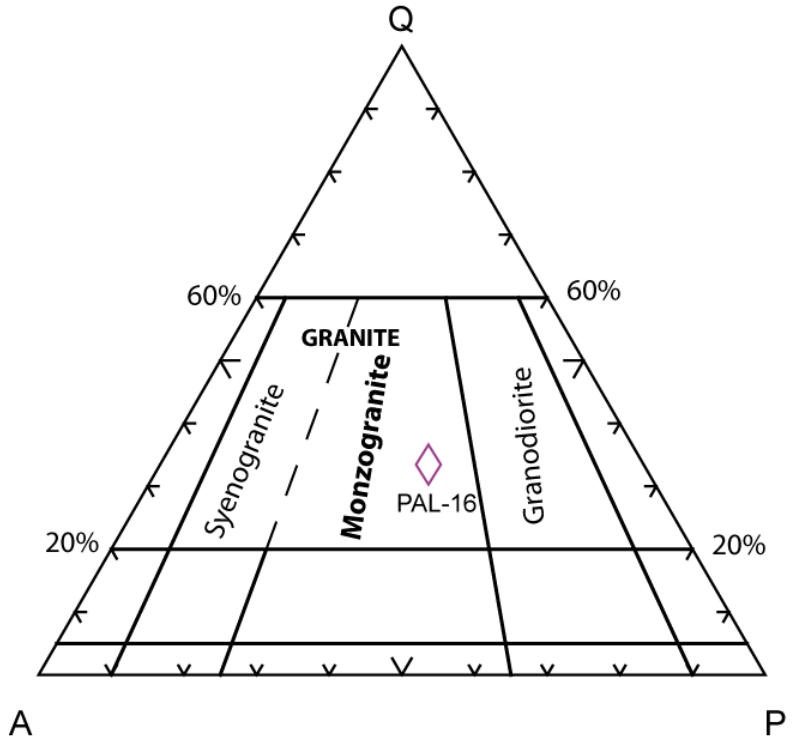

Fig. 3-85 Streckeisen 1979, showing that the PAL-16 sample protholit falling in the monzogranite field.

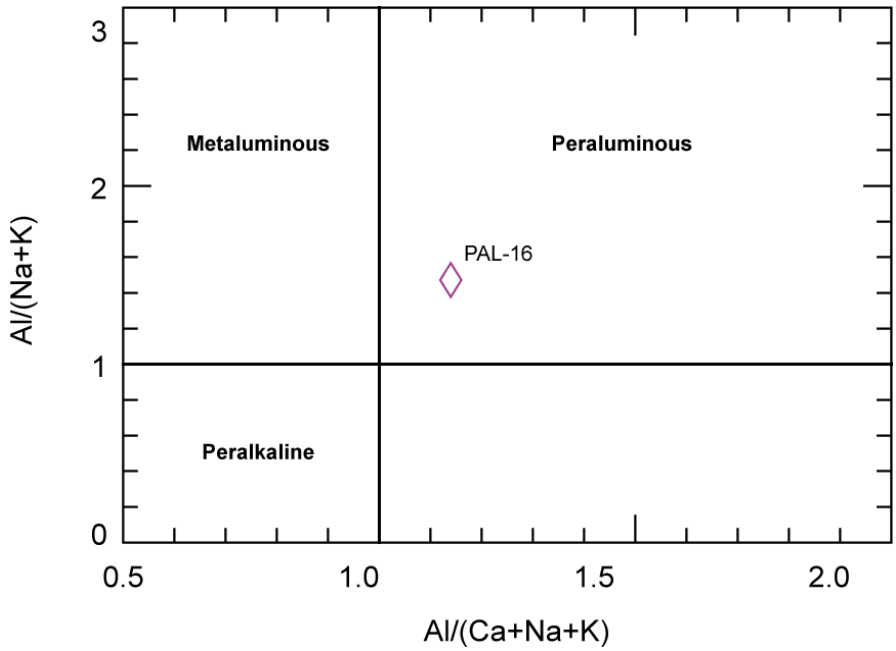

Fig. 3-86 Shand (1929) diagram where is shown the peraluminous features of PAL-16 sample.

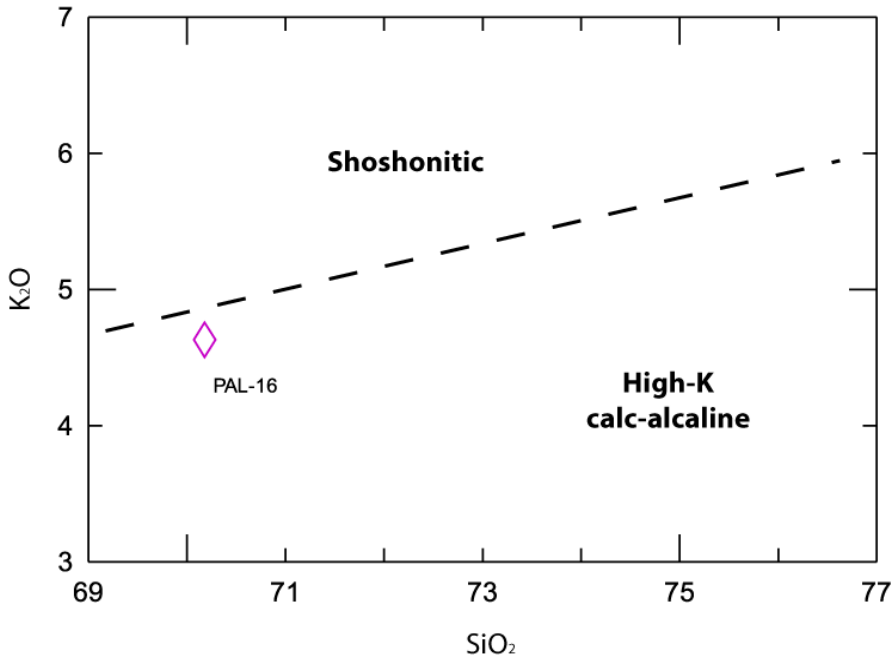

Fig. 3-87 K_2O versus SiO_2 plot showing the High-K cal-Alkaline signature of the PAL-16.

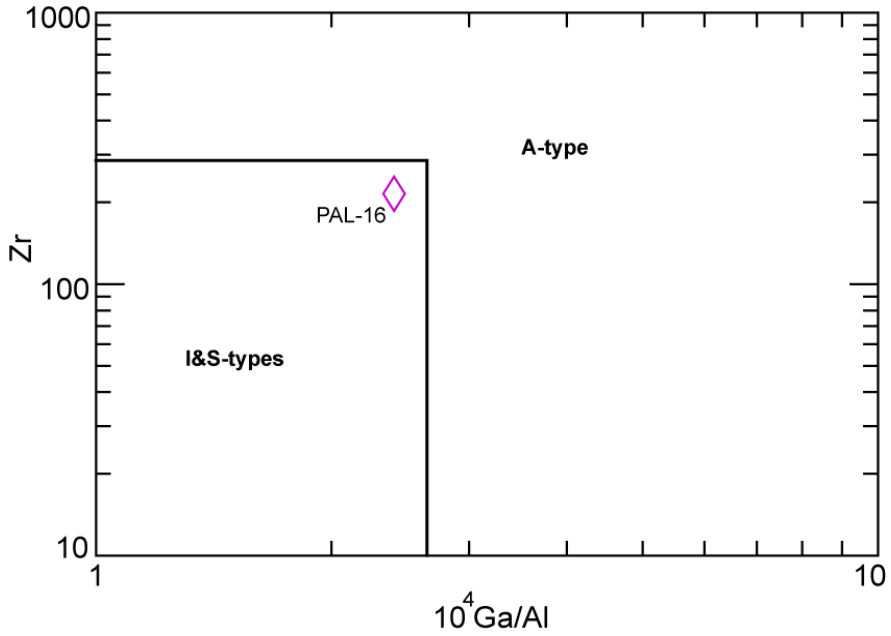

Fig. 3-88 Whalen et al., (1987) diagram showing the I&S-types of the PAL-16 granitoid.

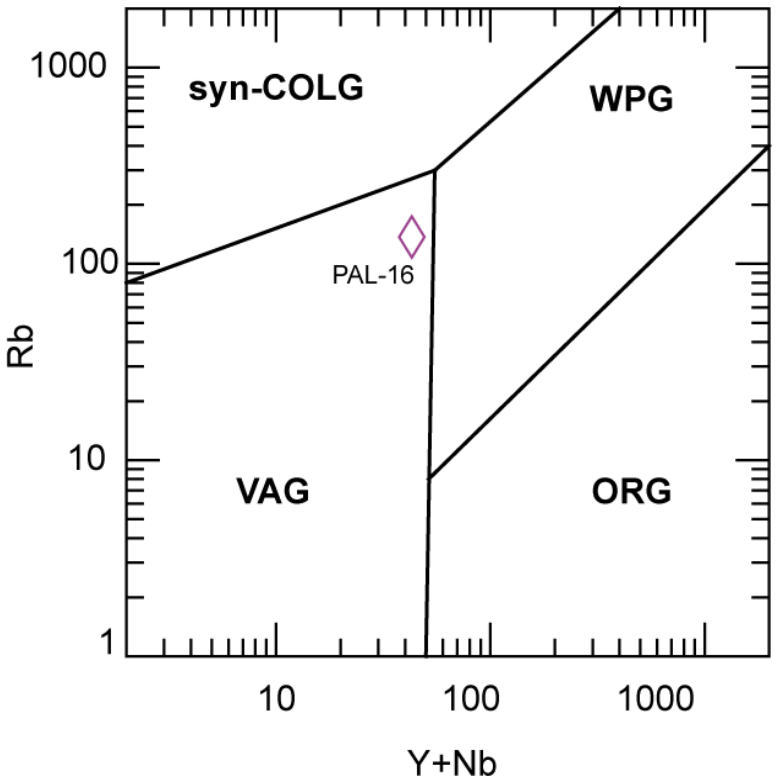

Fig. 3-89 Pearce et al., 1984 tectonic diagram suggesting the volcanic arc setting of PAL-16 protholit.

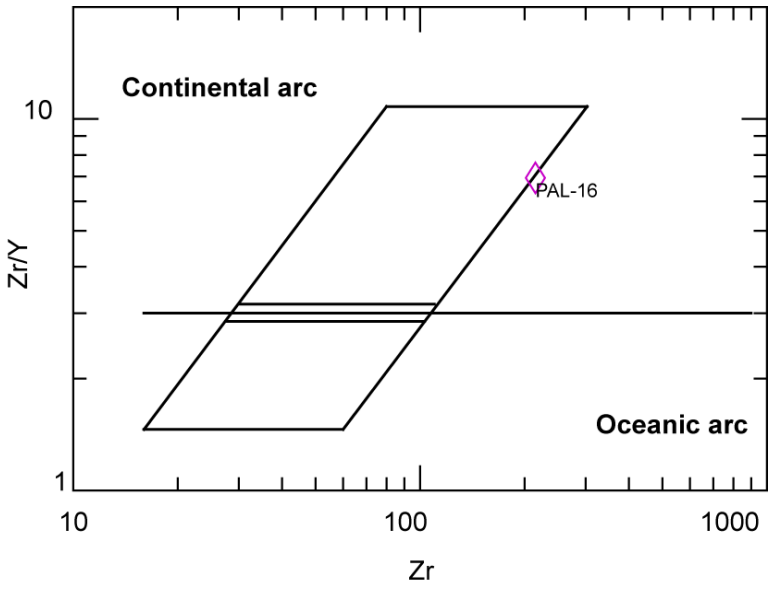

Fig. 3-90 Pearce et al., 1983 tectonic diagram showing the continental arc formation setting of PAL-16 protholit.

Chondrite-normalized rare earth patterns (Sun and McDonough, 1989 Fig. 3-91a) are LREE-enriched with flat HREE and a systematically negative Eu anomaly linked to the important fractionating plagioclase process. Trace element patterns normalized to the primitive mantle are homogeneous (Sun and McDonough, 1989 Fig. 3-91b) with negative anomalies in Ba, Nb, P and Ti.

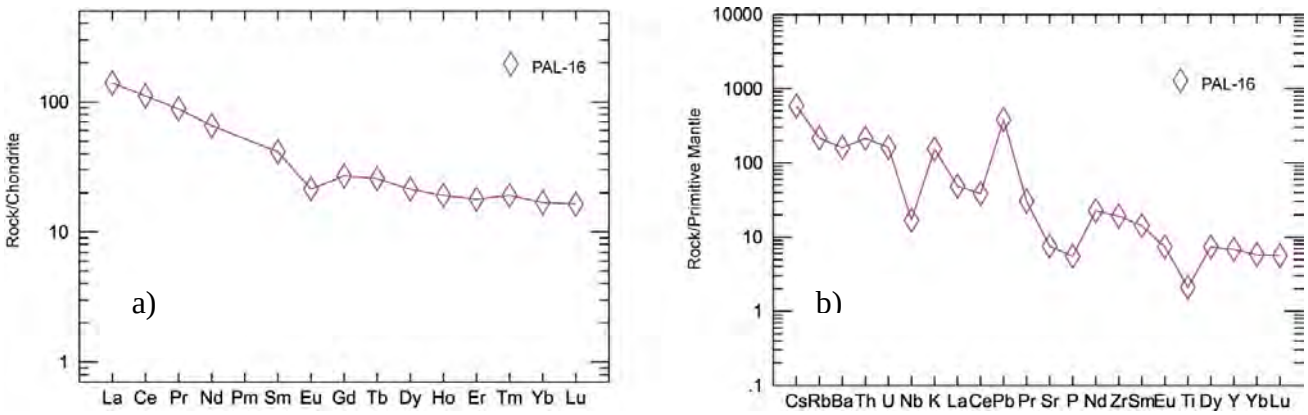

Fig. 3-91 Trace element spiders (Sun and McDonough, 1989) for PAL-16 Calabrian augen gneiss a) REE patterns normalized to chondrite and b) multi-element diagram normalized to primitive mantle.

3.2.2.2.1.1.1 U-Pb isotopes

From the PAL-16 sample 15 zircon grains have been analyzed (Table 2 in Annexes). They show a maximum length of 200 μm, are euhedral and prismatic (Fig. 3-92a) with strong magmatic zonation. Rare inherited cores have been found and they have given similar age respect of the rimes (zircon L3-33, Fig. 3-92a). The 8 zircon grains are concordant and show an average age of 553 ±4.1 Ma (Fig. 3-92b), interpreting like a crystallization age of augen-gneiss protholit.

Is possible to link this augen to the large bodies of granitic orthogneisses occurring in most segments of the European Variscan belt, from the Central Iberian Zone in Spain to the Bohemian Massif with emplacement ages mainly Latest Precambrian–Early Cambrian.

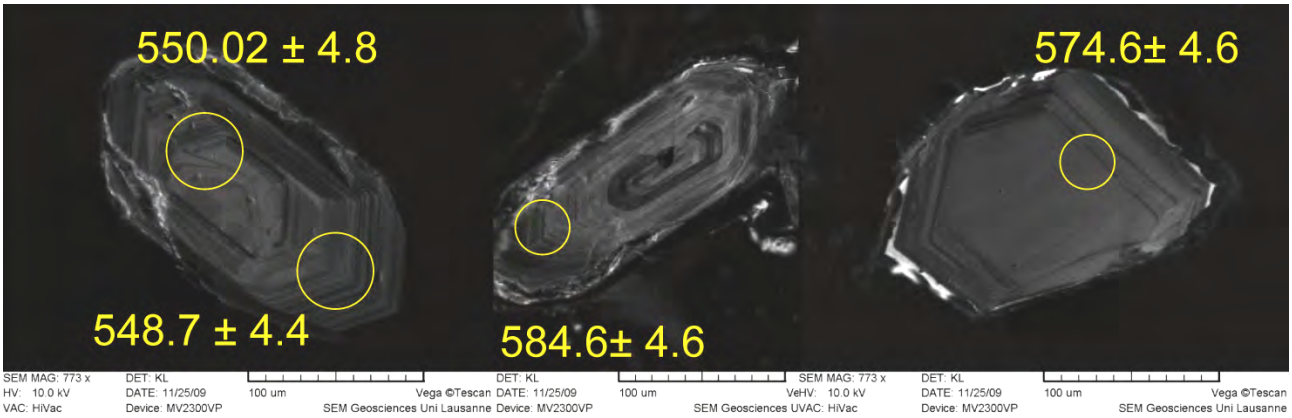

a)

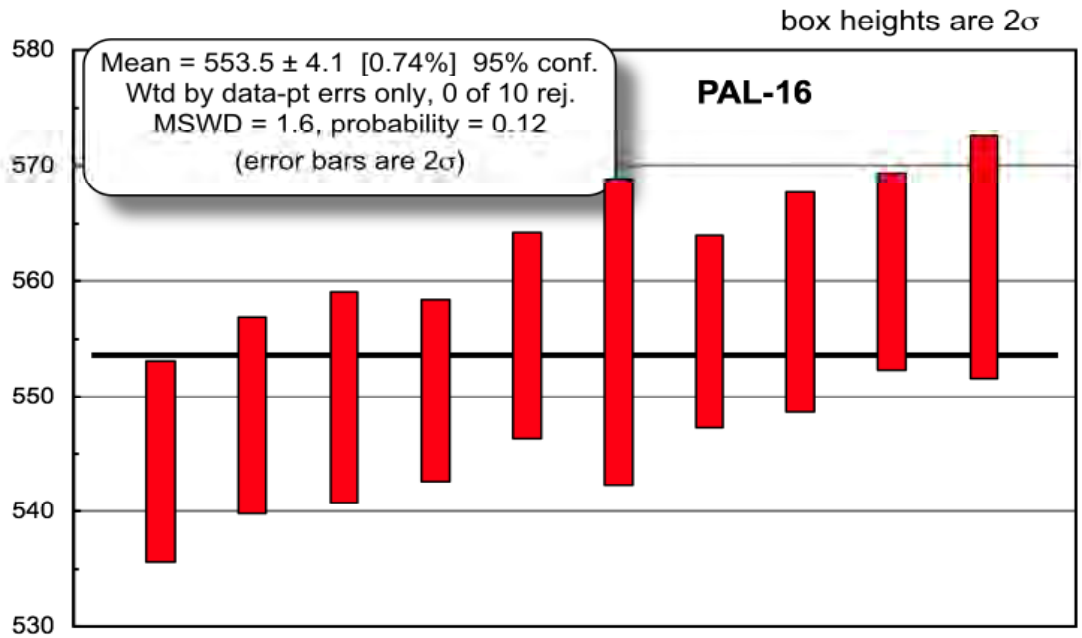

b)

Fig. 3-92 a) CL zircon images from PAL-16 sample: left) zircon L3- 33; centre) zircon L3- 26; right) zircon L3-16; b) $^{206}Pb/^{238}U$ of PAL-16 sample gives an average age of 553 ±4.1 Ma.

3.2.2.3 ASPROMONTE SUB-REGION COVERS

The southern sector of the Calabria–Peloritani Arc (Fig. 3-83) has been made by a crystalline basement nappe stack sealed by the late orogenic turbiditic deposits of the Stilo– Capo d'Orlando Formation.

The lowermost (Longi–Taormina Unit) and the uppermost (Stilo Unit) nappes of the tectonic stack are provided with a well developed pre-orogenic sedimentary cover, whereas an Alpine cover is either completely lacking or represented by small tectonic slices of Mesozoic rocks in the intermediate tectonic units (Fig. 3-94).

The Longi–Taormina U. is characterized by a continue sequence with the Frazzano Flysch at the top, Eo-Oligocene in age (Ogniben, 1960). The Stilo U. cropping out in the Southern sector of CPA, is characterized by Palaeozoic low metamorphic rocks and by Mesozoic deposits with age spanned from Trias to Cretaceous. To the Stilo U. belonged the Pignolo Fm. (Bonardi et al. 2002), the Palizzi Fm. and the Stilo Capo d'Orlando Fm. (at the top of the sequence). This last formation is until now debated because of its gaps and Cenozoic terranes.

The formation of the Southern Sector of the CPA is likely formed between the Upper Aquitanian to the Early Burdigalian (Bonardi et al., 2002). The deformation age is considered not older than Aquitanian (Capoa et al., 1997). The Stilo U. deformation also could be occurred at the limit Aquitanian–Burdigalian, between the end of deposition of Pignolo Fm and the oncoming sedimentation of Stilo Capo d'Orlando Fm. (Bonardi et al., 2002).

3.2.2.3.1 Aspromonte Sub-Region Tertiary Sample

The CA-PAL sample has been collected 2 km NNW from the Palizzi village (see coordinates in Tab. 3-3). The sample is part of the Stilo Capo d'Orlando Formation (Fig. 3-94), well extended from the Peloritain Mounts (Sicily) to the Serre Massif. This formation is constituted by silicoclastic torbidites (Fig. 3-93) stopped in the Langhian time, when occured the deposition of the "Argille Varicolori" belonging to the Antisicilidi units. the "Argille Varicolori" deposit is until now of doubtful provenance (Bonardi et al. 2002) but interpreted like a Sicilide Basin backthrust (Ogniben, 1960, 1969, 1973).

In the Stilo Capo d'Orlando Fm. three main sedimentary bodies have been distinguished (Cavazza et al., 1993) (Fig. 3-94):

i) Lutites and marbles belonging to the hemipelagic basin sedimentation.

ii) Conglomerates with debris linked to marine paleo-canyons.

iii) Turbidites finely stratified with thicker sandstone. At the top of the sequence silexites strata linked to the Burdigalian volcanoclastic event have been found (Lorenz, 1984). At the bottom conglomerates derived from phyllites and Giurassic carbonates of the Stilo U. have been found (Bonardi et al., 1984).

Fig. 3-93 Silico-clastic turbidites from where has been collected the sample CAV-05.

The conglomerates are constituted by granodiorites, andesites and limestone from the Stilo U. (Bonardi et al., 2002) and from the more metamorphic Aspromonte U. (Bonardi et al., 1980b; Cavazza, 1989).

Likely, the deposition of the Stilo Capo d'Orlando Fm. is linked to the Algerian Basin first step opening (Heymes et al., 2008). This kind of sedimentation could be interpreted as the erosion result consequent to the nappes formation in the whole southern sector of the CPA CPASS (Bonardi et al., 2002).

Considering the faunistic content found in the calcarenites belonging to the Stilo Capo d'Orlando Fm. several ages have been suggested:

- Early Oligocene (Weltje, 1992);
- Upper Oligocene (Cavazza et al., 1997; Courme & Mascle, 1988; Meulenkamp et al., 1986; Patterson et al., 1995);
- Upper Rupelian or Early Burdigalian (Heymes et al., 2008);

- Upper Aquitanian (Bonardi et al., 1980) ;
- Middle or Upper Burdigalian (Bonardi et al., 2002).

3.2.2.3.1.1 Zircon study

Almost 100 zircons have been analyzed and observed under optical microscope. They are brownish (the bigger grains), due, likely, to hydrothermal alteration that affected zircons during more sedimentary cycles, sub-euhedral with main length around 150-200 mμ, also grains up to 300 mμ have been found. Some zircons show apatite inclusions. Rare inherited cores have been found. As shown in the Fig 3.94a. zircon n.4 shows a core older ca. 20 Ma than near the rim. About the 30 % of zircons, because of their weak signal, likely done by small and thin size, have been ablated under LA-ICP-MS by a raster and not a spot (Fig. 3-95a: zircon n. 25). The majority of zircons are characterized by micro-fractures and inclusions.

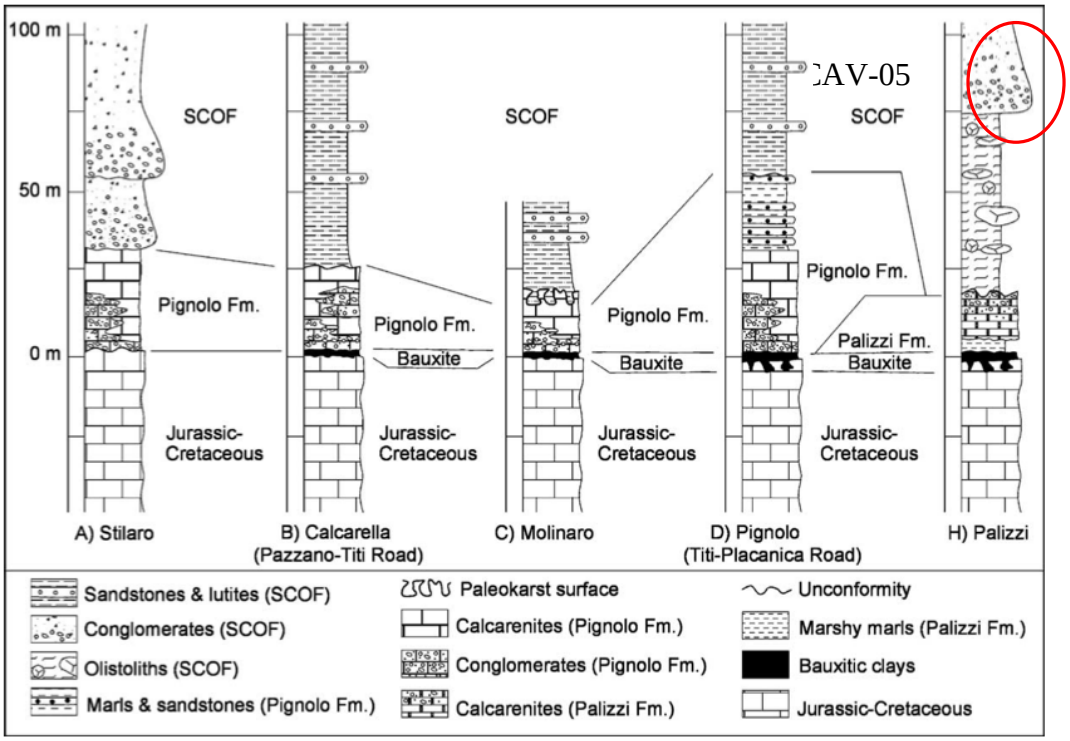

Fig. 3-94 Comparison between several Stilo Capo d'Orlando (SCOF) logs cropping out in different part of the Aspromonte from (from Bonardi et al., 2002). To collect the CAV-05 sample has been take in account the upper part of the H log characterized by micro-conglomerate and quartz-arenites.

3.2.2.3.1.1.1 U-Pb isotopes

Fifty-four U-Pb analyses (Table 2 in Annexes) on single grains from the Stilo Capo d'Orlando Fm. sample (CA-PAL), were performed and reported in the Concordia diagram (Wheterill, 1956; Fig. 3-95,b) They are concordant except for some slightly discordant Neoproterozoic and Archean zircons.

The frequency density histogram of the CA-PAL sample shows ages spanned from 300 Ma to 2,600 Ma (Fig. 3-96) with a main unimodal distribution of the ages with a main population (90% of all zircons) between 300 and 540 Ma zircon ages with a main Pan-african peaks at 530 Ma and a secondary peak at 650 Ma. Are also recognised sporadic Archean peaks. Between ca. 700 Ma and 2,400 Ma the sample are characterized by a lack of zircon ages.

3.2.2.3.1.1.2 Lu-Hf isotopes

Eight U–Pb zircon grains (Fig. 3-97), previously U-Pb measured, have been analyzed for their Hf isotopic compositions (Table 3 in Annexes). Two Carboniferous grains show εHf values spanned from −2.1 to 0.3 with Hf TDM model ages between 1.1 and 1.3 Ga. Four zircon grains related to Pan-african orogeny have negative ε Hf values between −3.3 to -1 with Hf TDM model ages between 1.4 and 1.5 Ga. A Cryogenian zircon grain shows a positive εHf value of 1.5 with Hf TDM model ages of 1.3 Ga. The Neoarchean zircon grain shows a negative εHf value of - 5 .7 with Hf TDM model ages of 3.2 Ga.

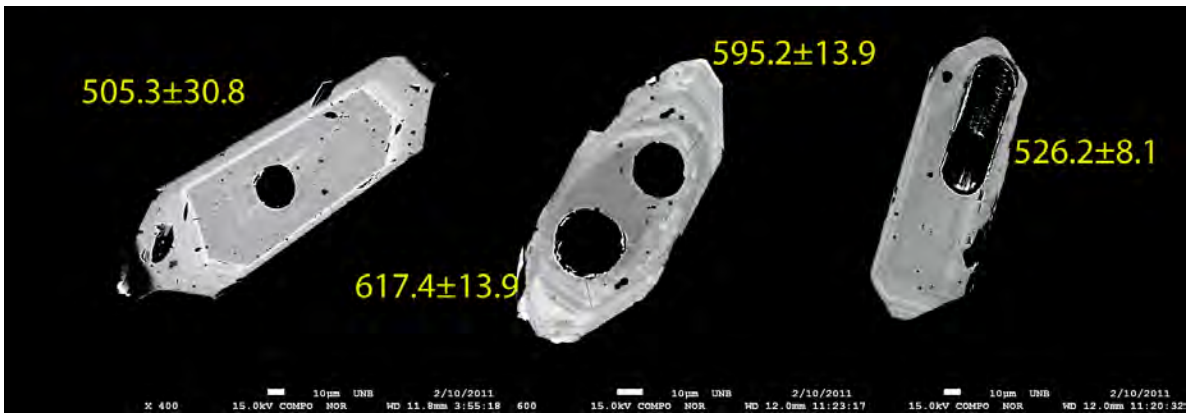

a)

b)

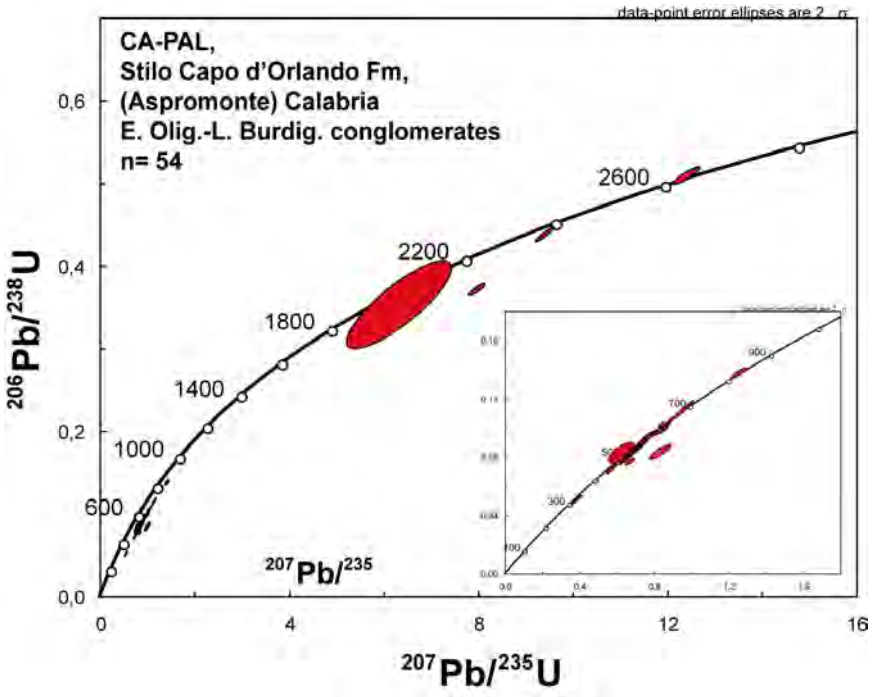

Fig. 3-95, a) BSE images with zircons n.12 (left), n.4 (centre), and n.25 (right) (measured by raster). b) Concordia diagram (Wetherill, 1956) with concordant age and a box with an expansion of measured from 100 Ma to 1,000 Ma.

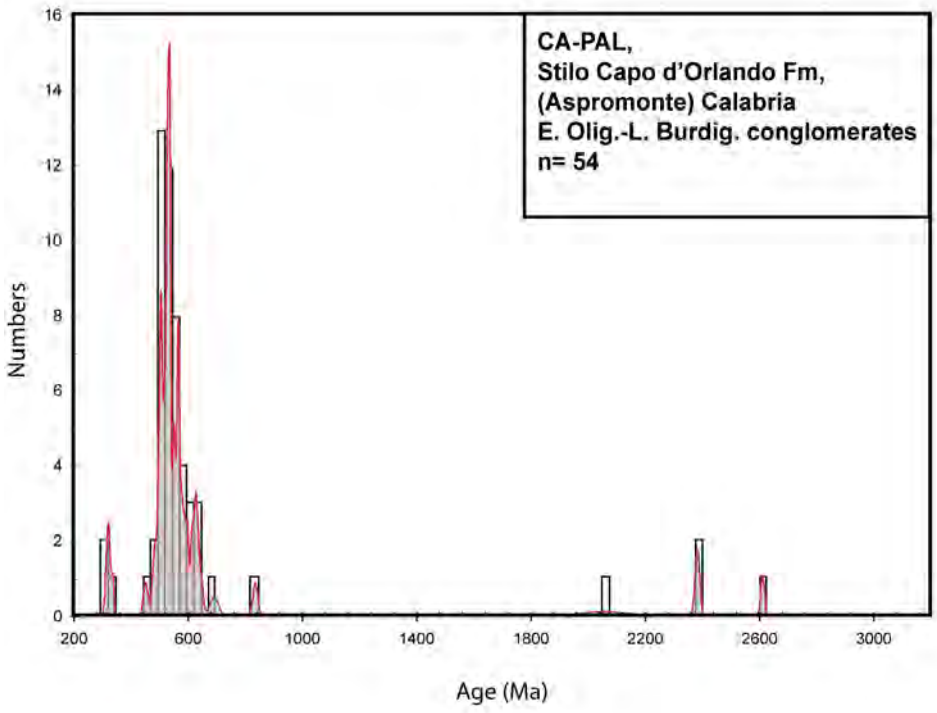

Fig. 3-96, U-Pb results shown in frequency histogram for the CA-PALsample, for the younger ages (< 900 Ma) have been used the $^{238}U/^{206}Pb$ ratios and for the older have been used the $^{207}Pb/^{206}Pb$. The histogram shows a polymodal distribution of ages, with a main population between 300 and 1,000 Ma.

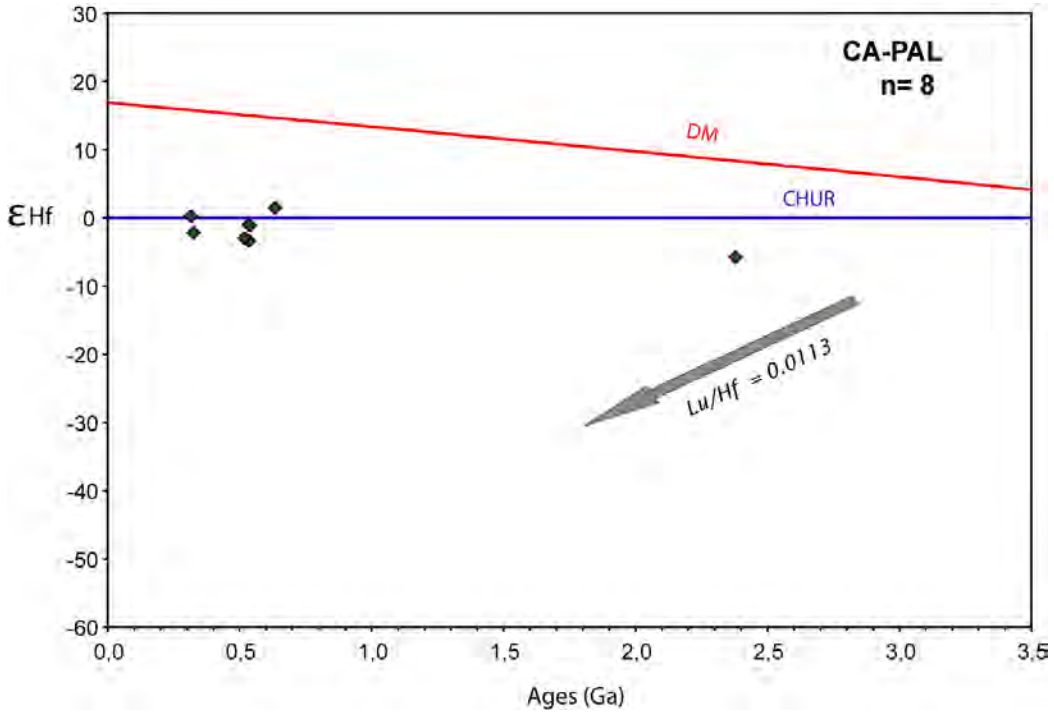

Fig. 3-97, Ages vs εHf values for the CA-PAL sample. The grey arrow represents the crustal evolution trend for Hf isotopic composition, calculated using $^{176}Lu/^{177}Hf$ = 0.0113 (Taylor and McLennan, 1985; Wedepohl, 1995).

4 DISCUSSION

In this chapter will be illustrate in a critical way the analogies and differences between the two blocks using the data illustrate in chapter 3. Here will be draft a Variscan magmatic evolution by the geochemical data performed from the basement rocks, will be take in account analogies or differences between the Sardinian nappe and foreland by magmatic and detrital zircons. Then will be discuss the Tertiary deposits cropping out in the SCB and in the CPA and theirs links with the main regional events registered by theirs zircons in order to suggest a re-location in the Gondwana peri-terranes, by detrital zircons ages and Lu-Hf isotopes.

4.1 PALAEOZOIC MAGMATIC SAMPLES

With the aim to give a new data and contributing to draft a comparison between terranes belonging to the Variscan European chain, have been studied few magmatic bodies collected in the SCB and CPA.

For their better exposition and literature knowledge respect of the Calabrian bodies, the Palaeozoic Sardinia formations are easier to insert them in the European Variscan scenario that fournishes more constraints for the reconstructing the Variscan evolution.

In fact one of the problems to study these Palaeozoic magmatic bodies is due to theirs complex evolution in terms of secondary magmatic pulses and metamorphic overprints. These troubles give difficult to constrain a detailed evolution without a more accurate petrographic studies that are not the focus of this thesis. So here will be furnish a general contextualization of the data in terms of tectonic and geodynamic setting. The geochemical data here performed in whole rocks help to better constrain the belonging of the “terranes” investigated in a wider context abroad the present-day Tyrrhenian basin.

4.1.1 MAGMATIC ORDOVICIAN SAMPLES

Even if the geodynamic Ordovician evolution of the SCB, particularly of the Nappe zone, is better understood because has been also recently deeply studied, and is constrained by an important amount of data, still lack a comparison between the different tectonic units and between Sardinian nappes and Calabria ambiguous units.

The older Ordovician volcanic rocks found in Sardinia region are recently dated back to Lower Ordovician time. They are rare, small outcrops scattered in the tectonic units either of the external and internal nappes. The huge amounts of volcanic rocks were emplaced during the Middle-Upper Ordovician period in the Nappe Zone of Sardinia above the so called Sardic unconformity. As the rocks range from andesite to rhyolite and have a calcalkaline geochemical imprint, an Andean-type volcanism related to Early Ordovician oceanic subduction has been proposed to explain this event (Cappelli et al., 1992, Oggiano et al., 2009; Gaggero et al., 2012). The Late Ordovician marks the end of this volcanism, the collapse of the continental arc and a Caradocian–Ashgillian transgression of the North-Gondwana margin. A third, new volcanic cycle represented by basalt and microgabbro with an alkaline to transitional signature encompassed the Ordovician– Silurian transition all over Sardinia.

Here all the Sardinian samples analysed have given an age of Middle-Upper Ordovician, in agreement with the stratigraphic position as inferred from published data.

The two samples collected from Sarrabus Unit (SM-200 and BS-125) have given an age of 458.7 ± 2.8 Ma, and 464.6 ± 7.3 Ma; the Arburese volcanites ("Porfidi grigi", CC-150) have given an age of 465.5 ± 5.4 Ma. Also the orthogneisses (SAR05-09 and 28 sample) collected in the Spartivento area have given an age of 462 ± 5.7 Ma and 459.6 ± 3.9 Ma. The ages here obtained are concordant with the Sandian dacites (457.01 ± 0.17 Ma) recently attributed (Pavanetto et al., 2012) to the Bithia Unit. metavolcanic rocks.

The data carried on from Sardinia Ordovician rocks well fit with the age found for the prophyroid collected in the northern part of the CPA, in the Sila sub-region. In fact this sample (VIV-11), belonging to the Bocchigliero Unit, gives an age of 466.4 ± 6.9 Ma.

Considering the comparison of these ages is plausible to corroborate a similar evolution of these blocks during the Ordovician time.

Following the tectonic classification of Pearce et al. (1984), the samples analysed in Sardinia show an anomaly respect to what described by other authors (Di Pisa & Oggiano, 1992; Oggiano et al., 2010; Gaggero et al., 2012). Whereas these authors considered the Middle-Upper Ordovician a

typical product of a volcanic arc on continental crust, since their calcalkaline signature, the Sarrabus volcanites (samples SM-200 and BS-125) have been developed in tectonic scenario of within plate (Fig. 3-10) as well as the Bithia U. dacite (Fig. 3-23) and granitic bodies (Fig. 3-31). Also considering the geochemical features REE patterns normalized to chondrite (Sun and McDonough, 1989) all the samples show the trend with are LREE-enriched with flat-decreasing HREE a Eu negative anomaly related to evoluted magma (Fig. 4-1).

The magmatic Ordovician samples studied here permit to well confine the two blocks (SCB and CPA) in the same Ordovician evolution.

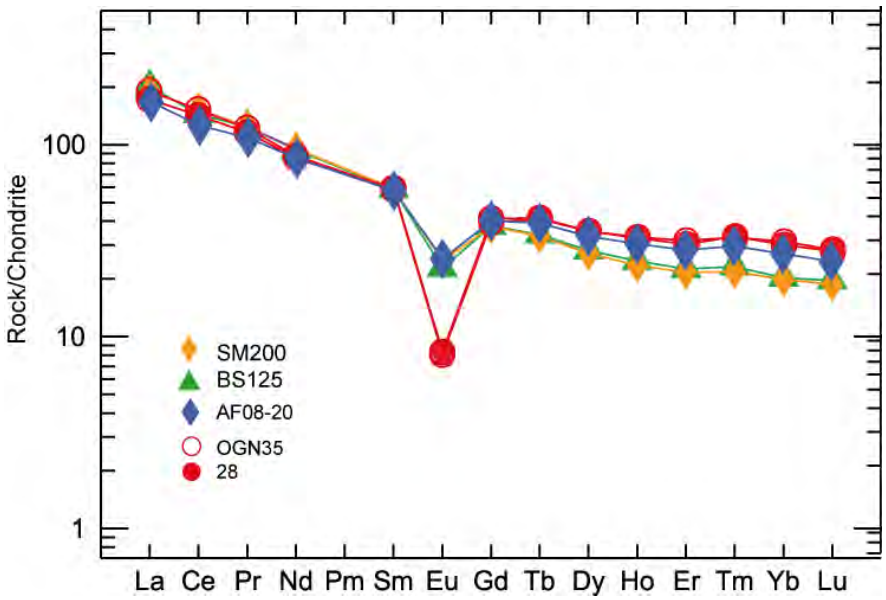

Fig. 4-1 Trace element spiders (Sun and McDonough, 1989) REE patterns normalized to chondrite for Sardinian sample.

4.1.2 MAGMATIC LATE PALAEOZOIC SAMPLES

With the collapse of the Variscan belt, has been placed the batholit that occupies large part of the Sardinia and Corsica islands. Also in Calabria huge amount of intrusion occur and here have been characterized some of these bodies. Here have been analysed only the magmatic bodies correlated with this event cropping out in Calabria with the aim to compare them with the data that well explain the Sardinian coeval bodies.

As know in the literature, the Sardinia-Corsica batholith intrusions were emplaced from 310 to 290 Ma (Late Carboniferous–Early Permian). The ages of the intermediate to acid intrusions range between 305 and 300 Ma, whereas the emplacement of the metaluminous to alkaline hyper-solvus

granite occurred around 290 Ma, synchronous with the leucocratic monzogranite and basic rocks (Cocherie et al., 2005).

The granitoids from Sila and Serre sub-regions here dated are correlated in age with the Sardinian-corse batholith, giving ages of Carboniferous-Permian. The samples colleted in the Northern sector of CPA, in the Sila sub-region (LON-02, LON-03) have given an age of 298.2 ±1.8 Ma and 303.6 ± 2 Ma, also the sample collected in the Serre sub-region (COR-13) is possible to associated at them for the age even if slightly younger (295.3 ± 1.5 Ma). These data well fit with the Sardinia-Corsica batholit characterized by an interval of age of ca. 40 Ma (320-280 Ma).

The Sila bodies are calc-alkaline granites (Fig. 3-55). The calc-alkaline suite has been interpreted as resulting from the interaction of mantle-derived magmas with crustal rocks, falling in the between of I-S type and A-type. Considering these peraluminous signature (Fig. 3-54) is more probable that they are S Type granites. The geochemical features of Sila samples show (Fig. 3-60) an enrichment of large ion lithophile elements (LILE), and an impoverishment of high field strength elements (HFSE). The negative anomaly of the Sr are linked to the plagioclase fractionating suggests a formation in a magma well differentiated. A negative anomaly has shown by Ba, Nb, Sr, and Ti.

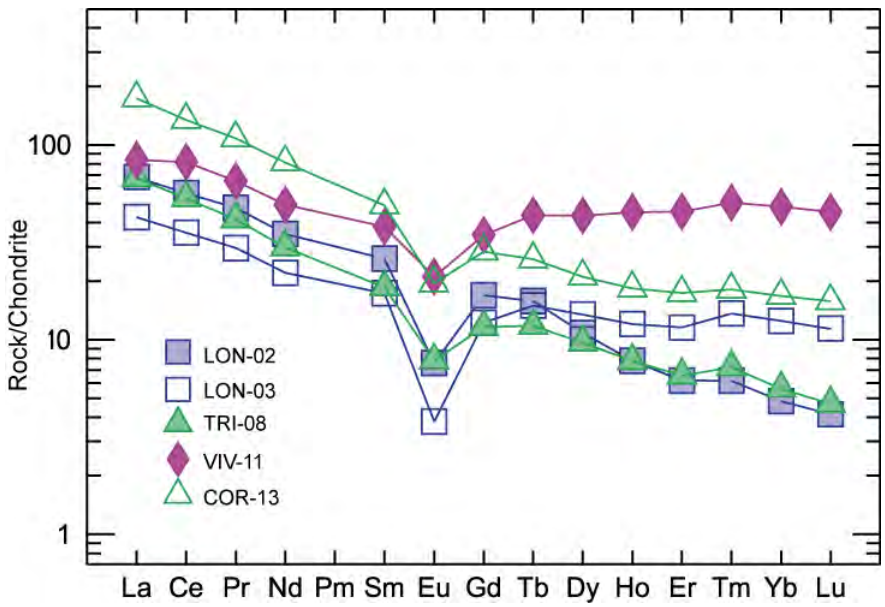

Fig. 4-2 Trace element spiders (Sun and McDonough, 1989) REE patterns normalized to chondrite for Calabrian sample

These bodies have been developed between the syn-collisional and the volcanic arc (Fig. 3-57) following the tectonic diagram of Pearce et al. (1984) likely in a continental field (Fig. 3-58)

considering the tectonic classification of Cabanis and Lecolle (1989). These characteristics of Sila products better fit with the Sardinian granitic bodies then with the Corsica ones, because of in Sardinia is present only the calc-alkaline suite.

Also the Serre granite studied (sample COR-13) is possible to considered like prosecution of Sardinian Batholit. The sample performed belongs to the peraluminous suite (Fig. 3-76) has been interpreted like I-S-type granites. As suggested by literature (D'Amico et al., 1982; Rottura et al., 1990) likely as S-type or as having a mixed mantle-crust origin.

Following Pearce et al., (1983, 1984), the tectonic setting shows the formation of the Serre sample in a volcanic arc in a continental setting (Fig. 3-79, 3-80). The geochemical features show a scenario with an enrichment of large ion lithophile elements (LILE) and an impoverishment of high field strength elements (HFSE) where crystallised Eu (Fig. 4-2), suggesting a fractioned magma.

In agree with Rottura et al. (1990) these bodies are late to post-tectonic and were probably emplaced along extensional ductile shear zones.

The time span during which the Calabria late Variscan granitoids have been emplaced into the middle crust is short and near-synchronous with the metamorphic peak (Graessner et al., 2000). This implies a sudden heating of the lithosphere and its consequent partial melting which is compatible with the geochemical nature of the magmas.

Slab detachment and post-collisional extensional tectonics have been proposed to explain the late Variscan magmatism of the French Massif Central (Lardeaux et al., 2001; Ledru et al., 2001) to which the Sardinia and Calabria regions would be palaeogeographically correlated (Stampfli and Borel, 2002).

As kinematic and structural data from all these regions tend to define a common tectonic framework (Faure, 1995; Burg et al., 1994; Carmignani et al., 1994c), similar evolution to the Serre and Sila massifs (Caggianelli et al., 2007) with the Sardinia region than the Corsica block, likely for the peleogeographic closure.

4.2 PALAEOZOIC DETRITAL SAMPLES

In this part of chapter will be discuss the results obtained by the comparison between the zircon populations (Fig. 4-3), analysed from the Palaeozoic deposits cropping out in the Sardinia Palaeozoic basement. We considered three sedimentary samples cropping out in different tectonic zone of the region: two samples have been collected in the Nappe zone, in the Sarrabus U. (SST-5100), one is collected in the Bithia tectonic unit (AF08-28) and one has been collected in the

foreland of the Variscan chain in the Iglesiente area (CORI). Beware that the Bithia unit has been identified as a part of the External Nappe just recently, as a branch stems out from this research, before it was considered a pre-Cambrian (Cadomian?) basement. Furthermore, the Sarrabus and foreland samples are collected in known stratigraphic positions (Upper Ordovician the nappe sample, Lower Ordovician the foreland sample, whereas the Bithia sample collected in the "quartzite unit", given its relationships with dated metavolcanics, given that was involved in a polyphase isoclinal folding events, could be either Lower or Upper Ordovician in age. One of the consequences of this analysis provide age constraint to this lithostratigraphic unit.

The new approach to study these deposits, taking into account theirs zircons population (associating theirs U-Pb age and Hf values) furnished more details to considered them as parts of the same terrane or not, providing also to give more information about theirs reciprocal paleo-position during the Palaeozoic era.

The sedimentary input that contributed to form the Palaeozoic deposits analysed suffered different important magmatic event zircon-formed, yet conventionally in literature.

The older input recognised in all samples is shown by the Archean population. This population is expressed by on average the 5% of whole zircons for each sample. This data suggests that the three samples analyzed likely were in nearby positions during Palaeozoic to receive the same sedimentary charge.

A modest Paleo-proterozoic input have been found in the foreland sample (CORI) and in the Bithia U. sample (AF08-28). Considering the lacking of Middle and Upper Mesoproterozoic input (1250-1600 Ma) in all samples analyzed is plausible to consider this like a period of igneous quiescence.

The Grenvillian population is well expressed in all the samples analysed even if the Tonian (850-1000) input is better expressed in the Nappe Zone samples (AF08-28 and SST-5100). The εHf values obtained in Tonian grains (U-Pb age of ~945 Ma) for Sarrabus Unit sample has positive values of εHf implying a link to an important juvenile contribution. These data also confirm the values found by Avigad et al. (2012) for the Cabitza Fm. sandstones. These data suggest that during the Tonian time, the Grenvillian magmatic sources with juvenile component contributed to form the provenance sedimentary basin. Here agree with Avigad et al., (2012) that suggests a likely the direct source could be a magmatic island arc, linked probably to the early crust evolution of the North Africa.

An important Cryogenian aged zircons presence has been found in the Foreland sample (CORI) and in the Bithia Unit (AF08-28) where the abundance give up 47 % of the whole zircons. This

occurrence do not means that the Ordovician magmatism developed in a Archean crust; rather, considering the strong negative εHf values detected, is possible to admit that Archean zircons have been reworked during different magmatic cycles from older sediments and finally deposited again in the Ordovician basin. The Sarrabus Unit sample is characterised by a paucity of this contribute that suggests its different location respect of the others samples, that is to say that during Upper Ordovician the basin corresponding to the present-day Nappe zone was in a different location, not fed by the reworked Cryogenian source. The Cryogenian magmatism (635-850 Ma) here is presented by the main peak at 650 Ma. The Cryogenian input as well the Grenvillian population represent the dominating signals in the Neoproterozoic populations.

The Ediacaran zircon population also is well represented in all samples with an important contribution (varying from 13% up to 18% respect of the whole populations). The peak reported is linked to a Pan-African orogeny (550 Ma). Taking in account the negative εHf values obtained in the Sarrabus U. zircon grains (550 Ma), in the Ediacaran period there has been or a reworking of an Archean crust (the εHf values spanned from -25 to -1).

Zircon populations younger than Ediacaran have been found only on Sarrabus U. sample. The main zircon population (53% of total zircons, Fig. 4-4) found in this sample is inferred to Ordovician magmatism that shows the main peak at 450 Ma, likely linked to the Middle Ordovician Andean-type arc (Oggiano et al., 2010), documented also in the whole European Variscan belt. The zircons analyzed show εHf negative values that suggest a recycling of Proterozoic crust during the Ordovician magmatism. The ε Hf values obtained (Fig. 4-5) suggest that during variscan magmatism the Grenvillian juvenil crust (violet elipse in the Fig. 4-5) has been recycled (red elipse in the Fig. 4-5).

Is possible to make a comparison between the εHf values here obtained and the features of the three cycles of the Ordovician magmatism recently subdivided by Gaggero et al. (2012).

The Upper Ordovician-Silurian cycle (~ 440 Ma) has alkaline signature (Gaggero et al. 2012). In the present study this cycle represents the majority of Ordovician grains (47%, Fig. 4-4) and the 4 Lu-Hf zircon performed show εHf negative values (εHf from -4 to -1) and εHf TDM model ages from 1.5 to 1.3 Ga. These values suggest a reworking of Mesoproterozoic crust.

The Middle Ordovician cycle (~ 465 Ma, Gaggero et al. 2012), here obtained by the U-Pb age in the Sarrabus U. dacites, gives a mean age of 458.7 ± 2.8 (SM-200 sample) and 464.6 ± 7.3 Ma (BS-125 sample). Considering the detrital zircon study this cycle is shows the 28% (Fig. 4-4) of Ordovician zircon population. The 2 zircons Lu-Hf performed have negative εHf values (εHf from -

8.4 to -2.3) with εHf TDM model ages ranging from 1.7 to 1.4 Ga. These data suggest a reworking of older crust during the middle Ordovician.

The Early Ordovician cycle (492–480 Ma) represents the 25% (Fig. 4-4) of Ordovician population here found. The single grain performed (age of ~ 474 Ma) shows a negative εHf value of -2.1 with a εHf TDM model age of 1.4 Ga, indicating a crustal reworking on Early Ordovician.

Considering the provenance ages of Ordovician zircons, is plausible that the deposition of SST-5100 sample has been developed during the dismantling of the Middle-Upper Ordovician Volcanic arc. This is totally in agreement with also sedimentological and stratigraphic data (Loi & Dabard 1997). A lesser consideration can be made about the relative age of the "quartzite unit" of the Bithia tectonic unit where the AF028 zircons were samples. As previously noted, this sample, although belong to the Nappe zone, according the last interpretation (Pavanetto et al., 2012), shows zircon sources analogous to the Lower Ordovician sample from the foreland, and lack at all the Middle Ordovician input largely diffused in the Upper Ordovician of the nappe zone. This means at first that the Bithia quartzite was deposited before the occurrence of the Middle-Upper Ordovician volcanism. If this assessment would be true, with some approximation, the basin of the Nappe zone units and that of the Foreland, generally referred to the North Gondwana passive margin, shared a close position up to Lower Ordovician time. This argument seems to indicate that the convergence that led to the development of the Middle-Upper Ordovician magmatic arc put closer two crustal block that up to the Middle Ordovician were enough far away to do not suffered the same sedimentary sources.

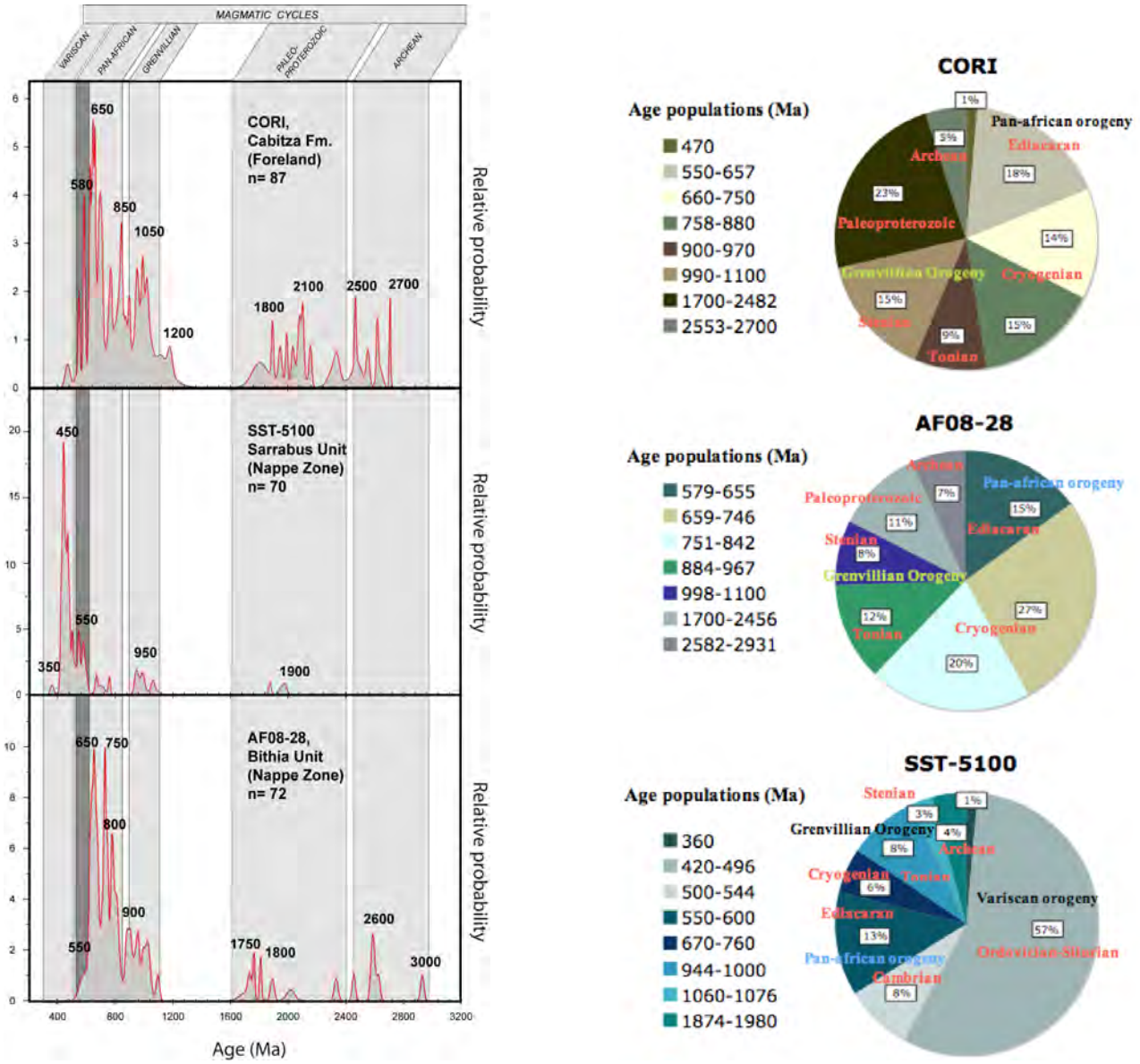

Fig. 4-3 On the left: U-Pb results shown in frequency histogram for the Palaeozoic Sardinian samples, for the younger ages (< 900 Ma) have been used the $^{238}U/^{206}Pb$ ratios and for the older have been used the $^{207}Pb/^{206}Pb$. The histogram shows a polymodal distribution of ages, with a main population between ca.400 and 750 Ma. On the right: population density with related percentage of the same samples.

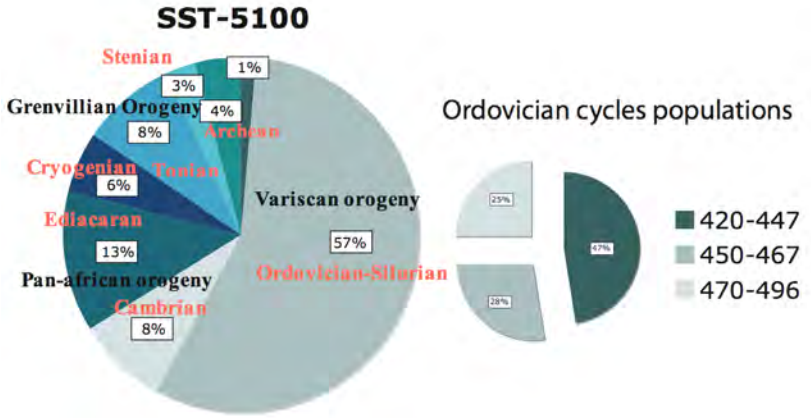

Fig. 4-4 Comparison of the population density of Sarrabus sample zircons (on the left) with the Ordovician cycle populations considering the three volcanic cycles defined by Gaggero et al., 2012 (on the right).

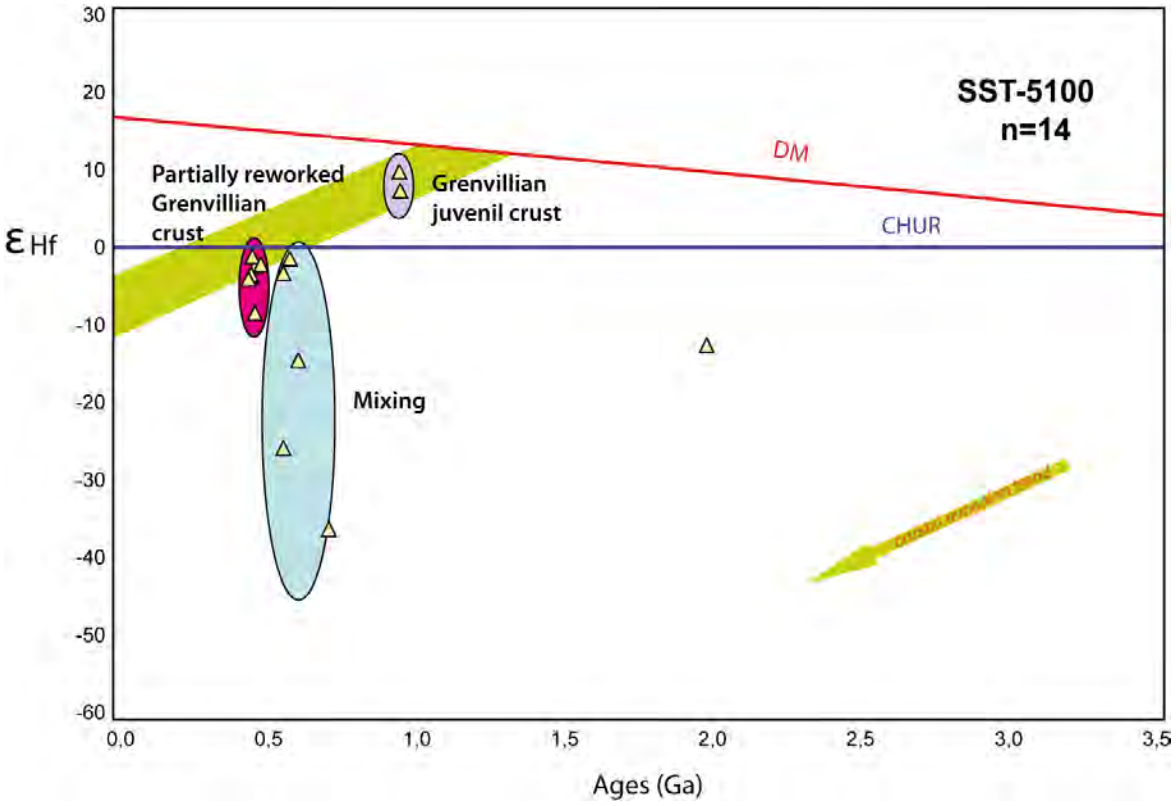

Fig. 4-5 Ages vs εHf values for the ST-5100 sample. The green arrow represents a juvenile Mesoproterozoic crustal evolution trend, yet calculated by Taylor and McLennan (1985) and Wedepohl (1995) with these values $^{176}Lu/^{177}Hf = 0.0113$

.

4.3 TERTIARY DETRITAL SAMPLES

The discussion and interpretation of data performed on detrital zircons sampled in Tertiary rocks closely related to tectonic structures linked to the evolution of the Central-western Mediterranean (see chapter 1) has to been considered as the more important of the work because of his relevant amounts of data that permit to suggest new paleo-geographic positions of the Sardinia-Corsica Block respect to the Calabria-Peloritani Arc and to the other peri-Gondwana terranes.

Here will be discuss the results obtained for the Tertiary deposits cropping out in Sardinia, Corsica, Northern part of CPA (Sila sub-region) and Southern part of CPA (Aspromonte sub-region). We consider these like key-deposits for better understanding the evolution of Southern Tyrrhenian basin opening. In fact these sedimentary bodies have been developed in the course of the convergence and collision between South-Europe and Adria during late Oligocene-Lower Miocene (Oggiano et al., 2009). So the study of zircons, associating the U-Pb ages with their Hf isotopes values, is a good tool to furnish more data for recognize the pre-Variscan inputs suffered by the peri-Tyrrhenian area, and to highlight differences and similarities between them. In fact the zircon populations found in these deposits furnish a spectrum of ages that focus in the basements evolution over where the deposits were developed. In order words, the deposits analysed, located at the bottom of the syn-tectonic sequences, have collected mainly the zircons formed during the magmatic events that contribute to form the basements. Different magmatic contribution in zircons population have been analysed that allow drafting the evolutions of these deposits by theirs sedimentary and magmatic input.

The study of the zircon populations from Tertiary deposits suggests important differences between the SCB and the Northern Calabria Sector with the Southern Sector.

All the samples (CO-SOL, CAV-05, CA-PAL) except for the Sardinian contribution (SA-ALB), present an important post-Variscan input. The zircons (between ~276 and ~362 Ma) analysed showing negative εHf values (except a single 314 Ma zircon from Calabria Southern sector) suggesting that during post-Variscan time there was crustal reworking of the older crust (εHf TDM model age give Early Paleo-Proterozoic and Mesoproterozoic ages). These considerations well fit with the geochemical data obtained from the Late Palaeozoic magmatic samples from the Northern sector of Calabria (paragraph 4.1.2) here dated and showing Carboniferous-Permian ages (LON-02 has a main age of 298.03 ± 1.8 and LON-03 shows a main age of 303.6 ± 2 Ma). This granites fall in the continental arc setting and in the between of volcanic arc and syn-collisional granites formation setting.

The lacking of this input, and as well the paucity of Ordovician input, in the Sardinian sample

(SA-ALB) still remain inquiring because the syn-tectonic deposits (Cuccuru 'e Flores Conglomerates CCF) are really nearby the Variscan crystalline basement ad is constituted for a large parts by elements fed by that source. The lack of Late Palaeozoic input is probably related to the study sample, because in outcrops the occurrence of fragments from the intrusive Carboniferous-Permian rocks is unquestionable. Some hypotheses can be made about the Ordovician paucity considering that the Ordovician magmatites are widespread more in the northern part of the area where the CCF crops out (othogneiss in the Posada valley and Lula-Lodè plateau) than in the central and southern surrounding areas (very small, scattered outcrops of metavolcanites in the Baronie region): i) the source area was the last one and not the first one; ii) it could be a consequence of an important effect of tectonic process occurred in this area that influenced the migration of sediments; iii) the area where magmatic Ordovician rocks crop out were not exposed at the time of CCF deposition. Finally a precautionary consideration may be made: the CCF consists of a large variability of rocks and sources, and its sedimentary and sedimentological features varied conspicuously during its deposition because of tectonic influence, so it is possible that the lower part was emplaced before that the tectonic would start to influence its deposition (Oggiano et al., 2010). Thus we may admit that a different sampling could overwhelms the Variscan paucity.

The Ordovician Variscan zircons (between ~440 and ~478 Ma) are well expressed in the Calabria Northern sector sample (CAV-05) and show negative εHf values. These εHf values (Fig. 4-7) suggest a reworking of Mesoarchean crust for the Upper Ordovician-Silurian zircon (~440 Ma) and a Mesoproterozoic crust reworking for the Middle and Lower Ordovician zircons. These data well fit with the Sardinian Palaeozoic detrital sample (SST-5100) which shows mainly reworking crust, suggesting that the Ordovician zircons from the two regions shared the same magmatic process.

Zircons linked to the lower Cambrian volcanism (here with ages spanned between ~482 and ~511 Ma) founded in Northern CPA and Corsica show mainly negative εHf values with plausible crustal reworking (showing Calymmian εHf TDM model age; Fig. 4-7). The CPA zircons have both negative εHf and positive εHf. The positive values are likely associated at crustal reworking of Grenville juvenile crust input.

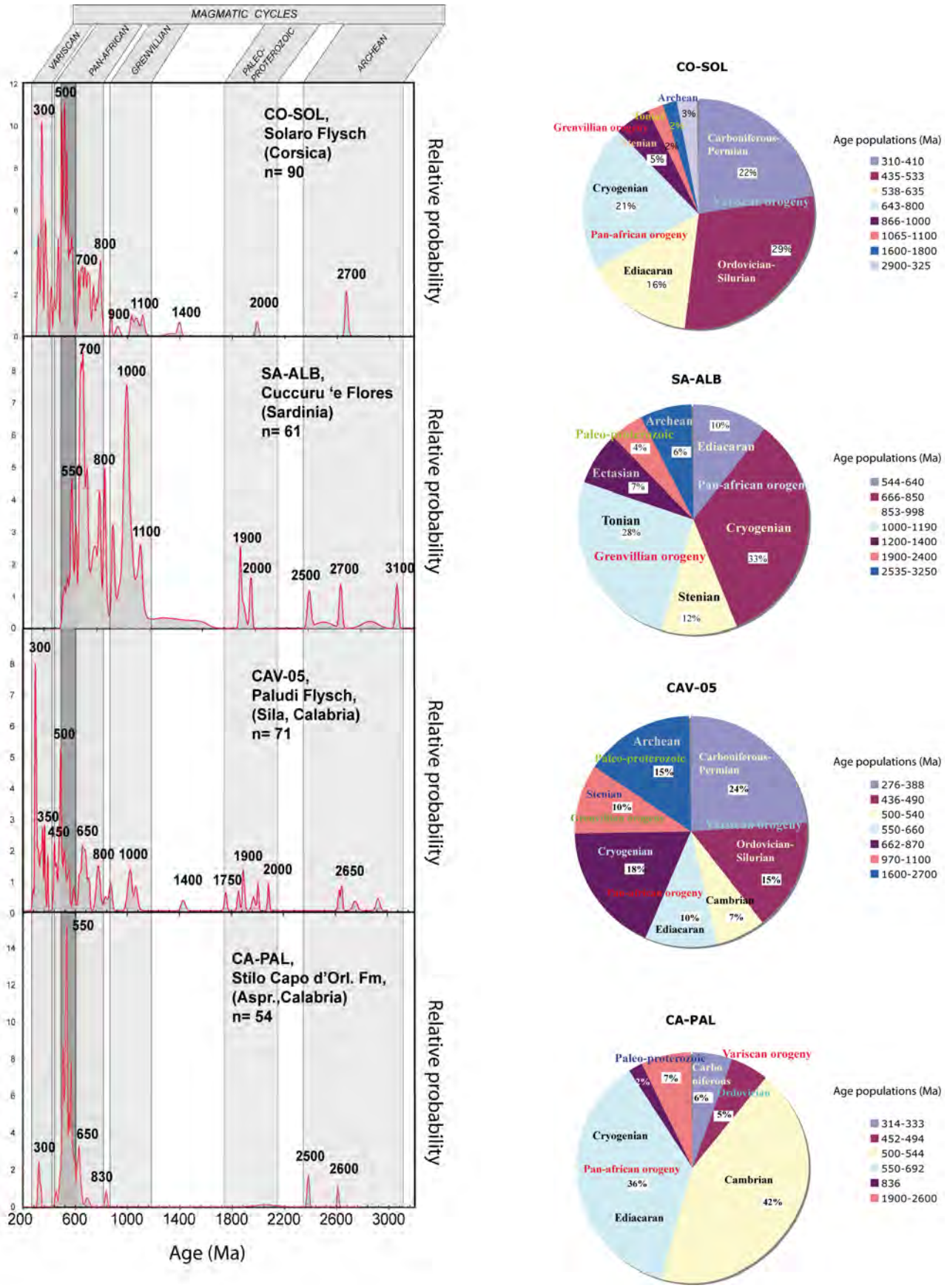

Fig. 4-6 On the left: U-Pb results shown in frequency histogram for the Tertiary samples, for the younger ages (< 900 Ma) have been used the $^{238}U/^{206}Pb$ ratios and for the older have been used the $^{207}Pb/^{206}Pb$. The histogram shows a polymodal distribution of ages, with a main population between ca.400 and 750 Ma. On the right: population density with related percentage of the same samples.

The Pan-African input (here ranging between ~544 and ~633 Ma) occurring in all the samples shows both positive and negative εHf values suggesting mainly reworked crust with mainly Paleoproterozoic model age (4/9 zircons with model age spanned between 1.82 and 3.92 Ga, Fig. 4-7). These data are also reinforced by the sample from the Aspromonte sub-region (PAL-16), having an age here measured of 553±4.1 Ma. This augen-gneiss shows the protholit with affinity in the continental arc formation setting (Fig. 3-90).

The Cryogenian input, presents moreover on the SCB (with ages between ~645 and ~781 Ma) and the Tonian input analysed on Sardinia and Northen CPA samples (with ages between ~816 and ~860 Ma), show mainly positive εHf values, suggesting a juvenile crust input.

The Grenvillian age (here represented with ages between 0.9-1.1 Ga) population recognized on the SCB samples and in the Northern sector of CPA sample (CAV-05) lacks in the Southern Calabro-peloritain Arc sample (CA-PAL). The Grenvillian zircons are characterized by a juvenile source all over for the Sardinian sample, confirming the important magmatism occurred during the Grenville period likely associated to volcanic arc. Also some negative εHf values have been found suggesting a mixing between juvenile and reworked crust.

The Archean input analysed shows different sources between CPA and Corsica. The Corsica sample shows an important juvenile direct source (also recycled in the Pan-African magmatism), the Southern Calabria sample shows a reworking crust as main process.

All over the Grenville lacking in the CA-PAL sample, suggests that the Southern sector of CPA during the Paleozoic time suffered different source areas input than SCB and Northern sector of Calabria. The Southern CPA probably was part of North Africa, well fitting with the Gondwanan European Variscan terranes, characterized by the lacking of Mesoproterozoic age (Kober et al., 2004). The Sardinia-Corsica block together with the Northern sector of CPA could suffered the Amazonian input, like as yet suggested for the Northwestern Iberia mesoproterozoic affinity (Friedl et al., 2000; Fernández-Suárez et al., 2000; Guttiérrez-Alonso et al., 2003) and for the Tuareg shield on Algeria (Linnemann et al., 2011). Is not possible exclude also a possible link to the Northeastern part of West African craton, recent proposed for the NW Iberia mesoproterozoic affinity (Villaseca et al., 2011).

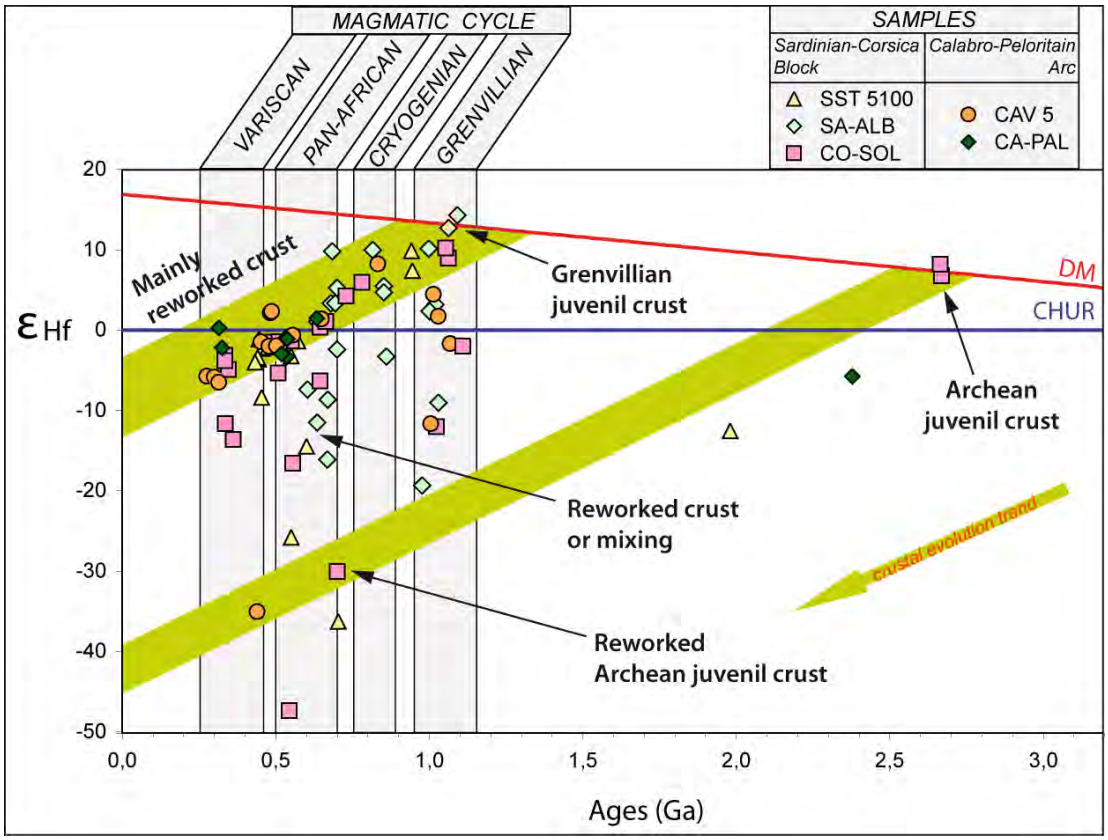

Fig. 4-7 Ages vs εHf values for the all samples analysed. The green arrow represents a juvenil Mesoproterozoic crustal evolution trend, yet calculated by Taylor and McLennan (1985) and Wedepohl (1995) with these values $^{176}Lu/^{177}Hf = 0.0113$.

4.4 GEODYNAMIC IMPLICATIONS

From the discussion and interpretation of the data above reported, taking in account also the data available in the published literature, some evaluations about the geodynamic constraints can be made that could answer to some of the questions reported in the Introduction (chapter 1):

i) Which was the position of SCB and CPA during the pre-Variscan evolution (and after the Variscan amalgamation)?

ii) Have they shared the same evolution after the opening and closing of Tethis?

iii) Did the CPA to be considered as a single terrane or different ones juxtaposed lately during the Tyrrhenian opening?

The value of the answers is mainly related to the quality and quantity of zircons associated to the different magmatic source. The paucity of Archean and Paleoproterozoic detrital zircons in the analysed populations of all samples allow us to just suggest some paleogeographic hypotheses about their links to the West African and Amazonian cratons.

The slight Paleoproterozoic zircons found could be associated to the Eburnean (c. 2–1.8 Ga) event. This event is recorded either in the West African craton (Liegeois et al., 1991; Hirdes and Davis, 2002; Thieblemont et al., 2004) and in the Amazonian craton (with the name of the Orosirian event; Basei et al., 2010 and Pereira et al., 2012). So, since these intervals are typical both in the West African and in the Amazonian cratons they are not resolving in which of them were the main potential source.

The Grenville zircons input (ca.0.9-1.05 Ga) furnished the main information about the difference between the CPA and the SCB. Their lacking in the CA-PAL sample (Fig. 4-6), suggests that the Southern sector of CPA during the Palaeozoic time suffered different source areas input than SCB and the Northern sector of Calabria.

This first assumption suggests that SCB and the Northern part of the CPA (Sila sub-region) were nearby, whereas the southern part (Aspromonte and Peloritani Mountains) would be separated from them. The Grenvillian lacking in the sedimentary input on the Southern CPA suggests that it was connected with the Cadomian European terranes belonging to the North Africa (Fig. 4-8, Fig. 4-9) that are characterized also by the lacking of mesoproterozoic age (Kober et al., 2004). The occurrence of abundant Cadomian zircon in the magmatic sample from Aspromonte (PAL-16) corroborate this hypothesis. Indeed, a provenance from anywhere north of the Congo Craton, including in the Tuareg Shield (Nance et al., 2008; Ennih and Liégeois 2008) and from the Saharan Metacraton (e.g. Abdelsalam et al., 2002; Schandelmier et al., 1988), where the Grenvillian-age detrital zircons are absent from the Lower Cambrian deposits, could be proposed also for the Southern CPA, as well as proposed for the Morocco (Avigad et al., 2011). Also could be supposed a derivation from the West African craton, as proposed for the Ossa–Morena and Saxo-Thuringia Ediacaran sediments, characterized by the he lack of Grenvillian-aged (Pereira, 2011).

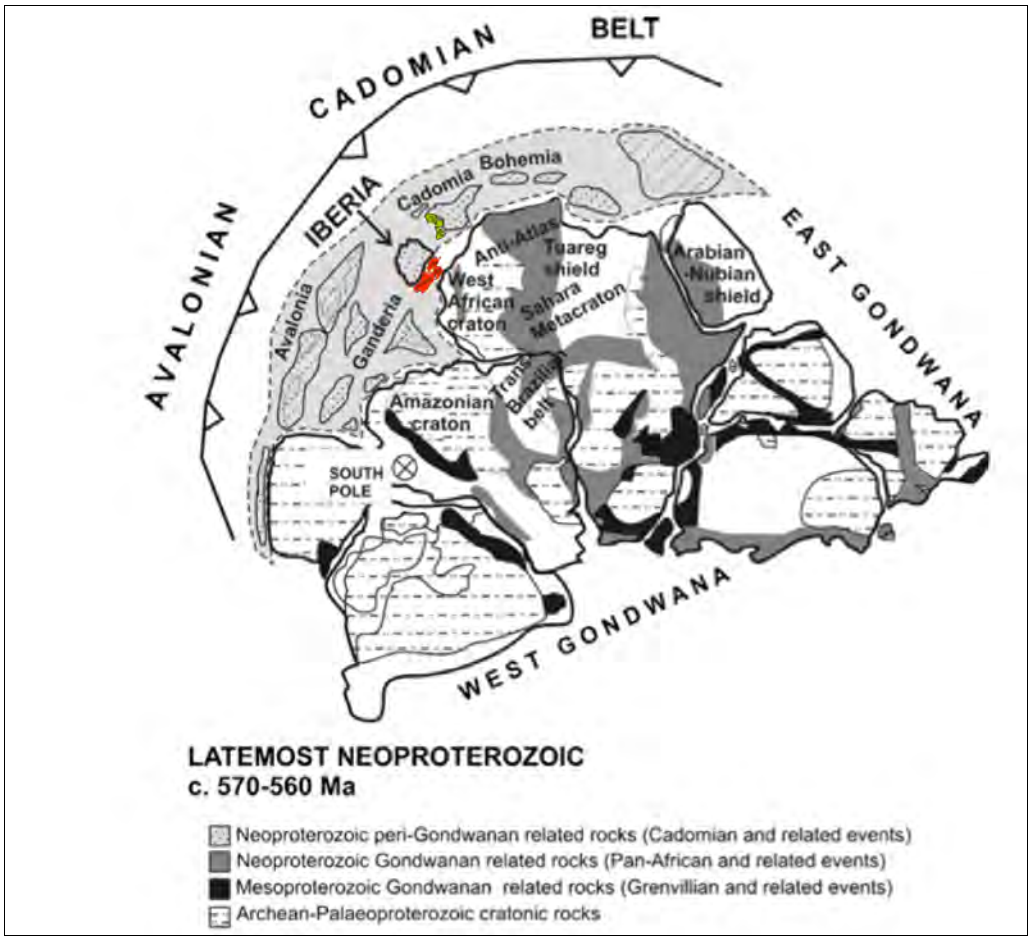

Fig. 4-8. Paleogeographical sketch of the Gondwana supercontinent at c. 570–560 Ma with possible paleoposition of Iberia, Sardinia, Corsica and Sila (in red color) and Aspromonte and Peloritani M. (in green color). Modified from Linnemann et al. (2004) and Pereira et al., (2012).

The zircons related to the Grenvillian event (ca.0.9-1.05 Ga) found in the Sardinia-Corsica block and in the Northern sector of CPA, might have been transported by large river systems to the northern margin of Gondwana (Zeh et al. 2001). These detrital zircons have been found (see Fig. 4-10) in the NW Iberia (Fernández-Suárez et al. 2002), in the NE Bohemian Massif (Hegner and Kröner 2000; Mingram et al. 2004), in the Moravo–Silesian Unit (Friedl et al. 2000, 2004), in the West Avalonia (Nance and Murphy 1994, 1996), in the East Avalonia (Strachan et al. 2007), in the Małopolska Unit (Belka et al. 2002) and in the Polish East European Platform (Belka et al. 2002). Such ages, however, are not known from the Meguma Terrane (Nance and Murphy 1996), Saxothuringia (Linnemann et al. 2004), SW Iberia and Brittany (Fernández-Suárez et al. 2002). The Grenvillian detrital zircons are absent in rocks that have their unambiguous source in the West African Craton (Meinhold et al., 2010).

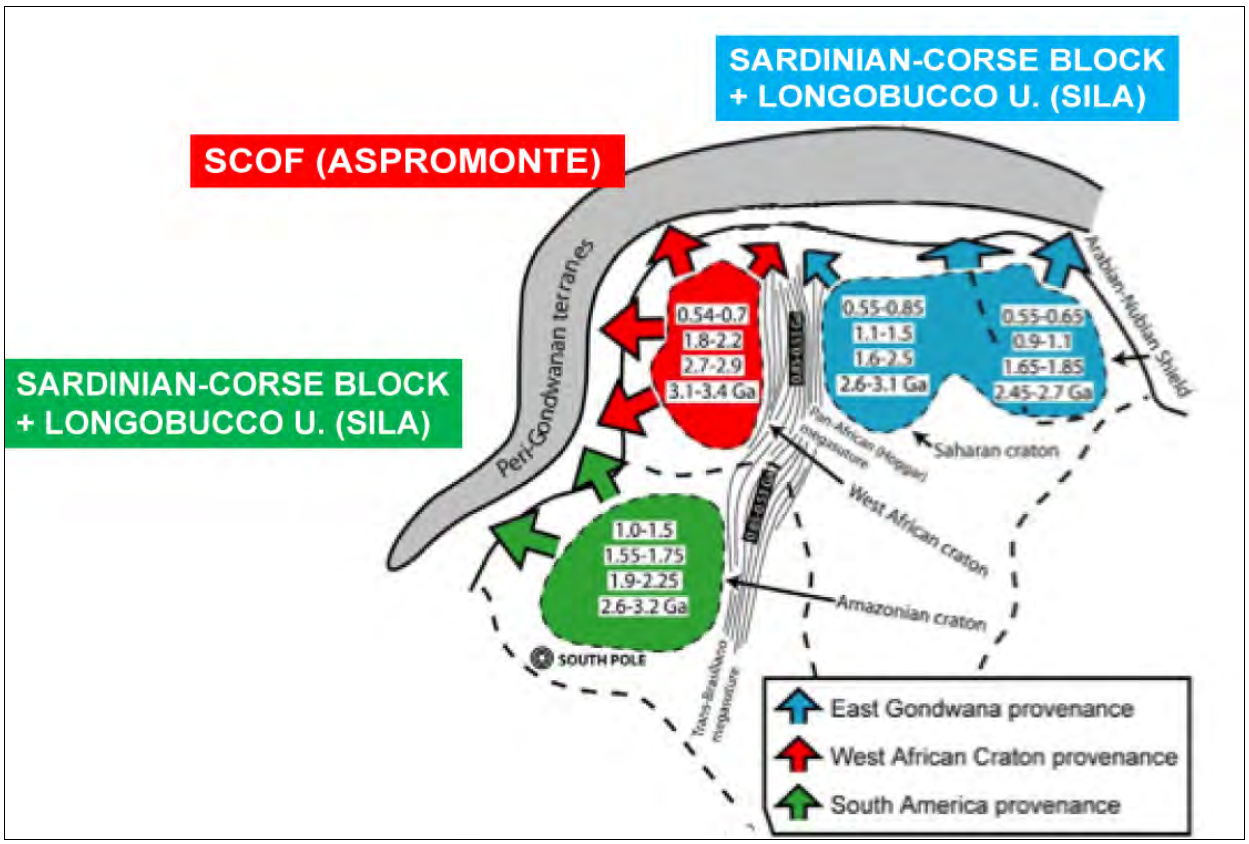

Fig.4-9. Simplified paleogeography of Gondwana and related major peri-Gondwanan terranes at ca. 570 Ma (modified after Nance and Murphy, 1994; Cordani and Teixeira, 2007; Linnemann et al., 2007; Ennih and Liégeois, 2008; Cordani et al., 2009). The main source areas for the Avalonian–Cadomian active margin and Peri-Gondwanan terranes are include cratons and the Trans-Brasiliano-Hoggar megasuture. Here it is proposed the likely sources of zircons forming the analysed tertiary samples.

Detrital zircons of Grenvillian age detected in several peri-Gondwana terranes (Fig. 4-8, Fig. 4-9) were generally assigned to the Amazonian provenance (Friedl et al., 2000; Fernández-Suárez et al., 2000; Guttiérrez-Alonso et al., 2003; Linnemann et al., 2011; Fig. 4-8, Fig. 4-9), but the recently discover of their presence in the detrital spectra of Morocco and Sardinia (Avigad et al., 2012 and reference therein) has given rise to a doubt about this provenance source. Avigad et al. (2012) suggest that the source of the sediment was in North Africa, even if they recognized it as a scarce viable source, admitting that Stenian-aged (Grenvillian) sources, if exist in North Africa, consist of crustal relics of very minor extent. Another plausible source for some European peri-Gondwana sequences with Grenville zircons, could be the Arabian-Nubian Shield (Bahlburg et al., 2010). This source has been recently excluded (Linneman, 2011) on the basis of the Upper Cambrian to Ordovician sandstones cropping out in the Algerian Sahara (Linneman, 2011). These data rejected the Arabian-Nubian shield and the East African belt as source, because of its total lack of ~ 1.0 Ga age.

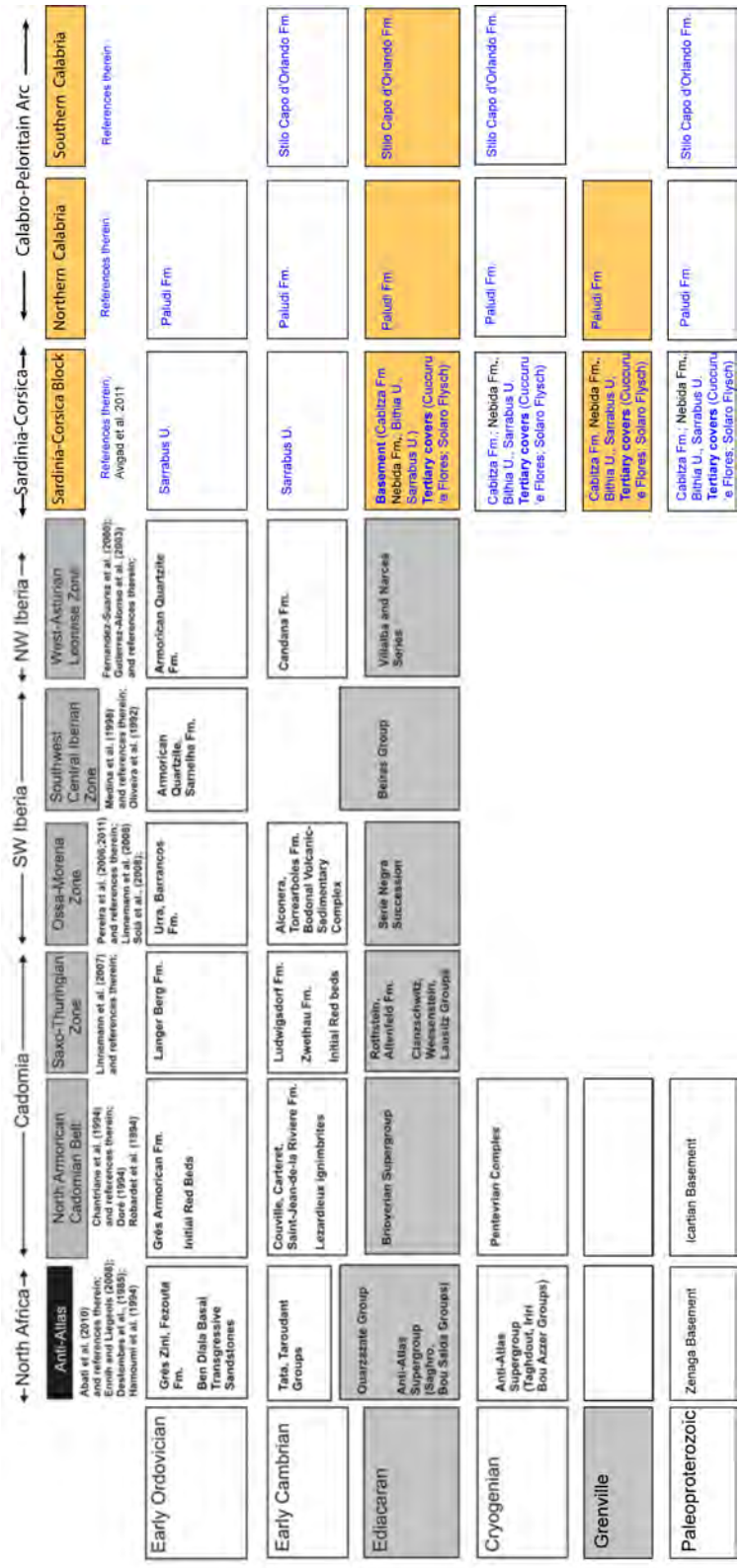

Fig. 4-10. Schematic chart showing correlations between peri-Gondwanan blocks: North Africa, Cadomia, SW Iberia, NW Iberia and Anti-Atlas (see refs. Destombes et al., 1985; Doré, 1994; Hamoumi et al., 1994; Robardet et al., 1994), Sardinia-Corsica and Calabro-Peloritain Arc (Avigad et al., 2012 and references therein). Modified from Pereira et al. (2006, 2012).

If the Amazonia craton most probably contributed to the formation of the early Paleozoic sands of West Gondwana (Linnemann et al., 2011) here has been excluded the derivation of the grenvillian zircons from the Cadomian terranes because of their Grenville input absence (Cahen et al. 1984).

Tonian zircon- forming events (c. 900–800Ma) have been recorded in the Arabian-Nubian shield (Stern, 2002) and in the Trans-Brazilian belt (Pimentel et al., 1999; Saalman et al., 2007; Fig. 4-8, Fig. 4-9), which may represent likely source areas with juvenile magmatism. The occurrence of zircons with Tonian ages in the analysed samples of SCB and Northern CAP (as well in the South Iberia (Pereira et al., 2012, Fig. 4-9) suggests the possibility of sources from outside the West African craton.

If the Ediacaran input is associated with the Tonian ages as found in SCB and Northern CPA (and also in the NW Iberia, Fernández-Suarez et al., 2002; Pereira et al., 2012) could be possible that these basins were located adjacent to sources of the Amazonian craton (Fernández-Suarez et al., 2002). A potential source has been recently related to the dispersion of sediments along the continental margin of North Gondwana (Pereira et al., 2012).

Considering these data is possible to put the SCB and the Sila (Northern part of CPA) near to the Iberia (Fig. 4-8), possibly on the W margin of the Iberia and the Aspromonte and Peloritani M. bordering the Cadomian terranes.

Also the presence of Cryogenian–Ediacaran (ca. 550–760 Ma) detrital zircons all over in the Southern CPA and in the Palaeozoic Sardinian deposits, suggest various linked with different sediments sources. This abundant input is likely derived from the erosion of and denudation of the North Africa interior Pan-African shields (Fig. 4-11): or the Trans-Sahara belt, the Arabian-Nubian shield or the West African craton like proposed for the SW Iberia by Abati et al. (2010) and Pereira et al. (2012). This deposits are linked to the Pan-African and Avalonian–Cadomian source rocks. Another plausible source for Ediacaran and Cryogenian zircons is individuated in the West Africa, which is connected to the relatively remote Trans-Braziliano belt, in South America (Kroner and Stern, 2004; Basei et al., 2010).

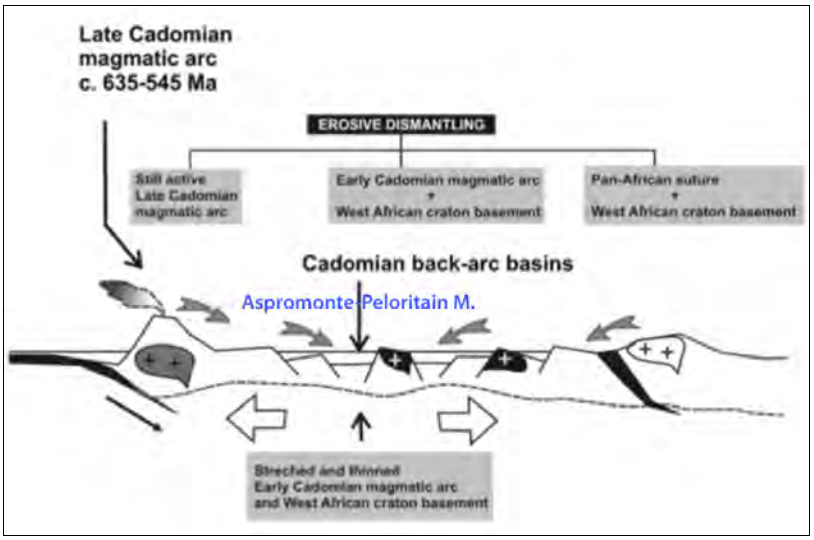

Fig. 4-11. Ediacaran evolutionary phases of the northern Gondwana active margin geodynamic evolution. In B-, grey arrows highlight the main source areas for the Aspromonte and Peloritani M. (as well the SW Iberia Cadomian basements) separated sufficiently to justify the differences in their detrital zircon content. After Pereira et al. 2012, modified.

As yet suggest by literature (Micheletti et al., 2008; Thomas et al. 2002; Walsh et al. 2002; Acef et al. 2003) by the population of detrital zircon here analysed, the analogies between Marocco and Southern Calabria can be reinforced. The Aspromonte samples both magmatic body (sample PAL-16) and sedimentary deposit (sample CA-PAL) have age related to the Pan-African magmatism found in the Anti-Atlas domain. The PAL-16 gneiss show an age of its protholit of 553 ±4.1 Ma, that represents the main peak of the last Pan-African stage. In the samples have been found zircons relatable to the three main stages recognized in Gasquet et al. (2005):

- 690– 790 Ma: ocean opening and subduction;
- 605–690 Ma: ocean closure and arc-continent collision. In the sample the anlyses in the zircon of 633 Ma show a positive εHf values linked to a juvenile crust. At this time also occurred the main phase of Avalonian arc magmatism and coeval synorogenic sedimentation (c. 640–570 Ma; Nance et al., 2002).
- 530–605 Ma: transition to a passive continental margin coupled with extension and development of foreland basins. In the detrital sample the analyses in the zircon of around 530 Ma, show negatives εHf values associated to recycling of older crust.

Considering also the Variscan magmatism, by the Hf analyses crustal reworking has been recognized, mixing process between juvenile and recycled crust. The mixing process better fits with also the literature data that correlate the Ordovician magmatism to subduction beyond the Gondwana northern rim.

Following the recent works about Ordovician volcanism in Sardinia (mainly Gaggero et al. 2012) is possible to fit the data here performed in the three magmatic cycles recognized:

- The Upper Ordovician-Silurian cycle (~ 440 Ma) has alkaline signature and is linked to the rift-drift stages (Gaggero et al. 2012, reference therein).
- The Middle Ordovician cycle (~ 465 Ma, Gaggero et al., 2012, reference therein), linked to within plate magmatism.
- The Early Ordovician cycle (492–480 Ma) with mildly alkaline signature is linked to a rifting stage (Gaggero et al. 2012) with a crustal reworking during on Early Ordovician.

Concerning the Post Variscan magmatism, here is studied in the igneous bodies collected in the Calabria region. The data performed supported the literature data that considering these bodies formed in a tectonic scenario of extensional tectonic regime linked to the Variscan orogen collapse.
All these data, added to that one from the literature, could be used to give new constrains in the geodynamic evolution of the southern Tyrrhenian basin and here the relative positions of CPA and SCB.
The data support once more the hypothesis of many authors (among them Alvarez & Shimabukuro, 2009) that CPA is made up by two different subterranes. The differences between them can be briefly report as follows:
- SCB and Northern CPA are characterized by the input of Grenvillian zircon, not found in the Southern CPA, which, conversely, has an important Cadomian zircon contribution.
- The carbonatic mesozoic covers (form Triassic to Lower Cretaceous) of the Northern CPA, in particular the Stilo U., have strong similarities with those that crops out in the eastern side of Sardinia (Supramonte).
From a field survey made in 2007 and as better reported in Patacca and Scandone (2011), the follow stratigraphic similarities can be summarized as follows:
- the so called calabrian Verrucano looks as the Middle Jurassic Genna Selole Fm. in Sardinia;
- the Tiriolo dolostones, belonging to the Stilo U., contain Eocene nummulites and could be correlate to the Dorgali Fm. cropping out in Sardinia (Supramonte area), and together considered like a pre-orogenic deposits

Indeed the Mesozoic succession of the Aspromonte and Peloritani Mt. (e.g. the Longi Taormina and Longobucco units) not fit well with the above scenario but, has suggested by Patacca & Scandone (2011) is more closed to the north of Tuscany.

In this correlation is important the interpretation of the Paludi Fm. According its lithostratigraphy and age (Oligo-Aquitanian, see Bonardi et al., 2005, cum biblio) it look really very similar to Cuccuru 'e Flores Conglomerates in NE Sardinia and Solaro flysch in E-Corsica. Since it is involved only by the "Apennine-vergent thrust", and post date the eo-alpine deformation (Bonardi et al., 2005). Is possible to argue that the Paludi fm. developed in the same tectono-sedimentary environment of the coeval Sardinian and Corse deposits above mentioned. Is also plausible admit that, from the field evidences, the Paludi fm. could represent a syn-orogenic deposit like suggested for the coeval deposits in SCB and is not more possible to consider it as a thrust-top deposit.
These concerns led to taking in account the option that Calabria is an amalgamation of two sub-terranes (like prospected in the four possibilities proposed by Alvarez & Shimabukuro, 2009 reported in Fig. 1-11). The model here proposed differs from the previous models mainly for the way to lead the two terranes and for the time of accretion of them.

Firstly, here is considered that the northern sub-terrane is composed by Sila and also by Serre sub-regions (and not only by Sila as proposed by Alvarez & Shimabukuro, 2009), which shared the early evolution with the Sardinia and Corsica regions (Fig. 4-12). Here is suggested that undoubtedly they shared the same evolution at least until the deposition of the coeval deposits (Paludi Flysch, Cuccuru 'e Flores Conglomerates and Solaro flysch).
The southern sub-terrane (e.g. Aspromonte and Peloritani) did not share the same evolution Sardinia and the northern sub-terrane, neither during late Palaeozoic neither up to Oligocene. (Fig. 4-12).
So, the two blocks, belonging to the present CPA, did not share the same position during Mesozoic and Paleogene.

An other divergence between the model here proposed and the tectonic sketches reported in Alvarez & Shimabukuro (2009) is about the subduction versus during the Oligocene. Here is admitted (like yet proposed by Patacca & Scandone, 2011) a westwards subduction occurred as main processus, refusing its east versus proposed in Alvarez & Shimabukuro (2009).

Following the proposal by Patacca and Scandone (2011) and considering the analogies about the Mesozoic sediments, the southern CPA may shared with northern Tuscany the same evolution, being involved in the Paleogene Mountain chain. Thus, northern Tuscany and southern CPA could be related, for its late evolution with the MesoMediterranean microplate proposed by Guerrera et al. (1993, 2005).

During the closure of the Piemontese -Liguride oceans, southern CPA was transported close to the southern European margin, facing the Sardinia-northern CPA blocks, and incorporated in the accretionary prism during Late Oligocene-Aquitanian.

Finally, here is considered that southern CPA shared the drifting of the northern CPA, due to the eastward slab rollback occurring during the Upper Miocene-Pliocene (Fig. 4-8).

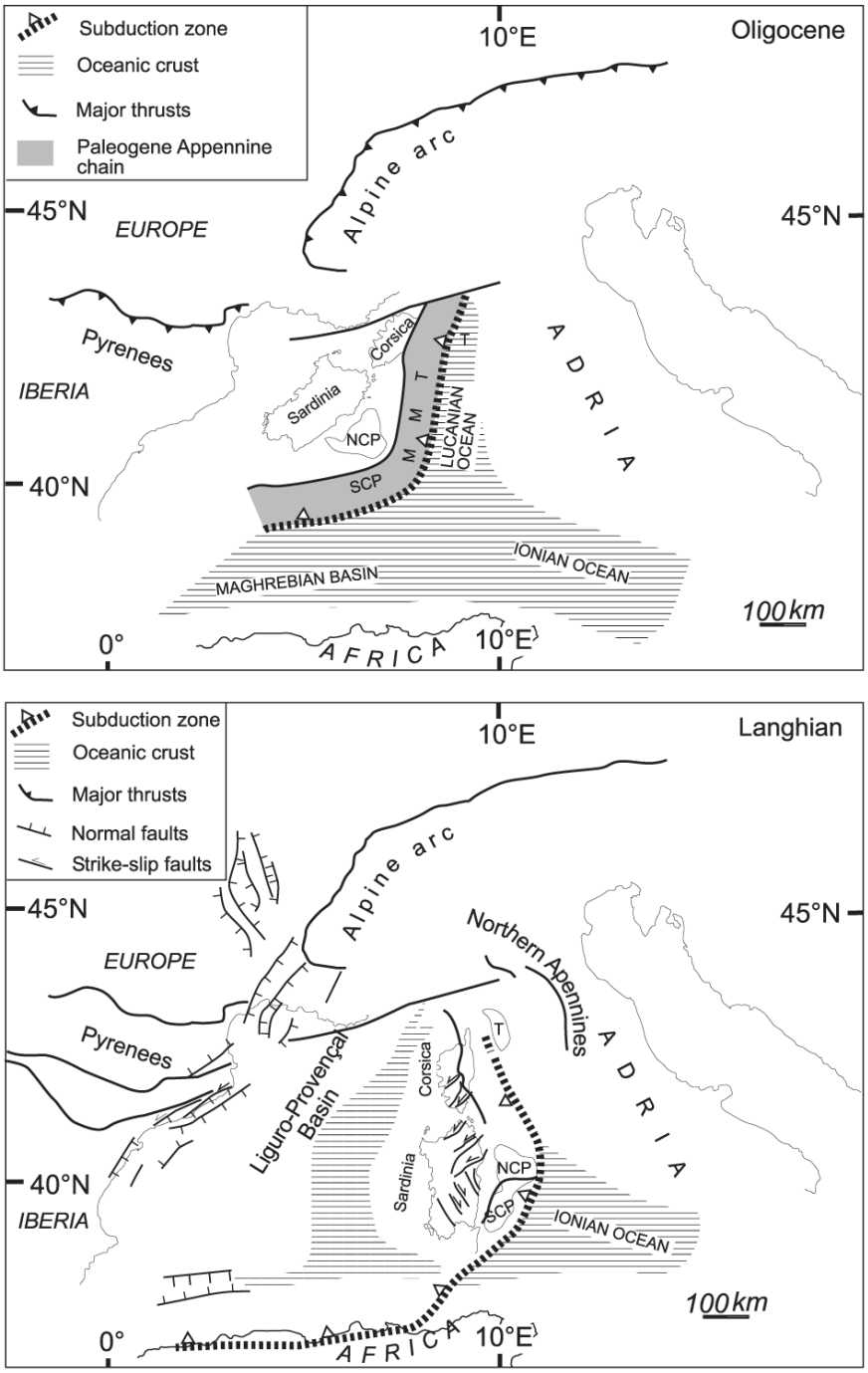

Fig. 4-12 - Sketch of central Mediterranean Basin at Oligocene and Langhian time.

5 CONCLUSIONS

5.1. ANSWERS TO THE MAIN QUESTIONS

To return to the main questions proposed at the beginning of the study, that are:

1. Did the Sardinia-Corsica block and Calabro-Peloritan Arc share the same tectonic evolution from their separation from the North-Gondwana (?) rim?
2. Have Sardinian-Corsica block and Calabro-Peloritani arc basements and Tertiary deposits the same age and geochemical features?
3. Are there alternative geodynamic models instead of the proposed models for these regions evolution?

and considering the data obtained here, the following conclusive considerations can be proposed:

1. is not possible to consider that the two blocks studied, Sardinia-Corsica block (SCB) and Calabro-Peloritan Arc (CPA), shared the same evolution from the spread out of the Gondwana paleo-continent up to the present configuration.
   Is more correct considered that only a part of the Calabro-Peloritan Arc, the Northern sector, shared the same evolution of the Sardinia-Corsica block, because of these similar geochemical features in terms of Variscan evolution (e.g. Ordovician magmatism studied here) and tertiary deposits (e.g. detrital zircon populations analysed here) linked to the Southern Tyrrhenian basin opening.

2. Only the Northern sector of CPA shows similar features to the SCB.

   Considering the Ordovician magmatism, here have been found that the Northern sector of CPA and the SCB, show the typical characteristics of the European Variscides.

   Also considering the Tertiary deposits, the Grenvillian input zircon found in the Sardinia-Corsica block and in the Northern part of the Calabria-Peloritani Arc, suggests that their source area was from the Grenvillian orogenic belt in the West part of Gondwana continent.

   The lacking of the Grenvillian input zircon in the Southern part of the Calabria-Peloritani Arc defines a different position respect of the others investigated zone. Likely, have been possible to correlate the Aspromonte region with the Cadomian terrane, deriving from the northern of Gondwana paleo-continent and then from the Northern Africa continent. Aspromonte zircon input shows affinity with the Morocco Palaeozoic sandstones whose evolution has been studied by Avigad et al. (2011). As yet suggest by literature (Micheletti et al., 2008; Thomas et al. 2002; Walsh et al. 2002; Acef et al. 2003) here is demonstrated the analogies between Morocco and Southern Calabria. The Aspromonte samples, both magmatic body (sample PAL-16) and sedimentary deposit (CA-PAL), are related to the Pan-African magmatism found in the Anti-Atlas domain.

   The Grenville detrital zircons found may have come from: (i) a sedimentary source located in a paleoposition external to the West African craton (Meinhold et al., 2010), closed to the Amazonian craton and displaced by large distances along the northern Gondwana active margin (Pereira et al., 2012); (ii) a sedimentary source located in a paleo-position closest to the West African craton (Arabian-Nubian shield and the Sahara metacraton).

3. Considering the differences between the northern and southern CPA, here is established the hypothesis of two subterranes model proposed by Alvarez & Shimabukuro (2009) about the CPA. The data here performed are in agreement to consider the Calabria like an amalgamation of two subterranes: a northern part of these terranes (Sila and likely Serre sub-regions) characterized by Ordovician magmatic rocks and similar detrital inputs found in Tertiary

samples, could be considered like part of Sardinia from the end of the Variscan orogeny until the almost the Eocene.

Considering the palinspastic restoration of the southern Tyrrhenian basin, in agreement with the model proposed by previously authors (Amodio Morelli et al., 1976; Boullin et al., 1986; Vai 1992; Oggiano et al., 2009; Patacca & Scandone, 2011) could be plausible to relocate the Stilo Unit close to Sardinia because of the remarkable analogies recognized both in the Palaeozoic basements and in the Mesozoic sedimentary covers.

The southern subterrane (Aspromonte, Peloritani) was part of a crustal block that did not collide with Sardinia. It collided with the northern subterrane (e.g. Sila and Serre) likely in the Early Miocene.

According to roll-back model proposed by many authors (among them: Royden et al., 1993; Doglioni et al, 1997; Rosenbaum and Lister, 2004) the whole CPA, likely jointed in the early Miocene, was tear apart from SCB and drifted away eastwards during the open of the South Tyrrhenian basin.

5.2. STILL OPEN QUESTIONS

From this research some questions remain still open, the more urgent are:

- When and in which way the two Calabrian subterranes did collide?
- When Northern sector of Calabria drifted away from SCB?
- Which relationships there were between the present day SCB and CPA and the others Hun super-terranes?

The answer to these questions could have a strong role in building an exhaustive model that considered all geological data (e.g. structural, stratigraphic and geochemical).

The performed data and analyses suggest also new development of the research:

The study of the pre-Variscan deposits of Sardinia here performed suggests that more data would be collected to solve the geodynamic evolution that led to the Middle Ordovician magmatic arc.

To improve the knowledge about Tyrrhenian opening the study of detrital zircon input in the Lower Miocene clastic deposits of Tuscany might be studied to investigated the analogies and differences with the CPA.

The Calabrian Variscan chain could not to be considered like a unique chain. Here is considered that CPA represent part a Variscan chain composed by almost two segments juxtaposed each others during the Tertiary. The modality how this conjunction has made, need to be better elaborated on.

If the external west Gondwana was really close to the SCB and Northern sector of CPA, the relationships between these last ones and the Amazonian craton would be better investigated.

REFERENCES

Abati, J., Aghzer, A.M., Gerdes, A., Ennih, N., 2010. Detrital zircon ages of Neopro-terozoic sequences of the Moroccan Anti-Atlas belt. Precambrian Research 181, 115–128.

Abdelsalam, M.G., Liegeois, J.P. & Stern, R.J., 2002. The Saharan Metacraton. Journal of African Earth Sciences 34, 119–136.

Acef, K., Liégeois, J.P., Ouabadi, A. & Latouche L., 2003. The Anfeg post-collisional Pan-African high-K calc-alkaline batholith (Central Hoggar, Algeria), result of the LATEA microcontinent metacratonization. Journal of African Earth Sciences 37, 295–311.

Acquafredda, P., Fornelli, A., Piccarreta, G. & Pascazio, A., 2008. Multi-stage dehydration–decompression in the metagabbros from the lower crustal rocks of the Serre (southern Calabria, Italy). Geological magazine 2008 v. 145 no. 3 p. 397-411

Acquafredda, P., Lorenzoni, S., Minzoni, N. & Zanettin Lorenzoni, E., 1987. The Palaeozoic sequence in the Stilo-Bivongi area (Central Calabria). Memorie Scienze Geologiche Università Padova 39, 117–127.

Acquafredda, P., Fornelli, A., Paglionico, A. & Piccarreta, G., 2006. Petrological evidence for crustal thickening and extension in the Serre granulite terrane (Calabria, southern Italy). Geol. Mag., 143, 145–163.

Alvarez, W., 1976. A former continuation of the Alps. Bull. Geol. Soc. Amer., 87, 891-896.

Alvarez, W., & Coccozza, T., 1974. The tectonics of central eastern Sardinia and the possible continuation of the Alpine Chain to the south of Corsica. In C. Maxia, & A. P. Cherchi Eds., paleogeografia del terziario sardo nell'ambito del Mediterraneo Occidentale. Rendiconti del Seminario della facolta' di Scienze dell' Universita' di Cagliari.

Alvarez, W., 2005. Structure of the Monte Reventino greenschist folds: a contribution to untangling the tectonic-transport history of Calabria, a key element in Italian tectonics. J. of Structural Geology, 27, 1355–1378.

Alvarez, W., & Shimaburo, D., 2009. The geological relationships between Sardinia and Calabria during Alpine and Hercynian times. Ital. J. Geosci. Boll. Soc. Geol. It., 128 2, 257-268.

Alvarez, W., Cocozza, T., & Wezel, F., 1974. Fragmentation of the Alpine orogenic belt by microplate dispersal. Nature, 248, 309-314.

Amaudric Du Chaffaut, 1973. Les relations entre Schistes lustrés et Flyschs autochtones dans le Sud de la Corse alpine. Géologie Alpine, t. 49, 1973, p. 5-12

Amelin, Y., Lee, D., & Halliday, A., 2000. Early-middle Archaean crustal evolution deduced from Lu-Hf and U-Pb isotopic studies of single zircon grains. Geochimica et Cosmochimica Acta, 64, 4205-4225.

Amodio Morelli L., Bonardi G., Colonna V., Dietrich D., Giunta G., Ippolito F., Liguori V., Lorenzoni S. Paglionico A., Perrone V., Piccaretta G., Russo M., Scandone P., Zanettin Lorenzoni E. & Zuppetta A. 1976. L'arco Calabro-peloritano nell'orogene Appenninico Maghrebide. Mem. Soc. Geol. It., 17, 1-60.

Andrieux, J., Fontbote, J. M., & Mattauer, M., 1971. Sur un modèle explicatif de l'arc de Gibraltar. Earth and Planetary Science Letters, 12, 191–198.

Arthaud, F. & Matte, P., 1977. Late Paleozoic strike slip faulting in southern Europe and northern Africa: result of right lateral shear zone between the Appalachians and Oural. Geol. Soc. Am. Bull., 88, 1305–1320.

Atzori, P., Carveni P., Lentini F., Pezzino A. & Vezzani L., 1977 Posizione strutturale dei lembi meso-cenozoici dell'unità di Rocca Novara nei Monti Peloritani (Sicilia nord orientale). Boll. Soc. Geol. It, 96, 331-338.

Augustsson, C., Münker, C., Bahlburg, H., & Fanning, C., 2006. Provenance of late Palaeozoic metasediments of the SW South American Gondwana margin: A combined U-Pb and Hf-isotope study of single detrital zircons. Journal of the Geological Society, 163, 983-995.

Avigad, D., Gerdes A., Morag N. & Bechstädt T., 2012. Coupled U–Pb–Hf of detrital zircons of Cambrian sandstones from Morocco and Sardinia: Implications for provenance and Precambrian crustal evolution of North Africa, Gondwana Res. 21, 2–3, pp. 690–703

Ayuso, R.A., Messina, A., De Vivo, B., Russo, S., Woodruff, L.G., Sutter, J.F. & Belkin, H.E., 1994. Geochemistry and argon thermochronology of the Variscan Sila Batholith, southern Italy: source rocks and magma evolution. Contrib. Mineral. Petrol., 117,87–109.

Bahlburg, H., Vervoort, J., & DuFrane, S. 2010. Plate tectonic significance of Middle Cambrian and Ordovician siliciclastic rocks of the Bavarian Facies, Armorican Terrane Assemblage, Germany - U-Pb and Hf isotope evidence from detrital zircons. Gondwana Research, 17, 223-235.

Bahlburg, H., Vervoort, J., Frane, S. D., Bock, B., Augustsson, C., & Reimann, C., 2009. Timing of crust formation and recycling in accretionary orogens: Insights learned from the western margin of South America. Earth-Science Reviews, 97, 227-253.

Bahlburg, H., Vervoort, J.D. & Du Frane, S.A., 2010. Plate tectonic significance of Middle Cambrian and Ordovician siliciclastic rocks of the Bavarian Facies, Armorican Terrane Assemblage, Germany. U–Pb and Hf isotope evidence from detrital zircons. Gondwana Research, 17, 223–235.

Barca, S. & Costamagna L. G., 2000. Il bacino paleogenico del Sulcis-Iglesiente (Sardegna SW): nuovi dati stratigrafico-strutturali per un modello geodinamico nell'ambito dell'orogenesi pirenaica. Boll. Soc. Geol. It., 119, 497-515.

Barca, S., & Gregorio, F., 1979. La successione ordoviciano-siluriana inferiore del Sarrabus Sardegna sud-orientale. Mem. Soc. Geo. It., 20, 189-202.

Barca, S., Ferretti A., Massa P. & Serpagli E., 1992. The Hercynian Arburese Tectonic Unit of SW Sardinia. New stratigraphic and structural data. Riv. Ital. Paleont. Strat. , 98, 119-136.

Basei, M.A.S., Brito Neves, B.B., Siga Júnior, O., Babinski, M., Pimentel, M.M., Tassinari, C.C.G., Hollanda, M.H.B., Nutman, A. & Cordani, U.G., 2010. Contribution of SHRIMP U–Pb zircon geochronology to unravelling the evolution of Brazilian Neoproterozoic fold belts. Precambrian Research 183, 122–144.

Bea, F., Montero, P., Talavera, C., Anbar, M. A., Scarrow, J., Molina, J., et al., 2010. The palaeogeographic position of Central Iberia in Gondwana during the Ordovician: evidence from zircon chronology and Nd isotopes. Terra Nova, 22, 341-346.

Beccaluva, L., Coltorti,, R. G., Macciotta, G., & Siena, F. 1994. The Cainozoic calcalkaline magmatism of the western Mediterranean and its geodynamic significance. Bollettino di Geofisica Teorica e Applicata , 36, 293-308.

Beccaluva, L., Deriu, M., Macciotta, G., Savelli, C., & Cantoni, M., 1981. Geopetrographic map of the Pliocene-Pleistocene volcanism from North-Western Sardinia. L.A.C.

Belka, Z., Valverde-Vaquero, P., Dörr, W., Ahrendt, H., Wemmer, K., Franke, W. & Schäfer J., 2002. Accretion of first Gondwana-derived terranes at the margin of Baltica. In: Winchester J.A., Pharaoh T.C. & Verniers J. (eds) Palaeozoic Amalgamation of Central Europe, 201. Geol. Soc. Lond. Spec. Publ., pp 19–36.

Belka, Z., Valverde-Vaquero, P., Dörr, W., Ahrendt, H., Wemmer, K., Franke, W., 2002. Accretion of first Gondwana-derived terranes at the margin of Baltica. Geological Society Special Publication , 201, 19-36.

Bezert, P. & Caby, R., 1988. Sur l'age post-bartonien des evenements tectono-metamorphiques alpins en bordure orientale de la Corse cristalline (Nord de Corte). Bull. Soc. geol. Fr. 6,965-971.

Boccaletti, M., & Guazzone, G., 1974. Remnant arcs and marginal basins in the Cainozoic development of the Mediterranean. Nature , 252, 18-21.

Bodet, F., & Schärer, U., 2000. Evolution of the SE-Asian continent from U-Pb and Hf isotopes in single grains of zircon and baddeleyite from large rivers. Geochimica et Cosmochimica Acta, 64, 2067-2091.

Bonardi, G., Compagnoni, R., Messina, A. & Perrone, V., 1984. Riequilibrazioni metamorfiche di probabile età alpina nell'unità dell'Aspromonte; Arco Calabro-Peloritano. Rend. Soc. Ital. Miner. Petr. 39, 613-628.

Bonardi G., Giunta G. , Perrone V., Russo M., Zuppetta A. & Ciampo G., 1980. Osservazioni sull'evoluzione dell'Arco Calabro-Peloritano nel Miocene inferiore: la Formazione di Stilo-Capo d'Orlando. Bollettino della Società Geologica Italiana, 99, 365–393.

Bonardi, G., & Giunta, G., 1982. L'estremità Nord-orientale della Sicilia nel quadro dell'evoluzione dell'Arco Calabro-Peloritano. Soc. Geol. It , 79-83.

Bonardi, G., Caggianelli, A., Critelli, S., Messina, A., Perrone, V., Acquafredda, P., Carbone, G., Careri, G., Cirrincione, R., D'Errico, M., Dominici, R., Festa, V., Iannace, A., Macaione, E., Mazzoli, S., Notaro, P., Parente, M., Perri, E., Piluso, E., Somma, R., Sonnino, M. & Vitale, S., 2004. Geotraverse across the Calabria-Peloritani Terrane (Southern Italy). Field Trip Guide Book-P66, 32nd International Geological Congress IUGS, Florence, 20–28 August 2004, pp. 1–60.

Bonardi, G., Capoa, P. D., Staso, A. D., Estévez, A., Martín-Martín, M., Martín-Rojas, I., 2002. New constraints to the geodynamic evolution of the southern sector of the Calabria-Peloritani Arc Italy. C.R. Geoscience , 334, 423-430.

Bonardi, G., Capoa, P. D., Staso, A. D., Estévez, A., Martín-Martín, M., Martín-Rojas, I., 2003. Oligocene to Early Miocene depositional and structural evolution of the Calabria-Peloritani southern terrane Italy and geodynamic correlations with the Spain Betics and Morocco Rif. Geodinamica Acta , 16, 149-169.

Bonardi, G., Capoa, P. D., Staso, A. D., Perrone, V., Sonnino, M., & Tramontana, M., 2005. The age of the Paludi Formation: a major constraint to the beginning of the Africa-verging orogenic transport in the northern sector of the Calabria-Peloritani Arc. Terra Nova, 17, 331-337.

Bonardi, G., Compagnoni, R., Moro, A. D., Macaione, E. & Messina, A. & Perrone V., 2008. Rb-Sr age constraints on the Alpine metamorphic overprint in the Aspromonte Nappe Calabria-Peloritani Composite Terrane, southern Italy. Boll. Soc. Geol. It. Ital. J. Geosci., 127, 173-190.

Bonardi, G., Cavazza, W., Perrone, V. & Rossi, S., 2001. Calabria–Peloritani Terrane and northern Ionian Sea. In: Anatomy of an Orogen: The Apennines and the Adjacent Mediterranean Basins (G.B.Vai and I.P. Martini, eds), pp. 287–306. Kluwer Academic Publishers, Dordrecht.

Bonjour, J., Peucat, J., Chauvel, J., Paris, F., & Cornichet, J., 1988. UPb zircon dating of the early paleozoic Arenigian transgression in Western Brittany France: A new constraint for the lower paleozoic time-scale. Chemical Geology: Isotope Geoscience Section, 72, 329-336.

Borsi, S. & Dubois, R., 1968. Donnes geochronologiques sue l'histoire hercynienne et alpine de la Calabre centrale, C. R. Acad. Sci. Paris, 266, 72–75.

Borsi, S., Hieke Merlin, O., Lorenzoni, S., Paglionico, A. & Zanettin Lorenzoni, E., 1976. Stilo Unit and "dioritic-kinzigitic" unit in Le Serre (Calabria, Italy). Geological, petrological, geochronological characters. Bollettino della Società Geologica Italiana 19, 501–510.

Bouillin, J., 1984. Nouvell de la liason Appennin-Maghrebides en Calabre; consequences sur la paleogeographie tethysienne entre Gibraltar et les Alpes. Rev. Geol. Dyn. Geogr. Phys., 25, 321-338.

Bouillin, J., Durand-Delga, M., & Oliver, P., 1986. Betic-Rifian and Tyrrhenian arcs: distinctive features, genesis and development stages. The origin of arcs. Conference papers, 281-304.

Brodie, K.H. & Rutter, E.H., 1987. Deep crustal extensional faulting in the Ivrea zone of northern Italy. Tectonophysics 140, 193-212.

Burg, J. P., Iglesias, M., Laurent, P., & Ribeiro, A., 1981. Variscan intracontinental deformation: the Coimbra-Cordoba shear zone SW Iberian Peninsula. Tectonophysics, 78, 161–177.

Burg, J.P., Van der Driessche, J. & Brun, J.P., 1994. Syn to post-thickening extension in the Variscan belt of western Europe: modes and structural consequences. Geol. Fr., 3, 33–51

Burg, J.P., Bale, P., Brun, J.P. & Girardeau, J., 1987. Stretching lineation and transport direction in the Ibero-Armorican arc during the Siluro-Devonian collision. Geodin. Acta, 1, 71–87.

Cabanis, B. & Lecolle M., 1989 Le diagramme La/10 Y/15-Nb/8: un outil pour la discrimination des series volcaniques et la mise en evidence des procesus de melange et/ou de contamination crustale. C.R. Acad. Sci. Ser. II 309. 2023-2029.

Caggianelli, A. & Prosser, G., 2002. Modelling the thermal perturbation of the continental crust after intraplating of thick granitoid sheets: a comparison with the crustal sections in Calabria (Italy). Geol. Mag., 139, 699–706.

Caggianelli, A., Prosser, G. & Rottura, A., 2000. Thermal history vs. fabric anisotropy in granitoids emplaced at different crustal levels: an example from Calabria, southern Italy. Terra Nova, 12, 109–116.

Caggianelli, A., Liotta, D., Prosser, G. & Ranalli, G., 2007. Pressure–temperature evolution of the late Hercynian Calabria continental crust: compatibility with post-collisional extensional tectonics. Terra Nova, 19: 502–514. doi: 10.1111/j.1365-3121.2007.00777.

Cahen, L., Snelling, N.J., Delhal, J. & Vail, J.R., 1984. The Geochronology and evolution of Africa. Clarendon Press, Oxford

Calvino, F., 1959. Lineamenti strutturali del Sarrabus-Gerrei (Sardegna sud-orientale). Boll. Serv. Geol. d'It.: 81, 489-556, Roma.

Calvino, F., 1972. Note Illustrative della Carta Geologica d'Italia, Foglio 227-Muravera, pp. 60, Servizio Geologico d'Italia, Roma.

Calvino, F., 1961. Lineamenti strutturali del Sarrabus-Gerrei. Boll. Soc. Geol , 81, 489-556.

Capelli, B., Carmignani, L., Castorina, F., Di Pisa A., Oggiano G, Petrini R., 1992. A Hercynian suture zone in Sardinia: geological and geochemical evidence. Geodin Acta , 51, 101-118.

Capoa, P.D., Guerrieri, F., V., P., & Serrano, F. 1997. New biostratigraphic data on the Frazzanò Formation Longi-Taormina unit: consequences on defining the deformation age of the Calabria-Peloritani arc southern sector. Riv. It. Paleont. Stratigr , 103, 343-356.

Carannante, G., Cocozza, T., & D'Argenio, B., 1984. Late Precambrian-Cambrian geodynamic setting and tectono-sedimentary evolution of Sardinia Italy. Bollettino della Società Geologica Italiana , 103, 121-128.

Carmignani, L., Franceschelli, M., Gattiglio, M., Pertusati, P.C., Ricci, C.A., 1982. Attuali conoscenze sul ciclo ercinico nella Sardegna settentrionale. In: Guida alla Geologia del Paleozoico sardo. Guide Geologiche Regionali. Mem. Soc. Geol. It. 129-135.

Carmignani, L., Oggiano, G. & Pertusati, P.C., 1994a. Geological outlines of the Hercynian basement of Sardinia. Petrology, Geology and ore deposits of the palaeozoic basement of Sardinia. Guide book to the field excursion Carmignani, L., Carosi, R., Di Pisa, A., Gattiglio, M., Musumeci, G., Oggiano, G. & Pertusati, P.C. 1994. The Hercynian chain in Sardinia (Italy). Geodin. Acta, 7, 31–47.

Carmignani, L., Barca, S., L., D., Fantozzi, P., Funedda, A., Oggiano, G. & Pasci, S., 1994b. Tertiary compression and extension in the Sardinian basement. Bollettino di Geofisica Teorica ed Applicata , 36, 45-62.

Carmignani, L., Carosi, R., Disperati, L., Funedda, A., Musumeci, G., Molli, G., 1992. Tertiary transpressional tectonics in NE Sardinia, Italy. In L. Carmignani, & F. P. Sassi Eds., «Contributions to the Geology of Italy with special regard to the Paleozoic Basements.A volume dedicated to Tommaso Cocozza» Vol. 7, pp. 83-96. NEWSLETTER.

Carmignani, L., Carosi, R., Pasa, A. D., Gattiglio, M., Musumeci, G., Oggiano, G., et al. 1994c. The Hercynian chain in Sardinia Italy. Geodinamica Acta , 7, 31-47.

Carmignani, L., Conti, P., Barca, S., Cerbai, N., Eltrudis, A., Funedda, A., Oggiano, G., Patta, E.D., Ulzega, A., Orrù, P. & Pintus, C., 2001. Note illustrative del Foglio 549 - Muravera. Memorie descrittive della Carta geologica d'Italia 1:50.000. Roma. 140 pp.

Carmignani, L., Decandia, F. A., Disperati, L., Fantozzi, P., Lazzarotto, A., Liotta, D., 1995. Relationships between the Tertiary structural evolution of the Sardinia-Corsica-Provençal Domain and the Northern Apennines. Terra Nova , 7, 128–137.

Carmignani, L., Funedda, A., Oggiano, G., & Pasci, S., 2004. Tectono-sedimentary evolution of southwest Sardinia in the Paleogene: Pyrenaic or Apenninic Dynamic? Geodinamica Acta, 17, 275-287.

Carmignani, L., Oggiano, G., Barca, S., Conti, P., Salvadori, I., Eltrudis, A., Funedda, A. & Pasci, S., 2001. Geologia della Sardegna. Note illustrative della Carta Geologica in scala 1:200.000. Servizio Geologico d'Italia: Roma .

Carosi R., Montomoli C. & Pertusati P.C., 1995 Zone di taglio nel Dominio Toscano Interno. Atti Societa Toscana de Scienze Naturali Residente in Pisa, Memorie, Serie A, 101, pp. 187–200.

Carosi, R., & Oggiano, G., 2002. Transpressional deformation in NW Sardinia Italy: insights on the tectonic evolution of the Variscan belt. Comptè Rendus Geoscience , 334, 273-278.

Carosi, R., Frassi, C., & Montomoli, C., 2009. Deformation during exhumation of medium- and high-grade metamorphic rocks in the Variscan chain in northern Sardinia Italy. Geol. J. , 44, 280-305.

Carosi, R., Lombardo, B., Molli, G., Musumeci, G. & Pertusati, P.C., 1998.The South Tibetan Detachment System in the Rongbuk valley, Everest region. Deformation features and geological implications. Journal of Asian Earth Science 16, 299–311.

Carosi, R., Montomoli,, R. D., & Visoná, D., 2006. Normal-sense shear zones in the core of the Higher Himalayan Crystallines Bhutan Himalaya: evidence for extrusion ? In S. MP, & L. Godin Eds., Channel Flow, Ductile Extrusion and Exhumation in Continental Collision Zones Vol. 268, pp. 425-444. Geol. Soc. London, Special Publications.

Carosi, R., Pisa, A. D., Iacopini, D., Montomoli, C., & Oggiano, G., 2004. The structural evolution of the Asinara Island NW Sardinia, Italy. Geod. Acta , 175, 309-329.

Casas J. M., Castiñeiras P., Navidad M., Liesa M. & Carreras J., 2010. New insights into the Late Ordovician magmatism in the Eastern Pyrenees: U–Pb SHRIMP zircon data from the Canigó massif. Gondwana Research 17, 317–324.

Casini, L., & Oggiano, G., 2008. Late orogenic collapse and thermal doming in the northern Gondwana margin incorporated in the Variscan Chain: A case study from the Ozieri Metamorphic Complex, northern Sardinia, Italy. Gondwana Research , 13, 396-406.

Cavazza, W. & De Celles, P., 1993. Geometry of a Miocene submarine canyon and associated sedimentary facies in southeastern Calabria, southern Italy. Bull. Geol. Soc. Amer., 105, 1297–1309.

Cavazza, W., Blenkinsop, J., Celles, P. D., Patterson, R., & Reinhardt, E., 1997. Stratigrafia e sedimentologia della sequenza sedimentaria oligocenico-quaternaria del bacino calabro-ionico. Boll. Soc. Geol. It. , 116, 52-77.

Cawood, P., Nemchin, A., & Strachan, R., 2007. Provenance record of Laurentian passive-margin strata in the northern Caledonides: Implications for paleodrainage and paleogeography. Bulletin of the Geological Society of America , 119, 993-1003.

Chabrier, G., 1967. Le synclinal cretace de Gorropu Sardaigne. C.R. Soc. geol. France , 7, 321-322.

Chabrier, G., 1969. Sur la stratigraphie et la tectonique des monts d'Oliena Sardaigne. C.R. Soc. geol. France , 6, 218-220.

Chabrier, G., 1970. Tectonique de socle d'age alpin en Sardaigne centro-orientale. C.R. Acad. Sci. Paris , 271, 1252-1255.

Chappel B. & White A.J.R., 1974. Two contrasting granite types. Pacific Geology 8, 173–174.

Cherchi, A., & L., M., 1984. Il sistema di rifting oligo-miocenico del Mediterraneo occidentale e sue conseguenze paleogeografiche sul Terziario sardo. Mem. Soc. Geol. It. , 24, 387-400.

Cherchi, A., & Montadert, L., 1982. Oligo-Miocene rift of Sardinia and the early history of the Western Mediterranean Basin. Nature , 298, 736-739.

Chiarabba, C., Gori, P. D., & Speranza, F., 2008. The southern Tyrrhenian subduction zone: Deep geometry, magmatism and Plio-Pleistocene evolution. Earth and Planetary Science Letters , 268, 408-423.

Cocherie A., Ph. Rossi, C.M. Fanning & Guerrot C., 2005. Comparative use of TIMS and SHRIMP for U–Pb zircon dating of A-type granites and mafic tholeiitic layered complexes and dykes from the Corsican batholith (France), Lithos 82 185–219.

Cocks, L., & Torsvik, T., 2002. Earth geography from 500 to 400 million years ago: a faunal and palaeomagnetic review. Journal of the Geological Society , 159, 631-644.

Cocozza, T. & Gandin, A., 1977. Età e significato ambientale delle facies detritico-carbonatiche dell'altopiano di Campumari (Sardegna sud-occidentale). Boll. Soc. Geol. Ital. 95, 1520–1540.

Cocozza, T., 1967. Il Permo-Carbonifero del bacino di San Giorgio (Iglesiente, Sardegna sud-occidentale). Memorie della Società Geologica Italiana 6, 607–642.

Cocozza, T., 1979. The Cambrian of Sardinia. Memorie della Società Geologica Italiana20, 163–187.

Colonna, V., Lorenzoni, S. & Zanettin Lorenzoni, E., 1973. Sull'esistenza di due complessi metamorfici lungo il bordo sud-orientale del massiccio 'granitico' delle Serre (Calabria). Boll. Soc. Geol. It., 92, 801–830.

Condie, K., O'Neill, C., & Aster, R., 2009. Evidence and implications for a widespread magmatic shutdown for 250 My on Earth. Earth and Planetary Science Letters , 282, 294-298.

Conti, P., Carmignani, L., & Funedda, A., 2001. Change of nappe transport direction during the Variscan collisional evolution of central-southern Sardinia Italy. Tectonophysics , 332, 255-273.

Cordani, U. G. & Teixeira, W., 2007. Proterozoic accretionary belts in the Amazonian Craton. In: Hatcher, R.D.Jr.; Carlson, M.P.; McBride, J.H.; Martínez-Catalán, J.R. (Org.). 4-D Framework of Continental Crust. Denver, USA: Geological Society of America, v. 200, 297–320.

Cordani, U.G., Teixeira, W., D'Agrella-Filho, M.S. & Trindade, R.I., 2009. The position of the Amazonian craton in supercontinents. Gondwana Research 15, 396–407.

Corrigan, D., & Hanmer, S., 1997. Anorthosites and related granitoids in the Grenville Orogen: a product of convective thinning of the lithosphere? Geology , 25, 61-64.

Corriveau, L., Heaman, L. M., Marcantonio, F., & Breemen, O., 1990. Ga K-rich alkaline plutonism in the SW Grenville Province. Ga K-rich alkaline plutonism in the SW Grenville Province , 105 4, 473-485.

Costamagna L.G. & Barca S., 2008. Depositional architecture and sedimentology of the Tuppa Niedda Conglomerates (Late Carboniferous, Arburese, SW Sardinia, Italy) vol. 127, n°3, pp. 625-636.

Courme, M.D. & Mascle, G., 1988. Nouvelles données stratigraphies sur les séries oligomiocénes des unités siciliennes: conséquences paléogéographiques. Bulletin de la Société géologique de France IV, 105–118.

Crisci, G.M., Maccarrone, E. & Rottura, A., 1979. Cittanova peraluminous granites (Calabria, Southern Italy). Mineralogica et Petrographica Acta 23, 279–302.

Crowley, Q., Floyd, P., Winchester, J., Franke, W., & Holland, J., 2000. Early Palaeozoic rift-related magmatism in Variscan Europe: fragmentation of the Armorican Terrane Assemblage. Terra Nova , 12, 171–180.

Dalziel, I., 1991. Pacific margins of Laurentia and East Antarctica-Australia as a conjugate rift pair: evidence and implications for an Eocambrian supercontinent. Geology , 19, 598-601.

Dalziel, I., 1992. On the organization of American plates in the Neoproterozoic and the breakout of Laurentia. GSA Today , 2, 237,240-241.

D'Amico, C., Rottura, A., Maccarrone, E. & Puglisi, G., 1982. Peraluminous granitic suite of Calabria-Peloritani Arc (Southern Italy). Rendiconti della Società Italiana di Mineralogia e Petrologia 38, 35–52.

Daniel, J.M., Jolivet, L., Goffé, B. & Poinssot, C., 1996. Crustal-scale strani partiotionning: Footwall deformation below the Alpine Oligo-Miocene detachment of Corsica. J. Struct. Geol., 18, 41-59.

De Capoa, P., Guerrera, F., Perrone,V. & Serrano, F., 1997. Newbiostratigraphic data on the Frazzanò Formation (Longi-Taormina Unit): consequences on defining the deformation age of the Calabria-Peloritani Arc Southern Sector. Rivista Italiana di Paleontologia e Stratigrafia 103, 343–356.

De Jong, K.A., Manzoni, M., & Zijdeverld, J.S., 1969. Paleomagnetism of the Alghero trachyandesites. Nature , 224, 64.

De Vivo, B., Ayuso, R.A., Belkin, H.E., Lima, A., Messina, A., & Viscardi, A., 1992. Whole-rock geochemistry and fluid inclusions as exploration tools for mineral deposit assessment in the Serre batholith, Calabria, Southern Italy. European Journal of Mineralogy 4, 1035–1051.

Del Moro, A, Pardini, G, Maccarrone, E, Rottura, A., 1982. Studio radiometrico Rb-Sr di granitoidi peraluminosi dell'Arco Calabro-Peloritano. Rend. Soc. Ital. Mineral. Petrol., 38:1015–1026.

Del Moro, A., Fornelli, A. & Paglionico, A., 1994 K-feldspar megacryst granitic suite in the Serre (southern Calabria – Italy). Periodico Miner., 63, 19-23.

Delaperrière, E. & Lancelot, J., 1989. Datation U–Pb sur zircons de l'orthogneiss du Capo Spartivento (Sardaigne, Italie), nouveau témoin d'unmagamatisme alcalin ordovicien dans le sud de l'Europe. Comptes Rendus Académie Sciences Paris 309, 835–842.

Destombes, J., Hollard, H. & Willefert, S., 1985. Lower Paleozoic rocks of Morocco. In: Hollard, H. (Ed.), Lower Paleozoic Rocks of the World. John Wiley, London, pp. 93–336.

Di Pisa, A., Gattiglio M. & Oggiano, G., 1992. Pre-Hercynian magmatic activity in the nappe zone (internal and external) of Sardinia: evidence of two within plate basaltic cycles. In: Carmignani, L., Sassi, F.P. (Eds.), Contribution to the Geology of Italy With Special Regards to the Palaeozoic basement. A volume dedicated to Tommaso Cocozza. IGCP Project N. 276. Newsletter, vol. 5. Siena, pp. 33–44.

Di Vincenzo G., Carosi R. & Calmieri R., 2004. The relationships between tectonometamorphic evolution and argon isotope records in white mica: constraints from in situ Ar/Ar laser analysis of the Variscan basement of Sardinia (Italy), J. Petrol.45, 1013–1043.

Dickinson, W., & Gehrels, G., 2003. U-Pb ages of detrital zircons from Permian and Jurassic eolian sandstones of the Colorado Plateau, USA: Paleogeographic implications. Sedimentary Geology , 163, 29-66.

Dieni, I., Massari, F. & Medus, J., 2008. Age, depositional environment and stratigraphic value of the Cuccuru 'e Flores Conglomerate: insight into the Palaeogene to early Miocene geodynamic evolution in Sardinia. Bull. Soc. Geol. Fr., 179-1, 51-72.

Dieni, I. & Massari, F., 1965. Il Neogene e Quaternario dei dintorni di Orosei (Sardegna). Memorie della Società Italiana di Scienze Naturali 15, 89–142.

Dieni, I., & Massari, F., 1970. Tettogenesi gravitativa di età oligocenica nella Sardegna centro-orientale. Bollettino della Societa geologica d' Italia , 89, 58-64.

Dieni, I., & Massari, F., 1987. Le Mesozoique de la sardaigne orientale. "Groupe Francais du Cretace", Sardaigne , 150-160.

Dietrich, D., 1988. Sense of overthrust shear in the Alpine nappes of Calabria Southern Italy. J. Struct. Geol., 10 4, 373-381.

Doglioni, C., Gueguen, E., Sabat, F., Fernandez, M., 1997. The western Mediterranean extensional basins and the Alpine orogen. Terra Nova 9 (3), 109–112.

Dojen, C., 2009. Late Silurian and Early Devonian Beyrichioidea from Gondwana and Perigondwanan terranes and their palaeobiogeographical implications. Bulletin de la Societe Geologique de France , 180, 309-315.

Doré, F., 1994. Cambrian of the Armorican Massif. In: Keppie, J.D. (Ed.), Pre-Mesozoic Geology in France and related areas. Springer-Verlag, Berlin/Heidelberg, pp. 136–141.

Dubois, R., 1971. Définition d'un socle antéhercynien en Calabre. Compte Rendu Academie Science de Paris 272, 2052–5.

Dubois, R., 1976. La suture calabro-apenninique crétacé–éocène et l'ouverture Tyrrhénienne néogène: étude pétrographique et structurale de la Calabre centrale. Thèse de Doctorat d'Etat, Université P. et M. Curie, Paris, pp.567, Egal, 1992

Elliot, D., & Fanning, C., 2008. Detrital zircons from upper Permian and lower Triassic Victoria Group sandstones, Shackleton Glacier region, Antarctica: Evidence for multiple sources along the Gondwana plate margin. Gondwana Research , 13, 259-274.

England, P.C., & Thompson, A.B., 1984. Pressure-temperature-time paths of regional metamorphism, I. Heat transfer during the evolution of regions of thickened continental crust. J. Petrol., 25 (1984), pp. 894–928

Ennih, N. & Liegeois, J.-P., 2008. The boundaries of the West African craton, with spe- cial reference to the basement of the Moroccan metacratonic Anti-Atlas belt. Geological Society, London, Special Publications 297 (1), 1–17.

Esu, D., & Kozakis, T., 1983. Les vertébrés et les mollusques continentaux du Tertiaire de la Sardaigne: Paléobiogeographie et biostratigraphie. Geol. Romana , 22, 177-206.

Faure, M., 1995. Late orogenic carboniferous extensions in the French Massif Central. Tectonics, 14, 132–153.

Faure, M., Leloix, C., & Roig, J., 1997. L'évolution polycyclique de la chaîne hercynienne. Bulletin de la Société géologique de France , 168, 695–705.

Fernández-Suarez, J., Gutierrez-Alonso, G. & Jeffries, T.E., 2002. The importance of along-margin terrane transport in northern Gondwana: insights from detrital zircon parentage in Neoproterozoic rocks from Iberia and Brittany. Earth and Planetary Science Letters 204 (1-2), 75–88.

Fernández-Suárez, J., Gutiérrez-Alonso, G., Jenner, G., & Tubrett, N.M., 2000. New ideas on the Proterozoic-Early Palaeozoic evolution of NW Iberia: Insights from U-Pb detrital zircon ages. Precambrian Research 102, 185-206.

Festa, V., Battista, P. D., Caggianelli, A., & Liotta, D., 2003. Exhumation and tilting of the late-Hercynian continental crust in the Serre Massif Southern Calabria, Italy. Boll. Soc. Geol. It., Spec. , 2, 79-88.

Fiannacca, P., Williams, I.S., Cirrincione, R. & Pezzino, A., 2008. Crustal contributions to Late-Hercynian peraluminous magmatism in the Southern Calabria–Peloritani Orogen, Southern Italy: petrogenetic inferences and the Gondwana connection.Journal of Petrology 48, 1497–1514.

Finetti, I., Boccaletti, M., B., Del, A. M., Pipan, M., Prizzon, A., 2005. Lithospheric tectono-stratigraphic setting of the Ligurian Sea-Northern Apennines-Adriatic foreland from integrated CROP seismic data. I. Finetti, Ed. CROP Project Book.

Flowerdew M.J., Millar I.L., Curtis, M.L., Vaughan, A.P.M., Horstwood, M.S.A., Whitehouse, M.J., & Fanning, C.M., 2007. Combined U-Pb geochronology and Hf isotope geochemistry of detrital zircons from early Paleozoic sedimentary rocks, Ellsworth-Whitmore Mountains block, Antarctica. Bulletin of the Geological Society of America , 119, 275-288.

Fornelli, A., Piccarreta, G., Acquafredda, P., Micheletti, F. & Paglionico, A., 2004.Geochemical fractionation in migmatitic rocks from Serre granulitic terrane (Calabria, southern Italy). Periodico di Mineralogia 73, 145–157.

Fornelli, A., Piccarreta, G., Del Moro, A. & Acquafredda, P. 2002. Multi-stage melting in the lower crust of the Serre (Southern Italy). Journal of Petrology 43 (12), 2191–2217.

Fornelli, A., Caggianelli, A., Del Moro, A., Bargossi, G.M., Paglionico, A., Piccarreta, G. & Rottura, A., 1994. Petrology and evolution of the central Serre granitoids (Southern Calabria – Italy). Per. Mineral., 63, 53–70.

Franceschelli, M., M., G. P., Dinandi, A., & Loi, M., 2005. Layered amphibolite sequence in NE Sardinia, Italy: Remnant of a pre-Variscan mafic silicic layered intrusion? Contributions to Mineralogy and Petrology , 149, 164-180.

Franke, W., 2000. The mid-European segment of the Variscides: tectono-stratigraphic units, terrane boundaries and plate tectonic evolution. J. Geol. Soc. London, Special Publications , 179, 35–61.

Friedl G., Finger F., Paquette J.L., von Quadt A., McNaughton N.J. & Fletcher I.R., 2004. Pre-Variscan geological events in the Austrian part of the Bohemian Massif deduced from U–Pb zircon ages. Int J Earth Sci 93:802–823. doi:10.1007/s00531- 004-0420-9

Friedl, G., Finger, F., McNaughton, N., & Fletcher, I., 2000. Deducing the ancestry of terranes: SHRIMP evidence for South America-derived Gondwana fragments in central Europe. Geology , 28, 1035-1038.

Funedda, A., 2009. Foreland- and hinterland-verging structures in fold-and- thrust belt: an example from the Variscan foreland of Sardinia. International Journal of Earth Sciences 98: 1625–1642.

Gaggero, L., Oggiano, G., Funedda, A. & Buzzi, L., 2012. Rifting and arc-related early Paleozoic volcanism along the North Gondwana margin: geochemical and geological evidence from Sardinia (Italy). The Journal of Geology.

Galassi, R. & Gandin, A., 1992. New structural data and their bearing on the Cambrian stratigraphy of the Iglesiente region (Sardinia, Italy). Comptes Rendus de l'Acadkmie des Sciences, Paris, 314,93-100.

Gandin, A., & Debrenne, F., 1984. Lower Cambrian bioconstructions in Southwestern sardinia Italy. Geobios. Memoire Special , 8, 231-240.

Gasquet, D., Levresse, G., Cheilletz, A., Azizi-Samir, M., & Mouttaqi, A., 2005. Contribution to a geodynamic reconstruction of the Anti-Atlas Morocco during Pan-African times with the emphasis on inversion tectonics and metallogenic activity at the Precambrian-Cambrian transition. Precambrian Research , 140, 157-182.

Gattacceca, J., & Rochette, P., 2004. Toward a robust relative paleointensity estimate in meteorites. Earth and Planetary Science Letters , 227, 377-393.

Giacomini, F., Bomparola, R., Grezzo, C., & Guldbransen, H., 2006. The geodynamic evolution of the Southern European Variscides: constraints from the U/Pb geochronology and geochemistry of the lower Paleozoic magmatic-sedimentary sequences of Sardinia Italy. Contrib Mineral Petrol , 152, 19–42.

Graessner, T. & Schenk, V., 2001. An exposed Hercynian deep crustal section in the Sila Massif of Northern Calabria: mineral chemistry, petrology and a P–T path of granulite-facies metapelitic migmatites and metabasites. J. Petrol., 42, 931–961

Graessner, T., Schenk, V., Bröcker, M. & Mezger, K., 2000. Geochronological constraints on the timing of granitoid magmatism, metamorphism and post-metamorphic cooling in the Hercynian crustal cross-section of Calabria. J. Metamorphic Geol., 18,409–421.

Grassner, T., & Schenk, V., 2001. An Exposed Hercynian Deep Crustal Section in the Sila Massif of Northern Calabria: Mineral Chemistry, Petrology and P-T Path of Granulite-facies Metapelitic Migmatites and Metabasites. Journal of Petrology , 42 5, 931-961.

Guerra-Merchán, A., & Serrano, F., 1993. Tectosedimentary setting and chronostratigraphy of the Neogene reefs in the Almanzora Corridor Betic Cordillera, Spain. Geobios , 26, 57-67.

Guerrera, F., Martìn-Algarra, A. & Perrone, V., 1993. Late Oligocene-Miocene syn-/-late-orogenic successions in Western and Central Mediterra- nean Chains from the Betic Cordillera to the Southern Apennines. Terra Nova, 5, 525–544.

Guerrera, F., Martìn- Martìn M. & Perrone, V. & Tramontana M., 2005. Tectonic-sedimentary evolution of the southern branch of the Western Tethys (Maghrebian Flysch Basin and Lucanian Ocean): consequences for Western Mediterranean geodynamics. Terra Nova, 17, 358–367.

Gutierrez-Alonso, G., Fernandez-Suarez, J., Jeffries, T., Jenner, G.A., Cox, R. & Jackson, S.E., 2003. Terrane accretion and dispersal in the northern Gondwana margin. An early Paleozoic analogue of a long-lived active margin. Tectonophysics 365, 221–232.

Haccard, D., Lorenz, C., & Grandja, C., 1972. Essai sur l'evolution tectogén~lique de la liaison AJpes·Apennines de lo Ligurie à lo Calabre. Mem. Soc. Geo!. It. , II, 309-341.

Hamoumi, N., Rabano, I., Gutierrez Marco, J.C., El Maazouz, B., Benbouida, M., Chakrone, Ch., Bensaou, M., Laaouar, R., De Sanjose, M.A., Aramburu, C., El Archi, A., Ezzouhairi, H. & Lackloufi, A., 1994. Guide book. Excursion à travers la Mesetacotiere, le Haut-Atlas central et Lánti-Atlas central et oriental. In: IGCP 351, Early Paleozoic Evolution of Gondwana, 2nd International Meeting, Morocco, Rabat, pp. 1–118.

Handy M.R. & Zingg A. 1991. The tectonic and rheological evolution of an attenuated cross section of the continental crust: Ivrea crustal section, southern Alps, northwestern Italy and southern Switzerland. Geol Soc Am Bull 103:236–253.

Hartnady, C., Joubert, P., & C.W., S., 1985. Proterozoic crustal evolution in southwestern Africa. Episodes , 2, 236–244.

Hegner, E. & Kröner, A., 2000. Review of Nd isotopic data and xenocrystic and detrital zircon ages from the pre-Variscan basement in the eastern Bohemian Massif: speculations on palinspastic reconstructions. In: Franke W., Haak V., Oncken O., Tanner D. (eds) Orogenic processes: quantification and modelling in the Variscan Belt, vol 179. Geol Soc Lond Spec Publ, pp 113– 129.

Helbing, H., & Tiepolo, M., 2005. Age determination of Ordovician magmatism in NE Sardinia and its bearing on Variscan basement evolution. Journal of the Geological Society , 162, 689-700.

Heymes, T., Bouillin, J.P., Pêcher A., Monié, P. & Compagnoni, R., 2008. Middle Oligocene extension in the Mediterranean Calabro-Peloritan belt (southern Italy): Insights from the Aspromonte nappes pile. Tectonics, 27, TC2006, doi: 10.1029/2007TC002157

Hirdes, W. & Davis, D.W., 2002. U–Pb geochronology of Paleoproterozoic rocks in the southern part of the Kedougou-Kenieba inlier, Senegal, West Africa: evidence for diachronous accretionary development of the Eburnean Province. Precambrian Research 118, 83–99.

Hoffman, P., 1991. Did the Breakout of Laurentia Turn Gondwanaland Inside-Out? Science , 252, 1409-1412.

Irvine, T.N., & Baragar, W.R.A., 1971. A guide to the chemical classification of the common volcanic rocks. Canadian Journal Earth Sciences 8, 523-548.

Jacobs, J., & Thomas, R., 2004. Himalayan-type indenter-escape tectonics model for the southern part of the late Neoproterozoic-early Paleozoic East African-Antarctic orogen. Geology , 32, 721-724.

Jolivet, L., Dubois, R., Fournier, M., Goffe, B., Michard, A. & Jourdan, C., 1990. Ductile extension in Alpine Corsica.Geology (Boulder) 18(10), 1007-1010.

Junker, B., & Schneider, H., 1983. The Infracambrian Bithia Formation - Its facies development in Southwest Sardinia. Neues Jahrbuch für Geologie und Paläontologie, Monatshefte , 24 Junker, B. and Schneider, H.H., 369-384.

Kalvoda, J., & Bábek, O., 2010. The Margins of Laurussia in Central and Southeast Europe and Southwest Asia. Gondwana Research , 17, 526–545.

Kober, B., Kalt, A., Hanel M. & Pidgeon R.T., 2004. SHRIMP dating of zircons from high-grade metasediments of the Schwarzwald/SW-Germany and implications for the evolution of the Moldanubian basement. Contributions to Mineralogy and Petrology V.147, N.3, 330-345, DOI: 10.1007/s00410-004-0560-8

Kroner, A. & Stern, R.J., 2004. Africa: Pan-African orogeny. In: Shelley, R., Cocks, L.R.M., Pilmer, I.R. (Eds.), Encyclopedia of Geology. Elsevier, pp. 1–12.

Langone A., Godard G., Prosser G., Caggianelli A., Rottura A. & Tiepolo M., 2010 P–T–t path of the Hercynian low-pressure rocks from the Mandatoriccio complex (Sila Massif, Calabria, Italy): new insights for crustal evolution. J. metamorphic Geol., 2010, 28, 137–162.

Lardeaux, J. M., Ledru, P., Daniel, I. & Duchêne, S., 2001. The Variscan French Massif Central—a new addition to the ultra-high pressure metamorphic 'club': exhumation processes and geodynamic consequences. Tectonophysics 332, 143–167.

Le Bas, M. J., Le Maitre, R. W., Streckeisen, A. & Zanettin, B., 1986. A chemical classification of volcanic rocks based on the total alkali-silica diagram. Journal of Petrology 27, 745-750.

Lecca, L., Lonis, R., Luxoro, S., Melis, E., Secchi, F., & Brotzu, P., 1997. Oligo-Miocene volcanic sequences and rifting stages in Sardinia. Periodico di Mineralogia , 66, 7-61.

Ledru, P., Courrioux, G., Dallain, C., Lardeaux, J.M., Montel, J.M., Vanderhaeghe, O. & Vitel, G., 2001. The Velay dome (French Massif Central): melt generation and granite emplacement during orogenic evolution. Tectonophysics, 342, 207–237.1

Ledru, P., Lardeaux, J.M., Santallier, D., Autran, A., Quenardel, J.M., Floc'h, J.P., Lerouge, G., Maillet, N., Marchand, J. & Ploquin, A., 1989. Où sont les nappes dans le Massif Central française. Bull. Soc. Géol. France, 5, 605–618.

Lefort, J., 1990. Cinématique de la collision Gondwana-Laurentia entre la Bretagne et la Floride d'après les données du socle submergé. Schweiz. Mineral. Petrogr. Mitt., 70, 3-16.

Lehman, J.T., 1975. Reconstructing the rate of accumulation of lake sediment: the effect of sediment focusing. Quat. Res. 5: 541-550.

Lentini F., Carbone S., Catalano, S., Stefano, A. D., Gargano, C., Romeo, M., Strazzulla, S. & Vinci G., 1995. Sedimentary evolution of basins in mobile belts: examples from the Tertiary terrigenous sequences of the Peloritani Mountains NE Sicily. Terra Nova , 7, 2, 161-170.

Leone, F., Hammann, W., Laske, R., Serpagli, E., & Villas, E. 1991. Lithostratigraphic units and biostratigraphy of the post-Sardic Ordovician sequence in southwest Sardinia. Bolletino della Società Paleontologica Italiana , 30, 201–235.

Lewandowski, M., 2003. Assembly of Pangea: Combned Paleomagnetic and Paleoclimatic Approach. Advances in Geophysics , 46, 199-236.

Liegeois, J.P., Claessens, W., Camara, D. & Klerkx, J., 1991. Short-lived Eburnian orogeny in southern Mali. Geology, Tectonics, U–Pb and Rb–Sr geochronology. Precam- brian Research 50 (1-2), 111–136.

Linnemann, U., Gehmlich, M., Tichomirowa, M., Buschmann, B., Nasdala, L., Jonas, P., Lützner, H. & Bombach, K., 2000. From Cadomian subduction to Early Palaeozoic rifting: the evolution of Saxo-Thuringia at the margin of Gondwana in the light of single zircon geochronology and basin development Central European Variscides, Germany. In W. Frank, V. Haak, O. Oncken, & D. Tanner Eds., Orogenic Processes — Quantification and Modelling in the Variscan Belt of Central Europe pp. 131–153. The Geological Society of London, London, Special Publication.

Linnemann, U., Gerdes, A., Drost, K. & Buschmann, B., 2007. The continuum between Cadomian Orogenesis and opening of the Rheic Ocean: constraints from LA-ICP- MS U–Pb zircon dating and analysis of plate-tectonic setting (Saxo-Thuringian Zone, NE Bohemian Massif, Germany). In: Linnemann, U., Nance, D., Kraft, P., Zulauf, G. (Eds.), The Evolution of the Rheic Ocean: From Avalonian–Cadomian Active Margin to Alleghenian–Variscan Collision, vol. 423. Geological Society of America, Special Paper, pp. 61–96.

Linnemann, U., McNaughton, N.J., Romer, R.L., Gehmlich, M., Drost, K. & Tonk, C., 2004. West African provenance for Saxo-Thuringia (Bohemian Massif): Did Armorica ever leave pre-Pangean Gondwana? — U/Pb-SHRIMP zircon evidence and the Nd- isotopic record. International Journal of Earth Sciences 93, 683–705.

Linnemann, U., McNaughton, N.J., Romer, R.L., Gehmlich, M., Drost, K. & Tonk, C., 2004. West African provenance for Saxo-Thuringia (Bohemian Massif): Did Armorica ever leave pre-Pangean Gondwana?—U/Pb-SHRIMP zircon evidence and the Nd- isotopic record. International Journal of Earth Sciences 93 (5), 683–705.

Linnemann, U., Ouzegane, K., Drareni, A., Hofmann, M., Becker, S., Gärtner, A. & Sagawe, A., 2011. Sands of West Gondwana: An archive of secular magmatism and plate interactions - A case study from the Cambro-Ordovician section of the Tassili Ouan Ahaggar (Algerian Sahara) using U-Pb-LA-ICP-MS detrital zircon ages. Lithos 123, 188–203.

Loi, A. & Dabard, M.P., 1997. Zircon typology and geochemistry in the palaeogeographic reconstruction of the Late Ordovician of Sardinia (Italy), Sedimentary Geology 112 263–279.

Loi, A., 1993. Sedimentological-petrographical study and paleogeographical approach of the Upper Ordovician of the central southern Sardinia. Eur. J. Mineral. 9, 81–86 ‘‘Plinius’’.

Loi, A., Barca, S., Chauvel, J.J., Dabard, M.P. & Leone, F., 1992. Storm deposits (placers and rhytmites) in the Caradocian transgressive sediments of the Sarrabus area (SE Sardinia–Italy). In: Carmignani, Sassi (Eds.), Contributions to the geology of Italy with special regards to the Paleozoic basement. A volume dedicated to Tommaso Cocozza. Siena, IGCP n. 276: Newletter, vol. 5, pp. 159–161.

Lorenz, V. & Nicholls, I.A., 1984. Plate and intraplate processes of Hercynian Europe during the Late Palaeozoic. Tectonophysics 107, 25-56.

Lorenzoni, S. & Zanettin-Lorenzoni, E., 1983. Note illustrative alla carta geologica della Sila alla scala 1:200000. Memorie della Società Geologica Italiana, 36, 317–342.

Maccarrone, E., Paglionico, A., Piccarreta, G. & Rottura, A., 1983. Granulite–amphibolites facies metasediments from the Serre (Calabria, Southern Italy): their protoliths and the processes controlling their chemistry. Lithos 16, 95–111.

Martini, I., Oggiano, G. & Mazzei, R., 1992. Siliciclastic–carbonate sequences of Miocenegrabens of northern Sardinia, western Mediterranean Sea. Sed. Geol. 76, 63–78

Matte, P., 1986. Tectonics and plate tectonics model for the Variscan belt of Europe. Tectonophysics , 126, 329–374.

Matte, P., 1991. Accretionary history and crustal evolution of the Variscan Belt in western Europe. Tectonophysics , 196, 309–339.

Matte, P., 2001. The Variscan collage and orogeny 480-290 Ma and the tectonic definition of the Armorica microplate: A review. Terra Nova , 13, 122-128.

Mazzoli, C. & Visonà, D., 1992. The gneisses of Monte Filau (Capo Spartivento, SW Sardinia): petrographic and chemical features. In: Carmignani, L. & Sassi, F.P. (eds) Contributions to the Geology of Italy with Special Regard to the Paleozoic Basements. IGCP 276, Newsletter, 5, 175–182.

McKerrow, W. S., & M., L. R., 1995. The use of biogeography in the terrane assembly of the Variscan Belt of Europe. Studia Geophysica et Geodetica , 39, 269-275.

McKerrow, W., Scortese, C., & M.D., B., 1992. Early Cambrian continental recostructions. Journ. Geol. Soc. London , 149, 599-606.

McMenamin, M., & McMenamin, S., 1990. The emergence of animals: the Cambrian breakthrough. The emergence of animals: the Cambrian breakthrough , 217.

Meinhold, G., Kostopoulos, D., Frei, D., Himmerkus, F. & Reischmann, T., 2010. U–Pb LA- SF-ICP-MS zircon geochronology of the Serbo-Macedonian Massif, Greece: palaeotectonic constraints for Gondwana-derived terranes in the Eastern Medi- terranean. International Journal of Earth Sciences 99, 813–832.

Melleton, J., Cocherie, A., Faure, M., & Rossi, P., 2010. Precambrian protoliths and Early Paleozoic magmatism in the French Massif Central: U-Pb data and the North Gondwana connection in the west European Variscan belt. Gondwana Research , 17, 13-25.

Memmi, I., Barca S., Carmignani, L., Cocozza, T., Franceschelli, M., Gattiglio, M., Grezzo, C., Minzolin, N., Naud, G., Pertusati, P.C. & Ricci, C.A., 1982. Il magmatismo pre- ercinico della Sardegna. In: Carmignani L., Cocozza T., Ghezzo C., Pertusati P.C. & Ricci C.A. (Eds.), Guida alla Geologia del Paleozoico Sardo. Guide Geologiche Regionali. Società Geologica Italiana: 157-164, Cagliari.

Memmi, I., Barca, S., Carmignani, L., Franceschelli, M., Gattiglio, M., Ghezzo, C., Minzoni, N., Naud, G., Pertusati, P.C. & Ricci, C.A., 1983. Further geochemical data on the Pre-Hercynian igneous activity of Sardinia and considerations on their geodynamic significance. IGCP Project no. 5 Newsletter, Padova, pp. 87–91

Messina, P., 1996. Tettonica meso-pleistocenica dei terrazzi nord-orientali del Fucino (Italia centrale), Il Quaternario, 9, 293–298

Meulenkamp, J.E. & Hilgen, F.J., 1986. Event stratigraphy, basin evolution and tectonics of the Hellenic and Calabro-Sicilian arcs. In:The Origin of Arcs (Ed. by F.C.Wezel), pp. 327–350. Elsevier Science Publishers B.V., Amsterdam.

Micheletti, F., Fornelli, A., Piccarreta, G., Barbey, P. & Tiepolo, M., 2008. The basement of Calabria (southern Italy) within the context of the Southern European Variscides: LA-ICPMS and SIMS U–Pb zircon study Lithos 104, 1–11

Micheletti, F., Barbey, P., Fornelli, A., Piccarreta, G. & Deloule, E., 2007. Latest Precambrian to Early Cambrian U–Pb zircon ages of augen gneisses from Calabria (Italy), with inference to the Alboran microplate in the evolution of the peri-Gondwana terranes. International Journal of Earth Sciences 96, 843–860.

Mingram, B., Kröner, A., Hegner, E. & Krentz, O., 2004. Zircon ages, geochemistry, and Nd isotopic systematics of pre-Variscan orthogneisses from the Erzgebirge, Saxony (Germany), and geodynamic interpretation. Int J Earth Sci 93:706–727. doi: 10.1007/s00531-004-0414-7

Minzoni, N., 1981. Il Precambriano del Sulcis meridionale Sardegna. Mineralogica et Petrographica Acta, 24, 51-56.

Moro, A. D., Fornelli, A., & Piccareta, G., 2000. Tectonothermal history of the Hercynian continental crust of the Serre southern Calabria, Italy monitored by Rb/Sr biotite resetting. Terra Nova , 12, 239-244.

Mosher, S., Levine, J., & Carlson, W., 2008. Mesoproterozoic plate tectonics: A collisional model for the Grenville-aged orogenic belt in the Llano uplift, central Texas. Geology , 36, 55-58.

Murphy, J., Strachan, R., Nance, R., Parker, K., & Fowler, M., 2000. Proto-Avalonia: A 1.2-1.0 Ga tectonothermal event and constraints for the evolution of Rodinia. Geology, 28, 1071-1074.

Nairn, A., & Westphal, M., 1968. Possible implications of the palaeomagnetic study of late palaeozoic igneous rocks of northwestern Corsica. Palaeogeography, Palaeoclimatology, Palaeoecology , 5, 179-204.

Nance, R.D. & Murphy, J.B., 1994. Contrastingbasementisotopicsignaturesandthe palinspatic restoration of peripheral orogens: example from the Neoproterozoic Avalonian–Cadomian belt. Geology 22, 617–620.

Nance, R.D. & Murphy, J.B., 1996. Basement isotopic signatures and Neoproterozoic paleogeography of Avalonian-Cadomian and related terranes in the circum-North Atlantic. In: Nance RD, Thompson MD (eds) Avalonian and related peri-Gondwana terranes of the circum-North Atlantic, vol 304. Geol Soc Am Spec Pap, pp 333–345

Nance, D. R., Gutiérrez-Alonso, G., Keppie, J., Linnemann, U., Murphy, J. B., Quesada, C., Strachan, R., Woodcock, N., 2010. Evolution of the Rheic Ocean. Gondwana Research , 17, 194-222.

Nance, R.D., Murphy, J.B. & Keppie, J.D., 2002. A Cordilleran model for the evolution of Avalonia. Tectonophysics 352, 11–32.

Nance, R.D., Murphy, J.B., Strachan, R.A., Keppie, J.D., Gutierrez-Alonso, G., Fernandez-Suarez, J., Quesada, C., Linnemann, U., D'Lemos, R. & Pisarevsky, S.A., 2008. Neoproterozoic–early Palaeozoic tectonostratigraphy and palaeogeogra- phy of the peri-Gondwanan terranes: Amazonian vs West African connections. Geological Society, London, Special Publications 297 (1), 345–383.

Naud, G., 1979. Le sales de Riu Cannoni, formation repère fossilifère dans l'Ordovicien supérieur de Sardaigne orientale. Conséquences stratigraphiques et structurales, Bull. Soc. Geol. France 21, 155–159.

Naud, G. & Pittau Demelia, P., 1987. Première decouverte d'Acritarches du Cambrien moyen à superieur basal et du Tremadoc – Arenigien dans la basse vallée du Flumendosa: mise en

evidence d'un nouveau témoin de la Phase Sarde en Sardaigne orientale. Padova, IGCP n. 5. New Letters 7, 85–86.

Naud, G., 1979. Tentative de synthèse sur l'évolution géodynamique de la Sardaigne antépermienne. Mem. Soc. Geol. Ital , 20, 85-96.

Naud, G., & Demelia, P. P., 1987. Première decouverte d'Acritarches du Cambrien moyen à superieur basal et du Tremadoc – Arenigien dans la basse vallée du Flumendosa: mise en evidence d'un nouveau témoin de la Phase Sarde en Sardaigne orientale. New Letters , 7, 85-86.

Navidad, M., Castiñeiras, P., Casas, J., Liesa, M., Suárez, J. & Barnolas, A., 2010. Geochemical characterization and isotopic age of Caradocian magmatism in the northeastern Iberian Peninsula: Insights into the Late Ordovician evolution of the northern Gondwana margin. Gondwana Research , 17 Navidad, M. and Castiñeiras, P. and Casas, J.M. and Liesa, M. and Suárez, J.F. and Barnolas, A. and Carreras,J. and Gil-Peña, I., 325-337.

Neugebauer, J., 1989. The Iapetus model: a plate tectonic concept for the Variscan belt of Europe. Tectonophysics , 169, 229–256.

Oggiano, G. & di Pisa A., 1992. Geologia della catena Ercinica in Sardegna-Zona Assiale. In: Carmignani L., Petrusati P.C., Barca S., Carosi R., Di Pisa A., Gattiglio M., Musumeci G., Oggiano G. (Eds), Struttura della catena ercinica in Sardegna. Guida all'escursione. GIGS, 147-177, Siena.

Oggiano, G., Funedda, A., Carmignani, L. & Pasci, S., 2009. The Sardinia-Corsica microplate and its role in the Northern Apennine Geodynamics: new insights from the Tertiary intraplate strike-slip tectonics of Sardinia. Italian Journal of Geosciences vol. 128, 2, pp. 527-539.

Oggiano G., Gaggero L., Funedda A., Buzzi L. & Tiepolo M. 2010. Multiple early Paleozoic volcanic events at the northern Gondwana margin: U–Pb age evidence from the Southern Variscan branch (Sardinia, Italy). Gondwana Research 17, 44–58.

Oggiano, G., Gaggero, L., Funedda, A., Buzzi, L., & Tiepolo, M., 2010. Multiple early Paleozoic volcanic events at the northern Gondwana margin: U–Pb age evidence from the Southern Variscan branch Sardinia, Italy. Gondwana Research , 17, 44–58.

Oggiano, G., Pasci, S. & Funedda, A., 1995. Il bacino di Chilivani-Berchidda: un esempio di struttura transtensiva. Possibili relazioni con la geodinamica cenozoica del mediterraneo occidentale. Boll. Soc. Geol. It. 114, 465–475.

Ogniben, L., 1960. Nota illustrativa dello schema geologico della Sicilia nord-orientale. Rivista Mineralogica Siciliana 11, 183–212.

Ogniben, L., 1969. Schema introduttivo alla geologia del confine calabro-lucano. Memorie della Societ`a Geologica Italiana 8, 453–763.

Ogniben, L., 1973. Schema geologico della Calabria in base ai dati odierni. Geologia Romana 12, 243–585.

Orszag-Sperber, F. & Pilot, M.D., 1976. Grands traits du Néogène de Corse. Bull. Soc. Géol. Fr. 7, 1183–1187.

Palagi, P., Laporte, D., Lardeaux, J., Ménot, R. R., & Orsini, J., 1985. Identification d'un complexe leptyno-amphibolique au sein des «gneiss de belgodère» Corse Occidentale. C. R. Acad. Sci. Paris , 301, 1047–1052.

Paris, F., & Robardet, M., 1990. Early Palaeozoic palaeobiogeography of the Variscan regions. Tectonophysics , 177, 193–213.

Pasci S., 1997. Tertiary transcurrent tectonics of North-Central Sardinia. Bulletin de la Société Géologique de France 168 (3):301-312.

Pasci, S., Oggiano, G. & Funedda, A., 1998. Rapporti tra tettonica e sedimentazione lungo le fasce trascorrenti oligo-aquitaniane della Sardegna NE. Bollettino della Società Geologica Italiana.vol. 117, 2, pp. 443-453.

Patacca, E. & Scandone, P., 2011. Calabria and Peloritani: Where did they stay before the Corsica-Sardinia rotation? Boundary conditions, internal geological constraints and first-order open problem. Rendiconti online Soc. Geol. It., Vol. 15, pp. 93-97.

Patchett, P., 1983. Hafnium isotope results from mid-ocean ridges and Kerguelen. Lithos , 16, 47-51.

Patterson, R.T., Blensikop, J. & Cavazza, W., 1995. Planktic foraminiferal biostratigraphy and 87Sr/86Sr isotopic stratigraphy of the Oligocene-to-Pleistocene sedimentary sequence in the southeastern Calabrian microplate, southern Italy, J. Paleontol. 69, 7–20.

Pavanetto, P., Funedda, A., Northrup, C. J., Schmitz, M., Crowley, J. & Loi, A., 2012. Structure and U–Pb zircon geochronology in the Variscan foreland of SW Sardinia, Italy. Geological Journal. doi: 10.1002/gj.1350

Pavanetto, P., Loi, A., Northrup, C.J. & Funedda, A., 2008. Zircon typology of magmatic rocks in the Southern Sulcis Complex (SW Sardinia). Rendiconti online della Società Geologica Italiana 3(2), 622–623.

Pearce, J.A. & Parkinson, I.J., 1983. Trace element models for mantle melting: application to volcanic arc petrogenesis.Geological Society, London, Special PublicationsJanuary 1, 1993, v. 76, p. 373-403

Pearce, J.A., Harris, N.B.W. & Tindle, A.G., 1984. Trace Element Discrimination Diagrams for the Tectonic Interpretation of Granitic RocksJ. Petrology 25(4): 956-983.

Peccerillo, A. & Taylor, S.R., 1976. Geochemistry of Eocene Calc-Alkaline volcanic rocks from Kastamonu area, Northern Turkey. contrib Mineral Petrol 58:63-81.

Pecorini, G. & Pomesano Cerchi, A., 1969. Ricerche geologiche e biostratigrafiche sul campidano meridionale (Sardegna) Mem. Soc. Geol. It .VIII Pisa

Pereira, M.F., Linnemann, U., Hofmann, M., Chichorro, M., Solá A.R., Medina J. & Silva J.B., 2012. The provenance of Late Ediacaran and Early Ordovician siliciclastic rocks in the Southwest Central Iberian Zone: Constraints from detrital zircon data on northern Gondwana margin evolution during the late Neoproterozoic. Precambrian Research 192–195, 166–189.

Pereira, M., Apraiz, A., Chichorro, M., Silva, J., & Armstrong, R., 2010. Exhumation of high-pressure rocks in northern Gondwana during the Early Carboniferours Coimbra–Cordoba shear zone, SW Iberian Massif: Tectonothermal analysis and U–Th–Pb SHRIMP in-situ zircon geochronology. Gondwana Research , 17, 440-460.

Pereira, M.F., Chichorro, M., Linnemann, U., Eguiluz, L. & Silva, J.B., 2006. Inherited arc signature in Ediacaran and Early Cambrian basins of the Ossa-Morena Zone (Iberian Massif, Portugal): paleogeographic link with European and North African Cadomian correlatives. Precambrian Research 144, 297–315.

Pereira, M.F., Chichorro, M., Solá, A.R., Silva, J.B., Sanchez-Garcia, T. & Bellido, F., 2011. Tracing the Cadomian magmatism with detrital/inherited zircon ages by in-situ U–Pb SHRIMP geochronology (Ossa-Morena Zone, SW Iberian Massif). Lithos 123, 204–217.

Pillola G, P., & Cherchi, A. P. 1969. Ricerche geologiche e biostratigrafiche sul Campidano meridionale Sardegna. Mem. Soc. Geo. It. , 8, 421-451.

Pillola, G.L., Leone, F. & Loi, A., 1995. The Lower Cambrian Nebida Group of Sardinia. Rendiconti del Seminario della Facoltà di Scienze dell'Università di Cagliari 65, 27–60.

Pillola, G., & Gross, U., 1982. Stratigrafia del Membro di Matoppa della Formazione di Nebida Cambrico inferiore nell'area M.te S. Giovanni-M.te Uda. In L. Carmignani, T. Cocozza, C. Ghezzo, P. Pertusati, & C. Ricci Eds., Guida alla Geologia del Paleozoico Sardo pp. 79-82. Società Geologica Italiana. Guide Geologiche Regionali.

Piluso, E., & Morten, L., 2004. Hercynian high temperature granulites and migmatites from the Catena Costiera, northern Calabria, southern Italy. Per. Mineral , 73, 159-172.

Pimentel, M.M., Fuck, R.A. & Botelho, N.F., 1999. Granites and the geodynamic history of the Neoproterozoic Brasilia belt, central Brazil. Lithos 46, 463–483.

Piqué, A., 1991. The ancient massifs of France, parts of the Variscan Belt of western Europe. Les massifs anciens de France, segments de la chaine varisque d'Europe occidentale. Sciences Geologiques - Bulletin, 44, 371-385.

Piqué, A., 1994. Géologie du Maroc. Les domaines régionaux et leur évolution structurale. Editons PUMAG, Marrakech , 284.

Pisarevsky, S., & Natapov, L. 2001. Siberia and Rodinia. Gondwana Research , 4, 734-735.

Pisarevsky, S., Natapov, L., Donskaya, T., Gladkochub, D., & Vernikovsky, V., 2008. Proterozoic Siberia: A promontory of Rodinia. Precambrian Research , 160, 66-76.

Pittau, P., Rio, M. D., & Funedda, A., 2008. Relationships between plant communities characterization and basin formation in the carboniferous-permian of Sardinia. Bollettino della Societa Geologica Italiana , 127, 637-653.

Pupin, J. P., 1980. Zircon and granite petrology. Contributions to Mineralogy and Petrology 73, 207–220.

Rasetti, F., 1972. Cambrian Trilobite faunas of Sardinia. Mem. Acc. Naz. Lincei , 11, 1-100.

Rey, P., Burg, J., & Casey, M., 1997. The Scandinavian Caledonides and their relationship to the Variscan belt. In: Orogeny Through Time. Spec. Publ. Geol. Soc. London , 121, 179–200.

Ricci, C.A. & Sabatini, G., 1978. Petrogenetic affinity and geodynamic significance of metabasic rocks from Sardinia, Corsica and Provence. Neues Jahrbuch fur Geologie und Palaeontologie. Monatschefte 1978, 23–38,

Robardet, M., 2000. An alternative approach to consider the Variscan belt in SW Europe: the pre-orogenic paleogeographical constraints. Variscan–Appalachian Dynamics: The Building of the Upper Paleozoic Basement, Basement Tectonics , 15, 23–26.

Robardet, M., 2003. The Armorica 'microplate': Fact or fiction? Critical review of the concept and contradictory palaeobiogeographical data. Palaeogeography, Palaeoclimatology, Palaeoecology , 195, 125-148.

Robardet, M., Bonjour, J.L., Paris, F., Morzadec, P. & Racheboeuf, P.R., 1994. Ordovician, Silurian and Devonian of the Medio-North-Armorican Domain. In: Keppie, J.D. (Ed.), Pre-Mesozoic Geology in France and Related Areas. Springer-Verlag, Berlin/Heidelberg, pp. 142–151.

Rosenbaum, G. & Lister, G.S., 2004. Neogene and Quaternary rollback evolution of the Tyrrhenian Sea, the Apennines and the Sicilian Maghrebides. Tectonics 23 (1), TC1013, doi:10.1029/2003TC001518.

Rossi, P., Oggiano, G. & Cocherie, A., 2009. A restored section of the “southern Variscan realm” across the Corsica – Sardinia microcontinent. Comptes Rendu Gèoscience 341, 2-3.

Rossi, Ph. & Rouire, J., 1980. Carte Géologique de la France a 1/250.000: Corse. BRGM, Orléans/ Maquet, Paris.

Rottura, A., Bargossi, G.M., Caironi, V., Del Moro, A., Maccarrone, E., Macera, P., Paglionico, A., Petrini, R., Piccarreta, G. & Poli, G., 1990. Petrogenesis of contrasting Hercynian granitoids from the Calabrian Arc, southern Italy. Lithos, 24, 97–119.

Rottura, A., Bargossi, G.M., Caironi, V., Del Moro, A., Maccarrone, E., Macera, P., Paglionico, A., Petrini, R., Piccarreta, G. & Poli, G., 1990. Petrogenesis of contrasting Hercynian granitoids from the Calabrian Arc, southern Italy. Lithos, 24, 97–119.

Royden, L., 1993. Evolution of retreating subduction boundaries formed during continental collision. Tectonics, 12, 629-638.

Ruban, D. A., Al-Husseini, M., & Iwasaki, Y., 2007. Review of Middle East Paleozoic plate tectonics. GeoArabia, 12, 35-56.

Saalman, K., Hartmann, L.A. & Remus, M.V.D., 2007. The assembly of West Gondwana—the view from the Rio de la Plata craton. In: Linnemann, U., Nance, R.D., Kraft, P., Zulauf, G. (Eds.), The Evolution of the Rheic Ocean: From Avalonian–Cadomian Active Margin to Alleghenian-Variscan Collision, vol. 423. Geological Society of America Special Paper, pp. 1–26.

Scandone, P., 1982. Structure and Evolution of the Calabrian Arc. In E. I. Mantovani, & R. Sartori Eds., Structure, Evolution and Present dynamics of the Calabrian Arc. Vol. 3, pp. 172-180. Earth Sci. Evol.

Schandelmier, H., Darbyshire, D.P.F., Harms, U. & Richter, A., 1988. The East Sahara Craton: evidence for pre-Pan-African crust in NE Africa west of the Nile. In: El, Gaby S., Greiling, R. (Eds.), The Pan-African belt of northeast Africa and adjacent areas: Wiesbaden. Vieweg, Earth Evolutionary Science, pp. 69–94.

Schätz, M., Bachtadse, V., Tait, J., & Soffel, H., 1997. Paleomagnetic reults from Lower Devonian sediments of the Souther Alps. Terra Nostra , 97, 152-155.

Schenk, V., 1980. U–Pb and Rb–Sr radiometric dates and their correlation with metamorphic events in the granulite-facies basement of the Serre, Southern Calabria Italy. Contrib. Mineral. Petrol., 73, 23–38.

Schenk, V., 1990. The exposed crustal cross section of southern Calabria, Italy: structure and evolution of a segment of Hercynian crust. In: Exposed Cross Sections of the Continental Crust (M.H.Salisbury and D.M.Fountain, eds), pp. 21–42. Kluwer Academic Publishers, The Netherlands.

Schenk, V., 1984. Petrology of felsic granulites, metapelites metabasics, ultramafics, and metacarbonates from southern Calabria (Italy): prograde metamorphism, uplift and cooling of a former lower crust. J. Petrol., 25, 255–298.

Schenk, V., 1989. P–T–t paths of the lower crust in the Hercynian fold belt of southern Calabria. In: Evolution of Metamorphic Belts (J.S. Daly, R.A. Cliff and B.W.D. Yardley, eds). Geol. Soc. London Spec. Publ., 43, 337–342.

Scherer, C., & Goldberg, K., 2007. Palaeowind patterns during the latest Jurassic-earliest Cretaceous in Gondwana: Evidence from aeolian cross-strata of the Botucatu Formation, Brazil. Palaeogeography, Palaeoclimatology, Palaeoecology , 205, 89-100.

Scotese, C., 2004. A continental drift flipbook. Journal of Geology , 112, 729-741.

Servais, T., & Sintubin, M., 2009. Avalonia, Armorica, Perunica: Terranes, microcontinents, microplates or palaeobiogeographical provinces? Geological Society Special Publication , 325, 103-115.

Shackleton, R., 1996. The final collision zone between East and West Gondwana: Where is it? Journal of African Earth Sciences , 23, 271-287.

Shand, S.J., 1929. Eruptive rocks. D. Von Nostrand Company, New York, 360 pp.

Sircombe, K., 1999. Tracing provenance through the isotope ages of littoral and sedimentary detrital zircon, eastern Australia. Sedimentary Geology , 124, 47-67.

Spina, A., & Vecoli, M., 2009. Palynostratigraphy and vegetational changes in the Siluro-Devonian of the Ghadamis Basin, North Africa. Palaeogeography, Palaeoclimatology, Palaeoecology , 282, 1-18.

Stampfli, G.M., von Raumer, J.F. & Borel, G.D., 2002, Paleozoic evolution of pre-Variscan terranes: From Gondwana to the Variscan collision. In: Martínez Catalán, J.R., Hatcher Jr., R.D., Arenas, R., Díaz García, F. (Eds.), Variscan-Appalachian dynamics: The building of the late Paleozoic basement: Boulder, Colorado. Geological Society of America Special Paper 364, pp. 263–280.

Stern, R., 1994. Arc Assembly and Continental Collision in the Neoproterozoic East African Orogen: Implications for the Consolidation of Gondwanaland. Annual Reviews Earth Planetary Sciences , 22, 319–351.

Stern, R.J., 2002. Crustal evolution in the East African Orogen: a Neodymium isotopic perspective. Journal of African Earth Sciences 34, 109–117.

Strachan R.A., Collins A.S., Buchan C., Nance R.D., Murphy J.B. & D'Lemos R.S., 2007. Terrane analysis along a Neoproterozoic active margin of Gondwana: insights from U–Pb zircon geochronology. J Geol Soc London 164:57–60. doi:10.1144/ 0016-76492006-014

Streckeisen, A. & Le Maitre, R.W., 1979. A chemical approximation to the modal QAPF classification of the igneous rocks. Neues Jahrb. Mineral., Abh. 136, 169–206.

Streepey, M., Lithgow-Bertelloni, C., der, B. v., & Magloughlin, J. F., 2004. Exhumation of a collisional orogen: A perspective from North American Grenville Province. Geological Society of America. Memoir , 197, 391-410.

Sun, S.S. & McDonough, W.F., 1989. Chemical and isotopic systematics of oceanic basalts:implications for mantle composition and processes. In: Saunders, A.D., Norry, M.J. (Eds.), Magmatism in ocean basins: Geological Society, London, Special publications, vol. 42, pp. 313–345.

Tait, J., 1999. New Early Devonian paleomagnetic data from NW France: Paleogeography and implications for the Armorican microplate hypothesis. Journal of Geophysical Research B: Solid Earth , 104, 2831-2839.

Tait, J., Bachtadse, V., & Soffel, H., 1994. New palaeomagnetic constraints on the position of central Bohemia during Early Ordovician times. Geophys J. Int. , 116, 131-140.

Tait, J., Bachtadse, V., Franke, W., & Soffel, H., 1997. Geodynamic evolution of the European Variscan fold belt: paleomagnetic and geological constraints. Geol. Rndsch., 86, 585–598.

Tait, J., Schätz, M., & Bachtadse, V., 2000. Palaeomagnetism and palaeozoic palaeogeography of Gondwana and European terranes. Geological Society Special Publication , 179, 21-34.

Taylor, S. R. & McLennan, S. M., 1985. The Continental Crust: Its Composition and Evolution. Oxford University Press, New York, New York, USA. 312 pp.

Thieblemont, D., Goujou, J.C., Egal, E., Cocherie, A., Delor, C., Lafon, J.M. & Fanning, C.M., 2004. Archean evolution of the Leo Rise and its Eburnean reworking. Journal of African Earth Sciences 39 (3–5), 97–104

Thomas, R.J., Chevallier, L.P., Gresse, P.G., Harmer, R.E., Eglington, B.M., Armstrong, R.A., De Beer, C.H., Martini, J.E.J., De Kock, G.S., Macey, P.H. & Ingram, B.A., 2002. Precambrian evolution of the Sirwa Window. Anti-Atlas Orogen, Morocco, Precambrian Research 118, 1–57.

Thomson, S.N., 1994. Fission track analysis of the crystalline basement rocks of the Calabrian Arc, southern Italy: evidence of Oligo-Miocene late-orogenic extension and erosion. Tectonophysics, 238, 331–352.

Torsvik, T., & Rehnström E.F., 2003. The Tornquist Sea and Baltica-Avalonia docking. Tectonophysics , 362, 67-82.

Tortoricci, L., Catalan, S., & Monaco, C., 2009. Ophiolite-bearing mélanges in southern Italy. Geol. J. , 44, 153-166.

Trombetta, A., Cirrincione, R., Corfu, F., Mazzoleni, P., & Pezzino, A., 2004. Mid-Ordovician U–Pb ages of porphyroids in the Peloritan Mountains NE Sicily: palaeogeographical implications for the evolution of the Alboran microplate. Journal of the Geological Society , 161, 265-276.

Trompette, R., 1994. Geology of western Gondwana 2000-500 Ma Pan-African-Brasiliano aggregation of South America and Africa. Geology of Western GondwanaBalkema , 350.

Tucci P. 1983. Le metamorfiti dinamometamorfiche di Capo Malfatano (Sulcis, Sardegna). Period. Min. 52, 149-176, Roma.

Vai, G., 1992. Il segmento calabro-peloritano dell'orogene ercinico. Disaggregazione palinspastica. Boll. Soc. Geol. Ital., 111, 109–129.

Vai, G., & Martini, I., 2001. Anatomy of an Orogen: the Apenninesand Adjacent Mediterranean Basins. Dordrecht, Kluwer Academic Publishers , 632.

van der Voo, R. and French, A.N. and French, R.B der, R. V., French, A., & French, R., 1979. A paleomagnetic pole position from the folded Upper Devonian Catskill red beds, and its tectonic implication. Geology , 7, 345-348.

van der Voo, R. V., 1988. Palaeozoic palaeogeography of North America, Gondwana, and intervening displaced terranes: comparisons of palaeomagnetism with palaeoclimatology and biogeographical patterns. Geol. Soc. Am. Bull. , 100, 311–324.

Veevers, J., & Saeed, A., 2008. Gamburtsev Subglacial Mountains provenance of Permian-Triassic sandstones in the Prince Charles Mountains and offshore Prydz Bay: Integrated U-Pb and TDM ages and host-rock affinity from detrital zircons. Gondwana Research , 14, 316-342.

Villaseca, C., Belousova E., Orejana D., Castiñeiras P. & Pérez-Soba C., 2011 Presence of Palaeoproterozoic and Archean components in the granulite-facies rocks of central Iberia: The Hf isotopic evidence. Precambrian Research 187, 143–154.

von Raumer, J., Stampfli, G., & Bussy, F., 2003. Gondwana-derived microcontinents — the constituents of the Variscan and Alpine collisional orogens. Tectonophysics , 365, 7–22.

von Raumer, J., Stampfli, G., Borel, G., & Bussy, F., 2002. Organizationn of pre-Variscan basement areas at the North-Gondwanan margin. International Journal of Earth Sciences , 91, 35-52.

von Raumer, J., Stampfli, G., Borel, G., & Bussy, F., 2004. Organization of pre-Variscan basement areas at the north-Gondwanan margin. International Journal of Earth Science , 91, 35-52.

von Raumer, J., & Stampfli, G., 2008. The birth of the Rheic Ocean-Early Palaeozoic subsidence patterns and subsequent tectonic plate scenarios. Tectonophysics , 461, 9-20.

Walsh, G.J., Aleinikoff, J.N., Benziane, F., Yazidi, A. & Armstrong, T.R., 2002. U–Pb zircon geochronology of the Paleoproterozoic Tagragra de Tata inlier and its Neoproter- ozoic cover, western Anti-Atlas, Morocco. Precambrian Research 117, 1–20.

Wang, X., Liou, J., & Mao, H., 1989. Coesite-bearing eclogite from the Dabie Mountains in central China. Geology , 17, 1085-1088.

Wedepohl, K.H., 1995. The compositions of the continental crust. Geochimica et Cosmochima. Acta 59, 1217–1232.

Weltje, G., 1992. Oligocene to Early Miocene sedimentation and tectonics in the southern part of the Calabria-Peloritani Arc (Aspromonte, Southern Italy): a record of mixed-mode piggy-back basin evolution. Basin Research , 4, 37-68.

Wetherill, G.W., 1956. Discordant uranium-lead ages: 1. Transactions of the American Geophysical Union, 37, 320-326.

Whalen, J.B., Currie, K.L. & Chappell, B.W., 1987. A-type granites: geochemical characteristics, discrimination and petrogenesis. Contributions to Mineralogy and Petrology 95, 407-418.

Williams, M., Floyd, J., Salas, M., Siveter, D., Stone, P., & Vannier, J., 2003. Patterns of ostracod migration for the 'North Atlantic' region during the Ordovician. Palaeogeography, Palaeoclimatology, Palaeoecology , 195, 193–228.

Willner, A., Gerdes, A., & Massonne, H.J., 2008. History of crustal growth and recycling at the Pacific convergent margin of South America at latitudes 29°-36° S revealed by a U-Pb and Lu-Hf isotope study of detrital zircon from late Paleozoic accretionary systems. Chemical Geology , 253, 114-129.

Winchester, J., Floyd, P., Crowley, Q., Piasecki, M., Lee, M., Pharaoh, T., 2002. Palaeozoic amalgamation of Central Europe: New results from recent geological and geophysical investigations. Tectonophysics , 360, 5-21.

Zeh, A., Bratz, H., Millar, I.L. & Williams, I.S., 2001. A combined zircon SHRIMP and Sm–Nd isotope study of high-grade paragneisses from the mid-German crystalline rise: evidence for northern Gondwanan and Grenvillian provenance. Journal of the Geological Society of London 158, 983–994.

Ziegler, P., 1990. Geological Atlas of Western and Central Europe. Shell International Petroleum Mij., Dist. Geol. Soc , 239.

ANNEXES

Tab. 1. Whole rocks with geohemical data

	Calabria						Sardinia					
Sample	**LON-02**	**LON-03**	**TRI-08**	**COR-13**	**PAL-16**	**VIV-11**	**BS-125**	**SM-200**	**CC-150**	**AF08-20**	**OGN-35**	**28**
Major oxides (wt%)												
SiO_2	74,6	76,5	73,28	71,8	70,18	69,18	64,55	68,51	81,56	66,16	74,51	75,49
Al_2O_3	13,9	13,12	14,09	14,4	14,92	14,4	16,06	16,26	11,18	15,5	13,59	13,16
Fe2O3(T)	1,95	0,94	2,12	2,51	3,69	2,63	7,72	4,19	0,98	6,59	1,42	0,65
MnO	0,019	0,013	0,021	0,054	0,044	0,007	0,029	0,012	0,014	0,072	0,015	0,006
MgO	0,29	0,18	0,41	0,56	1,04	0,57	1,42	0,95	0,21	1,43	0,21	0,11
CaO	0,34	0,12	0,45	1,6	1,62	1,19	1,15	0,19	0,23	0,43	0,48	0,27
Na2O	3,31	3,19	3,53	2,9	3,12	1,21	1,1	0,61	3,83	4,12	3,16	2,77
K2O	4,96	5	3,8	4,01	4,63	6,57	5,68	4,61	1,39	2,8	5,27	5,32
TiO2	0,175	0,065	0,176	0,281	0,455	0,372	0,775	0,8	0,078	0,99	0,257	0,184
P2O5	0,23	0,17	0,22	0,07	0,12	0,89	0,17	0,16	0,03	0,21	0,11	0,05
LOI	1,11	0,76	1,02	1,08	0,81	1,86	1,59	2,65	1,05	2,41	1,2	0,9
Total	100,9	100,1	99,12	99,27	100,6	98,88	100,3	98,93	100,5	100,7	100,2	98,9
Trace elements (ppm)												
Sc	4	3	5	6	8	7	14	13	4	18	7	7
Be	1	1	< 1	1	2	2	5	3	2	3	3	3
V	9	< 5	8	15	49	28	66	65	< 5	98	14	8
Cr	< 20	< 20	< 20	< 20	40	30	60	60	< 20	40	20	< 20
Co	3	2	2	3	8	2	7	9	2	13	3	1
Ni	1	1	2	3	14	9	22	19	3	11	4	2
Cu	1	2	7	5	22	6	10	33	5	19	2	5
Zn	52	37	17	62	42	25	51	101	19	80	48	6
Cd	< 0.5	< 0.5	< 0.5	< 0.5	< 0.5	< 0.5	< 0.5	< 0.5	< 0.5	< 0.5	< 0.5	< 0.5
Ga	20	16	20	20	19	19	23	21	9	21	23	21
Ge	1,6	1,6	2,1	1,6	1,6	1,7	1,8	1,5	1,1	1,6	1,5	1,7
As	< 5	9	< 5	< 5	< 5	7	< 5	10	< 5	20	6	< 5
Rb	234	217	152	113	137	243	196	138	54	103	222	203
Sr	69	27	106	205	159	69	188	53	192	119	39	49
Y	12,7	20,4	13,5	31,7	31	85,9	40,5	36,7	20,5	47,9	53,4	54,5
Zr	93	47	70	156	215	170	283	293	54	263	207	168

Tab. 1. Whole rocks with geohemical data (continuous)

	Calabria							Sardinia					
Sample	**LON-02**	**LON-03**	**TRI-08**	**COR-13**	**PAL-16**	**VIV-11**		**BS-125**	**SM-200**	**CC-150**	**AF08-20**	**OGN-35**	**28**
Trace elements (ppm)													
Nb	13,4	7	16	11,9	12	10,6		17,1	16,3	9	14,9	19,1	19,7
Mo	< 2	< 2	< 2	< 2	< 2	< 2		< 2	< 2	< 2	< 2	< 2	< 2
Ag	0,3	< 0.3	< 0.3	< 0.3	< 0.3	< 0.3		< 0.3	< 0.3	< 0.3	< 0.3	< 0.3	< 0.3
In	< 0.1	< 0.1	< 0.1	< 0.1	< 0.1	< 0.1		< 0.1	< 0.1	< 0.1	< 0.1	< 0.1	< 0.1
Sn	10	3	5	2	3	4		4	4	5	5	14	9
Sb	0,6	0,6	0,6	0,6	0,6	0,7		1,3	1,5	1	15,2	0,6	0,8
Cs	4,4	1,9	2,1	1,7	4,6	6,1		17,2	12,2	4,4	8,7	2,3	2
Ba	352	214	258	1041	1120	1293		1782	890	245	710	262	243
Hf	2,6	1,9	2,1	4,2	5,6	4,6		7,2	7,1	2	6,7	6	5,1
Ta	1,65	1,12	1,98	0,93	0,87	0,86		1,19	1,18	1,15	1,12	1,85	1,78
W	1,1	0,8	1,2	0,6	1,3	4,4		2,4	2,3	1,4	3,7	3,1	3,7
Tl	1,12	1,07	0,63	0,5	0,54	1,06		0,99	0,67	0,28	0,57	1,08	0,97
Pb	18	16	9	31	27	30		16	14	13	10	14	17
Bi	1,1	0,2	< 0.1	< 0.1	< 0.1	1,8		< 0.1	< 0.1	0,5	0,2	0,5	0,1
Th	9,1	5,68	6,01	14,1	18,2	13,8		16,5	18,2	5,55	14	23,9	20,5
U	4,01	2,06	1,78	2,24	3,39	18,9		3,01	3,65	3,99	3,27	6,04	4,17
Rare earth elements (ppm)													
La	16,2	10,1	16	41,2	33,2	19,9		47,6	44,9	11,8	39,5	46	41,5
Ce	34,6	21,7	32,6	82,5	68,1	50,1		88,3	93,5	24,4	76,8	95	88,7
Pr	4,52	2,81	3,94	10,3	8,4	6,21		11,8	11,8	3,1	10,3	11,8	11,2
Nd	16,3	10,3	13,9	38,1	30,6	23,1		44	44,5	11,4	39,4	41,6	40,7
Sm	3,99	2,65	2,84	7,51	6,33	5,82		8,98	9,08	2,9	8,76	9,13	9,26
Eu	0,439	0,22	0,454	1,13	1,24	1,22		1,32	1,44	0,406	1,46	0,477	0,493
Gd	3,47	2,51	2,39	5,83	5,54	7,09		7,74	7,7	2,73	8,2	8,26	8,64
Tb	0,59	0,56	0,44	0,97	0,96	1,63		1,27	1,25	0,58	1,45	1,56	1,58
Dy	2,75	3,42	2,45	5,36	5,41	11		7,14	6,9	3,44	8,41	9,17	9,17
Ho	0,44	0,68	0,44	1,04	1,08	2,56		1,4	1,33	0,71	1,71	1,9	1,88
Er	1,02	1,91	1,08	2,88	2,95	7,53		3,72	3,57	1,86	4,64	5,34	5,1
Tm	0,157	0,347	0,184	0,462	0,487	1,29		0,59	0,556	0,331	0,75	0,853	0,865
Yb	0,82	2,12	0,95	2,86	2,86	8,19		3,44	3,37	1,9	4,56	5,41	5,19
Lu	0,105	0,289	0,119	0,401	0,415	1,15		0,498	0,476	0,248	0,621	0,735	0,721

Tab. 2. U-Pb analyses data

Sample °	Ratios						Ages						rho	% Disc
	$^{207}Pb/^{206}Pb$	2σ(%)	$^{207}Pb/^{235}U$	2σ(%)	$^{206}Pb/^{238}U$	2σ(%)	$^{207}Pb/^{206}Pb$	2σ(%)	$^{207}Pb/^{235}U$	2σ(%)	$^{206}Pb/^{238}U$	2σ(%)		
CAV-05														
Z01	0,05418	2,6	0,5239	3,7	0,07013	2,6	378,5	59,3	427,7	13,0	436,9	11,1	0,71	115,43
Z02	0,06121	1,0	0,8952	1,9	0,10608	1,6	646,5	22,3	649,2	9,1	649,9	9,8	0,84	100,54
Z03	0,06584	26,8	0,7060	27,6	0,07776	6,6	801,4	478,6	542,4	109,6	482,8	30,5	0,24	60,24
Z05	0,05653	31,5	0,7032	41,4	0,09023	22,3	473,1	577,4	540,7	160,2	556,9	141,8	0,58	117,72
Z07	0,11342	1,0	4,4465	2,3	0,28432	2,1	1855,0	17,4	1721,1	19,1	1613,1	29,9	0,91	86,96
Z08	0,05449	3,3	0,6107	4,8	0,08128	3,5	391,5	73,2	484,0	18,4	503,8	16,9	0,73	128,68
Z09	0,05089	4,5	0,3506	7,4	0,04996	5,9	235,9	103,4	305,1	19,6	314,3	18,1	0,80	133,25
Z10	0,05566	1,7	0,5576	2,6	0,07266	2,0	438,8	36,9	450,0	9,4	452,2	8,6	0,76	103,05
Z11	0,06630	3,1	1,2599	4,4	0,13782	3,2	815,9	64,8	827,9	25,0	832,3	24,7	0,71	102,02
Z12	0,07268	1,3	1,6370	2,2	0,16336	1,7	1005,1	26,8	984,6	13,7	975,4	15,8	0,79	97,05
Z13	0,05391	2,5	0,5723	3,9	0,07699	3,0	367,3	57,1	459,5	14,6	478,2	13,9	0,77	130,19
Z14	0,05170	2,7	0,3397	4,5	0,04766	3,6	272,0	61,9	297,0	11,6	300,2	10,6	0,80	110,34
Z15	0,05174	1,9	0,3128	5,7	0,04385	5,3	273,9	44,1	276,3	13,7	276,6	14,5	0,94	101,00
Z16	0,05574	1,8	0,4474	2,4	0,05821	1,6	442,2	40,4	375,5	7,6	364,7	5,7	0,67	82,48
Z17	0,07303	1,1	1,7842	2,3	0,17718	2,0	1014,9	22,9	1039,7	14,8	1051,6	19,2	0,87	103,62
Z18	0,06166	1,3	0,6005	2,5	0,07063	2,1	662,3	27,2	477,5	9,4	440,0	9,0	0,86	66,43
Z19	0,07359	2,6	1,4725	3,7	0,14513	2,6	1030,2	52,1	919,2	22,1	873,6	21,3	0,71	84,80
Z20	0,05043	3,5	0,3445	4,8	0,04955	3,4	214,7	80,4	300,6	12,6	311,8	10,2	0,70	145,19
Z21	0,06109	2,6	0,6607	3,0	0,07844	1,6	642,4	54,2	515,1	12,1	486,8	7,4	0,52	75,78
Z25	0,07499	1,0	1,7875	2,6	0,17287	2,4	1068,3	20,7	1040,9	16,8	1027,9	22,5	0,92	96,22
Z26	0,11560	0,6	5,2595	1,8	0,32997	1,7	1889,3	10,4	1862,3	14,9	1838,2	26,6	0,94	97,30
Z28	0,17974	0,7	10,7784	1,7	0,43491	1,6	2650,5	11,7	2504,2	16,1	2327,8	30,8	0,91	87,83
Z31	0,21289	1,8	15,3611	2,6	0,52332	1,9	2927,7	28,5	2837,9	25,1	2713,2	43,2	0,74	92,68
Z38	0,05313	1,0	0,3963	4,5	0,05410	4,4	334,4	22,7	339,0	13,0	339,6	14,5	0,97	101,56
Z39	0,05469	2,3	0,5915	3,5	0,07845	2,6	399,5	50,6	471,8	13,1	486,8	12,3	0,76	121,87
Z42	0,05176	1,7	0,3370	3,2	0,04723	2,8	274,7	38,8	294,9	8,3	297,5	8,1	0,85	108,29
Z45	0,06051	1,3	0,9265	3,5	0,11106	3,2	621,7	28,9	665,8	16,9	678,9	20,6	0,92	109,20
Z46	0,04830	3,4	0,3698	6,9	0,05553	6,1	114,1	79,5	319,5	19,0	348,4	20,6	0,87	305,37
Z47	0,06414	1,5	1,1377	4,4	0,12864	4,1	746,3	32,3	771,4	23,6	780,1	30,0	0,94	104,53

Tab. 2. U-Pb analyses data (continuous)

Sample °	Ratios						Ages						rho	% Disc
	$^{207}Pb/^{206}Pb$	2σ(%)	$^{207}Pb/^{235}U$	2σ(%)	$^{206}Pb/^{238}U$	2σ(%)	$^{207}Pb/^{206}Pb$	2σ(%)	$^{207}Pb/^{235}U$	2σ(%)	$^{206}Pb/^{238}U$	2σ(%)		
CAV-05														
Z50	0,06336	1,1	1,1225	3,8	0,12849	3,6	720,5	23,6	764,2	20,2	779,2	26,4	0,96	108,16
Z51	0,05691	3,2	0,5812	6,0	0,07407	5,0	488,1	69,2	465,3	22,1	460,6	22,4	0,84	94,37
Z55	0,06001	1,9	0,8506	4,5	0,10280	4,1	603,9	41,2	625,0	21,1	630,8	24,6	0,91	104,45
Z56	0,05724	2,0	0,6722	4,0	0,08518	3,5	500,7	43,1	522,1	16,2	526,9	17,5	0,87	105,24
Z57	0,05309	3,0	0,4269	5,2	0,05832	4,2	332,7	68,6	361,0	15,7	365,4	14,9	0,81	109,85
Z61	0,10746	1,0	4,9104	2,1	0,33142	1,9	1756,8	18,2	1804,0	17,8	1845,2	29,9	0,88	105,04
Z63	0,07100	3,6	0,7515	5,2	0,07676	3,7	957,5	72,0	569,1	22,3	476,8	17,0	0,72	49,80
Z64	0,07458	2,5	1,7283	4,1	0,16808	3,2	1057,1	49,8	1019,1	25,8	1001,5	29,5	0,79	94,74
Z66	0,17740	1,0	11,5992	4,3	0,47422	4,2	2628,7	16,3	2572,6	40,1	2502,0	86,6	0,97	95,18
Z69	0,05794	1,3	0,7004	3,2	0,08767	3,0	527,5	28,7	539,0	13,5	541,7	15,4	0,91	102,70
Z70	0,07249	0,9	1,7227	1,8	0,17236	1,6	999,7	17,7	1017,0	11,8	1025,1	15,4	0,88	102,54
Z72	0,05258	1,7	0,3914	4,8	0,05399	4,5	310,7	38,3	335,4	13,7	339,0	14,8	0,94	109,11
Z73	0,06124	1,8	0,9793	2,4	0,11598	1,6	647,7	39,0	693,3	12,3	707,4	11,0	0,67	109,23
Z74	0,05817	3,6	0,7653	4,6	0,09541	2,9	536,2	79,4	577,0	20,4	587,5	16,2	0,62	109,57
Z75	0,06351	1,3	0,9700	2,6	0,11077	2,2	725,2	27,9	688,4	12,7	677,2	14,1	0,85	93,38
Z76	0,09023	1,7	2,4213	4,2	0,19462	3,8	1430,4	32,3	1248,9	29,7	1146,4	40,1	0,91	80,14
Z77	0,05271	1,1	0,3787	2,5	0,05211	2,2	316,5	25,3	326,1	6,9	327,4	7,0	0,89	103,45
Z79	0,05645	2,6	0,6133	4,1	0,07880	3,1	470,1	56,9	485,6	15,7	489,0	14,8	0,77	104,02
Z81	0,05782	1,4	0,6546	5,2	0,08211	5,0	522,9	30,9	511,3	20,8	508,7	24,6	0,96	97,28
Z82	0,05310	5,8	0,3625	6,0	0,04950	1,4	333,3	132,1	314,1	16,2	311,5	4,3	0,24	93,46
Z83	0,05594	1,3	0,6075	2,4	0,07875	2,1	450,1	29,6	482,0	9,4	488,7	9,7	0,84	108,57
Z85	0,11622	0,8	5,4202	1,6	0,33825	1,3	1898,8	14,9	1888,0	13,4	1878,3	21,7	0,85	98,92
Z86	0,06394	0,9	1,1214	4,6	0,12720	4,5	739,7	19,2	763,6	24,8	771,9	33,0	0,98	104,35
Z87	0,12341	0,7	6,4505	1,8	0,37908	1,7	2006,1	11,8	2039,2	16,1	2072,0	30,3	0,93	103,28
Z88	0,06195	0,8	0,9246	2,5	0,10824	2,4	672,5	17,8	664,8	12,4	662,5	15,1	0,94	98,52
Z89	0,05426	1,0	0,4646	1,8	0,06210	1,5	382,0	23,1	387,5	5,9	388,4	5,6	0,82	101,66
Z91	0,05094	2,1	0,3328	3,1	0,04739	2,2	238,0	49,2	291,7	7,8	298,5	6,4	0,72	125,41
Z93	0,06168	1,2	0,9652	2,7	0,11349	2,4	663,0	26,1	686,0	13,4	693,0	15,8	0,89	104,53
Z94	0,05893	4,1	0,7270	4,5	0,08947	1,9	564,6	87,7	554,8	19,3	552,4	10,0	0,42	97,83
Z95	0,06116	1,1	0,8691	2,4	0,10306	2,1	645,0	24,6	635,1	11,4	632,3	12,8	0,88	98,04

Tab. 2. U-Pb analyses data (continuous)

	Ratios						Ages						rho	% Disc
Sample °	$^{207}Pb/^{206}Pb$	2σ(%)	$^{207}Pb/^{235}U$	2σ(%)	$^{206}Pb/^{238}U$	2σ(%)	$^{207}Pb/^{206}Pb$	2σ(%)	$^{207}Pb/^{235}U$	2σ(%)	$^{206}Pb/^{238}U$	2σ(%)		
CAV-05														
Z97	0,05240	0,6	0,3334	1,6	0,04614	1,5	303,1	14,4	292,1	4,2	290,8	4,3	0,92	95,93
Z98	0,05342	1,5	0,3412	2,3	0,04633	1,8	346,5	33,2	298,1	6,0	291,9	5,1	0,77	84,25
Z99	0,06321	0,9	1,1139	4,1	0,12782	4,0	715,2	18,5	760,1	22,0	775,4	29,4	0,98	108,41
Z100	0,07352	0,9	2,0225	3,6	0,19952	3,5	1028,3	17,4	1123,1	24,2	1172,7	37,1	0,97	114,04
Z101	0,05843	3,5	0,6725	3,9	0,08348	1,8	545,8	74,8	522,3	16,0	516,9	8,9	0,45	94,69
Z103	0,19116	2,2	9,3882	4,5	0,35620	4,0	2752,1	35,6	2376,7	41,7	1964,1	67,6	0,88	71,37
Z104	0,06448	2,2	1,2801	3,9	0,14399	3,2	757,4	46,6	836,9	22,2	867,2	26,0	0,82	114,49
Z106	0,12914	0,7	7,1029	4,1	0,39889	4,0	2086,4	12,3	2124,4	36,5	2163,9	74,3	0,99	103,72
Z107	0,05982	2,1	0,8887	3,5	0,10775	2,8	597,0	45,4	645,7	16,8	659,7	17,8	0,80	110,50
Z108	0,06339	0,9	0,9522	4,2	0,10894	4,1	721,4	19,2	679,2	20,4	666,6	25,6	0,98	92,39
Z109	0,05154	4,0	0,3338	4,8	0,04697	2,6	265,1	92,4	292,4	12,2	295,9	7,6	0,55	111,60
Z111	0,12095	1,4	6,4191	4,9	0,38492	4,7	1970,3	25,1	2034,9	43,4	2099,2	84,9	0,96	106,55
Z113	0,05186	1,3	0,3309	2,1	0,04628	1,6	279,4	30,0	290,3	5,2	291,6	4,5	0,77	104,36
CA-PAL														
Z01	0,06064	0,8	0,8560	1,7	0,10237	1,6	626,6	17,4	627,9	8,2	628,3	9,3	0,89	100,27
Z01*	0,05818	1,5	0,7346	2,3	0,09158	1,8	536,4	32,8	559,3	10,0	564,9	9,6	0,76	105,30
Z02	0,05950	1,1	0,7224	5,6	0,08806	5,5	585,4	23,6	552,1	23,9	544,0	28,7	0,98	92,94
Z03	0,12696	8,1	6,2231	14,8	0,35551	12,4	2056,3	143,0	2007,7	129,4	1960,8	209,2	0,84	95,36
Z03*	0,06106	2,2	0,8415	3,5	0,09995	2,7	641,3	47,7	619,9	16,1	614,1	15,7	0,77	95,76
Z04	0,06151	0,8	0,8524	2,5	0,10051	2,4	657,2	16,3	626,0	11,6	617,4	13,9	0,95	93,95
Z04*	0,05989	1,4	0,7987	2,1	0,09672	1,5	599,8	31,3	596,1	9,5	595,2	8,8	0,73	99,23
Z05	0,17553	0,8	12,3997	1,9	0,51235	1,7	2611,1	13,0	2635,2	17,4	2666,6	36,8	0,91	102,13
Z06	0,05476	4,1	0,6019	5,6	0,07971	3,7	402,4	92,6	478,4	21,3	494,4	17,8	0,67	122,86
Z07	0,05849	0,6	0,6992	1,5	0,08669	1,3	548,2	13,2	538,3	6,2	536,0	6,9	0,91	97,77
Z08	0,05859	0,7	0,6806	4,3	0,08426	4,2	551,8	15,9	527,2	17,7	521,5	21,3	0,99	94,51
Z09	0,05346	6,0	0,6180	9,1	0,08384	6,9	348,4	134,9	488,6	35,2	519,0	34,2	0,75	148,99
Z10	0,05881	1,0	0,7119	2,6	0,08779	2,4	560,2	21,6	545,9	11,0	542,4	12,5	0,92	96,83
Z11	0,07130	2,9	0,8293	5,9	0,08436	5,1	965,9	60,2	613,2	27,3	522,1	25,8	0,87	54,05
Z12	0,05876	1,8	0,6607	6,6	0,08155	6,3	558,3	39,5	515,1	26,7	505,3	30,8	0,96	90,51

Tab. 2. U-Pb analyses data (continuous)

Sample °	Ratios						Ages						rho	% Disc
	$^{207}Pb/^{206}Pb$	2σ(%)	$^{207}Pb/^{235}U$	2σ(%)	$^{206}Pb/^{238}U$	2σ(%)	$^{207}Pb/^{206}Pb$	2σ(%)	$^{207}Pb/^{235}U$	2σ(%)	$^{206}Pb/^{238}U$	2σ(%)		
CA-P4L														
Z13	0,05819	1,9	0,6751	4,8	0,08415	4,4	536,7	40,5	523,8	19,5	520,8	21,9	0,92	97,04
Z15	0,05678	1,8	0,5686	4,2	0,07263	3,9	482,9	39,1	457,1	15,6	452,0	16,8	0,91	93,60
Z15*	0,05302	2,5	0,3652	3,7	0,04995	2,7	329,6	57,5	316,1	10,0	314,2	8,2	0,72	95,34
Z16	0,05926	1,0	0,7055	1,4	0,08635	1,0	576,5	21,4	542,1	5,8	533,9	5,0	0,70	92,60
Z17*	0,05793	1,1	0,7503	4,1	0,09393	4,0	527,2	23,3	568,4	17,9	578,8	22,0	0,97	109,78
Z18	0,06080	1,3	0,8435	4,3	0,10061	4,1	632,3	27,2	621,1	19,8	618,0	24,0	0,96	97,73
Z19	0,05874	0,8	0,7449	1,6	0,09197	1,4	557,6	17,6	565,3	6,9	567,2	7,5	0,86	101,71
Z19*	0,05809	1,3	0,7427	2,7	0,09274	2,4	533,1	27,8	564,0	11,7	571,7	13,1	0,88	107,24
Z20	0,06115	1,3	0,9558	4,7	0,11335	4,5	644,7	27,3	681,1	23,4	692,2	29,8	0,96	107,36
Z21	0,06036	1,0	0,8769	2,5	0,10537	2,2	616,5	22,0	639,3	11,7	645,8	13,8	0,91	104,76
Z22	0,05862	1,8	0,6537	4,5	0,08088	4,2	552,9	38,8	510,7	18,2	501,4	20,1	0,92	90,68
Z23	0,05862	1,9	0,6526	3,1	0,08075	2,4	552,8	41,1	510,1	12,3	500,6	11,7	0,79	90,55
Z24	0,05894	0,8	0,6686	1,6	0,08227	1,4	564,8	17,1	519,8	6,6	509,7	6,9	0,87	90,24
Z25	0,05812	1,3	0,6816	2,1	0,08505	1,6	534,3	28,4	527,7	8,5	526,2	8,1	0,78	98,49
Z26	0,05937	1,3	0,6647	2,1	0,08120	1,6	580,7	29,0	517,5	8,4	503,3	7,6	0,76	86,67
Z27	0,05852	0,7	0,6828	1,3	0,08462	1,0	549,3	16,0	528,5	5,2	523,6	5,1	0,81	95,33
Z28	0,05847	0,9	0,6596	2,2	0,08181	2,0	547,6	20,6	514,4	8,8	506,9	9,6	0,90	92,57
Z29	0,15293	0,7	7,8857	1,7	0,37399	1,6	2378,9	12,5	2218,0	15,5	2048,1	27,3	0,90	86,09
Z29*	0,05396	1,9	0,3952	3,0	0,05312	2,4	369,2	43,1	338,2	8,7	333,7	7,7	0,78	90,38
Z30	0,05867	1,0	0,7450	1,5	0,09209	1,1	555,0	22,2	565,3	6,6	567,9	6,2	0,75	102,34
Z30*	0,05909	0,8	0,7836	2,6	0,09619	2,5	570,3	18,3	587,5	11,6	592,0	13,9	0,95	103,80
Z31	0,05865	2,6	0,7039	2,9	0,08705	1,2	554,0	57,4	541,1	12,1	538,1	6,2	0,42	97,12
Z32	0,05854	1,9	0,7599	2,5	0,09413	1,7	550,2	41,0	573,9	11,0	579,9	9,2	0,66	105,41
Z33	0,05287	1,1	0,3762	1,7	0,05160	1,3	323,4	24,3	324,2	4,7	324,3	4,2	0,78	100,29
Z34	0,05906	1,2	0,7071	1,6	0,08683	1,1	569,5	26,3	543,0	6,9	536,8	5,7	0,68	94,26
Z34*	0,05844	1,7	0,7464	4,0	0,09264	3,6	546,2	37,9	566,2	17,3	571,2	19,7	0,90	104,58
Z35	0,05874	0,9	0,6947	1,2	0,08578	0,8	557,4	20,0	535,6	5,2	530,5	4,3	0,68	95,17
Z36	0,05897	1,2	0,7364	2,0	0,09057	1,6	566,0	27,2	560,3	8,8	558,9	8,6	0,79	98,75
Z37*	0,15384	0,7	9,3556	1,8	0,44106	1,6	2389,1	11,4	2373,5	16,3	2355,4	32,5	0,93	98,59
Z39	0,06549	1,3	1,2512	2,5	0,13856	2,1	790,1	27,4	823,9	13,9	836,5	16,5	0,85	105,87

Tab. 2. U-Pb analyses data (continuous)

Sample °	Ratios						Ages						rho	% Disc
	$^{207}Pb/^{206}Pb$	2σ(%)	$^{207}Pb/^{235}U$	2σ(%)	$^{206}Pb/^{238}U$	2σ(%)	$^{207}Pb/^{206}Pb$	2σ(%)	$^{207}Pb/^{235}U$	2σ(%)	$^{206}Pb/^{238}U$	2σ(%)		
CA-PAL														
Z40	0,05841	0,8	0,7218	1,2	0,08962	0,9	545,3	17,0	551,7	5,1	553,3	4,8	0,76	101,46
Z41	0,05856	0,6	0,6889	1,0	0,08532	0,8	550,9	13,3	532,1	4,2	527,8	4,1	0,80	95,81
Z42	0,05857	0,8	0,8340	1,8	0,10328	1,7	551,2	16,6	615,8	8,5	633,6	10,1	0,91	114,94
Z43	0,05839	0,7	0,6900	1,0	0,08571	0,8	544,5	14,2	532,8	4,3	530,1	4,1	0,77	97,36
Z45	0,05808	0,9	0,6534	2,6	0,08159	2,4	532,8	19,6	510,5	10,3	505,6	11,6	0,94	94,89
Z47	0,05821	2,2	0,7150	3,2	0,08909	2,3	537,7	49,2	547,7	13,7	550,2	12,3	0,72	102,33
Z48	0,06237	1,9	0,6658	3,3	0,07742	2,6	687,0	41,5	518,2	13,2	480,7	12,1	0,80	69,97
Z49	0,05920	1,1	0,7069	1,4	0,08661	0,9	574,3	23,0	542,9	5,8	535,4	4,5	0,64	93,23
Z50	0,05900	1,1	0,6809	1,5	0,08370	1,1	567,1	23,2	527,3	6,3	518,1	5,5	0,72	91,37
Z51	0,05892	0,8	0,7069	2,0	0,08702	1,8	564,2	16,8	542,9	8,4	537,9	9,5	0,92	95,34
CORI														
Z02	0,06519	3,0	1,1651	6,0	0,12962	5,2	780,6	63,0	784,4	32,8	785,7	38,5	0,87	100,65
Z03	0,06264	2,9	1,0191	8,6	0,11798	8,0	696,2	62,1	713,5	43,8	718,9	54,7	0,94	103,27
Z05	0,06274	6,4	0,9967	10,5	0,11522	8,3	699,4	136,5	702,1	53,2	703,0	55,4	0,79	100,52
Z06	0,17808	2,4	12,2765	6,9	0,49998	6,4	2635,1	39,4	2625,8	64,3	2613,7	138,1	0,94	99,19
Z08	0,06229	2,8	0,9608	4,9	0,11186	4,0	684,1	59,1	683,7	24,4	683,6	26,2	0,83	99,92
Z09	0,06426	0,8	1,1055	2,5	0,12478	2,4	750,2	17,4	756,0	13,5	758,0	17,1	0,95	101,04
Z11	0,07394	2,4	1,7931	3,3	0,17587	2,3	1039,9	48,1	1042,9	21,4	1044,4	21,7	0,69	100,43
Z13	0,06305	2,5	0,9323	4,4	0,10724	3,7	710,0	52,2	668,9	21,6	656,7	22,9	0,83	92,50
Z15	0,06468	40,2	1,1219	41,1	0,12580	8,4	764,1	847,6	763,9	220,6	763,8	60,6	0,20	99,97
Z15*	0,06190	2,4	0,8634	4,1	0,10116	3,4	670,7	51,8	632,0	19,5	621,2	20,0	0,81	92,62
Z16	0,16192	5,1	9,4065	6,7	0,42134	4,3	2475,8	86,4	2378,5	61,1	2266,6	81,2	0,64	91,55
Z17	0,12781	2,0	6,0211	9,4	0,34167	9,2	2068,1	34,8	1978,9	81,7	1894,7	150,6	0,98	91,62
Z20	0,06529	4,3	1,1773	7,0	0,13078	5,5	783,7	90,9	790,1	38,2	792,3	40,7	0,78	101,10
Z22	0,07167	1,0	1,6504	2,1	0,16701	1,9	976,6	20,0	989,7	13,4	995,6	17,3	0,89	101,95
Z24	0,11678	6,5	5,6991	10,2	0,35394	7,8	1907,5	117,6	1931,2	88,2	1953,4	132,1	0,77	102,41
Z26	0,06768	10,4	1,4590	12,0	0,15635	6,0	858,8	215,9	913,6	72,5	936,5	52,7	0,50	109,04
Z26*	0,06079	1,8	0,9081	4,2	0,10833	3,7	632,0	39,1	656,0	20,1	663,1	23,5	0,90	104,92
Z28	0,06034	1,1	0,8490	3,8	0,10205	3,6	615,8	22,9	624,1	17,3	626,4	21,4	0,96	101,72

Tab. 2. U-Pb analyses data (continuous)

Sample °	Ratios						Ages						rho	% Disc
	$^{207}Pb/^{206}Pb$	2σ(%)	$^{207}Pb/^{235}U$	2σ(%)	$^{206}Pb/^{238}U$	2σ(%)	$^{207}Pb/^{206}Pb$	2σ(%)	$^{207}Pb/^{235}U$	2σ(%)	$^{206}Pb/^{238}U$	2σ(%)		
CORI														
Z29	0,06657	1,5	1,2401	4,2	0,13511	3,9	824,3	30,5	818,9	23,4	817,0	29,9	0,94	99,10
Z31	0,13431	1,1	7,9694	5,2	0,43034	5,0	2155,1	18,7	2227,6	46,5	2307,3	97,9	0,98	107,06
Z31*	0,07316	1,3	1,7045	3,4	0,16897	3,1	1018,5	26,7	1010,2	21,5	1006,4	29,0	0,92	98,82
Z33	0,06128	3,9	0,9603	4,5	0,11365	2,2	649,2	83,4	683,4	22,2	693,9	14,6	0,50	106,89
Z34	0,17643	0,8	12,7722	3,9	0,52504	3,8	2619,6	13,1	2663,0	36,9	2720,5	85,2	0,98	103,85
Z36	0,07669	3,0	1,9921	5,0	0,18841	4,0	1113,0	60,1	1112,8	33,9	1112,7	41,0	0,80	99,97
Z36*	0,13034	0,8	1,9567	10,0	0,10888	9,9	2102,6	14,6	1100,7	65,0	666,2	62,7	1,00	31,69
Z39	0,07165	1,3	1,6010	4,2	0,16206	4,0	976,0	27,4	970,6	26,1	968,2	35,6	0,95	99,20
Z40	0,06284	3,3	0,9919	8,6	0,11447	8,0	702,9	71,2	699,7	43,7	698,7	52,8	0,92	99,39
Z41	0,07316	14,1	1,8269	15,2	0,18111	5,5	1018,4	286,4	1055,2	99,5	1073,0	54,1	0,36	105,37
Z41*	0,13028	2,1	7,1211	4,7	0,39643	4,2	2101,7	36,1	2126,7	41,5	2152,6	76,5	0,90	102,42
Z42	0,06898	8,8	1,3330	9,3	0,14015	2,9	898,2	181,0	860,2	53,7	845,5	23,3	0,32	94,14
Z42*	0,14684	3,6	6,6183	7,0	0,32688	6,0	2309,5	60,0	2061,8	59,9	1823,3	94,9	0,86	78,95
Z43	0,12235	0,9	6,1819	2,2	0,36644	2,0	1990,8	15,2	2001,9	19,0	2012,6	34,5	0,92	101,10
Z46	0,06122	6,0	0,8880	7,9	0,10520	5,1	646,9	128,0	645,3	37,6	644,8	31,5	0,65	99,67
Z46*	0,15170	9,2	10,3929	14,2	0,49689	10,8	2365,1	156,8	2470,4	131,4	2600,4	231,4	0,76	109,95
Z48	0,16960	1,4	10,8693	6,4	0,46480	6,3	2553,7	22,8	2512,0	59,6	2460,7	128,2	0,98	96,36
Z49	0,06330	1,9	0,9857	2,8	0,11293	2,1	718,4	39,6	696,5	14,3	689,7	14,0	0,75	96,01
Z49*	0,07836	7,1	2,2510	9,5	0,20836	6,3	1155,9	134,5	1197,1	65,0	1220,1	70,7	0,67	105,55
Z50	0,07322	1,1	1,8560	2,5	0,18385	2,3	1020,0	21,4	1065,6	16,6	1088,0	22,9	0,91	106,66
Z50*	0,07266	5,3	1,7059	8,9	0,17028	7,2	1004,5	107,7	1010,8	57,0	1013,7	67,1	0,80	100,91
Z53	0,06748	2,2	1,3913	7,1	0,14955	6,7	852,5	45,1	885,3	41,2	898,4	56,5	0,95	105,39
Z53*	0,16254	3,3	11,1417	5,6	0,49715	4,4	2482,3	56,4	2535,1	51,8	2601,5	95,0	0,80	104,80
Z55b	0,07046	3,4	1,6785	8,4	0,17278	7,7	941,7	69,6	1000,4	53,4	1027,4	72,8	0,91	109,10
Z56	0,06870	2,4	1,4890	6,6	0,15720	6,2	889,7	49,5	925,9	40,1	941,2	53,9	0,93	105,80
Z59	0,10953	5,0	5,4131	6,9	0,35843	4,7	1791,6	90,4	1886,9	58,9	1974,7	80,7	0,69	110,22
Z63	0,07745	5,1	2,2497	8,6	0,21067	6,9	1132,8	101,2	1196,7	60,5	1232,4	77,8	0,81	108,79
Z66	0,11127	5,2	4,8004	8,2	0,31288	6,3	1820,3	91,7	1785,0	66,4	1754,9	95,8	0,77	96,40
Z76	0,10870	6,2	4,8882	8,7	0,32616	6,0	1777,7	113,7	1800,2	73,2	1819,7	95,8	0,70	102,37
Z80	0,07605	12,0	2,0687	14,7	0,19728	8,4	1096,4	239,8	1138,5	100,3	1160,7	89,7	0,58	105,86

Tab. 2. U-Pb analyses data (continuous)

	Ratios						Ages						rho	% Disc
Sample °	$^{207}Pb/^{206}Pb$	2σ(%)	$^{207}Pb/^{235}U$	2σ(%)	$^{206}Pb/^{238}U$	2σ(%)	$^{207}Pb/^{206}Pb$	2σ(%)	$^{207}Pb/^{235}U$	2σ(%)	$^{206}Pb/^{238}U$	2σ(%)		
CORI														
Z045	0,06998	0,9	1,3703	4,2	0,14201	4,1	927,9	18,1	876,3	24,4	856,0	32,5	0,98	92,25
Z047	0,06303	0,9	0,9380	1,8	0,10794	1,6	709,3	19,3	671,9	9,0	660,7	10,0	0,87	93,16
Z050	0,06874	1,4	1,3034	3,9	0,13751	3,6	891,1	28,6	847,2	22,3	830,6	28,4	0,93	93,21
Z052	0,06063	0,9	0,8973	1,6	0,10735	1,4	626,0	19,4	650,3	7,9	657,3	8,6	0,84	105,01
Z052	0,07105	0,9	1,5547	2,1	0,15871	1,9	958,8	17,6	952,4	13,1	949,6	17,2	0,91	99,04
Z055	0,06216	1,6	0,9968	2,6	0,11631	2,1	679,6	33,7	702,2	13,3	709,3	14,1	0,80	104,37
Z058	0,05967	3,1	0,8570	3,6	0,10417	1,7	591,5	68,0	628,5	16,7	638,8	10,2	0,47	107,99
Z061	0,05833	3,7	0,7160	4,2	0,08902	1,9	542,3	79,7	548,3	17,6	549,8	9,9	0,45	101,37
Z064	0,05559	1,8	0,5810	7,8	0,07580	7,5	435,9	38,9	465,1	28,7	471,0	34,4	0,97	108,07
Z067	0,07009	1,3	1,3514	2,1	0,13983	1,7	931,0	25,5	868,1	12,1	843,7	13,2	0,80	90,62
Z070	0,06973	1,2	1,4372	1,9	0,14948	1,4	920,5	25,3	904,5	11,2	898,0	11,9	0,75	97,56
Z072	0,12524	1,2	7,0884	5,4	0,41050	5,3	2032,2	21,2	2122,6	48,4	2217,2	99,6	0,98	109,11
Z073	0,06310	3,1	1,1060	3,5	0,12712	1,7	711,6	65,7	756,2	18,9	771,4	12,6	0,49	108,41
Z079	0,14944	2,3	8,5290	3,7	0,41392	2,9	2339,6	38,0	2289,0	33,2	2232,8	55,6	0,79	95,44
Z081	0,05944	1,3	0,7712	2,0	0,09410	1,5	583,3	28,5	580,4	8,8	579,7	8,4	0,75	99,39
Z083	0,07186	1,1	1,5972	3,0	0,16121	2,8	982,0	22,5	969,1	18,7	963,5	24,9	0,93	98,12
Z091	0,07110	1,4	1,4285	2,8	0,14572	2,4	960,2	28,0	900,9	16,5	876,9	19,8	0,87	91,32
Z099	0,11578	0,8	5,7578	5,8	0,36068	5,7	1892,1	13,7	1940,1	50,2	1985,4	98,2	0,99	104,93
Z100	0,18602	0,5	13,2218	1,7	0,51551	1,6	2707,3	8,8	2695,6	16,3	2680,1	35,9	0,95	99,00
Z102	0,07379	2,4	1,8464	3,0	0,18148	1,9	1035,7	47,9	1062,1	20,0	1075,0	18,8	0,62	103,80
Z103	0,06189	1,6	0,9874	2,8	0,11571	2,3	670,4	34,3	697,4	14,2	705,8	15,5	0,82	105,28
Z104	0,05977	0,9	0,7926	2,2	0,09618	2,0	595,2	18,8	592,7	9,7	592,0	11,3	0,92	99,47
Z105	0,05876	1,3	0,7700	1,8	0,09504	1,3	558,2	28,5	579,7	8,1	585,3	7,2	0,70	104,85
Z108	0,07935	1,7	2,0536	2,2	0,18770	1,5	1180,9	32,6	1133,5	15,2	1108,9	15,3	0,67	93,90
Z109	0,05863	2,5	0,7183	8,6	0,08886	8,1	553,3	54,1	549,7	36,0	548,8	43,2	0,96	99,19
Z110	0,12865	1,1	6,8364	2,8	0,38540	2,5	2079,6	19,2	2090,5	24,4	2101,5	45,3	0,92	101,05
Z112	0,11929	1,3	6,1552	2,9	0,37424	2,6	1945,6	23,0	1998,1	25,1	2049,3	45,1	0,89	105,33
Z115	0,16109	0,7	9,2941	6,6	0,41843	6,5	2467,2	11,9	2367,4	58,4	2253,4	122,7	0,99	91,33
Z117	0,06089	2,1	0,8715	3,3	0,10381	2,5	635,2	46,1	636,4	15,6	636,7	15,2	0,76	100,23
ZBB	0,07123	1,0	1,6280	1,9	0,16576	1,7	964,1	20,0	981,1	12,1	988,7	15,2	0,86	102,55

Tab. 2. U-Pb analyses data (continuous)

Sample °	Ratios						Ages						rho	% Disc
	$^{207}Pb/^{206}Pb$	2σ(%)	$^{207}Pb/^{235}U$	2σ(%)	$^{206}Pb/^{238}U$	2σ(%)	$^{207}Pb/^{206}Pb$	2σ(%)	$^{207}Pb/^{235}U$	2σ(%)	$^{206}Pb/^{238}U$	2σ(%)		
CORI														
Z012	0,06071	2,3	0,8827	2,5	0,10546	1,0	628,8	49,0	642,4	11,8	646,3	6,0	0,40	102,78
Z018*	0,06749	1,0	1,2885	4,5	0,13847	4,4	852,9	20,9	840,6	25,9	836,0	34,7	0,98	98,02
Z019	0,06128	1,7	0,8595	2,1	0,10173	1,2	649,2	35,4	629,9	9,6	624,5	7,3	0,60	96,20
CO-SOL														
Z01	0,05219	2,6	0,3644	6,4	0,05064	5,8	293,9	58,7	315,5	17,3	318,5	18,2	0,92	108,37
Z02	0,05755	1,0	0,6816	1,4	0,08590	0,9	512,5	22,4	527,7	5,7	531,2	4,7	0,67	103,65
Z03	0,06219	1,0	0,9835	3,8	0,11469	3,6	680,8	22,0	695,4	19,0	700,0	24,1	0,96	102,82
Z04	0,05672	0,9	0,6188	1,8	0,07912	1,6	480,6	19,4	489,1	7,1	490,9	7,6	0,88	102,13
Z05	0,05643	0,8	0,5694	1,4	0,07318	1,1	469,4	18,5	457,6	5,0	455,3	4,8	0,79	97,00
Z07	0,06037	1,1	0,9085	2,3	0,10914	2,1	616,9	22,9	656,3	11,2	667,8	13,1	0,89	108,25
Z08	0,05877	1,3	0,6120	1,6	0,07553	0,9	558,5	28,8	484,8	6,3	469,4	4,3	0,58	84,04
Z09	0,06221	1,9	1,0526	4,5	0,12271	4,1	681,4	41,0	730,2	23,5	746,2	28,8	0,91	109,50
Z10	0,06063	1,0	0,9447	1,9	0,11300	1,6	626,3	22,1	675,4	9,4	690,2	10,5	0,84	110,20
Z11	0,05615	1,0	0,5485	1,8	0,07085	1,5	458,3	22,2	444,0	6,4	441,3	6,3	0,83	96,29
Z11	0,05845	1,7	0,8451	2,8	0,10486	2,2	546,8	37,6	622,0	13,0	642,8	13,5	0,79	117,55
Z12	0,05412	1,2	0,4017	1,4	0,05383	0,8	376,1	26,9	342,9	4,1	338,0	2,5	0,54	89,88
Z13	0,05597	1,0	0,6380	1,3	0,08268	0,8	451,0	21,5	501,1	5,1	512,1	4,2	0,66	113,55
Z14	0,06224	2,7	0,6805	3,5	0,07930	2,3	682,3	57,0	527,1	14,5	491,9	11,0	0,66	72,10
Z15	0,05607	1,2	0,6123	2,7	0,07920	2,4	455,3	27,2	485,0	10,3	491,3	11,3	0,89	107,91
Z17	0,05475	1,0	0,5238	1,7	0,06939	1,4	402,0	22,2	427,7	6,0	432,5	5,9	0,82	107,58
Z19	0,12176	1,2	5,2589	2,1	0,31325	1,7	1982,1	21,7	1862,2	17,9	1756,7	26,2	0,81	88,63
Z20	0,05308	1,3	0,4799	2,0	0,06558	1,5	332,1	30,2	398,0	6,7	409,4	6,1	0,75	123,27
Z21	0,18126	1,0	16,3977	1,5	0,65612	1,1	2664,4	17,0	2900,3	14,1	3252,1	27,1	0,72	122,06
Z22	0,05196	1,7	0,4182	2,1	0,05838	1,2	283,5	39,7	354,8	6,3	365,8	4,2	0,56	129,02
Z24	0,06398	1,9	1,1365	2,5	0,12884	1,7	740,9	40,2	770,9	13,6	781,2	12,3	0,66	105,44
Z25	0,05700	1,7	0,6496	2,3	0,08265	1,5	491,5	37,8	508,2	9,2	511,9	7,6	0,67	104,14
Z26	0,05243	1,3	0,4113	1,9	0,05689	1,3	304,3	30,3	349,8	5,5	356,7	4,5	0,70	117,21
Z31	0,06243	4,7	0,7763	6,6	0,09019	4,6	688,7	100,7	583,4	29,2	556,7	24,5	0,70	80,83
Z32	0,05802	1,2	0,8959	2,2	0,11199	1,8	530,3	25,5	649,5	10,3	684,3	11,8	0,84	129,04

Tab. 2. U-Pb analyses data (continuous)

	Ratios						Ages						rho	% Disc
Sample °	$^{207}Pb/^{206}Pb$	2σ(%)	$^{207}Pb/^{235}U$	2σ(%)	$^{206}Pb/^{238}U$	2σ(%)	$^{207}Pb/^{206}Pb$	2σ(%)	$^{207}Pb/^{235}U$	2σ(%)	$^{206}Pb/^{238}U$	2σ(%)		
CO-SOL														
Z33	0,08833	1,3	3,3224	1,7	0,27279	1,1	1389,7	24,2	1486,3	13,0	1555,0	15,1	0,65	111,89
Z34	0,05508	1,6	0,6789	2,4	0,08939	1,8	415,6	36,2	526,1	10,0	551,9	9,7	0,75	132,81
Z35	0,05731	0,9	0,6749	1,5	0,08541	1,1	503,3	20,6	523,7	6,0	528,4	5,7	0,77	104,97
Z39	0,06410	1,5	0,7688	2,3	0,08699	1,7	744,9	32,6	579,1	10,1	537,7	8,8	0,74	72,18
Z40	0,05764	1,7	0,6271	2,1	0,07890	1,3	516,1	37,4	494,3	8,3	489,6	5,9	0,60	94,86
Z40	0,06530	1,5	1,3814	3,9	0,15342	3,6	784,1	31,6	881,0	23,0	920,1	31,0	0,92	117,34
Z41	0,05607	0,9	0,6043	5,9	0,07817	5,8	455,2	20,3	480,0	22,4	485,2	27,0	0,99	106,58
Z42	0,05967	1,6	0,7763	3,3	0,09436	2,9	591,6	35,6	583,4	14,8	581,3	16,1	0,87	98,26
Z43	0,05294	1,4	0,3887	1,9	0,05325	1,3	326,1	31,8	333,4	5,4	334,4	4,1	0,67	102,56
Z44	0,06257	2,1	1,0347	2,9	0,11993	2,0	693,8	44,0	721,3	14,7	730,2	13,6	0,69	105,25
Z45	0,05445	1,1	0,6831	1,6	0,09100	1,2	389,5	24,8	528,7	6,8	561,5	6,5	0,74	144,15
Z46	0,05523	1,3	0,6406	1,7	0,08413	1,1	421,5	28,6	502,7	6,6	520,7	5,4	0,64	123,53
Z47	0,05432	1,3	0,4471	2,8	0,05969	2,5	384,4	28,7	375,2	8,7	373,7	9,0	0,89	97,24
Z48	0,05337	1,3	0,4188	1,7	0,05691	1,0	344,7	30,1	355,2	5,0	356,8	3,5	0,61	103,52
Z51	0,05671	1,4	0,4777	2,5	0,06110	2,1	480,2	30,3	396,5	8,3	382,3	7,9	0,84	79,61
Z52	0,06179	1,2	0,7273	1,8	0,08537	1,4	666,9	24,8	555,0	7,6	528,1	6,9	0,76	79,19
Z53	0,07160	1,2	1,6950	1,9	0,17171	1,4	974,5	24,7	1006,7	12,0	1021,5	13,6	0,76	104,83
Z54	0,06339	1,4	1,1143	2,3	0,12750	1,9	721,2	29,0	760,2	12,6	773,6	13,9	0,81	107,27
Z55	0,07167	1,8	1,0486	2,4	0,10612	1,6	976,4	37,4	728,2	12,6	650,2	9,8	0,65	66,59
Z56	0,07659	1,0	2,0093	1,6	0,19026	1,2	1110,6	20,5	1118,6	10,7	1122,8	12,5	0,76	101,10
Z57	0,06193	1,0	1,0651	2,0	0,12474	1,7	671,6	22,2	736,3	10,4	757,8	12,0	0,85	112,83
Z58	0,05273	0,9	0,3991	1,7	0,05489	1,5	317,1	20,8	341,0	5,1	344,5	5,0	0,85	108,62
Z59	0,06243	1,1	1,0400	2,2	0,12082	1,9	688,8	24,2	723,9	11,3	735,3	13,0	0,85	106,76
Z60	0,05703	0,9	0,6514	1,6	0,08285	1,3	492,7	20,0	509,4	6,4	513,1	6,5	0,82	104,14
Z62	0,06088	1,0	0,9221	1,9	0,10985	1,6	634,9	22,2	663,5	9,3	671,9	10,3	0,84	105,83
Z63	0,06411	1,8	1,2723	2,2	0,14394	1,4	745,2	37,2	833,4	12,7	866,9	11,2	0,62	116,33
Z64	0,06338	1,0	0,8020	1,6	0,09177	1,3	721,1	20,2	598,0	7,4	566,0	7,3	0,82	78,49
Z65	0,05886	1,3	0,7495	2,9	0,09235	2,5	562,0	28,2	567,9	12,4	569,4	13,9	0,89	101,33
Z66	0,18090	1,2	14,3064	2,2	0,57358	1,9	2661,1	19,5	2770,2	21,0	2922,5	44,1	0,85	109,82
Z66	0,05643	1,7	0,6858	2,1	0,08814	1,3	469,4	36,6	530,3	8,6	544,5	6,7	0,61	115,99

Tab. 2. U-Pb analyses data (continuous)

	Ratios						Ages						rho	% Disc
Sample °	$^{207}Pb/^{206}Pb$	2σ(%)	$^{207}Pb/^{235}U$	2σ(%)	$^{206}Pb/^{238}U$	2σ(%)	$^{207}Pb/^{206}Pb$	2σ(%)	$^{207}Pb/^{235}U$	2σ(%)	$^{206}Pb/^{238}U$	2σ(%)		
CO-SOL														
Z69	0,05848	1,1	0,6614	1,7	0,08202	1,3	547,9	23,8	515,5	6,9	508,2	6,4	0,77	92,75
Z70	0,05615	1,6	0,4473	2,3	0,05777	1,6	458,3	35,8	375,4	7,2	362,1	5,7	0,71	79,00
Z71	0,05471	2,3	0,4015	2,8	0,05322	1,6	400,3	52,0	342,7	8,3	334,3	5,4	0,58	83,52
Z72	0,05602	1,2	0,6777	2,8	0,08774	2,5	453,2	27,0	525,4	11,4	542,2	13,0	0,90	119,62
Z73	0,06030	1,1	0,6528	1,6	0,07852	1,2	614,5	24,7	510,2	6,5	487,3	5,4	0,71	79,29
Z74	0,07445	1,8	1,6393	2,5	0,15969	1,7	1053,8	36,3	985,5	15,5	955,1	14,7	0,68	90,63
Z75	0,05384	1,6	0,3979	3,0	0,05360	2,6	364,5	36,2	340,1	8,8	336,6	8,5	0,85	92,34
Z76	0,05269	1,0	0,4013	1,8	0,05524	1,5	315,3	23,0	342,6	5,3	346,6	5,1	0,83	109,92
Z77	0,05967	1,5	0,6765	2,7	0,08223	2,2	591,5	31,7	524,6	11,0	509,4	11,0	0,84	86,13
Z78	0,05391	1,1	0,3692	2,3	0,04967	2,1	367,1	24,0	319,1	6,4	312,5	6,3	0,89	85,13
Z80	0,05915	0,8	0,8231	1,4	0,10093	1,2	572,7	17,8	609,8	6,5	619,8	6,8	0,82	108,23
Z81	0,06295	1,0	1,0014	2,5	0,11537	2,3	706,6	21,4	704,5	12,9	703,9	15,6	0,92	99,62
Z83	0,05761	1,4	0,6713	2,9	0,08451	2,5	515,0	31,3	521,5	11,7	523,0	12,5	0,87	101,55
Z84	0,05777	2,6	0,6389	4,2	0,08022	3,3	520,9	57,6	501,6	16,8	497,4	15,9	0,79	95,50
Z86	0,06491	0,9	1,1535	3,2	0,12889	3,0	771,4	19,6	778,9	17,3	781,5	22,4	0,96	101,31
Z87	0,05190	1,2	0,3530	3,4	0,04933	3,2	280,9	26,8	307,0	8,9	310,4	9,6	0,94	110,49
Z88	0,05540	1,5	0,5706	2,6	0,07470	2,2	428,6	32,9	458,4	9,7	464,4	9,8	0,83	108,36
Z89	0,06226	1,4	0,8883	2,4	0,10347	2,0	683,2	29,3	645,5	11,6	634,7	12,1	0,83	92,91
Z90	0,05767	1,3	0,6863	1,7	0,08632	1,2	517,1	27,5	530,6	7,1	533,7	6,0	0,68	103,22
Z92	0,05418	1,3	0,4131	1,8	0,05530	1,3	378,6	28,7	351,1	5,4	347,0	4,4	0,71	91,65
Z93	0,06613	1,2	1,1860	1,7	0,13007	1,1	810,5	25,9	794,1	9,1	788,3	8,1	0,66	97,26
Z94	0,05665	0,8	0,6401	1,9	0,08195	1,7	478,0	18,4	502,4	7,6	507,7	8,4	0,90	106,23
Z95	0,05769	2,4	0,4127	3,9	0,05188	3,0	518,0	52,7	350,8	11,5	326,1	9,6	0,78	62,95
Z96	0,06103	1,3	0,7823	1,8	0,09297	1,3	640,1	28,4	586,8	8,2	573,1	7,0	0,70	89,52
Z97	0,05868	1,7	0,7032	2,3	0,08691	1,5	555,2	38,1	540,7	9,7	537,2	7,8	0,66	96,76
Z98	0,06724	4,7	0,9341	6,5	0,10075	4,4	845,3	98,6	669,8	31,7	618,8	26,0	0,68	73,20
Z99	0,06484	3,2	0,7144	3,6	0,07991	1,7	769,3	66,6	547,4	15,3	495,6	8,3	0,48	64,42
Z100	0,18181	1,5	14,2649	4,5	0,56904	4,2	2669,5	25,3	2767,5	42,3	2903,9	97,8	0,94	108,78
Z101	0,06283	1,6	0,9968	2,2	0,11506	1,5	702,5	34,0	702,2	11,1	702,1	10,0	0,68	99,93
Z102	0,05697	2,6	0,4757	3,9	0,06057	2,9	490,2	56,9	395,1	12,8	379,1	10,8	0,75	77,33

Tab. 2. U-Pb analyses data (continuous)

Sample °	Ratios						Ages						rho	% Disc
	$^{207}Pb/^{206}Pb$	2σ(%)	$^{207}Pb/^{235}U$	2σ(%)	$^{206}Pb/^{238}U$	2σ(%)	$^{207}Pb/^{206}Pb$	2σ(%)	$^{207}Pb/^{235}U$	2σ(%)	$^{206}Pb/^{238}U$	2σ(%)		
CO-SOL														
Z103	0,05559	1,2	0,4514	2,0	0,05889	1,6	436,1	26,7	378,3	6,3	368,9	5,7	0,80	84,60
Z104	0,06024	1,2	0,5506	2,7	0,06629	2,4	612,0	25,3	445,4	9,8	413,8	9,8	0,90	67,61
Z105	0,07481	1,8	1,6637	2,2	0,16130	1,3	1063,3	36,9	994,8	14,2	964,0	11,5	0,57	90,67
Z106	0,05841	1,3	0,5990	1,8	0,07437	1,3	545,3	28,2	476,6	7,0	462,4	5,8	0,71	84,81
Z107	0,08547	5,2	1,2412	8,4	0,10532	6,6	1326,3	100,3	819,4	47,3	645,5	40,7	0,79	48,67
Z108	0,06789	1,8	1,2340	2,7	0,13183	2,0	865,2	36,6	816,2	15,1	798,3	15,3	0,76	92,27
Z109	0,05639	3,1	0,3835	4,3	0,04932	3,0	467,6	69,5	329,6	12,2	310,4	9,0	0,69	66,38
Z110	0,07335	0,9	1,8165	1,5	0,17961	1,3	1023,6	18,3	1051,4	10,1	1064,9	12,4	0,81	104,03
Z112	0,05677	1,3	0,6406	2,1	0,08185	1,6	482,5	28,7	502,7	8,3	507,2	8,0	0,79	105,11
Z113	0,06450	1,1	0,9361	4,2	0,10525	4,1	758,2	22,9	670,8	20,8	645,1	25,2	0,97	85,09
Z114	0,05888	1,2	0,7227	2,1	0,08902	1,7	562,7	26,1	552,3	9,0	549,7	9,1	0,82	97,71
Z115	0,07633	3,1	0,8473	3,7	0,08051	2,2	1103,7	61,4	623,2	17,5	499,2	10,3	0,57	45,23
Z116	0,06274	2,4	0,9381	3,5	0,10845	2,5	699,5	51,1	671,9	17,1	663,7	15,9	0,72	94,89
Z116	0,05977	2,8	0,6690	4,2	0,08119	3,1	595,1	60,7	520,1	16,9	503,2	14,9	0,74	84,56
AF08-28														
Z05b	0,06015	1,6	0,8926	2,9	0,10764	2,3	608,9	35,2	647,8	13,7	659,0	14,7	0,82	108,23
Z06a	0,10632	1,5	4,8967	2,4	0,33402	1,9	1737,3	26,7	1801,7	20,1	1857,8	30,5	0,79	106,94
Z06b	0,17731	1,4	13,6015	2,2	0,55635	1,8	2627,9	23,4	2722,4	21,3	2851,5	40,5	0,78	108,51
Z07b	0,06164	1,7	0,9955	2,7	0,11713	2,2	661,7	35,7	701,5	13,8	714,0	14,6	0,79	107,90
Z08b	0,11588	1,5	5,6073	2,5	0,35096	2,1	1893,5	26,8	1917,2	21,9	1939,2	34,5	0,81	102,41
Z09b	0,17249	1,4	11,8729	3,3	0,49922	3,0	2581,9	24,1	2594,4	31,4	2610,4	64,9	0,90	101,10
Z10a	0,06229	1,8	1,0671	2,3	0,12425	1,5	684,2	37,9	737,3	12,2	755,0	10,8	0,65	110,34
Z10b	0,07070	1,7	1,7029	3,8	0,17469	3,4	948,8	35,6	1009,6	24,4	1037,9	32,6	0,89	109,39
Z11b	0,07146	1,6	1,6502	2,7	0,16748	2,2	970,7	33,1	989,6	17,1	998,2	20,0	0,80	102,84
Z12a	0,06256	2,6	0,9235	4,0	0,10706	3,0	693,4	54,9	664,2	19,2	655,6	18,6	0,75	94,56
Z12b	0,06062	1,7	0,9386	2,8	0,11230	2,2	625,7	36,5	672,2	13,6	686,1	14,3	0,79	109,65
Z13b	0,06190	2,3	1,0298	3,3	0,12067	2,4	670,6	49,6	718,8	17,2	734,4	16,7	0,72	109,52
Z14b	0,06184	10,5	1,0079	12,9	0,11821	7,4	668,5	225,3	707,8	65,6	720,3	50,6	0,58	107,74
Z15a	0,07233	1,5	1,8408	2,5	0,18459	2,0	995,2	30,0	1060,2	16,5	1092,0	20,3	0,81	109,73

Tab. 2. U-Pb analyses data (continuous)

Sample °	Ratios						Ages						rho	% Disc
	$^{207}Pb/^{206}Pb$	2σ(%)	$^{207}Pb/^{235}U$	2σ(%)	$^{206}Pb/^{238}U$	2σ(%)	$^{207}Pb/^{206}Pb$	2σ(%)	$^{207}Pb/^{235}U$	2σ(%)	$^{206}Pb/^{238}U$	2σ(%)		
AF08-28														
Z15b	0,06403	1,7	1,1829	3,6	0,13398	3,2	742,7	36,3	792,7	20,0	810,5	24,4	0,88	109,13
Z16b	0,06311	2,1	1,1230	2,8	0,12905	1,8	712,1	45,5	764,4	15,1	782,4	13,3	0,64	109,88
Z17b	0,06521	2,0	1,1703	3,0	0,13016	2,2	781,0	42,1	786,8	16,2	788,8	16,1	0,73	101,00
Z18b	0,06245	4,0	1,0480	4,9	0,12171	2,9	689,6	84,7	727,9	25,7	740,4	20,6	0,60	107,38
Z19b	0,06712	17,1	1,2054	17,4	0,13024	3,2	841,6	320,1	803,1	92,2	789,2	24,6	0,18	93,77
Z19b	0,06642	1,6	1,3462	2,8	0,14700	2,3	819,6	32,7	865,9	16,2	884,1	19,1	0,83	107,88
Z20b	0,05892	1,7	0,8981	3,1	0,11055	2,6	564,1	37,5	650,7	15,1	676,0	16,8	0,84	119,83
Z20b	0,06891	1,4	1,4425	3,6	0,15181	3,3	896,2	29,3	906,7	21,7	911,1	28,3	0,92	101,66
Z21a	0,06170	3,8	0,9307	6,1	0,10941	4,8	663,7	78,6	668,0	29,6	669,3	30,7	0,79	100,85
Z22a	0,06028	3,0	0,9007	4,4	0,10836	3,2	613,8	65,2	652,1	21,3	663,2	20,3	0,73	108,05
Z23a	0,06373	1,9	1,1584	4,5	0,13183	4,1	732,7	40,8	781,2	24,6	798,3	30,6	0,90	108,95
Z25a	0,06047	1,4	0,8741	3,0	0,10483	2,6	620,6	31,1	637,8	14,1	642,6	15,9	0,87	103,55
Z25a	0,06087	3,9	0,8681	7,8	0,10343	6,8	634,7	81,2	634,5	36,2	634,5	40,8	0,87	99,96
Z27b	0,06012	1,4	0,8505	2,5	0,10260	2,1	607,9	29,2	624,9	11,6	629,6	12,5	0,84	103,57
Z28a	0,06515	3,2	1,2051	5,0	0,13415	3,8	779,3	68,2	802,9	27,9	811,5	29,2	0,76	104,12
Z28b	0,06328	1,8	1,1260	4,9	0,12906	4,5	717,5	37,3	765,9	26,1	782,5	33,4	0,93	109,06
Z28b	0,06560	1,5	1,2292	3,0	0,13590	2,6	793,6	31,0	814,0	17,0	821,5	20,4	0,87	103,51
Z29a	0,06158	4,9	0,9084	5,8	0,10698	3,1	659,6	104,1	656,2	27,9	655,2	19,3	0,54	99,33
Z29b	0,06110	2,3	0,8669	3,3	0,10291	2,4	642,6	48,1	633,9	15,3	631,4	14,1	0,72	98,26
Z30b	0,06041	1,8	0,8995	3,5	0,10799	3,0	618,4	38,2	651,5	16,7	661,1	18,8	0,86	106,90
Z31b	0,06331	2,8	1,0797	4,2	0,12369	3,2	718,6	59,8	743,5	22,3	751,8	22,4	0,75	104,62
Z32a	0,06021	7,7	0,7807	10,8	0,09404	7,6	611,1	158,5	585,9	47,1	579,4	42,0	0,70	94,82
Z32b	0,17374	1,4	12,3854	2,4	0,51701	1,9	2594,0	22,8	2634,1	22,3	2686,5	42,6	0,82	103,56
Z33b	0,06132	1,7	1,0203	2,5	0,12068	1,7	650,3	37,2	714,1	12,6	734,5	12,1	0,71	112,94
Z35b	0,06220	1,4	0,9407	5,0	0,10969	4,8	681,0	30,3	673,3	24,3	671,0	30,5	0,96	98,53
Z36b	0,06170	2,4	1,0077	4,3	0,11845	3,5	663,8	50,6	707,7	21,7	721,6	24,2	0,83	108,71
Z38a	0,06171	1,9	0,9750	4,3	0,11459	3,8	664,2	41,4	691,1	21,5	699,3	25,4	0,89	105,30
Z40a	0,16012	1,3	10,0428	2,3	0,45489	1,9	2456,9	22,4	2438,7	21,2	2416,9	38,1	0,82	98,37
Z40a	0,06023	5,4	0,8544	8,2	0,10289	6,2	611,9	117,6	627,1	38,4	631,3	37,0	0,75	103,18
Z40a-r	0,05890	3,1	0,7724	12,8	0,09511	12,2	563,2	65,8	581,1	55,3	585,7	69,4	0,97	103,99

Tab. 2. U-Pb analyses data (continuous)

Sample °	Ratios						Ages						rho	% Disc
	$^{207}Pb/^{206}Pb$	2σ(%)	$^{207}Pb/^{235}U$	2σ(%)	$^{206}Pb/^{238}U$	2σ(%)	$^{207}Pb/^{206}Pb$	2σ(%)	$^{207}Pb/^{235}U$	2σ(%)	$^{206}Pb/^{238}U$	2σ(%)		
AF08-28														
Z41a	0,06192	1,9	1,0265	2,8	0,12023	2,1	671,3	39,6	717,2	14,2	731,9	14,2	0,74	109,02
Z43a	0,06155	12,4	0,8892	17,2	0,10478	12,0	658,6	264,8	646,0	82,2	642,4	73,1	0,70	97,54
Z44a	0,06183	1,6	0,9602	3,0	0,11264	2,6	668,1	33,4	683,4	15,0	688,0	16,9	0,86	102,99
Z45a	0,06317	4,1	1,1232	5,4	0,12895	3,6	714,1	87,2	764,5	29,2	781,9	26,3	0,66	109,49
Z47a	0,12441	3,1	6,7697	5,0	0,39464	3,9	2020,5	55,7	2081,8	44,5	2144,3	71,7	0,78	106,13
Z48a	0,07329	1,4	1,9075	3,8	0,18875	3,5	1022,1	27,9	1083,7	25,2	1114,6	36,0	0,93	109,05
Z49	0,06031	2,1	0,8707	2,7	0,10472	1,6	614,6	45,5	635,9	12,6	642,0	10,0	0,61	104,46
Z49a	0,06300	1,8	1,1098	6,9	0,12775	6,7	708,4	37,9	758,1	37,0	775,0	48,9	0,97	109,40
Z50	0,07291	2,0	1,8192	3,4	0,18097	2,7	1011,4	40,1	1052,4	22,0	1072,2	26,9	0,81	106,01
Z50a-c	0,06903	2,3	1,4244	4,9	0,14966	4,3	899,5	47,3	899,2	28,7	899,1	35,9	0,88	99,95
Z50a-r	0,06128	1,7	0,9271	3,4	0,10973	2,9	649,1	35,9	666,1	16,5	671,2	18,7	0,87	103,40
Z51	0,06778	1,7	1,3045	4,7	0,13959	4,3	861,8	35,5	847,7	26,8	842,3	34,3	0,93	97,74
Z57	0,06917	2,0	1,5112	5,0	0,15845	4,6	903,9	40,5	934,9	30,6	948,1	40,6	0,92	104,90
Z61b	0,10446	4,4	4,1174	8,4	0,28588	7,2	1704,8	78,3	1657,8	66,4	1620,9	102,1	0,85	95,08
Z69b	0,07127	0,9	1,6616	3,0	0,16907	2,9	965,3	18,9	994,0	19,0	1007,0	26,6	0,95	104,32
Z73	0,06157	2,1	0,9146	6,0	0,10774	5,6	659,2	45,3	659,5	29,1	659,6	35,3	0,94	100,05
Z74	0,06425	2,3	1,2146	4,7	0,13710	4,1	750,0	47,8	807,3	26,1	828,3	31,9	0,88	110,44
Z77	0,07010	0,7	1,4272	3,9	0,14767	3,8	931,2	15,2	900,4	23,1	887,9	31,8	0,98	95,35
Z80	0,21338	1,4	18,3117	3,2	0,62240	2,9	2931,4	23,4	3006,3	30,8	3119,5	70,7	0,89	106,42
Z81b	0,06778	1,4	1,4194	3,0	0,15188	2,7	861,7	29,8	897,1	18,2	911,5	22,8	0,88	105,78
Z82b	0,06231	1,7	1,0636	4,5	0,12380	4,1	684,7	35,4	735,6	23,3	752,4	29,4	0,93	109,90
Z91b	0,14905	1,6	9,4658	3,4	0,46060	3,1	2335,1	26,8	2384,2	31,6	2442,2	62,3	0,89	104,59
Z95	0,10801	0,7	5,0719	2,3	0,34057	2,2	1766,1	12,5	1831,4	19,9	1889,4	36,8	0,96	106,98
Z97	0,11080	0,7	4,8444	2,5	0,31711	2,3	1812,5	13,3	1792,6	20,5	1775,6	36,4	0,95	97,96
Z100	0,07396	1,7	1,7410	3,2	0,17072	2,7	1040,5	33,0	1023,8	20,1	1016,1	25,2	0,85	97,66
Z102	0,17349	1,6	7,1530	5,4	0,29903	5,2	2591,6	26,4	2130,7	48,2	1686,5	76,7	0,96	65,08
Z103	0,07625	1,2	1,8760	3,7	0,17845	3,5	1101,6	23,3	1072,7	24,1	1058,5	34,0	0,95	96,09
Z106	0,06305	0,7	1,0500	2,1	0,12078	2,0	709,8	14,4	728,9	11,0	735,1	13,9	0,95	103,56
Z109	0,06412	0,7	1,0852	2,7	0,12274	2,6	745,7	15,2	746,2	14,1	746,3	18,3	0,96	100,08
Z112b	0,07110	1,6	1,5880	3,7	0,16199	3,3	960,3	31,8	965,5	22,9	967,9	29,9	0,91	100,79

Tab. 2. U-Pb analyses data (continuous)

Sample °	Ratios						Ages						rho	% Disc
	$^{207}Pb/^{206}Pb$	2σ(%)	$^{207}Pb/^{235}U$	2σ(%)	$^{206}Pb/^{238}U$	2σ(%)	$^{207}Pb/^{206}Pb$	2σ(%)	$^{207}Pb/^{235}U$	2σ(%)	$^{206}Pb/^{238}U$	2σ(%)		
AF08-28														
Z122	0,06802	1,9	1,4788	3,5	0,15768	2,9	869,1	38,5	921,7	20,9	943,9	25,6	0,84	108,61
SA-ALB														
Z01	0,23252	1,3	21,0213	3,4	0,65569	3,1	3069,5	20,8	3139,6	32,5	3250,4	78,9	0,92	105,89
Z04	0,05380	2,6	0,7216	4,1	0,09727	3,1	362,8	56,5	551,6	17,2	598,4	18,2	0,78	164,92
Z05	0,06332	1,2	0,8561	2,3	0,09806	2,0	719,1	25,3	628,0	10,9	603,0	11,5	0,86	83,86
Z06	0,06494	3,3	1,1534	4,7	0,12881	3,4	772,5	68,9	778,8	25,6	781,0	24,9	0,72	101,11
Z08	0,07178	7,3	1,0937	10,3	0,11050	7,3	979,8	148,8	750,3	54,9	675,6	47,0	0,71	68,95
Z09	0,06383	2,3	1,0395	3,0	0,11811	1,8	736,0	49,0	723,7	15,3	719,7	12,5	0,62	97,78
Z10	0,07720	1,1	2,0337	2,3	0,19106	2,0	1126,3	22,7	1126,9	16,0	1127,1	21,2	0,87	100,07
Z11	0,06054	4,9	1,0224	6,2	0,12248	3,9	622,9	105,1	715,1	31,9	744,8	27,1	0,62	119,57
Z12	0,08388	7,5	2,3980	10,6	0,20735	7,5	1289,7	138,7	1242,0	73,0	1214,7	82,2	0,71	94,18
Z13	0,12033	0,9	5,9424	2,7	0,35818	2,6	1961,1	16,7	1967,5	23,8	1973,5	43,7	0,94	100,64
Z14	0,05700	2,0	0,7849	4,5	0,09988	4,0	491,4	43,9	588,3	19,9	613,7	23,4	0,89	124,90
Z15	0,05385	3,0	0,6544	5,3	0,08813	4,4	364,9	67,0	511,2	21,4	544,5	23,1	0,83	149,22
Z17	0,07318	1,2	1,8419	2,0	0,18255	1,6	1019,0	23,4	1060,6	13,1	1080,9	16,1	0,81	106,08
Z18	0,05718	4,3	0,9102	5,5	0,11546	3,5	498,4	94,1	657,2	26,6	704,4	23,0	0,63	141,32
Z19	0,05691	2,0	0,8582	2,8	0,10937	2,0	488,2	44,3	629,1	13,3	669,1	12,6	0,70	137,05
Z20	0,20466	7,6	17,4327	12,9	0,61777	10,3	2863,7	124,3	2959,0	123,4	3101,0	254,3	0,80	108,29
Z21	0,07224	5,2	2,2003	5,7	0,22091	2,4	992,7	105,7	1181,1	40,0	1286,7	28,0	0,42	129,62
Z22	0,08095	13,3	1,9590	18,4	0,17551	12,7	1220,3	261,4	1101,5	123,6	1042,4	122,2	0,69	85,42
Z23	0,07104	3,3	1,2785	4,7	0,13053	3,3	958,5	67,9	836,2	26,6	790,9	24,4	0,70	82,52
Z24	0,09010	7,6	2,9259	11,0	0,23552	8,0	1427,6	138,0	1388,6	80,1	1363,4	97,6	0,73	95,50
Z25	0,07142	1,6	1,4988	2,4	0,15220	1,8	969,5	31,6	929,9	14,6	913,3	15,7	0,76	94,20
Z26	0,06174	1,1	0,9620	2,1	0,11301	1,8	665,2	24,5	684,4	10,5	690,2	11,6	0,84	103,76
Z27	0,07333	1,5	1,9011	2,6	0,18802	2,1	1023,1	30,7	1081,5	17,4	1110,7	21,7	0,81	108,56
Z28	0,09711	7,4	3,2447	11,2	0,24234	8,4	1569,3	132,7	1467,9	83,4	1398,8	104,6	0,75	89,14
Z29	0,07269	1,5	1,3820	3,1	0,13788	2,7	1005,4	30,1	881,3	18,0	832,7	21,1	0,87	82,82
Z30	0,07388	1,5	2,0662	3,4	0,20283	3,1	1038,2	29,9	1137,7	23,2	1190,5	33,2	0,90	114,67
Z31	0,06483	1,8	0,8303	4,1	0,09289	3,6	768,7	38,3	613,8	18,5	572,6	19,8	0,89	74,49

Tab. 2. U-Pb analyses data (continuous)

	Ratios						Ages						rho	% Disc
Sample °	$^{207}Pb/^{206}Pb$	2σ(%)	$^{207}Pb/^{235}U$	2σ(%)	$^{206}Pb/^{238}U$	2σ(%)	$^{207}Pb/^{206}Pb$	2σ(%)	$^{207}Pb/^{235}U$	2σ(%)	$^{206}Pb/^{238}U$	2σ(%)		
SA-ALB														
Z63	0,11635	2,0	7,1409	4,2	0,44512	3,7	1900,9	36,1	2129,2	37,8	2373,5	74,2	0,88	124,86
Z64	0,06018	4,1	0,9508	5,7	0,11460	3,9	609,9	89,2	678,5	28,0	699,4	25,7	0,68	114,67
Z66	0,06627	1,4	1,3994	3,0	0,15315	2,7	815,0	28,7	888,7	17,8	918,6	22,8	0,89	112,72
Z68	0,11509	0,8	6,8774	3,8	0,43341	3,7	1881,2	13,8	2095,8	33,4	2321,1	71,8	0,98	123,38
Z69	0,07361	1,1	1,8731	2,8	0,18454	2,6	1030,9	22,8	1071,6	18,8	1091,7	26,1	0,92	105,91
Z70	0,06502	1,1	1,2100	2,4	0,13498	2,1	774,9	22,3	805,2	13,3	816,2	16,5	0,90	105,33
Z71	0,06141	1,2	1,0662	3,3	0,12593	3,0	653,5	25,7	736,9	17,1	764,6	21,8	0,93	116,99
Z72	0,06017	5,1	0,9294	5,5	0,11203	2,0	609,7	111,1	667,3	27,0	684,5	13,0	0,36	112,28
SST-5100														
Z01	0,05558	1,3	0,5468	2,4	0,07135	2,0	435,7	28,6	442,9	8,6	444,3	8,6	0,84	101,97
Z02	0,05606	1,8	0,5366	2,9	0,06943	2,3	454,6	39,0	436,2	10,2	432,7	9,6	0,79	95,20
Z03	0,05655	1,8	0,5493	2,6	0,07045	1,9	473,9	39,1	444,5	9,5	438,9	8,3	0,74	92,61
Z04	0,12159	1,4	5,4505	2,3	0,32510	1,8	1979,8	25,2	1892,8	19,4	1814,6	28,2	0,78	91,66
Z05	0,05591	2,2	0,5312	4,0	0,06891	3,4	448,8	47,4	432,6	14,2	429,6	14,2	0,84	95,73
Z06	0,05551	2,5	0,5279	3,3	0,06897	2,1	432,7	54,8	430,4	11,5	430,0	8,9	0,65	99,38
Z07	0,05768	3,1	0,5967	4,8	0,07504	3,6	517,5	67,2	475,2	18,0	466,4	16,4	0,77	90,14
Z08	0,07528	2,6	1,8966	3,9	0,18272	2,9	1076,0	51,7	1079,9	26,0	1081,8	29,2	0,75	100,54
Z09	0,05751	2,0	0,6449	3,1	0,08133	2,3	511,2	44,9	505,3	12,3	504,0	11,2	0,75	98,60
Z10	0,05754	1,8	0,6199	2,4	0,07813	1,6	512,3	39,3	489,8	9,3	484,9	7,4	0,66	94,65
Z11	0,05829	1,7	0,6601	3,8	0,08213	3,4	540,8	36,6	514,7	15,2	508,8	16,5	0,90	94,08
Z12	0,05850	1,8	0,7185	3,0	0,08908	2,4	548,6	39,3	549,8	12,8	550,1	12,7	0,80	100,28
Z14	0,05563	1,9	0,5763	4,8	0,07513	4,4	437,5	43,4	462,1	18,0	467,0	20,0	0,92	106,74
Z15	0,05767	1,0	0,6027	2,7	0,07580	2,5	517,2	22,4	478,9	10,3	471,0	11,3	0,93	91,07
Z15b	0,05670	9,2	0,6256	13,1	0,08003	9,2	479,8	191,9	493,3	49,9	496,3	44,3	0,71	103,44
Z16	0,05902	1,8	0,6934	4,1	0,08521	3,6	567,8	39,4	534,8	17,1	527,1	18,8	0,89	92,84
Z17	0,05591	2,9	0,5884	4,8	0,07633	3,8	448,9	65,0	469,9	17,9	474,2	17,2	0,79	105,62
Z18	0,07017	3,2	1,5276	4,5	0,15789	3,1	933,4	66,4	941,6	27,4	945,1	26,9	0,69	101,25
Z19b	0,07233	1,2	1,6688	2,7	0,16733	2,4	995,3	24,5	996,7	17,0	997,4	22,0	0,89	100,20
Z20	0,05974	2,2	0,7760	3,2	0,09421	2,4	594,3	47,2	583,2	14,3	580,4	13,2	0,74	97,65

Tab. 2. U-Pb analyses data (continuous)

Sample °	Ratios						Ages						rho	% Disc
	$^{207}Pb/^{206}Pb$	2σ(%)	$^{207}Pb/^{235}U$	2σ(%)	$^{206}Pb/^{238}U$	2σ(%)	$^{207}Pb/^{206}Pb$	2σ(%)	$^{207}Pb/^{235}U$	2σ(%)	$^{206}Pb/^{238}U$	2σ(%)		
SST-5100														
Z21	0,11985	1,8	5,5344	2,6	0,33492	1,8	1954,0	31,7	1906,0	22,0	1862,2	29,8	0,72	95,30
Z21b	0,06336	25,1	1,0068	26,3	0,11523	7,8	720,5	532,2	707,2	133,7	703,1	51,8	0,30	97,59
Z22	0,07187	1,1	1,5597	2,6	0,15739	2,4	982,2	21,4	954,3	16,0	942,3	20,8	0,91	95,93
Z23	0,05596	2,3	0,5470	3,4	0,07089	2,5	450,7	50,4	443,0	12,2	441,5	10,8	0,74	97,97
Z23b	0,07098	2,8	1,6146	3,6	0,16499	2,2	956,7	57,4	975,9	22,4	984,4	20,1	0,62	102,90
Z25b	0,05877	2,5	0,7635	4,2	0,09422	3,4	558,6	54,3	576,0	18,4	580,5	18,7	0,80	103,92
Z26	0,05872	2,6	0,7501	4,4	0,09265	3,6	556,6	55,7	568,3	19,1	571,2	19,5	0,81	102,61
Z27	0,05730	1,2	0,5789	2,4	0,07328	2,1	503,1	25,9	463,8	8,8	455,9	9,1	0,87	90,62
Z27b	0,05825	18,3	0,7212	19,6	0,08980	6,7	539,2	356,8	551,4	80,1	554,4	37,1	0,34	102,81
Z28	0,05616	2,6	0,5679	4,1	0,07335	3,2	458,7	56,4	456,7	15,1	456,3	14,2	0,78	99,47
Z28b	0,05487	2,6	0,5346	3,0	0,07066	1,6	407,0	56,2	434,9	10,6	440,2	6,8	0,52	108,15
Z30	0,05322	5,6	0,4225	8,9	0,05758	6,2	338,1	122,5	357,9	26,6	360,9	24,3	0,74	106,74
Z30b	0,05550	8,0	0,5360	8,3	0,07005	2,2	432,5	177,4	435,8	29,2	436,4	9,2	0,26	100,91
Z31	0,05525	1,4	0,5147	2,8	0,06756	2,4	422,3	31,9	421,6	9,7	421,5	9,9	0,86	99,81
Z31b	0,05672	2,6	0,6133	5,8	0,07842	5,1	480,6	57,9	485,6	22,2	486,7	24,1	0,89	101,26
Z32	0,05940	1,9	0,7292	3,1	0,08903	2,4	582,0	41,2	556,1	13,2	549,8	12,9	0,79	94,48
Z32b	0,05687	4,4	0,5796	6,0	0,07392	4,0	486,5	93,4	464,2	22,0	459,7	18,0	0,68	94,49
Z34	0,05559	3,4	0,5222	4,0	0,06813	2,2	436,1	74,0	426,6	14,0	424,9	8,9	0,54	97,42
Z34b	0,05702	6,6	0,6701	8,3	0,08524	5,0	492,2	138,6	520,8	33,3	527,3	25,6	0,60	107,13
Z36	0,05619	1,8	0,5486	2,7	0,07080	2,0	460,0	39,7	444,1	9,7	441,0	8,6	0,74	95,88
Z37	0,05547	2,0	0,5328	3,4	0,06966	2,8	431,4	45,1	433,6	12,1	434,1	11,6	0,81	100,63
Z39	0,05608	1,6	0,5632	3,0	0,07283	2,5	455,7	36,1	453,6	11,0	453,2	11,1	0,84	99,45
Z40	0,06031	2,6	0,5833	3,2	0,07014	1,9	614,7	54,8	466,6	12,0	437,0	8,2	0,60	71,09
Z41	0,05634	1,4	0,5831	2,5	0,07506	2,1	465,8	31,5	466,5	9,5	466,6	9,5	0,83	100,17
Z42	0,05534	1,7	0,5449	2,5	0,07141	1,9	426,0	37,2	441,7	9,1	444,7	8,2	0,75	104,37
Z42b	0,05737	33,2	0,5892	34,4	0,07448	8,8	505,9	730,9	470,4	129,4	463,1	39,5	0,26	91,53
Z43	0,05651	9,3	0,5696	9,6	0,07310	2,5	472,6	205,2	457,8	35,4	454,8	11,0	0,26	96,24
Z44	0,05637	2,2	0,5618	3,3	0,07228	2,4	467,0	48,8	452,7	11,9	449,9	10,4	0,73	96,34
Z45	0,05628	1,4	0,5922	2,4	0,07632	2,0	463,6	31,1	472,3	9,1	474,1	8,9	0,81	102,27
Z45b	0,05838	11,3	0,7472	11,9	0,09282	3,7	544,2	228,7	566,6	50,4	572,2	21,0	0,32	105,14

Tab. 2. U-Pb analyses data (continuous)

	Ratios						Ages						rho	% Disc
Sample °	$^{207}Pb/^{206}Pb$	2σ(%)	$^{207}Pb/^{235}U$	2σ(%)	$^{206}Pb/^{238}U$	2σ(%)	$^{207}Pb/^{206}Pb$	2σ(%)	$^{207}Pb/^{235}U$	2σ(%)	$^{206}Pb/^{238}U$	2σ(%)		
SST-5100														
Z46	0,05603	2,2	0,5550	2,6	0,07184	1,3	453,4	49,9	448,3	9,4	447,3	5,5	0,50	98,65
Z47	0,05724	1,4	0,6019	4,0	0,07627	3,8	500,8	30,3	478,4	15,2	473,8	17,1	0,94	94,61
Z48	0,05647	1,1	0,6279	2,4	0,08065	2,2	470,9	23,7	494,8	9,4	500,0	10,4	0,90	106,19
Z49	0,05584	1,6	0,5830	2,4	0,07572	1,8	446,0	35,8	466,4	9,1	470,5	8,3	0,75	105,49
Z57b	0,06991	7,5	1,6133	10,6	0,16736	7,5	925,8	154,3	975,4	66,6	997,6	69,5	0,71	107,75
Z57b	0,06363	1,6	0,9596	2,9	0,10938	2,4	729,4	33,5	683,1	14,3	669,1	15,4	0,83	91,73
Z60b	0,05620	2,1	0,6010	2,9	0,07755	2,0	460,4	46,4	477,8	11,0	481,5	9,2	0,69	104,58
Z61b	0,07473	1,1	1,6835	2,1	0,16340	1,8	1061,2	22,9	1002,3	13,3	975,6	15,9	0,84	91,94
Z62b	0,07077	1,2	1,5692	2,7	0,16083	2,4	950,6	24,8	958,1	16,8	961,4	21,7	0,90	101,13
Z63b	0,05635	2,6	0,5312	3,7	0,06837	2,5	466,3	56,6	432,6	12,9	426,3	10,8	0,69	91,42
Z64b	0,06135	1,7	0,8200	3,5	0,09695	3,1	651,4	35,9	608,1	16,1	596,5	17,7	0,88	91,57
Z671b	0,11462	1,0	5,4009	3,6	0,34173	3,4	1874,0	18,5	1885,0	30,4	1895,0	55,9	0,96	101,12
Z71b	0,05586	2,3	0,5533	3,3	0,07183	2,3	447,0	50,9	447,1	11,8	447,2	10,1	0,71	100,04
Z81b	0,06005	6,8	0,8085	8,0	0,09766	4,2	605,3	146,8	601,6	36,1	600,7	23,8	0,52	99,24
Z88b	0,06475	1,5	1,1167	2,3	0,12508	1,8	766,2	30,3	761,4	12,5	759,8	13,2	0,79	99,16
Z89b	0,05838	15,7	0,6402	18,8	0,07953	10,0	544,1	311,3	502,4	72,0	493,3	48,8	0,54	90,66
Z90b	0,05655	6,1	0,5553	6,4	0,07122	2,2	474,0	128,5	448,5	23,0	443,5	9,2	0,34	93,57
Z91b	0,05882	2,6	0,7148	3,3	0,08815	1,9	560,3	57,5	547,6	13,8	544,6	10,0	0,59	97,19
Z92b	0,06134	8,2	0,9632	11,3	0,11388	7,7	651,3	176,5	685,0	56,2	695,2	51,0	0,69	106,74
Z94b	0,05520	8,6	0,5108	9,3	0,06712	3,7	420,3	191,3	419,0	32,0	418,8	14,8	0,39	99,63
Z100	0,05594	2,3	0,5702	3,4	0,07394	2,4	449,9	51,7	458,2	12,4	459,8	10,8	0,72	102,21

	Ratios						Ages						rho	% Disc
Sample #	$^{207}Pb/^{206}Pb$	1σ(%)	$^{207}Pb/^{235}U$	1σ(%)	$^{206}Pb/^{238}U$	1σ(%)	$^{207}Pb/^{206}Pb$	±2 S.D.	$^{207}Pb/^{235}U$	±2 S.D.	$^{206}Pb/^{238}U$	±2 S.D.		
28														
S14	0,05825	0,94	0,6	1,32000	0,1	0,41	538,0	40,0	458,4	9,7	443,7	3,5	0,9	82,47
S15b	0,05715	0,62	0,6	0,73000	0,1	0,39	496,0	28,0	453,7	5,3	453,3	3,4	0,5	91,39
S18	0,06818	1,57	0,7	1,88000	0,1	0,7	872,0	66,0	548,6	15,9	468,8	6,3	0,6	53,76
S18	0,05617	1,16	0,6	1,46000	0,1	0,57	458,0	52,0	459,5	10,8	461,3	5	0,7	100,72

Tab. 2. U-Pb analyses data (continuous)

Sample #	Ratios						Ages					rho	% Disc
	$^{207}Pb/^{206}Pb$	1σ(%)	$^{207}Pb/^{235}U$	1σ(%)	$^{206}Pb/^{238}U$	1σ(%)	$^{207}Pb/^{206}Pb$	±2 S.D.	$^{207}Pb/^{235}U$	±2 S.D.	$^{206}Pb/^{238}U$	±2 S.D.		
28														
S20a	0,05854	1,17	0,6	1,57000	0,1	0,63	446,0	66,0	458,5	14,8	465,2	6,7	0,8	104,30
S24a	0,05595	0,87	0,6	1,16000	0,1	0,43	450,0	38,0	456,2	8,5	460,0	3,8	0,8	102,22
S25a	0,05878	1,27	0,6	1,64000	0,1	0,5	558,0	56,0	472,5	12,4	453,4	4,4	0,8	81,25
S27a	0,05755	1,72	0,6	2,79000	0,1	0,71	512,0	76,0	461,6	20,7	454,6	6,2	1,3	88,79
S27b	0,05587	1,49	0,6	2,00000	0,1	0,74	642,0	58,0	510,1	13,2	468,9	4,8	0,8	73,04
S28b	0,05726	1,05	0,6	1,18000	0,1	0,54	500,0	46,0	464,6	8,8	459,0	4,7	0,5	91,80
S29	0,06112	1,35	0,7	1,65000	0,1	0,53	482,0	70,0	465,2	14,3	465,1	7	0,7	96,49
S31a	0,0587	1,86	0,6	2,98000	0,1	0,75	556,0	82,0	488,9	23,1	461,8	6,7	1,3	83,06
SAR05-09														
S34b	**0,07337**	**1,6**	0,8	2,32000	0,1	0,68	1024,0	66,0	576,6	20,4	467,8	6,2	1,0	45,68
S37	**0,0571**	**1,48**	0,6	2,03000	0,1	0,58	494,0	64,0	461,1	15,0	458,4	5,2	1,0	92,79
S39b	**0,05656**	**0,97**	0,6	1,22000	0,1	0,86	474,0	42,0	459,0	9,0	456,4	7,5	0,6	96,29
S41	0,0568	1,59	0,6	1,92000	0,1	0,78	482,0	70,0	465,2	14,3	465,1	7	0,6	96,49
S43b	**0,06619**	**1,51**	0,7	2,00000	0,1	0,88	812,0	62,0	527,2	16,5	463,2	7,9	0,7	57,04
CC-150														
L3-57	0,05729	1,12	0,6	1,51000	0,1	0,61	502,0	50,0	465,2	11,3	466,6	5,5	0,8	92,95
L3-60	0,06156	1,47	0,6	2,11000	0,1	0,62	658,0	64,0	494,2	16,5	460,8	5,5	1,0	70,03
L3-61	0,05747	1,67	0,6	2,31000	0,1	0,69	508,0	74,0	473,1	17,5	459,8	6,1	0,9	90,51
L3-64	0,06377	1,14	0,7	1,72000	0,1	0,55	732,0	48,0	516,2	14,0	469,1	5	1,0	64,08
BS-125														
L3-71	0,05764	1,49	0,6	1,59000	0,1	0,75	514,0	66,0	470,0	11,9	462,5	6,7	0,4	89,98
L3-75	0,05775	1,26	0,6	1,60000	0,1	0,44	520,0	54,0	476,1	12,2	471,0	4	0,8	90,58
L3-77	0,05965	1,24	0,6	1,50000	0,1	0,45	590,0	54,0	489,0	11,6	455,6	3,9	0,7	77,22
L3-81	0,06007	1,08	0,6	1,67000	0,1	0,57	606,0	46,0	500,2	13,2	466,1	5,1	1,0	76,91
L3-82	0,05755	1,16	0,6	1,60000	0,1	0,76	512,0	50,0	480,7	12,2	471,0	6,9	0,7	91,99
L3-88	0,06076	0,98	0,6	1,42000	0,1	0,93	630,0	42,0	496,7	11,2	467,9	8,4	0,7	74,27

Tab. 2. U-Pb analyses data (continuous)

	Ratios						Ages					rho	% Disc
Sample #	**$^{207}Pb/^{206}Pb$**	**1σ(%)**	**$^{207}Pb/^{235}U$**	**1σ(%)**	**$^{206}Pb/^{238}U$**	**1σ(%)**	**$^{207}Pb/^{206}Pb$**	**±2 S.D.**	**$^{207}Pb/^{235}U$**	**±2 S.D.**	**$^{206}Pb/^{238}U$**	**±2 S.D.**		
SM-200														
L1-43 (r)	0,06	1,07	0,6	1,57000	0,1	0,41	478,0	48,0	460,8	11,6	454,8	3,6	1,2	95,15
L1-43 ©	0,06	1,13	0,6	1,19000	0,1	0,46	528,0	50,0	470,2	9,0	453,7	4	0,3	85,93
L1-46	0,06	1,06	0,6	1,32000	0,1	0,49	508,0	48,0	462,2	9,8	457,2	4,4	0,7	90,00
L1-48	0,06	1,22	0,6	1,47000	0,1	0,45	458,0	54,0	453,8	10,8	458,3	4	0,7	100,07
L1-50	0,06	1,08	0,6	1,67000	0,1	0,44	526,0	46,0	465,5	12,5	460,1	3,9	1,2	87,47
L1-53 (r)	0,056	1,080	0,6	1,68000	0,1	1,05	468,0	48,0	450,6	12,2	456,3	9,2	0,8	97,50
L1-53 ©	0,058	1,960	0,6	2,37000	0,1	1,08	536,0	86,0	473,6	18,0	462,7	9,7	0,6	86,32
L1-65	0,057	1,570	0,6	2,04000	0,1	0,52	490,0	68,0	456,6	15,0	456,0	4,6	0,9	93,06
L1-71 (r)	0,057	1,020	0,6	1,47000	0,1	0,45	506,0	46,0	473,6	11,1	467,4	4,1	1,0	92,37
L1-71 ©	0,056	1,180	0,6	1,59000	0,1	0,56	438,0	52,0	454,4	11,7	464,4	5	0,8	106,03
LON-03														
L1-109	0,05	1,61	0,4	2,02000	0,0	0,58	356,0	72,0	308,3	10,8	300,2	3,4	0,8	84,33
L1-110(c)	0,05	1,78	0,4	2,07000	0,0	0,67	320,0	80,0	317,3	11,3	311,0	4	0,6	97,19
L1-110(r)	0,06	2,81	0,4	2,82000	0,0	0,85	462,0	124,0	324,9	15,7	299,0	4,9	0,2	64,72
L1-112	0,06	2,12	0,4	2,53000	0,0	0,62	518,0	94,0	333,8	14,4	299,5	3,7	0,7	57,82
L1-113	0,05	1,03	0,4	1,36000	0,0	0,62	328,0	46,0	310,6	7,3	308,1	3,7	0,7	93,93
L1-115(c)	0,05	2,45	0,4	2,99000	0,0	0,77	310,0	112,0	310,4	16,0	303,9	4,6	0,8	98,03
L1-115(r)	0,05	1,80	0,4	2,17000	0,0	0,62	382,0	80,0	311,5	11,7	302,8	3,7	0,7	79,27
L1-116	0,05	1,48	0,4	1,76000	0,0	0,55	376,0	66,0	315,1	9,5	305,6	3,3	0,6	81,28
L1-118	0,06	2,54	0,4	3,25000	0,0	0,8	454,0	114,0	319,3	17,8	302,7	4,7	0,9	66,67
L1-122	0,06156	9,93	0,4	9,57000	0,0	0,93	658,0	428,0	348,5	56,5	305,7	5,5	-0,3	46,46
L1-123 (c)	0,05582	9,28	0,4	10,30000	0,0	0,63	444,0	414,0	323,5	57,1	305,5	3,7	1,6	68,81
L1-123 (r)	0,05539	1,61	0,4	3,26000	0,0	0,41	426,0	72,0	316,1	17,7	300,2	2,4	3,1	70,47
L1-125	0,05478	0,78	0,4	0,72000	0,0	0,92	402,0	36,0	317,4	3,9	306,8	5,5	0,6	76,32
L1-126 ®	0,06704	19,05	0,5	21,48000	0,0	1,59	838,0	810,0	384,0	137,6	308,0	9,6	1,5	36,75
L1-126(c)	0,0648	16,62	0,4	18,09000	0,0	1,16	766,0	710,0	356,0	108,8	300,7	6,8	1,2	39,26
L1-127	0,05899	15,19	0,4	15,03000	0,0	0,65	566,0	670,0	338,9	86,7	306,1	3,9	-0,2	54,08

Tab. 2. U-Pb analyses data (continuous)

Sample #	Ratios						Ages					rho	% Disc
	$^{207}Pb/^{206}Pb$	1σ(%)	$^{207}Pb/^{235}U$	1σ(%)	$^{206}Pb/^{238}U$	1σ(%)	$^{207}Pb/^{206}Pb$	±2 S.D.	$^{207}Pb/^{235}U$	±2 S.D.	$^{206}Pb/^{238}U$	±2 S.D.		
COR-13														
L1-75	0,05305	0,88	0,3	0,96000	0,0	0,38	330,0	40,0	296,5	5,0	294,9	2,2	0,4	89,36
L1-76	0,05177	1,1	0,3	1,45000	0,0	0,48	274,0	52,0	287,0	7,2	292,7	2,7	0,8	106,82
L1-77	0,05238	1,14	0,3	1,32000	0,0	0,44	302,0	54,0	292,9	6,7	293,2	2,5	0,5	97,09
L1-78	0,05538	2,94	0,4	3,98000	0,0	1,01	426,0	132,0	316,3	21,6	294,5	5,8	1,0	69,13
L1-82	0,06777	3,62	0,4	5,49000	0,0	1,18	860,0	150,0	358,5	33,2	293,4	6,8	1,4	34,12
L1-85	0,05149	1,37	0,3	1,56000	0,0	0,57	262,0	62,0	291,7	7,9	295,6	3,3	0,5	112,82
L1-86	0,05347	1,54	0,3	1,67000	0,0	0,57	348,0	70,0	297,2	8,6	294,5	3,3	0,4	84,63
L1-89 (c)	0,05472	1,47	0,3	1,76000	0,0	0,71	400,0	66,0	295,5	9,0	290,6	4	0,6	72,65
L1-89 (r)	0,0525	0,76	0,3	0,81000	0,0	0,51	306,0	36,0	292,8	4,1	291,8	2,9	0,4	95,36
L1-90	0,05252	0,63	0,3	0,75000	0,0	0,38	308,0	30,0	297,1	3,9	286,0	2,1	0,5	92,86
L1-92 (c)	0,05425	1,48	0,3	1,64000	0,0	0,61	380,0	68,0	303,1	8,6	295,3	3,5	0,4	77,71
L1-92 (r)	0,05396	1,57	0,3	1,91000	0,0	0,59	368,0	72,0	303,5	10,0	299,2	3,4	0,7	81,30
L1-93 (c)	0,05494	1,99	0,3	2,10000	0,0	0,69	408,0	88,0	304,2	11,0	296,9	4	0,3	72,77
L1-93 (r)	0,05303	1,11	0,4	1,60000	0,0	0,62	330,0	50,0	305,3	8,4	299,1	3,6	0,9	90,64
L1-97	0,05622	1,08	0,4	1,36000	0,0	0,43	460,0	48,0	319,3	7,4	300,3	2,5	0,7	65,28
L1-98	0,05218	0,76	0,3	0,99000	0,0	0,37	292,0	36,0	299,8	5,1	303,9	2,2	0,7	104,08
L1-103	0,05212	0,98	0,3	1,18000	0,0	0,5	290,0	46,0	289,6	5,9	293,9	2,9	0,6	101,34
L1-104	0,05421	1,57	0,4	2,17000	0,0	0,52	378,0	70,0	304,8	11,4	297,8	3	1,1	78,78
PAL-16														
L3-01	0,0603	1,21	0,8	1,60000	0,1	0,62	614,0	52,0	573,6	14,0	555,5	6,7	0,7	90,47
L3-05 (r)	0,06	0,86	0,7	1,06000	0,1	0,4	0,1	0,9	557,1	9,1	560,8	4,3	0,6	952607,44
L3-05 ©	0,06	0,87	0,8	1,18000	0,1	0,39	0,1	0,9	573,3	10,3	555,6	4,2	0,9	920019,87
L3-11	0,05871	0,99	0,7	1,40000	0,1	0,49	556,0	42,0	558,3	12,1	562,1	5,3	0,9	101,10
L3-14	0,05837	0,81	0,7	1,12000	0,1	0,38	542,0	36,0	546,2	9,4	550,4	4	0,9	101,55
L3-30	0,05882	0,93	0,8	1,22000	0,1	0,45	560,0	42,0	569,6	10,7	558,2	4,8	0,8	99,68
L3-31	0,05961	1,05	0,7	1,47000	0,1	0,42	588,0	44,0	567,3	12,7	555,3	4,5	1,0	94,44
L3-32	0,05932	0,83	0,7	1,41000	0,1	0,42	578,0	36,0	546,2	11,9	544,2	4,4	1,2	94,15
L3-33 (r)	0,05891	0,85	0,7	1,29000	0,1	0,44	562,0	38,0	555,2	11,0	549,8	4,6	1,0	97,83
L3-33(c)	0,05911	0,82	0,7	1,28000	0,1	0,41	570,0	36,0	553,4	10,9	548,2	4,3	1,1	96,18

Tab. 2. U-Pb analyses data (continuous)

	Ratios						Ages					rho	% Disc
Sample #	**$^{207}Pb/^{206}Pb$**	**1σ(%)**	**$^{207}Pb/^{235}U$**	**1σ(%)**	**$^{206}Pb/^{238}U$**	**1σ(%)**	**$^{207}Pb/^{206}Pb$**	**±2 S.D.**	**$^{207}Pb/^{235}U$**	**±2 S.D.**	**$^{206}Pb/^{238}U$**	**±2 S.D.**		
VIV-11														
L3-36	0,06	1,26	0,6	1,60000	0,1	0,69	572,0	54,0	480,5	12,2	462,1	6,2	0,7	80,79
L3-39	0,05904	0,81	0,6	1,10000	0,1	0,64	568,0	36,0	474,2	8,3	453,5	5,6	0,7	79,84
L3-41 (r)	0,05838	1,21	0,6	1,56000	0,1	0,45	544,0	54,0	472,6	11,8	463,5	4	0,8	85,20
L3-41 ©	0,05876	1,25	0,6	1,83000	0,1	0,5	558,0	54,0	482,4	14,1	461,7	4,5	1,1	82,74
L3-45	0,06	1,08	0,6	1,32000	0,1	0,48	464,0	48,0	469,9	10,0	465,1	4,3	0,6	100,24
L3-48	0,06	0,72	0,6	0,99000	0,1	0,41	568,0	32,0	483,4	7,6	473,1	3,7	0,8	83,29
L3-52	0,05926	0,87	0,6	1,09000	0,1	0,49	576,0	38,0	486,0	8,4	477,2	4,5	0,6	82,85
TRI-O8														
S1-37	0,053	1,380	0,4	1,50000	0,0	0,97	310,0	62,0	309,5	8,0	313,5	5,9	0,4	101,13
S1-40	0,052	2,210	0,3	3,54000	0,0	1,76	272,0	102,0	293,5	18,1	298,4	10,3	0,9	109,71
S1-43	0,052	2,270	0,4	2,30000	0,0	2,45	280,0	104,0	312,0	12,4	309,2	14,8	0,5	110,43
S2-17	0,06	2,24	0,4	2,34000	0,0	0,76	524,0	98,0	333,0	13,3	300,0	4,4	0,3	57,25
S2-20	0,052	1,420	0,3	1,83000	0,0	0,77	292,0	66,0	301,2	9,5	300,7	4,5	0,7	102,98
S2-21	0,06	1,76	0,4	2,19000	0,0	0,92	420,0	78,0	315,3	11,9	296,7	5,3	0,6	70,64
S2-22	0,06	2,46	0,4	3,15000	0,0	0,72	420,0	110,0	307,8	16,7	298,2	4,2	1,0	71,00
S2-23	0,053	4,200	0,4	6,58000	0,0	1,24	346,0	190,0	322,1	36,3	296,7	7,2	1,7	85,75
S2-24	0,093	2,240	0,6	3,53000	0,1	0,95	1482,0	86,0	506,8	28,2	316,1	5,9	1,2	21,33
L1-139	0,0	1345,9	0,7	65,60236	1,6	7,43	298,0	140,0	302,2	21,0	303,3	5,1	-1853,7	101,78
L1-140	0,0	1040,6	0,4	82,48684	1,0	9,61	362,0	82,0	313,7	11,1	306,4	4,2	-678,6	84,64
LON-02														
L1-01	0,05	1,61	0,3	1,84000	0,0	0,57	338,0	74,0	299,0	9,5	302,2	3,4	0,5	89,41
L1--04	0,05	1,49	0,3	1,70000	0,0	0,8	332,0	68,0	304,5	8,9	299,6	4,7	0,5	90,24
L1--06	0,05	2,01	0,3	2,37000	0,0	0,65	328,0	90,0	302,8	12,4	298,7	3,8	0,6	91,07
L1--08	0,05	1,81	0,4	2,17000	0,0	0,78	322,0	82,0	307,9	11,5	303,0	4,6	0,6	94,10
L1-10	0,06	1,91	0,4	2,27000	0,0	0,97	542,0	82,0	330,8	12,8	303,8	5,8	0,6	56,05
L1--18	0,05	0,90	0,3	1,17000	0,0	0,48	364,0	42,0	300,3	6,1	295,6	2,8	0,7	81,21
L1-25	0,05	0,83	0,3	0,97000	0,0	0,35	334,0	38,0	300,4	5,0	298,0	2	0,6	89,22
L1-26	0,05	1,37	0,4	1,73000	0,0	0,53	368,0	62,0	307,3	9,2	298,1	3,1	0,8	81,01

Tab. 2. U-Pb analyses data (continuous)

	Ratios						Ages							
Sample #	$^{207}Pb/^{206}Pb$	1σ(%)	$^{207}Pb/^{235}U$	1σ(%)	$^{206}Pb/^{238}U$	1σ(%)	$^{207}Pb/^{206}Pb$	±2 S.D.	$^{207}Pb/^{235}U$	±2 S.D.	$^{206}Pb/^{238}U$	±2 S.D.	rho	% Disc
L1-27	0,05	1,59	0,3	1,82000	0,0	0,55	362,0	72,0	299,7	9,5	296,3	3,2	0,5	81,85
L1-30	0,05	2,42	0,4	2,88000	0,0	0,86	390,0	108,0	309,2	15,3	303,9	5,1	0,6	77,92
L1-31 ©	0,05	1,88	0,3	2,32000	0,0	0,88	400,0	84,0	298,5	12,0	288,3	5	0,6	72,08
L1-31 ®	0,05	1,96	0,4	2,45000	0,0	0,87	380,0	88,0	305,4	12,9	295,8	5	0,7	77,84
L1--32	0,05	1,27	0,3	1,40000	0,0	0,71	276,0	58,0	295,9	7,2	300,3	4,2	0,4	108,80
L1-33	0,05	1,75	0,3	2,74000	0,0	0,76	332,0	78,0	296,9	14,1	297,0	4,4	1,2	89,46
L1-34	0,06	2,16	0,4	2,81000	0,0	0,79	436,0	96,0	305,5	14,8	298,0	4,6	0,9	68,35

Sample ° have been performed at Geochronological Laboratory at University of Brasilia

Sample # have been performed at Mineralogy and Geochemical Institute at the University of Lausanne

Tab. 3. Lu-Hf analyses data

Sample	T(Ma)	$(^{176}Lu/^{177}Hf)_{meas}$	±2⊠	$(^{176}Hf/^{177}Hf)_{meas}$	±2⊠	$^{176}Hf/^{177}Hf_{(T)}$	±2⊠	⊠$Hf_{(T)}$	±2⊠	T_{DM}(Ga)
SST 5100										
Z01	444	0,0021687	0,000033	0,282424	0,000020	0,282405	0,000018	-3,62	0,13	1,48
Z02	432	0,0022463	0,000045	0,282422	0,000031	0,282403	0,000031	-3,96	0,37	1,49
Z04	1980	0,0008550	0,000012	0,281206	0,000173	0,281172	0,000013	-12,54	-0,63	3,24
Z12	550	0,0011386	0,000007	0,282362	0,000017	0,282349	0,000016	-3,23	0,05	1,55
Z18	945	0,0024258	0,000115	0,282443	0,000055	0,282399	0,000055	7,39	0,57	1,29
Z21	703	0,0012710	0,000017	0,281336	0,000019	0,281319	0,000019	-36,29	0,04	3,46
Z22	942	0,0022164	0,000009	0,282512	0,000019	0,282471	0,000019	9,89	-0,07	1,14
Z26	571	0,0019006	0,000019	0,282410	0,000035	0,282389	0,000035	-1,35	0,39	1,46
Z32	550	0,0005266	0,000005	0,281717	0,000024	0,281712	0,000024	-25,80	0,19	2,77
Z36	441	0,0020355	0,000010	0,282431	0,000021	0,282413	0,000021	-3,40	0,19	1,47
Z39	453	0,0015493	0,000012	0,282279	0,000025	0,282265	0,000025	-8,38	0,26	1,75
Z42	445	0,0024422	0,000065	0,282497	0,000026	0,282476	0,000026	-1,10	0,28	1,34
Z43	455	0,0012888	0,000020	0,282447	0,000023	0,282435	0,000023	-2,30	0,22	1,42
Z45	474	0,0019476	0,000093	0,282446	0,000018	0,282429	0,000018	-2,12	0,11	1,42
SA-ALB										
Z05	603	0,0007252	0,000002	0,282207	0,000051	0,282198	0,000051	-7,39	1,31	1,82
Z19	669	0,0006288	0,000008	0,282129	0,000026	0,282121	0,000026	-8,66	0,37	1,94
Z33	667	0,0010543	0,000010	0,281926	0,000030	0,281912	0,000030	-16,09	0,24	2,35
Z35	1019	0,0008744	0,000009	0,282251	0,000030	0,282234	0,000030	3,21	0,10	1,58
Z37	860	0,0006138	0,000005	0,282163	0,000024	0,282152	0,000024	-3,25	0,06	1,80
Z38	1000	0,0006025	0,000004	0,282234	0,000020	0,282223	0,000020	2,39	-0,08	1,61
Z39	1091	0,0010792	0,000005	0,282524	0,000021	0,282501	0,000021	14,30	-0,09	1,02
Z40	699	0,0007913	0,000007	0,282507	0,000024	0,282496	0,000024	5,30	0,24	1,20
Z43	852	0,0005028	0,000017	0,282392	0,000024	0,282383	0,000024	4,75	0,06	1,36
Z44	1063	0,0007687	0,000014	0,282490	0,000027	0,282474	0,000027	12,73	0,02	1,09
Z49	679	0,0020724	0,000037	0,282482	0,000022	0,282455	0,000022	3,39	0,21	1,29
Z50	851	0,0007080	0,000015	0,282417	0,000019	0,282405	0,000019	5,49	-0,03	1,31
Z51	998	0,0007548	0,000004	0,282457	0,000031	0,282443	0,000031	10,14	0,12	1,18
Z57	976	0,0011160	0,000034	0,281646	0,000018	0,281625	0,000018	-19,34	-0,19	2,78
Z58	635	0,0004907	0,000003	0,282069	0,000021	0,282063	0,000021	-11,46	0,20	2,07

Tab. 3. Lu-Hf analyses data (continous)

Sample	T(Ma)	$(^{176}Lu/^{177}Hf)_{meas}$	±2σ	$(^{176}Hf/^{177}Hf)_{meas}$	±2σ	$^{176}Hf/^{177}Hf_{(T)}$	±2σ	εHf$_{(T)}$	±2σ	T_{DM}(Ga)
SA-ALB										
Z58B	635	0,0006574	0,000020	0,282425	0,000019	0,282417	0,000019	1,07	0,14	1,38
Z64	699	0,0011829	0,000020	0,282294	0,000026	0,282278	0,000026	-2,40	0,33	1,62
Z65	693	0,0007606	0,000016	0,282456	0,000016	0,282446	0,000016	3,39	-0,02	1,30
Z69	1030	0,0003290	0,000007	0,281888	0,000022	0,281882	0,000022	-9,02	-0,05	2,26
Z70	816	0,0018502	0,000008	0,282584	0,000017	0,282555	0,000017	10,01	-0,05	1,03
Z72	684	0,0010180	0,000021	0,282647	0,000022	0,282634	0,000022	9,85	0,19	0,93
CO-SOL										
Z03	700	0,0008178	0,000018	0,281508	0,000025	0,281496	0,000025	-30,08	0,31	3,13
Z14	491	0,0014638	0,000015	0,282448	0,000020	0,282434	0,000020	-1,53	0,29	1,40
Z21	2664	0,0007175	0,000015	0,281347	0,000023	0,281310	0,000023	8,20	-1,52	2,66
Z24	781	0,0005745	0,000007	0,282470	0,000030	0,282462	0,000030	5,93	0,41	1,23
Z25	511	0,0011093	0,000014	0,282435	0,000032	0,282424	0,000032	-1,45	0,69	1,42
Z31	556	0,0006187	0,000010	0,281974	0,000035	0,281968	0,000035	-16,61	0,78	2,28
Z34	551	0,0015789	0,000040	0,282418	0,000030	0,282401	0,000030	-1,36	0,59	1,44
Z43	334	0,0008101	0,000009	0,282474	0,000021	0,282469	0,000021	-3,83	0,46	1,40
Z44	730	0,0020946	0,000067	0,282477	0,000026	0,282447	0,000026	4,26	0,30	1,28
Z56	1110	0,0015659	0,000012	0,282063	0,000051	0,282029	0,000051	-2,00	0,88	1,94
Z66	544	0,0006305	0,000003	0,281112	0,000031	0,281105	0,000031	-47,41	0,63	3,92
Z69	508	0,0019662	0,000009	0,282334	0,000047	0,282315	0,000047	-5,38	1,22	1,63
Z70	362	0,0005814	0,000004	0,282177	0,000034	0,282173	0,000034	-13,65	0,89	1,96
Z71	334	0,0010018	0,000004	0,282493	0,000036	0,282487	0,000036	-3,18	0,99	1,36
Z74	1054	0,0008128	0,000019	0,282426	0,000079	0,282409	0,000079	10,22	1,89	1,22
Z75	336	0,0008371	0,000015	0,282252	0,000056	0,282246	0,000056	-11,65	1,70	1,83
Z76	346	0,0018909	0,000023	0,282443	0,000035	0,282431	0,000035	-4,89	0,96	1,47
Z100	2669	0,0006611	0,000004	0,281301	0,000049	0,281266	0,000049	6,78	-0,59	2,74
Z105	1063	0,0011050	0,000002	0,282390	0,000059	0,282367	0,000059	8,93	1,19	1,30
Z107	645	0,0004930	0,000005	0,282207	0,000054	0,282201	0,000054	-6,35	1,36	1,80
Z110	1023	0,0008978	0,000017	0,281819	0,000029	0,281801	0,000029	-12,03	0,17	2,42
Z113	645	0,0017246	0,000028	0,282412	0,000041	0,282390	0,000041	0,35	0,90	1,43
Z116	663	0,0014794	0,000025	0,282417	0,000051	0,282398	0,000051	1,03	1,25	1,41

Tab. 3. Lu-Hf analyses data (continous)

Sample	T(Ma)	$(^{176}Lu/^{177}Hf)_{meas}$	±2⊠	$(^{176}Hf/^{177}Hf)_{meas}$	±2⊠	$^{176}Hf/^{177}Hf_{(T)}$	±2⊠	⊠$Hf_{(T)}$	±2⊠	T_{DM}(Ga)
CAV 05										
Z02	649	0,0013054	0,000007	0,282434	0,000018	0,282418	0,000018	1,41	0,08	1,37
Z03	482	0,0031298	0,000090	0,282574	0,000020	0,282544	0,000020	2,15	0,29	1,19
Z05	536	0,0024361	0,000055	0,282445	0,000024	0,282418	0,000024	-0,65	0,37	1,41
Z08	503	0,0019485	0,000044	0,282434	0,000019	0,282415	0,000019	-1,97	0,24	1,44
Z09	314	0,0015989	0,000015	0,282415	0,000020	0,282405	0,000020	-6,50	0,43	1,53
Z10	452	0,0022727	0,000067	0,282481	0,000025	0,282461	0,000025	-1,46	0,51	1,37
Z11	832	0,0007679	0,000010	0,282508	0,000020	0,282495	0,000020	8,27	0,01	1,14
Z12	1005	0,0005810	0,000010	0,281834	0,000014	0,281823	0,000014	-11,67	-0,35	2,39
Z13	478	0,0023016	0,000084	0,282451	0,000018	0,282429	0,000018	-2,01	0,22	1,42
Z14	300	0,0015181	0,000023	0,282441	0,000016	0,282433	0,000016	-5,85	0,33	1,48
Z15	276	0,0018084	0,000035	0,282460	0,000021	0,282451	0,000021	-5,74	0,50	1,46
Z17	1014	0,0027024	0,000026	0,282326	0,000019	0,282272	0,000019	4,46	-0,17	1,51
Z18	440	0,0009341	0,000015	0,281527	0,000025	0,281519	0,000025	-35,07	0,52	3,18
Z19	1030	0,0000590	0,000000	0,282186	0,000013	0,282184	0,000013	1,71	-0,41	1,67
Z20	311	0,0020833	0,000054	0,282425	0,000017	0,282413	0,000017	-6,32	0,35	1,52
Z21	486	0,0008342	0,000015	0,282555	0,000016	0,282547	0,000016	2,35	0,17	1,19
Z25	1068	0,0014858	0,000021	0,282095	0,000026	0,282064	0,000026	-1,71	0,03	1,89
CA-PAL										
Z15	**314**	0,0024997	0,000032	0,282613	0,000060	0,282598	0,000060	0,29	1,86	1,16
Z29	**2378**	0,0004543	0,000006	0,281127	0,000016	0,281106	0,000016	-5,72	-1,51	3,19
Z33	**324**	0,0050348	0,000096	0,282553	0,000219	0,282521	0,000219	-2,19	7,46	1,30
Z37	**2389**	0,0010112	0,000017	0,282450	0,000017	0,282402	0,000017	40,64	-1,50	0,59
Z40	**533**	0,0010195	0,000018	0,282434	0,000019	0,282423	0,000019	-0,99	0,24	1,41
Z42	**633**	0,0014669	0,000032	0,282448	0,000019	0,282430	0,000019	1,48	0,15	1,36
Z49	**535**	0,0013942	0,000019	0,282371	0,000014	0,282356	0,000014	-3,32	0,06	1,54
Z50	**518**	0,0016187	0,000019	0,282393	0,000021	0,282377	0,000021	-2,96	0,32	1,51
Z51	**537**	0,0011234	0,000020	0,282430	0,000018	0,282419	0,000018	-1,07	0,17	1,42